

CRANFIELD UNIVERSITY

DOMINIKA A. GASTOL

MICROFABRICATION PROCESSING OF TITANIUM FOR BIOMEDICAL DEVICES
WITH REDUCED IMPACT ON THE ENVIRONMENT

SCHOOL OF APPLIED SCIENCES

PhD THESIS

Academic Year 2009 -12

Supervisors:

Prof. David M. Allen

Dr Heather J. A. Almond

September 2012

CRANFIELD UNIVERSITY

SCHOOL OF APPLIED SCIENCES

PhD THESIS

Academic Year 2009-2012

DOMINIKA A. GASTOL

Microfabrication Processing of Titanium for Biomedical Devices with Reduced
Impact on the Environment

Supervisors:

Prof. David M. Allen

Dr Heather J. A. Almond

Sponsor Company: Datum Alloys Ltd.

September 2012

This thesis is submitted in partial fulfilment of the requirements for the degree of Doctor of
Philosophy

© Cranfield University 2012. All rights reserved. No part of this publication may be
reproduced without the written permission of the copyright owner.

Abstract

This thesis presents research on a novel method of microfabrication of titanium (Ti) biomedical devices. The aim of the work was to develop a commercial process to fabricate Ti in a more environmentally friendly manner than current chemical etching techniques. The emphasis was placed on electrolytic etching, which enables the replacement of hazardous hydrofluoric acid-based etchants that are used by necessity when using Photochemical Machining (PCM) to produce intricate features in sheet Ti on a mass scale. Titanium is inherently difficult to etch (it is designed for its corrosion-resistant attributes) and as a result, Hydrofluoric acid (HF) is used in combination with a strong and durable mask to achieve selective etching. The use of HF introduces serious health and safety implications for those working with the process.

The new technique introduces the use of a “sandwich structure”, comprising anode/insulator/cathode, directly in contact with each other and placed in an electrolytic etching cell.

In this technique the same photolithography process is utilised to achieve selective etching on a metal substrate as in the PCM process. However, for the electrolytic etching stage, the inter-electrode gap (IEG) is reduced significantly from a few centimetres, as usually applied in electrochemical processes, to 4 μm . The intention behind this was to improve the current distribution experienced at the anode (Ti) during subsequent electrolytic etching.

The sandwich structure was developed by deposition of a photoresist S1818 and Copper (Cu) on top of Ti. Firstly, a manual sanding of the substrate was applied in order to eliminate the oxide layers which could strongly affect a final electrolytic etching. The soft- and hard-bake stages involved in the processing of the S1818 resist were optimised to produce a stress-free Ti/S1818/Cu/S1818 structure. Ultimately a pattern would be imparted onto the S1818/Cu/S1818 that would ultimately be imparted through to the Ti layer during the last stage, electrolytic etching. In order to achieve this, a Cu electroless deposition was developed as a technique to obtain a conductive film which would act as a cathode during the electrolytic etching of the target, Ti layer.

The results of the electrolytic etching of the Ti sandwich structure revealed flat-base profiles of half-etched (“half-etch” is the term used to signify an etch that does not penetrate completely through the thickness of the metal sheet) micro-holes in the Ti layer. The problem

of delamination of the electroless Cu, in 10 % w/v HCl electrolyte used as an etchant, was solved by electroplating a 12 μm layer of Cu on top of the 60 nm Cu electroless deposited film.

Using this technique, micro-features were achieved in Ti. The half-etched micro-holes were characterised to have an overall spherical shape corresponding to the imaged pattern and a preferred flat-base profiles (typically a raised land of material arises in conventional electrolytic etching).

A series of parameters were tested in order to control the process of electrolytic etching through the Ti sandwich structure by measuring etch rate, surface roughness of the etched pattern and the etch factor. The applied current densities (CD) of 10, 15, 20, and 25 A/cm^2 showed proportional dissolution to the applied current. Electrolytic etching with a CD of 20 A/cm^2 demonstrated a high etch rate of 40 $\mu\text{m}/\text{min}$. and a relatively low Ra of 2.8 μm , therefore, it was utilised in further experimental work. The highest etch rate of 50 $\mu\text{m}/\text{min}$. and an improved distribution of half-etched micro-holes was achieved by the introduction of 4 crocodile connectors (2 per electrode) and mechanically stirring of the electrolyte (800 rpm) while performing the electrolytic etching. The maximum etch depth of 143.9 μm was produced in Ti when the electrolytic etching was performed at the same conditions for 3 minutes. The incorporation of ultrasonic agitation to the electrolytic etching and an electrolyte temperature of 13⁰C resulted in a decrease of the surface roughness of the etched micro-holes to 0.5 μm .

The results of the Ti sandwich structure electrolytic etching proved the concept of minimising the IEG in order to obtain a uniform Ti dissolution on a feature scale, improved control of the electrolytic dissolution over the whole area of the sample with utilisation of the lower hazard etchant at the same time.

Acknowledgement

I wish to express my sincere thanks to my supervisors: Prof. David M. Allen and Dr Heather J. A. Almond for their first class supervision, the advice and support throughout the project.

I would like to thank Datum Alloys Ltd. for sponsoring this project and Dr Peter Jefferies, CTO, for the external supervision of the project.

I also wish to thank Mr Andrew Dyer for his technical assistance.

My special thanks go to my family for their support during the PhD course.

List of contents

1. Aims and objectives	1
2. Literature review of titanium biomedical devices and microfabrication techniques	2
2.1 Introduction to biomedical devices	1
2.1.2 Titanium – what makes it special for biomedical devices?	4
2.1.3 Ti as a biomaterial	10
2.1.4 Ti in biomedical applications	14
2.1.5 Ti biomedical devices in humans	16
2.2 Ti microfabrication techniques	20
2.2.1 Dry etching techniques	20
2.2.2. Physical techniques	21
2.2.3 Mechanical techniques	22
2.2.4 Chemical techniques	24
2.2.5 Electrochemical microfabrication	27
2.2.6 Sandwich structure microfabrication	38
2.2.7 Microfabrication with reduced impact on the environment	40
2.2.8 Summary of literature review	41
3. Background to experimental methodology	45
3.1 Determination of the configuration of the sandwich structure	46
3.1.1 Exploratory sandwich structure	46
3.1.2 Sandwich structure	48
3.2 Determination of materials of the sandwich structure	48
3.2.1 Insulator	48
3.2.2 The cathode	53
3.3 Permanent sandwich structure building	55
3.3.1 Ti substrate preparation	55
3.3.2 Photoresist coating	55
3.3.3 Metallisation of the photoresist	55
4. Experimental procedures – stage 1 of sandwich structure building using Titanium as the anode	81
4.1 Introduction	81

4.2 Titanium substrate preparation	83
4.2.1 Sanding	83
4.2.2 Cleaning	83
4.2.3 Electrical resistivity measurements of Ti substrate	83
4.2.4 Roughness measurements	85
4.2.5 XRD analysis	86
4.2.6 Ti microstructure	88
5. Experimental procedures – stage 2 of sandwich structure building using photoresist as a dielectric	90
5.1 S1818 constituents characterisation	90
5.1.2 Chemical composition of the S1818 resist	91
5.2 Processing stages of the S1818 resist in the sandwich structure	93
5.2.1 Photoresist coating	95
5.2.2 Softbake	96
5.2.3 Exposure	97
5.2.4 Development	98
5.2.5 Hardbake	98
5.2.6 Photoresist removal	99
5.3 Baking stage optimisation of the S1818 resist	99
5.4 Mechanical properties of the S1818 photoresist cured at different temperatures	103
5.4.1 Nanoindentation	104
5.4.2 Nanoindentation tests	106
5.5 Investigation of the Ti/S1818 resist interface	110
6. Experimental procedures – stage 3 of sandwich structure building using a copper cathode	113
6.1 Role of Cu layer in Ti sandwich structure	113
6.2 Cu electroless deposition	113
6.2.1 Mechanism of Cu electroless deposition	114
6.2.2 Cu electroless process for Ti sandwich structure	116
6.2.3. Cu electroless deposit modification	125
6.3 Cu electroplating	152
6.4 Summary of fabrication of the cathode in the Ti sandwich structure	159

7. Experimental procedure – Titanium sandwich structure microfabrication	160
7.1 Ti sandwich structure microfabrication	160
7.2 Mechanism of electrolytic etching of Ti sandwich structure	160
7.3 Chemicals	163
7.4 Equipment	163
7.5 DC electrolytic etching of Ti sandwich structure	164
7.5.1 DC electrolytic etching of Ti sandwich structure with an electroless Cu cathode	164
7.5.2 DC electrolytic etching of Ti sandwich structure with the Cu cathode obtained from electroless and electrodeposition	172
8. Experimental procedure – scale-up of titanium sandwich structure process	202
8.1 Introduction	202
8.2 Test pattern	203
8.3 Equipment	203
8.3.1 Electrolytic etching machine	203
8.3.2 Chemicals	207
8.4 Future work on the scale-up of Ti sandwich structure	207
9. Discussion and summary of the feasibility of producing titanium microparts using a novel sandwich structure	208
10. Conclusions and recommendations for future work	211
10.1 Conclusions	211
10.2 Recommendations for future work and its relevance to industry	212
10.2.1 Current distribution control	212
10.2.2 Double-sided sandwich structure	213
10.2.3 Scale-up process	214
References	215
Appendices	231
Appendix A	231
Appendix B	232
Appendix C	233
Appendix D	236
Appendix E	237
Appendix F	238

List of figures

1	Yield strength-to-density ratios of selected implant materials. Amended from [9], [17].	9
2	Schematic illustration of the molecular processes at the interface between Ti and the surrounding biological environments; A) Processes at Ti oxide and biological fluid interface; B) An interaction of cells with the layer of water, ions and biomolecules [19], [20].	12
3	Applications of Ti and its alloys, author's analysis based on [9].	15
4	Titanium biomedical devices in human body [26], [27].	18
5	Layout of electrochemical photoetching reaction cell.	34
6	Schematic diagram of ECM experimental system applied by [67].	39
7	Cross section schemat of the "sandwich structure".	45
8	RF sputtering system [77].	56
9	Undeveloped pattern in the sandwich structure. The photoresist S1818 remained in the spherical- shape pattern.	63
10	Cell layout of DC electrolytic etching of the sandwich structure.	65
11	Tarnished ring on the Ti.	66
12	SEM micrograph of Cu electroless plated deposit with an indication of the thicknesses of the film.	69
13	XRD spectra for the Cu depositions obtained from two differently activated samples.	71
14	XRD spectrum of nickel electroless deposition.	77
15	SEM micrograph of Ni electroless plated deposit with an indication of the thicknesses of the film.	77
16	Surface roughness of the as-received and sanded Ti samples with the corresponding SEM micrographs of the surface textures.	86
17	XRD spectra for titanium as-received and manually sanded samples.	87
18	Microstructure of Kroll etched, cross-sectioned cp-Ti samples; a) surface as-received specimen, b) sanded specimen.	89
19	Cross section schemat of the complete sandwich structure prior patterning.	90

20	An optical micrograph of the chrome-on-glass pattern used in the sandwich structure.	98
21	Sketch of nanoindentation profile, modified from [116].	105
22	The Berkovich-shaped nano indenter from [117].	106
23	An optical micrograph of a trace of the Berkovich indent at the S1818 surface.	106
24	Load vs. displacement of the S1818 resist soft baked at 50 ⁰ C and 100 ⁰ C for 60 min.	108
25	Reduced elastic modulus of the S1818 resist soft baked at 50 ⁰ C and 100 ⁰ C for 60 min.	108
26	Hardness of the S1818 resist soft baked at 50 ⁰ C and 100 ⁰ C for 60 min.	109
27	FIB micrographs of the milled specimens: a) sample 1; b) sample 2 in Table 25.	111
28	Cu electroless process stages. The colours of the solutions a) and b) do not present their actual appearance. The colours were selected to differentiate the solutions one from the other.	118
29	Cross section of the process of Cu electroless deposition in the Ti sandwich structure.	118
30	Experimental set-up for the Cu electroless plating. Left picture: equipment used for the Cu electroless plating. Right picture: vertical immersion of the substrate - Ti/S1818.	120
31	SEM micrograph of the Cu deposit obtained from the standard Cu electroless solution.	122
32	EDX spectra in statistics for Ti structure: Ti/S1818/Cu - Cu obtained from standard solution.	123
33	XRD spectra of Ti/S1818/Cu structure with the Cu coatings obtained from stirred and unstirred solutions.	125
34	SEM micrographs of Cu electroless coating deposited on the S1818 resist. The Cu coatings were obtained from the electroless solutions with new organic additives: a) Gelatin, b) Glycerol, c) Glycerol 2, d) Sorbitol, e) Saccharin, f) Saccharin + Glycerol, g) Cytosine.	130
35	EDX spectra in statistics for Ti/S1818/Cu structure. The Cu coating obtained from the modified solutions.	131
36	XRD spectra for the Cu depositions obtained from the electroless solutions containing tested organic additives.	132

37	Roughness of Cu electroless deposits obtained from the solutions containing the following additives: 1 –standard, 2 – glycerol, 3- glycerol 2, 4 – sorbitol, 5 –cytosine, 6 – saccharin, 7 – glycerol + saccharin, 8 – gelatine.	137
38	Resistivity of Cu electroless films; where: 1 –standard, 2 – glycerol, 3- glycerol 2, 4 – sorbitol, 5 –cytosine, 6 – saccharin, 7 – glycerol + saccharin.	142
39	Plating rates for the Cu electroless solutions containing additions of glycerol and three different surfactants.	147
40	Optical micrograph of the Cu electroless coating obtained from the Cu electroless solution containing the additions of glycerol and Triton X-100.	148
41	SEM micrograph of the Cu deposit obtained from the Cu electroless solution containing the additions of glycerol and TX-100.	149
42	EDX spectra in statistics for Ti structure: Ti/S1818/Cu - Cu obtained from the Cu electroless solution containing the additions of glycerol and Triton X-100.	149
43	Cross section of the sandwich structure with the Cu double layer.	153
44	FIB cross section of the Ti/S1818/Cu structure with the Cu electroplated at different times on top of Cu electroless deposit.	156
45	Thickness of Cu electroplated deposit measured with FIB vs. plating time.	157
46	Plating rates for Cu electrodeposition.	157
47	Optical micrographs illustrating the deposition process steps; from left: specimen coated with the S1818 resist, then coated with the Cu electroless deposit, and Cu electro-plated layer on top of electroless deposit.	158
48	Schematic diagram of the Ti sandwich structure during electrolytic etching.	162
49	SEM micrographs of a) half-etched micro-holes, b) selected half-etched micro-hole, and c) the edge of the micro-hole.	167
50	Olympus Lext Confocal Laser Microscope micrographs of half-etched microholes etched at $CD = 20 \text{ A/cm}^2$, for 1 min. 1a), 2a) 3D scans of the half-etched microholes with corresponding 2D images of the profiles of the etched micro-holes: 1b), 2b).	169
51	Etch rate vs. surface roughness of half-etched micro-holes in Ti with the use of Cu electroless cathode.	170
52	Etch factor of half-etched micro-holes in Ti with the use of Cu electroless cathode.	171

53	SEM micrographs of a) half-etched micro-holes, b) selected half-etched micro-hole, and c) the edge of the micro-hole, produced by applying 20 A/cm^2 for 1 minute at ambient temperature.	175
54	Olympus Lext Confocal Laser Microscope micrographs of half-etched microholes etched at $CD = 20 \text{ A/cm}^2$ for 1 min. 1a), 2a) 3D scans of the half-etched microholes with corresponding 2D images of the profiles of the etched micro-holes: 1b), 2b).	177
55	Etch rate vs. current density.	178
56	Surface roughness vs. current density.	179
57	Etch rate vs. surface roughness.	179
58	Etch factor vs. current density.	180
59	Etch rate vs. surface roughness of etched Ti in sandwich structure electrolytic etching process utilising different number of electrode connectors.	182
60	Etch factor of etched Ti in sandwich structure electrolytic etching process utilising different number of electrode connectors.	182
61	Etch rate vs. surface roughness of the etched Ti at two mechanical stirring speeds.	186
62	Etch factor of the etched Ti at two mechanical stirring speeds.	186
63	Etch depth vs. time of etching of Ti at high mechanical stirring speed.	189
64	Etch rate vs. surface roughness of the etched Ti at a high mechanical stirring speed.	189
65	Etch factor of the etched Ti at a high mechanical stirring speed.	190
66	a) An optical micrograph of the cathode after electrolytic etching; b) SEM micrograph of the black film on top of the Cu cathode.	192
67	XRD spectrum of the Cu cathode from the Ti sandwich structure after electrolytic etching where the dot above the peak indicates detection of CuO.	192
68	Etch rate vs. surface roughness of the etched Ti micro-holes at ambient temperature and with an ice jacket applied.	194
69	Etch factor of the etched Ti micro-holes at ambient temperature and with an ice jacket applied.	195
70	Etch rate vs. surface roughness of the etched Ti micro-holes at ambient temperature and cooled electrolyte in the ultrasonic bath.	197
71	Etch factor of the etched Ti micro-holes at ambient temperature and cooled electrolyte in the ultrasonic bath.	197

72	4 inch diameter polished Ti substrate.	202
73	A design of the phototool for patterning the scaled-up Ti sandwich structure.	203
74	New electrolytic etching machine for the scaled-up process of the Ti sandwich structure, a) side view of the machine; b) front view of the loaded Ti workpiece to the Ti sandwich structure holder; c) top view of the machine with the indicated electrical connections to the sandwich structure and the electrolyte pump.	204

List of Tables

1	Biomaterials – their advantages and disadvantages with selected medical applications.	5
2	Specific gravities of the selected metallic biomaterials [10], [17].	9
3	Methods of Ti microfabrication.	40
4	The experimental conditions for the non-permanent “sandwich structure” etching.	47
5	Alternative processing stages investigated in the formation of the “sandwich structure”.	52
6	Resistivity of metals potentially involved in the processing of the “sandwich structure” [71].	54
7	Processing stages to obtain Ti/photoresist/Au sandwich structure.	58
8	Processing stages to obtain Ti/photoresist/Al sandwich structure.	60
9	Processing stages to obtain Ti/photoresist/Cu sandwich structure.	61
10	Processing stages to obtain Ti/photoresist/Cu structure incorporating electroless copper process.	72
11	Processing stages to obtain Ti/photoresist/Ni sandwich structure incorporating nickel electroless plating process.	78
12	Properties of α , $\alpha+\beta$ and β Ti alloys [9].	81
13	Chemical compositions of four cp Ti alloys compared with $\alpha+\beta$ alloy [10].	82
14	Chemical composition of the investigated Ti substrate [73].	83
15	The measured resistivity with standard deviation of the as-received and sanded titanium samples.	84
16	Chemical composition of the positive photoresist MICROPOSIT TM S1818 [74].	92
17	Process steps for the fabrication of the sandwich structure with an indication of the photoresist processing conditions.	94
18	The S1818 resist spin coating conditions using the EMS vacuum spinner.	96
19	Review of applied temperatures and time to soft/hardbake of the S1818 photoresist.	100
20	The S1818 resist baking parameters for the hot plate (Approach I).	101
21	The S1818 resist baking parameters for the hot plate (Approach II).	101

22	The S1818 resist baking parameters for the hot plate and the oven.	102
23	The S1818 resist baking parameters for the oven (Approach I).	102
24	The S1818 resist baking parameters for the oven (Approach II).	102
25	The parameters used to evaluate the Ti and the S1818 resist interface.	110
26	Sensitisation solution constituents with the quantities per litre.	116
27	Activation solution constituents with the quantities per litre.	117
28	Copper electroless plating solution constituents with the quantities per l.	117
29	Operating conditions for the sensitisation solution, activation solution and the Cu electroless plating bath.	121
30	Effect of a mechanical stirring on Cu electroless deposit.	124
31	Copper electroless plating solution organic additives with the quantities per litre.	127
32	Time needed to obtain a uniform copper coating by electroless deposition with the use of solution with the organic additive/s.	128
33	Olympus Lext Confocal Laser Microscope micrographs of the Cu deposits from Cu electroless modified solutions.	135
34	FIB cross-section thickness measurement of Cu electroless deposits in the Ti/S1818/Cu structure.	139
35	Non-ionic surfactants applied to Cu electroless plating solution.	145
36	The parameters obtained from the Cu coating deposited from the Cu electroless solution containing the additions of glycerol and TX-100.	150
37	Cu electroplating electrolyte constituents with quantities used per litre.	155
38	Process steps for the fabrication of the Ti sandwich structure with Cu cathode electrolessly deposited.	165
39	Process steps for the fabrication of the Ti sandwich structure with Cu cathode obtained from electroless and electrodeposition.	173
40	Conditions applied for electrolytic etching of Ti sandwich structure with 2 stirring speeds with the observations of the electrodes.	185
41	Conditions applied for electrolytic etching of Ti sandwich structure with a high mechanical stirring speed.	188
42	Summary of the Ti sandwich structure electrolytic etching results.	199
43	Process steps and required equipment for the scaled-up Ti sandwich structure microfabrication process.	205

Nomenclature

Symbol	Definition	Unit
m	mass of metal liberated	g
M	molecular weight of metal	g/mol
I	current	A
t	time	s
n	valence number of dissolved metal	-
F	Faraday's constant	96500 C/mol
J	Current density (CD)	A/cm ²
U	Electric potential difference	V
ρ	Resistivity	$\Omega \cdot \text{cm}$
t	Thickness of the specimen	cm
F	Force	N
P	Load	N
A	Projected area	m ²
E _r	Reduced elastic modulus	Pa
S	Contact stiffness	N/m
H	Hardness	Pa
h _c	Contact depth	m
R _a	Roughness	μm
R	Resistance	Ω
E	Young's Modulus	Pa

Chapter 1: Aims and objectives

The aim of the work, presented in this thesis, was to develop a fully commercial process to fabricate micro-features in titanium for biomedical devices with a reduced impact on the environment. Conventional etching of titanium entails the use of hazardous and environmentally dangerous etchants such as hydrofluoric acid.

The fabrication method of titanium, detailed in this work, relied on electrolytic etching with an application of a novel “sandwich structure”. The new structure comprising of the anode/insulator/cathode was introduced in order to significantly reduce the inter-electrode gap. This was aimed at overcoming the problems of non-uniform current distribution over the substrate, as typically experienced in conventional electrolytic etching.

The process was examined by using a test pattern comprising of an array of circular holes of 125 μm (in diameter). The pattern was used to test the capabilities of the sandwich structure to produce micro-features in titanium with the use of a less hazardous etchant, such as 10% w/v HCl. Direct current (DC) continuous electrolytic etching was utilised as the main method to electrolytically etch the micro-features in titanium.

The bulk of the work was aimed at optimising the process over a working area of 4 x 5 cm in order to subsequently enable a further scale-up of a working area up to 4 inch in diameter.

The main objective of the project was to produce high-quality components with controlled parameters, such as: side wall profile i.e. straight edges, flat base profile, desirable dimensions as well as surface roughness dependant on the application.

Chapter 2: Literature review of titanium biomedical devices and microfabrication techniques

2.1 Introduction to biomedical devices

The objectives of introducing new technology to medicine are prevention of disease, remediation of disease, and rehabilitation from disease [1]. In the current state of health care, life-saving and life-enhancing procedures would not have been so advanced without the development of medical devices.

Medical devices have been introduced to all areas of the medical practice, which are:

- a) Analysis,
- b) Diagnosis,
- c) Therapy,
- d) Rehabilitation.

Development of medical devices has provided numerous benefits for medicine, technology, and the economy. An implementation of technologically-assisted procedures effects an increase in the chances of a positive outcome of a treatment. In addition, the use of medical devices raises patients' quality of life and improves the availability of health care by reducing the costs of provided services. Medical challenges draw the attention of physicians, biologists, engineers, entrepreneurs and businessmen. Their collaboration in the last few decades has resulted in the spin out of technological advances in the medical field.

All parties involved in medical technology are obliged to employ international (within European Union) and national standards in order to assure that the final product is safe and has met all requirements. Medical devices have been regulated in the new approach to technical harmonization and standardization in the European Union (EU) in the 1990s [2], [3]. The core legal framework consists of three directives which group medical devices into the following categories, depending on their applications:

- a) **Active implantable devices**, Directive 90/385/EEC,
- b) **Medical devices**, Directive 93/42/EEC,
- c) ***In vitro* diagnostic medical devices**, Directive 98/79/EC, [4].

These directives introduce definitions, classification, as well as essential requirements regarding design and manufacture of medical devices.

‘**Active medical device**’ is defined as “any medical device that relies for its functionality on a source of electrical energy or any source of power that is not generated by the human body or gravity”, such as a pacemaker or insulin pump. An active implantable device is totally or partially introduced into the human body or into a natural orifice during a medical intervention. Such devices are intended to remain there after the procedure [5].

A directive released in 1993 provides a definition of a **medical device**. It is any instrument, apparatus, appliance, software, material or other article that can be used for the purposes of:

- Diagnosis, prevention, monitoring, treatment or alleviation of disease, an injury or handicap,
- Investigation, replacement or modification of the anatomy or of a physiological process,
- Control of conception [3].

The following devices can be classified in this category: X-ray equipment, dental equipment, aids for handicapped and disposables [6].

The last group of the medical devices is ***in vitro* diagnostic medical devices**. This term covers reagent, reagent product, calibrator, control material, kit, instrument, apparatus system, used alone or in combination. They are processed for *in vitro* examination of physiological or pathological state, congenital abnormality, determine the safety and compatibility with potential recipients, or to monitor therapeutic measures [6]. Reagents and analytical products represent described medical devices.

Manufacturers of the Member States of the EU have to meet the conditions covered in the Directives which replace the corresponding national provisions. These specific rules include the area of: health and safety requirements of design and manufacture, implementation on the market, conformity assessment procedures, procedures packs including the procedure for sterilization as well as clinical investigation.

CE marking of medical devices, described in the Directives, is required from the manufacturer, in order to implement it on the market. The CE marking of conformity assures

that the medical device is constructed and built according to the essential requirements applicable for the specific use [6].

2.1.2. Titanium– what makes it special for biomedical devices?

➤ **Biomaterials**

When a medical device is designed, particular attention must be paid to [5]:

- The choice of materials used, especially as regards toxicity and flammability,
- The compatibility between the materials applied and biological tissues, cells and body fluids,
- Where appropriate, the results of biophysical or modeling research.

These requirements are met by **biomaterials**, also called **biocompatible materials** which are employed to replace a part or a function in the body [4]. The term ‘biomaterial’ is applied to natural or synthetic material that is used in contact with living tissue and/or biological fluids [7]. It is intended for use in prosthetic, diagnostic, therapeutic, and storage applications without adversely affecting the living organism and its components [8].

From the engineering perspective, the success of biomaterials in the human organism depends on material properties, design, and its compatibility with the surrounding tissues.

Therefore, to achieve a medical objective, a biomaterial must fulfil the criteria [9]:

- a) Corrosion resistance,
- b) Biocompatibility,
- c) Bioadhesion, also called osseointegration,
- d) Favorable mechanical properties, e.g. Young’s Modulus, similar to that of bone, fatigue strength in accordance with the application,
- e) Processability (casting, deformation, powder metallurgy, machinability, welding, etc.),
- f) Availability.

Each of these properties plays a crucial role in the decision making process of what material should be employed for specific medical demands.

There are four main materials which are used as the biomaterials. They are:

- Metals,
- Ceramics,
- Polymers, and
- Composites.

All of them have their strengths and weaknesses which have been listed in Table 1 with selected applications in medicine.

Table 1: Biomaterials – their advantages and disadvantages with selected medical applications [10].

Biomaterials	Advantages	Disadvantages	Examples
Metals (Ti and its alloys, Co-Cr alloys, stainless steel, Au, Ag, Pt, etc.)	Strong, tough, ductile	May corrode, dense, difficult to fabricate	Joint replacements, bone plates and screws, stents, pacemakers
Ceramics (aluminum oxide, calcium phosphates)	Very biocompatible, inert, strong in compression	Brittle, not resilient, difficult to make	Dental, femoral head of hip replacement, coating of dental and orthopedic implants
Polymers	Resilient, easy to fabricate	Deforms with time, may degrade	Sutures, blood vessels, hip socket, ear, nose, other soft tissues
Composites	Strong, tailor-made	Difficult to make	Joint implants, heart valves

These biomaterials can be applied either separately or in various combinations.

Ceramic biomaterials are used for their hardness and wear resistance. They exhibit excellent biocompatibility with body fluids and tissues. Depending on the material used, they can be divided into bioinert, bioactive or biodegradable. Alumina (Al_2O_3), Zirconia (ZrO_2), and Pyrolytic Carbon are bioinert ceramics. Thromboresistance of Pyrolytic Carbon finds an application in artificial mechanical heart valves. Alumina is used for orthopaedic applications and in dentistry. In contrast, glass ceramics like SiO_2 , CaO possess bioactive properties. They are capable of direct chemical bonding with host tissues making them ideal for cement fillers and coatings. The last group of ceramics – biodegradable, such as Tricalcium phosphate ($\text{Ca}_3(\text{PO}_4)_2$) have been used for formation of new bone [11]. In spite of their outstanding properties, ceramics are not designed for load bearing applications.

Polymers, in contrast to ceramics, are flexible and have highly varying mechanical properties [4]. They exhibit time-dependent mechanical behaviour and are known to be viscoelastic [12]. However, sustained loads can result in progressing strain or creep. Due to their resistance to attack from body-fluids, polymers find a broad range of applications in medical devices. What is more, polymers are easy to fabricate, enhancing their availability. Typical applications include dentistry, ophthalmology, orthopaedics, cardiology, drug delivery, and wound healing aids. Materials such as Polyurethane compounds offer superior mechanical properties with regard to durability and flexibility [4]. These polymers have been used for pump membranes in artificial hearts. Polytetrafluoroethylene (PTFE) is employed in intravascular balloon catheters, in the deployment of a coronary stent.

Recently, **composites** have been gaining attention as biomaterials. The strategy of designing composites is to combine various materials such as: metals, ceramics, and polymers in order to put together the advantages of the individual components [13]. Some applications of composites include: dental filling composites, reinforced methyl methacrylate bone cement, or orthopaedic implants with porous surfaces. Increasing interest has been shown in ceramic-polymer composites as potential fillers of bone defects. The most commonly used ceramics are tricalcium phosphate or 44S5 Bioglass® which exhibit biocompatibility, osteoconduction, osseointegration and vascularization. However, these ceramics are considered too stiff and brittle to be used alone [14]. Composites have been successful in bone and neurological systems, but are limited for vascular systems, particularly heart valve replacements [14]. The

introduction of composites as biomaterials has been recent. Therefore, their importance in the biomedical field may increase in the future.

Metals are used as biomaterials due to their excellent electrical and thermal conductivity and preferential mechanical properties. They have been utilized as biomaterials since the 16th century [15]. Since that time metal properties have been closely investigated along with their ability to be used in *in vivo* applications.

Nowadays, metals are employed as passive materials for hard tissue replacement such as total hip or knee joints, for fracture healing aids, such as bone plates and screws, spinal fixation devices, and in dentistry because of their excellent mechanical properties and corrosion resistance. Certain metallic alloys exhibit more active roles in medical devices such as vascular stents, catheter guide wires, orthodontic wires, and cochlea implants [10]. Because of the requirements for biomaterials (see page 3) the number of metallic materials is limited. Noble metals such as gold, silver, and platinum exhibit superior corrosion resistance. However, their inadequate mechanical properties limit their use [15].

Nowadays, the following groups of **metallic materials** are being used for **biomedical devices** [9]:

- a) Stainless steel, i.e. X2CrNiMo1812 (AISI 316L),
- b) CoCr-based alloys (Vitallium) in the as-cast condition, i.e. CoCr30Mo6, or in the as-wrought condition, i.e. CoNi35Cr20,
- c) Commercially pure (cp) tantalum,
- d) Cp-niobium,
- e) Cp-titanium and titanium alloys, i.e. Ti-6Al-4V.

Most widely used for implant fabrication amongst steels are the **austenitic stainless steels**, types AISI 316 and 316L. However, even 316L can corrode in a *in vivo* environment under certain circumstances, such as a highly stressed and oxygen-depleted region. Therefore, stainless steels are suitable for temporary implant devices such as fracture plates, screws, and hip nails [10].

Cobalt-chromium alloys are divided into castable CoCrMo alloy and CoNiCrMo which is usually wrought by hot forging. These two CoCr alloys are used extensively in implant fabrication. The superior fatigue and ultimate tensile strength of wrought CoNiCrMo alloy

makes it suitable for medical devices which require long service life without being subject to fracture or stress fatigue. Therefore, wrought CoNiCrMo is used for heavily loaded joints such as the knee and hip and for stems of prostheses. The castable CoCrMo alloys have been used in dentistry for decades and recently applied to making artificial joints. However, the toxicity tests of metal contents *in vitro* indicate that Co and Ni at 50% concentration appear to be highly toxic, whereas, Cr was found to be less toxic than Ni and Co [10].

Biocompatibility of the metallic material with the body tissues, so as not to harm them or cause an inflammatory reaction, has already been emphasized as an essential requirement for medical applications. Tantalum, niobium, titanium, platinum, and zirconium have been identified as the most biocompatible metals [16].

Tantalum, one of the most biocompatible metals, has poor mechanical properties. Due to this and its high density (see Table 2) it is restricted to a few applications, such as wire sutures in plastic surgery, neurosurgery and as a radioisotope for bladder tumours [10].

Unalloyed Niobium has good corrosion resistance and excellent biocompatibility [17]. Pure niobium is reported to possess better electrochemical properties and biocompatibility than titanium and its alloys. Therefore, it is to be considered in developing new implant material [16]. Its lower mechanical strength than Ti and its alloys is improved by cold-working. This process could raise its competitiveness as a biomaterial.

Niobium-based alloys, such as Nb-Ti, Nb-Sn are used in the superconducting magnets in Magnetic Resonance Imaging –MRI [16].

Ti-Nb alloys, i.e. Ti-13Nb-13Zr exhibit excellent wear and corrosion resistance with superior biocompatibility.

A new family of shape memory alloys containing Ti, Nb, and Sn is under development for bio-applications. So far, a Ni-free alloy: Ti-Nb-Sn was investigated. It was found that it possesses excellent deformability at ambient temperature in comparison with TiNi alloys [16].

The density of a metal incorporated in the body is an important factor too. The lower weight of the implant becomes especially important in older individuals and to people with frail builds, such as children [15]. The specific gravities of metallic biomaterials indicate the advantage of Ti and its alloys.

Table 2: Specific gravities of the selected metallic biomaterials [10], [17].

Alloys	Density [g/cm ³]
Ti and its alloys	4.5
NiTi	6.7
316L SS	7.9
CoCrMo	8.3
Nb	8.6
CoNiCrMo	9.2
Ta	16.6

Ti and its alloys represent the lightest metallic materials for medical devices. The most biocompatible metals apart from Ti (Nb and Ta) have much higher densities. Moreover, comparing the specific strength (strength per density) of metallic biomaterials, the titanium alloys exceed any other implant material, as shown in Figure 1.

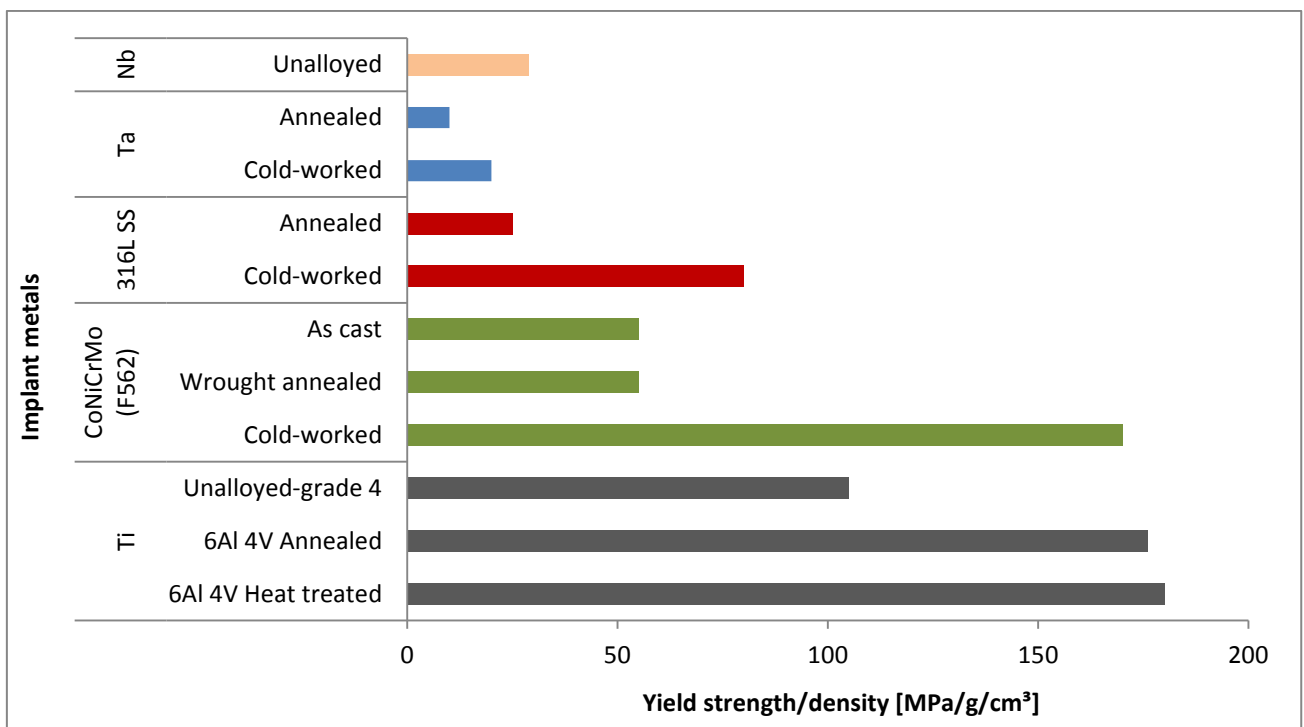


Figure 1: Yield strength-to-density ratios of selected implant materials. Amended from [9], [17].

Titanium's properties enable it to replace medical devices made of 316L stainless steel or CoCrMo alloys [15]. Due to its combination of strength, corrosion resistance, light weight, and biocompatibility; it has become the metal of choice for prostheses, internal fixation, inner body devices and instrumentation [15], [18].

The properties of Titanium as a metallic biomaterial, together with the applications for medical devices, will be discussed in the following sections.

2.1.3 Ti as a biomaterial

Titanium and its alloys continue to receive much attention in the medical field because of the balance between lightness (4.5g/cm^3), excellent mechanical properties and corrosion resistance. Most importantly, titanium meets the requirements necessary to define the metal as a biomaterial. These criteria are:

a) Corrosion resistance:

Titanium is resistant to general corrosion, pitting attack, and crevice corrosion, which occur in several other alloys as a consequence of aggressive organic fluids [15]. It withstands the changing pH of human body fluids because of its inert oxide layer [9]. The corrosion behaviour of Ti and its alloys was analysed and compared with other metallic biomaterials. It was found that:

- Commercially pure titanium (cp-Ti) and Ti-6Al-4V have the highest breakdown potential of 2.4 V and 2.0 V respectively. In comparison, stainless steel has 0.2 - 0.3 V, CoCr alloys (cast) 0.42 V, as measured in Hank's solution.
- cp-Ti and Ti-6Al-4V repassivation times of the passive oxide layer, measured in 0.9% NaCl, pH=7.4 are over 1500 times faster (potential = -0.5V) in comparison with stainless steel 316L, and over 100 times faster compared to CoCr cast.
- The oxide growth on cp-Ti and its alloys, measured with the same parameters in the same medium as the example above, is also 15000 faster compared to other materials [9].

b) Biocompatibility:

Titanium is a non-magnetic metal, therefore, it does not interfere with the magnetic field of medical equipment or implanted electronic devices. Furthermore, the protective surface layer of titanium dioxide exhibits semi-conductive properties, which makes it an insulator and prevents the flow of ions. It has a dielectric constant similar

to that of water. Therefore, Ti implants are not recognized *in vivo* as a foreign body [9].

c) Bioadhesion (osseointegration):

Osseointegration is defined as “direct contact without intervening soft tissue between viable remodelled bone and an implant” [10]. The Ti implant surface consists of a thin oxide layer which is in contact with water molecules in biofluids, dissolved ions, and biomolecules (proteins with surrounding water shell) as shown in Figure 2 A [10].

In a pH region from 2.9 – 12.7 the titanium oxide is hydroxylated, which means that, at the surface, OH⁻ groups are able to react chemically with biomolecules. In the oxide layer, mineral ions from the biosystem, e.g. calcium and phosphorous, are deposited. Then, the larger structures, like cells reach the surface to bridge the gap between the collagen fibrils and the oxide surface layer with maximum mechanical stability, see Figure 2 B [9], [19].

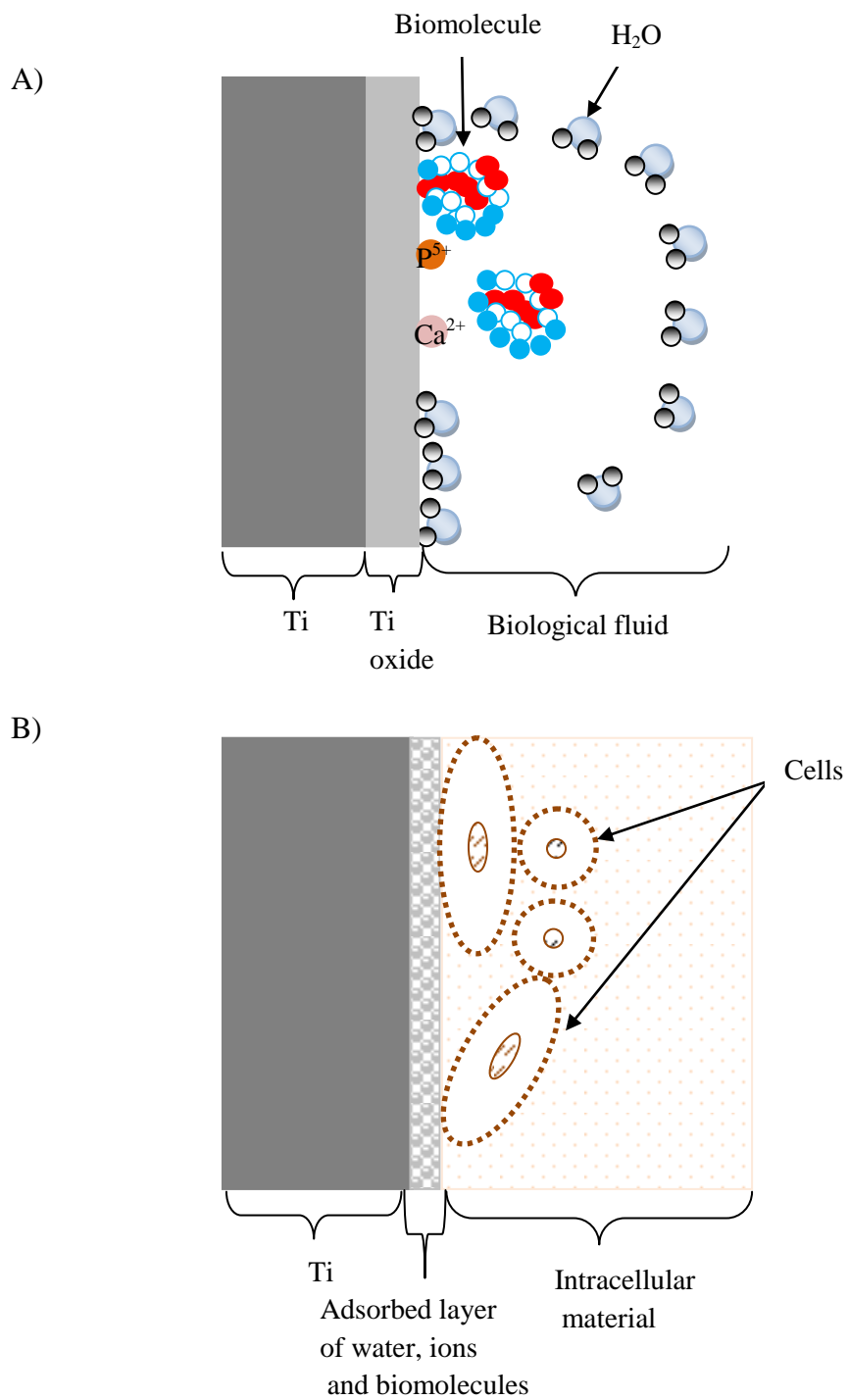


Figure 2: Schematic illustration of the molecular processes at the interface between Ti and the surrounding biological environments; A) Processes at Ti oxide and biological fluid interface; B) An interaction of cells with the layer of water, ions and biomolecules [19], [20].

d) Mechanical properties:

The mechanical properties of titanium and its alloys surpass the requirements for an implant material. It is recommended that surgical implants have strength levels greater than that of bone and an elastic modulus close to that of bone [15].

- Titanium shows the best Young's Modulus (E) in the group of biomaterials (titanium alloys: 105GPa, cp-Ti: 100GPa). The lower the value of E, the better transmission of the load on the implant with stimulation of bone formation [8].
- Yield strength (YS) of Ti alloys is 900MPa. For cp-Ti it is 3 times lower. In comparison, a YS of 316L = 450MPa, CoCr cast = 500MPa. High YS is critical in applications, where the load is increased such as in hip prostheses [15].

e) Processability:

All current processing procedures are applicable to Ti and its alloys [9]. These are discussed in the section 1.2.

However, Ti and its alloys belong to the group of metals that are difficult to etch. This raises issues with producing micro-parts and micro-features in Ti components by chemical etching without the use of hazardous chemicals in a production scale. The following chapters are dedicated to the presentation of available methods for Ti microfabrication and introduce a novel "triple sandwich structure" for Ti etching, which is the subject of this thesis.

f) Availability:

Titanium is one of the most abundant minerals in the earth's crust [15]. The Ti ores are spread throughout the world. The reserves and locations in the world make Ti a geopolitically secure metal. From the economic aspect, the volume price for titanium is lower than that of CoCr-alloys, niobium, and tantalum [9].

The natural selection of Ti and its alloys for medical devices is determined by a combination of most favourable properties including: corrosion resistance, biocompatibility, high Yield Strength, low Young's Modulus and density, and finally the capacity for joining with bone and other tissue – osseointegration.

2.1.4 Ti in biomedical applications

The utilisation of the unique properties of Ti and its alloys results in high popularity in biomedical applications. More than 1000 tonnes of titanium medical devices are implanted in patients worldwide every year [21].

Four grades of cp titanium, $\alpha + \beta$ alloys, metastable β , and NiTi shape memory alloys have found a wide range of applications in the medical sector.

- a) Cp Ti Grades 1 – 4 are fully α phases of titanium and oxygen. They exhibit superior corrosion resistant behaviour. In addition to this, cp Ti grades are characterized by higher resistance to plastic deformation and reduced ductility [9].
- b) $\alpha + \beta$ alloys are used where high strength-to-weight ratios are required. The most popular alloy among this class is Ti-6Al-4V. However, new vanadium-free titanium alloys have been developed due to the concerns about the toxicity of this element [22].
- c) Metastable β alloy can be aged to a high strength level of more than 1400 MPa. What is more, they have low Young's modulus, which is closer to that of human bone i.e. 10-30 GPa. Beta Ti alloys exhibit better notch properties and toughness than $\alpha + \beta$ alloys. By design, they contain non-toxic and non-allergic alloying elements [23].
- d) NiTi shape memory alloys (SMAs) exhibit the unique properties of shape-memory effect and superelasticity, alongside excellent corrosion resistance. SMAs are capable of transforming from an austenite crystal structure to martensite and back again at low temperatures (-200°C to 110°C). The shape of the metal can be different in the two phases. The shape memory effect does not affect the mechanical properties of the SMA [24].

In the case of superelasticity, thermal transformation has been replaced by a mechanical one. The superelasticity occurs when an applied stress deforms martensite above its transformation temperature. This phase is stable as long as the stress is present. As the shape memory alloy has been formed above its normal temperature, the martensite reverts to undeformed austenite shape when the stress is removed. No shape change is noticed after stress release.

All available Ti alloys with their current areas of applications have been presented in Figure 3.

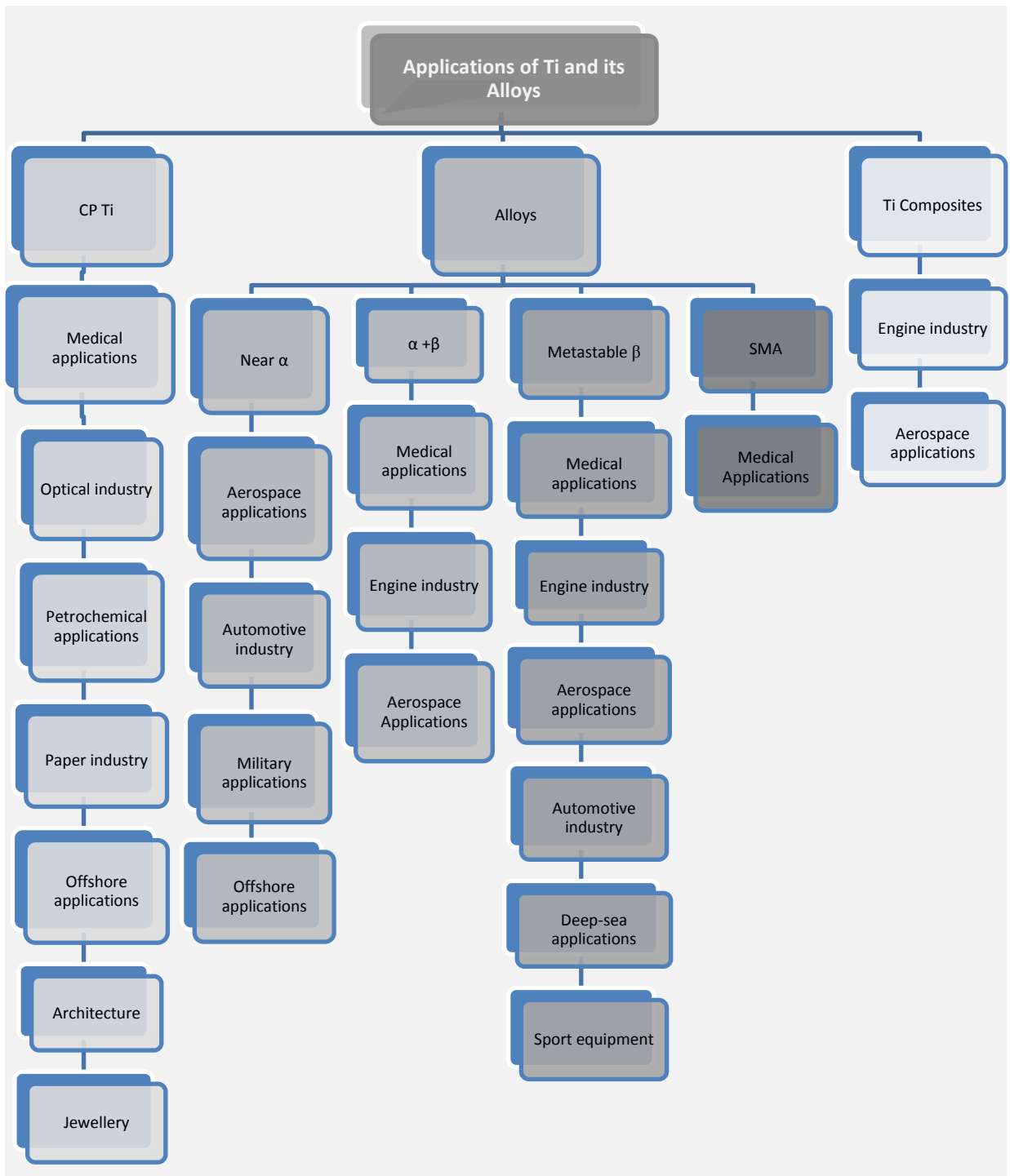


Figure 3: Applications of Ti and its alloys, author's analysis based on [9].

The range of available Ti alloys enables biomedical engineers to select materials to design medical devices tailored to the needs of the application. 'Fit and forget' is a standard requirement for the equipment in applications, where once installed it cannot be readily maintained or replaced [21].

2.1.5 Ti biomedical devices in humans

There is a diversity of Ti medical devices used *in vivo*. They can be divided into:

- Craniofacial and maxillofacial treatments

Under conditions where part of a face or a skull has to be replaced in order to restore the ability to speak or eat, as well as for cosmetic appearance, artificial parts made of titanium are applied [21]. Plates and screws are used for the fixation and stabilization of osteotomized or fractured bone segments [25], whereas, custom-made parts are applied in maxillofacial surgeries.

Cp Ti (phase α) and Ti6Al4V (phase $\alpha + \beta$) are incorporated for craniofacial and maxillofacial treatments.

- Dental treatments

Ti-based materials are used in orthodontics, prosthetics, and implantology [9]. Ti dental implants had a major input in changing restorative dental practice. A Ti 'root' is introduced into the jaw bone and after some time, allowing for osseointegration, the tooth is built onto the implant [21]. Cp Ti grades from 1 to 4 (phase α), TiMo11Zr6Sn4, Ti-30Ta (phase β), Ti6Al64V, and NiTi SMA alloys are utilized in dentistry. Ti and its alloys have a dominant position in this area of medicine because of their biocompatibility, mechanical and aesthetic properties as well as cost efficiency [9].

- Bone and joint replacement

The preferred Ti alloys for orthopaedic applications are metastable β alloys. Nowadays, the most common biomedical application of Ti is hip replacement [23]. Hip joints usually have a metallic femoral stem and head which is located in a polyethylene socket, secured in position with polymethyl methacrylate bone cement [21]. Other joint replacements include: knee – nearly half of all replacements are made of Ti, and also shoulder and elbow. Furthermore, internal and external bone-fracture fixation provides a major application for Ti as spinal fusion devices, pins, bone-plates, screws, intramedullary nail, and external fixators [21].

The following Ti (phase β) alloys have been introduced for described applications: Ti-12Mo-6Zr-2Fe, Ti-13Nb-13Zr, Ti-15Mo, TIMETAL[®] 21SRx, and Tiadyne 1610 [22], [23].

- External prostheses

Ti is used for both temporary and long term external fixations and devices as well as for orthotic callipers and artificial limbs [21].

- Cardiovascular devices

Ti is found in applications for pacemaker cases and defibrillators. It is also used as a carrier structure for heart valve replacement and for intra-vascular stents [21]. NiTi SMA and Ti-15Mo alloys have been employed in fabrication of cardiovascular devices.

- Surgical instruments

Ti is a popular solution for surgical instrumentation because of its lightness. Where required, instruments are additionally anodised to achieve a non-reflecting surface, important in microsurgical operations such as in eye surgery. Ti is a non-magnetic metal, therefore, it does not interfere with implanted electronic devices. Ti instruments withstand repeated sterilisation without a change in their surface quality, corrosion resistance or strength [21].

The localisation of Ti medical devices in humans has been illustrated in Figure 4.

Ti biomedical devices in humans

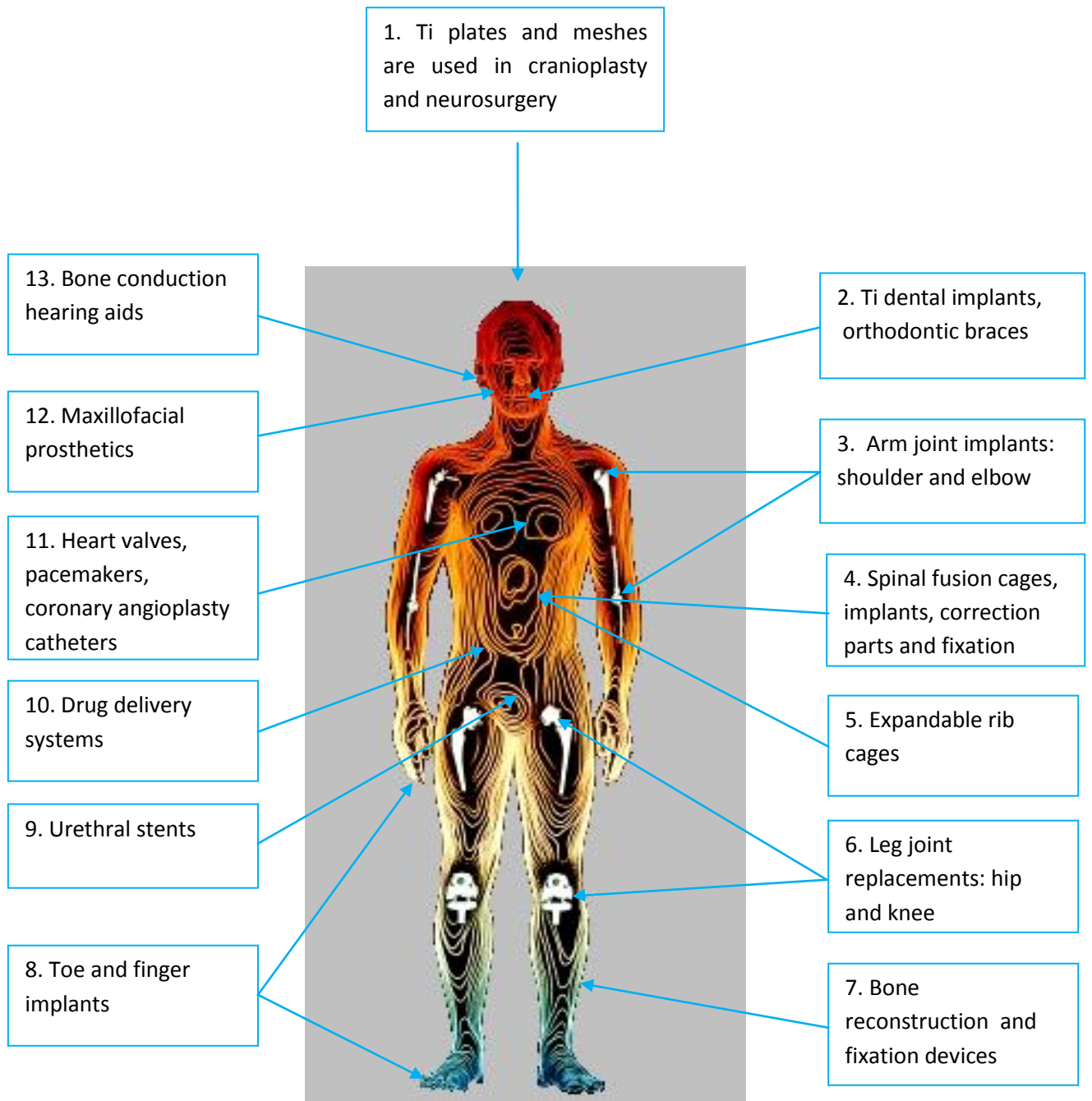


Figure 4: Titanium biomedical devices in human body [26], [27].

Summary

Metallic biomaterials have proven over ceramics, polymers and composites their preferential mechanical properties, i.e. Yield strength and excellent electrical and thermal conductivity.

Amongst the class of metals, Ti and its alloys have established a strong position as the **biomaterial of choice**. They are characterized by high corrosion resistance, due to a Ti oxide layer which is responsible for the inertness in a *in vivo* environment. In addition to this, Ti exhibits high Yield strength, creep resistance and a low Young's modulus.

2.2 Ti microfabrication techniques

The corrosion resistance of Ti and its alloys is due to a surface oxide layer. It passivates the metal and forms a tenacious protective layer [28]. Because of this, Ti and its alloys belong to the group of difficult to etch metals.

The aim of this section is to compare microfabrication techniques which are currently being used to produce micro-features in Ti. The emphasis will be placed on fabrication methods which enable industrial production on large-scale.

2.2.1 Dry etching techniques

Dry etching includes the methods by which a solid surface is fabricated in the gas or vapour phase. Three types of reactions that take place depending on the process can be distinguished: physical, when ion bombardment is responsible for etching; chemical – a chemical reaction on the surface of a specimen, and finally, a combined physical and chemical mechanism of material removal [29].

Reactive Ion Etching (RIE) belongs to the physical/chemical methods, where impacting ions, electrons, or photons initiate chemical reactions in a diode-type reactor.

- **RIE**

A dry etching technique has been designed for thin film etching [30]. It can remove material with very high precision. RIE is used to etch features larger than hundreds of microns on the titanium substrate. There are several disadvantages of this process, such as: very low etch rate, expensive equipment, and the possibility of redeposition of material on the specimen substrate.

- **RIE Lag** where etching of small features lags behind that of large structures to enable fabrication of complex 3D surface profiles by using a single mask [31]. This method employs a mask design with different-sized openings closely spaced apart in order to differentiate etch rate through the mask and applies a secondary etch step to smooth the surface. The utility of this approach was shown in the fabrication of sloping electrodes in a bulk Ti substrate [32].

TiO₂ acting as an etch mask was deposited on the polished Ti substrate during DC reactive sputtering. Ti oxide imaged by a standard lithographic technique is then etched using a CHF₃-

based dry etching. In order to etch the underlying Ti substrate, the developed **Titanium Inductively Coupled Plasma (ICP) Deep Etch (TIDE)** process is applied. It incorporates a high density Cl/Ar-based plasma which enables highly anisotropic etching of Ti with etch rates of up to **2 $\mu\text{m}/\text{min}$** . After etching the bulk Ti with the TIDE process, the superstructure above the etched floor is removed using hydrofluoric acid (HF) wet etching, which results in a surface topography defined by the dry etch process. However, the limitation of this technique appears as the sharp, peak like protrusions are left beneath the original structure sidewalls and causes an increase of the surface roughness. Further HF etching could smooth the surface but in the meantime damages structural integrity of the thin interconnected parts.

2.2.2 Physical techniques

- **Laser micromachining**

Laser micromachining is based on the interaction of laser light with the material [30]. Machining takes place when pulsed light energy, in the form of a coherent beam, focuses on a small spot and removes material by vaporization and ablation. During this thermal process, the volume expansion of the vaporized material generates pressure to blow the molten material out to create a cavity [33].

Metal melting caused by laser processing, affects the chemical properties. What is more, residues on the surface create stress which changes the mechanical properties of the material. This method is being utilised to manufacture Nitinol stents typically using nanosecond diode pumped solid state Nd-YAG lasers [34]. **Nanosecond pulses** (5 ns) at 532-nm wavelength of the **Nd-YAG laser** were used to micromachine Ti rods, grade 2 [35]. The topographical and chemical effect was studied by varying the incident fluence (1-100 J/cm^2) and focal spot size (10, 20, 50, and 100 μm) of the beam.

Material in the case of laser micromachining is mainly removed by a melt ejection.

The produced pattern with pulsed Nd-YAG laser had a crater-like profile, with a formed ridge localized around a central intrusion and an ablated material present in a heat-affected zone (HAZ).

It was reported that by increasing the irradiated laser fluence produces craters of larger diameter. For instance, the fluence at 3 J/cm^2 and focal spot size (FSS) of 10 μm produced crater of 17 μm in diameter and 0.4 μm in depth, while the fluence at 495 J/cm^2 and FSS of 10

μm resulted in a wider crater of **60 μm in diameter** and approx. **2 μm in depth** but only in the centre of the pattern.

A correlation was noticed between crater depth and fluence as well as the crater diameter.

The shape of the micromachined pattern became more irregular with the increase of the fluence.

There was no influence of FSS on the crater depth.

The chemical composition of the laser ablated patterns was studied in order to investigate oxide and nitride formation. X-ray photoelectron spectroscopy (XPS) revealed that the oxide layer outside the crater in the HAZ grows logarithmically with increasing fluence, whereas, thickness of the oxide inside the crater was constant with increasing fluence. In addition to this, titanium nitride was formed in the crater.

Laser surface texturing is used to modify the surface of the material.

The femtosecond laser was employed to create a regular pattern and bioactive layer on the surface of cp Ti [36]. A Ti: sapphire laser of 800 nm wavelength with pulses of 50 fs in duration was used to fabricate grooves. Two pulse laser energies of 10 μJ and 100 μJ fabricated regular grooves with a width of approx. 20 μm . The comparison of the micromachined specimens showed that

the lower energy of the laser produces grooves with small ripples on both the ridges and valleys of the pattern, whereas, the higher energy laser results in smaller ripples being formed. Increased surface roughness, demonstrated by the presence of grooves, small ripples, and holes was found to be favourable for the entrance of biomacromolecules.

Using this method it was possible to micromachine a three order roughness pattern, consisting of $\sim 20 \mu\text{m}$ grooves, $\sim 0.8 \mu\text{m}$ ripples and $\sim 500 \text{ nm}$ TiO particles periodically aligned into rows, when a laser energy of 10 μJ was applied.

2.2.3 Mechanical techniques

- **Mechanical micro-milling**

Micro-milling can be defined as the process that incorporates endmills varying in diameter from 100 – 500 μm , with edge radii in the range from 1 – 10 μm [37].

Titanium belongs to the category of hard-to-machine metals. Micro-machining of Ti is challenging because of a few reasons, which are: high tool wear associated with the reactivity of Ti with tool materials and its low thermal conductivity. Moreover, a development of suitable tool coatings is still in progress for Ti and its alloys. The tool failure is mostly because of its chipping or breakage. In addition, heat build-up restricts the increase of cutting speed [38]. Therefore, any modification to the micro-milling process which can decrease the cutting forces has the potential of improving this process.

- **Laser –assisted micro-milling (LAMM)** applies a focused laser beam ahead of the material cutting location [39]. The laser heating thermally degrades the mechanical properties of a workpiece which allows reduced cutting forces and makes the material easier to micro-mill.

By applying LAMM it is possible to overcome low shear plane temperatures when a small tool diameter is used.

In the experiment described by [39], a spindle with a max. rotation speed of 90 k rpm was used, with 100 – 300 μm diameter two-flute tungsten carbide endmills of an average edge radius of 1 μm . The micro-milling was assisted with a CO_2 laser pointed at 45° to the cutting plane and FSS from 150 to 300 μm . An inert gas (argon) was used in order to prevent the work material, Ti6Al4V, from combustion in an atmospheric environment.

The performed experiment on the bulk workpiece, with a 100 μm diameter tool at a spindle speed of 60 k rpm, and a cutting speed of 18.85 m min^{-1} showed that the surface **roughness** of the **Ti6Al4V** workpiece **increased by 36 %** compared to conventional micro-milling.

LAMM was found to almost completely **eliminate the top edge burrs** at the material-removal temperature (T_{mr}) of 420°C . This phenomenon was explained by a direct melting by laser of the burrs, which was also responsible for **eliminating chips** of the milled material blown away from the workpiece.

The examination of the used tool showed no significant difference between the amounts of wear on LAMM and conventional tools for Ti6Al4V fins. It was reported that the larger diameter of the tools (300 μm) were protected from total failure during machining. LAMM process was found to reduce the large edge burrs formed during conventional side cutting of Ti6Al4V.

The numerical study of thermal and mechanical effect of LAMM of difficult-to-machine alloys, including Ti6Al4V was conducted [40]. It revealed a feasibility of this process to eliminate or reduce built-up edge (BUE) formation with proper heating of the workpiece ahead of the cutting tool.

2.2.4 Chemical techniques

- **Photochemical machining (PCM)**

This is a process that combines photolithography, through the use of a patterned resist or stencil placed on the substrate, with chemical etching to produce selective metal removal [41]. It is a controlled-corrosion machining technique which is used to fabricate highly complex shapes in thin sheet metallic material (typically of thickness less than 3 mm). PCM allows economical processing **in bulk quantities on an industrial scale**.

However, highly corrosion resistant metals and alloys require more reactive etchants, very often aggressive and hazardous to both the operator and the environment. Titanium, with its passive oxide (TiO₂) on the surface, has an exceptional corrosion resistance. This property makes titanium very difficult to etch in the conventional PCM process. Only a few chemicals, very aggressive and hazardous, are capable of attacking Ti and its alloys.

The following Ti etchants have been reported [28]:

- i. **Hydrofluoric-based etchants: HF**, the reaction with titanium has been presented below (1).



As a consequence of formed hydrogen, the ductility and fatigue strength of the metal are reduced (otherwise known as “hydrogen embrittlement”).

The hydrogen can be absorbed with the addition of HNO₃ (concentration from 20% to 50%) in a 2% HF solution, ammonium formate and citric acid. Additions of nitric acid (HNO₃) give a more controlled reaction rate.

- ii. **Ammonium bifluoride (NH₄HF₂)** improves Ra.

- iii. **Aqua regia fluoride:** 32⁰Bé Hydrochloric acid + 40⁰Bé HNO₃ + 70%HF + anhydrous FeCl₃ (to adjust specific gravity to 1.26), 60 - 70⁰ C.

The following etchants were reported for the **NiTi SMA** [15]:

- i. **HF/HNO₃** – the presence of nitric acid prevents hydrogen embrittlement. The addition of HNO₃ in the proportion: HF:HNO₃: H₂O 1:4:5 increases the etch rate and produces a good bright finish.
- ii. **Diluted HF.**

Hydrofluoric acid process implications

Aggressive Hydrofluoric-based etchants dictate the use of more durable and stronger photoresists. The disintegration of mask from a substrate has been reported as a common difficulty.

The research on Ti-alloy wing fabrication [42], applied HF-based solution to etch Ti6Al4V. The concentration used for this purpose, **5% HF/ 2% HNO₃**, was found to damage the dry film resist (DFR-4713), which would peel off before etching was finished. The etching rate under such conditions were reported to be **2.5 µm/min**.

In the experiments conducted by [43] two cp Ti grades 1 and 2 were etched in HF: HNO₃: H₂O (1:1:30) for 20 minutes at ambient temperature. The results showed that the surface roughness of Ti grade 2 specimen was several orders larger than that of grade 1. Moreover, the mask used in order to pattern the substrate peeled off. Therefore, further tests were conducted on Ti grade 1 and the Parylene was replaced with a sputtered nickel layer in order to pattern the Ti substrate. Six fluoride based etchants were tested, however only **40% HF/ 70% HNO₃/ H₂O (1:1:30)** revealed constant etching rate of **2.26 µm/min**. The octagonal shape of mask produced sharp microneedles of the height between 20 – 100 µm in 500 µm thick Ti substrate.

The use of more durable resists to protect the areas of the substrate that do not need to be etched, and ultimately, stronger strippers to remove the resist from the substrate afterwards, increases the total environmental impact of the titanium PCM process.

Uneven fabrication of parts in Ti or NiTi SMA, are the additional implications of HF-based etching.

Two Cranfield University's researchers investigated this problem. In the work carried out by [44] nine different etchants based on the mixture of 40% HF, 70% HNO₃, and H₂O were tested in order to produce a stent. NiTi specimens, coated with negative-working photoresist SU-85, were imaged and etched. The results demonstrated non-uniform etching of the stent with rough surface finish due to the limited chemical resistance of the resist stencil.

In order to improve etching uniformity and increase the dissolution rate, a Hull cell filled with HF-based electrolyte was employed [24].

The electrolyte consisting of 4% HF, 20% HNO₃, and H₂O was used to etch three different materials: Ti, NiTi SMA and Ni. The results from the experiments conducted in the Hull cell indicated variations in the etching rates, where Ti showed the highest differences between top, centre and bottom areas of the specimens.

Hydrofluoric acid impact on humans and environment

All etchants for titanium and its alloys contain hydrofluoric acid, which is classified, according to the UK Regulations and UE Directive 67/548/EEC [20] as a **very toxic** and **corrosive chemical**.

Contact with HF is severe in consequences for both human and environment.

- Human health

HF is found to be fatal in contact with skin, when swallowed or inhaled and to cause severe skin burns and eye damage [45]. Serious metabolic derangements are due to the high electronegativity of the fluoride anion which holds on to the hydrogen cation.

In case of systemic complications, it can result in liquefactive necrosis of soft tissue, bone erosion, hypocalcemia, hyperkalemia, hypomagnesemia, and metabolic acidosis. The hypocalcemia and hyperkalemia can lead to cardiac arrest and death due to refractory ventricular fibrillation and torsades de pointes. The treatment, of the person affected, should be immediate and include clinical monitoring due to an insidious nature of the poison and the potential for lethal outcome from apparently minor injury [46].

- Environment

HF waste should be disposed in accordance with local regulations, whereas, empty containers should be taken for local recycling, recovery or waste disposal.

A concentration of hydrogen fluoride of 660 mg/l was found to be lethal to 50% of freshwater fish in 48 hours [45].

HF-based etchants are dangerous for human health and the environment. In addition to this, in the production environment they can damage parts of the conveyORIZED etching machines [24].

2.2.5 Electrochemical microfabrication

Introduction to electrochemical processes

The relationship between charge (i.e. quantity of electricity passed in a given time) and the amount of a substance oxidised or reduced at an electrode has been embodied in Faraday's laws, which state:

- A. The mass of electrolysis product is proportional to the quantity of electricity passed (i.e. the mass of metal liberated at the anode is proportional to current x time).
- B. For a given quantity of electricity passed, the masses of the product liberated are proportional to the chemical equivalent of that material.

These statements can be express in the following equation:

$$m = \frac{M \cdot I \cdot t}{n \cdot F} \quad (1)$$

Where:

m= mass of metal liberated (g),

M= molecular weight of metal (g/mol),

I= current (A),

t= time (s),

n= valence number of dissolved metal

F= Faraday's constant (96500 C/mol)

As M and n are a constant for a given material and t is set for a process, the only variable is the current. The current is a function of the corrosion potential that develops between the

anode and the cathode. Potentials will vary for different metal/electrolyte combinations and operational parameters [28].

Faraday's laws give a theoretical value of the change in mass of a sample for a specified amount of electricity passed [47]. These laws are not affected by alteration of temperature, solution concentration or electrode size.

There are numerous causes for a deviation from the theoretical value of the change in the sample mass, such as [47]:

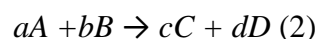
- Some of the charge is being consumed in parasitic processes, i.e. hydrogen evolution,
- All of the reactants are not consumed,
- The postulated electrochemical process is not the actual process occurring, or
- Some of the material from the sample falls off so that a larger mass reduction is recorded than actually occurred in the electrolytic reaction.

It should be noted that the deviations can provide a measure of the efficiency of a process.

A fundamental expression for characterizing redox systems under equilibrium conditions is the Nernst equation. It allows the calculation of relative activities of the species in a redox reaction as a function of the measured electrode potential (E) and the standard reduction potential (E^0) for the half reaction.

The Nernst equation relates concentration changes to change in reversible potential.

For the galvanic cell, where the following reaction occurs [48]:



Where: a and b are moles of substances A and B respectively, which react to give c and d moles of C and D respectively. The Nernst equation for the cell has the following form:

$$E = \frac{RT}{zF} \ln K - \frac{RT}{zF} \frac{C^c D^d}{A^a B^b} \quad (3)$$

Where: E – e.m.f. of the cell (V), R = gas constant (8.314 (J)/(K mol), T = temperature in K, zF = the quantity of electricity flowing when a moles of A (or b moles of B etc.) react (F = 96500 C/mol), and K denotes the equilibrium constant for the cell reaction.

The equation above can be simplified to:

$$E = E^\circ - \frac{2.303 RT}{zF} \lg \frac{C^c D^d}{A^a B^b} \quad (4)$$

Where:

$$E^\circ = \frac{RT}{nF} \ln K \quad (5)$$

E° is known as the standard e.m.f. of the cell. It is the value of the e.m.f. when all the concentrations (activities) are equal to unity.

The equation can be presented in the following form for a temperature of 25°C by substituting the appropriate values of R, F, and T (298 K):

$$E = E^\circ - \frac{0.059}{z} \lg \frac{C^c D^d}{A^a B^b} \quad (6)$$

The electrochemical processes, that are governed by Faraday's laws and have been employed in the sandwich structure building and its microfabrication, were: electroplating and electrolytic etching.

Electroplating is restricted to electrically conductive materials. The process takes place when an electrical potential is applied to a conductive cathode (-ve) and an anode (+ve), submerged in an electrolyte. As a result, a chemical redox process takes place. In this instance an electrically conducting coating is require in order to precede the deposition.

Electroplating is performed by passing a direct electric current through the solution between one or more anodes, connected to the positive terminal of the dc power source, and one or more cathodes (the part to be plated), connected to the negative terminal.

In the external circuit, negatively charged electrons flow from anode to cathode via the power source. In the solution, all the cations migrate under the influence of the electric field towards the cathodes and all the anions towards the anions. Different types of ion move at different rates, depending mainly on the size and the magnitude of their charge. The sum of their movements in both directions produces a total flow of charge (current) equal to the external

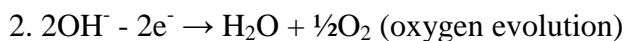
current [49]. The detailed reactions that occur of the electrodes will be discussed in the Chapter dedicated to Cu electroplating (6.3).

In order to coat a non-conductor or a conductor with a film of a metal, without the benefit of an external source of electric current, **electroless plating** can be employed. It is characterised by a selective reduction of metal ions, with continued deposition of metal on the substrate through the catalytic action of the deposit itself [56] [50]. The chemical deposition of a metal occurs in an aqueous solution of a salt of said metal and involves an electrochemical mechanism, both oxidation and reduction [50].

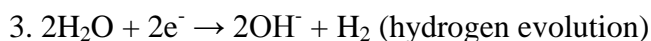
Electrochemical microfabrication (electrolytic etching) represents electrolytic processes, where metal is removed away atom by atom, without the use of mechanical and thermal energy. The mechanism relies on the use of electrical energy, combined with a chemical to produce a reaction of metal dissolution [44]. It is carried out in an electrolytic cell by applying a positive (anodic) potential to the workpiece and a negative (cathodic) potential, whereby, a current is passed through a conductive electrolyte between the positive and the negative electrodes. Electrochemical microfabrication involves the cathodic and anodic partial reactions following the electrochemical laws [51].

The following reactions take place at the electrodes in the electrolytic cell [28]:

At the anode (workpiece) (+ve):



At the cathode (tool) (-ve):



Where: M is the metal under dissolution

In order to achieve uniform machining, a uniform current distribution is required. To obtain this effect the following factors should be eliminated: electric field disruptions (such as sharp

edges, high points), any build up of waste product from the inter-electrode gap, heating between the electrodes. The current distribution can be affected also by: the conductance of the electrolyte, depending on temperature, pH, amount and type of dissolved metal ions in the solution, and volume of hydrogen produced at the cathode.

Electrochemical microfabrication is capable of machining high strength and heat resistant alloys and the metal dissolution is independent of the thermal or mechanical properties of the material [28]. In addition to this, the nature of the material removal does not introduce surface property changes [52].

The electrochemical techniques which enable the fabrication of titanium and its alloys have been described in this subchapter. They have been divided into two categories. The first does not require the application of the lithography process and the second which use a mask to protect and pattern the substrate.

A) Maskless

- **Electric discharge machining (EDM)**

This is a non-contact method of machining any conductive material regardless of its hardness [53]. Therefore, it is very effective in producing small holes, blind holes, deep holes and irregular holes.

The mechanism of EDM relies on feeding the shaped tool (cathode) towards the workpiece (anode) under high voltage [54]. Both anode and a cathode are submerged in a dielectric i.e. hydrocarbon oil. Material from both sides undergoes dissolution and the debris is removed by a dielectric flushed at high flow rates.

The quality of surface finish obtained in EDM depends on the material being machined, the type of the electrolyte, current density applied and the dielectric flow rate [44].

EDM becomes unstable when applied to machine Ti. Moreover, the debris from the inter electrode gap (IEG) cannot be removed easily. It is due to Ti's low heat conduction efficiency which causes difficulties in machining small and deep holes with this method.

The researchers [55] found that introducing ultrasonic vibration into micro-hole EDM can improve the dielectric flow dynamics and avoid the sedimentation of the erosion-products. The machining under an open voltage of 100 V in Ti6Al4V with assistance of ultrasonic agitation of 20 kHz showed an increase in the machining efficiency and an improvement in

the shape of the fabricated hole. It was possible to machine a 3 mm deep hole by using ultrasonic EDM with “single-notch” electrode, whereas normal EDM was capable to achieve 1.6 mm deep hole after 10 minutes of machining. It was assumed that an addition of a rotating single-notch microelectrode to EDM can result in a bigger space for by-products to flow away, the improvement of the machining efficiency and a minimisation of the machining taper.

- **Jet electrochemical micromachining (Jet-EMM)**

Jet-EMM is based on electrochemical reactions with an addition of a pressurized charge electrolyte jet. This process can utilize micro- and macro-holes as well as grooves [56].

In the research of [52] Jet-EMM process was employed to produce micro-holes on Ti specimens. An Ti6Al4V alloy cylinder, 12 mm in diameter and 50 mm in length was connected as an anode and impinged on with a stream of 5 mol/l NaBr aqueous solution through the metal nozzle of 300 μm in diameter, acting as a cathode. The machining was performed under a voltage of 150 to 200 V and average current of 45 mA.

The results showed that Jet-EMM can machine Ti at high speed. The micro-holes of approx. **1000 μm in depth** and **800 μm in diameter** were fabricated in **2 min**. The micro-holes produced by Jet-EMM indicated that this technique can be compared to drilling rather than isotropic etching.

Due to the shape of the specimen used in the experiment, it was concluded that this technique is able to machine surfaces of any type of curvature. In addition to this, it generated micro-holes with high aspect ratios without implementation of a photolithography stage. However, the high operating voltage (up to 200 V) makes the process less economical. Moreover, the higher depth-machining rate can be achieved at higher voltages, whereas it was found that 250 V and jet pressure greater than 280 kPa caused sparking which affected the surface finish of the titanium.

In the work on Jet-EMM, presented by [56], a number of parameters, such as: applied voltage, capillary outside diameter (from 0.20 to 0.60 mm), feed rate, electrolyte concentration and inlet electrolyte pressure were evaluated on the productivity of the quality small holes. The machining of a nickel base superalloy (containing 2.1% of Ti) resulted in a finding an optimal parameters like 340 V, capillary outside diameter 0.4 mm, feed rate 0.5 mm/min,

concentration of 17.5 % NaNO₃, and inlet electrolyte pressure of 300 kPa. However, in this case, the higher applied voltage led to better surface finish but with larger overcut and higher roundness error.

B) Through mask ECM (TMECM)

- One step patterning process

• TM Jet-EMM

Jet-EMM was applied to machine a pattern in a flat Ti surface, (achieved through a photoresist) [52]. It showed capability of producing semi-spherical holes in Ti6Al4V plate. The etched holes were approx. 500 µm in diameter and 113 µm in depth. Each hole required approx. 2 min of machining. Whereas, the depth etching rate of 12.1 µm/min. and the width etching rate 10.7 µm/min were produced.

• Electrochemical photoetching

In the electrochemical photoetching reaction cell, the conductive substrate to be etched is connected as the anode (positive electrode). A non-reactive metal is connected as the cathode (negative electrode). Both are immersed in an electrolyte and connected to a power supply, as shown in Fig. 5. For through-etching¹ two cathodes – one either side of the anode is used in order to minimize the degree of undercut² on the workpiece [41].

The electrochemical photoetching utilises the same lithography processes as in the PCM process to pattern the workpiece. But on the contrary to the PCM, the etching power is enhanced by the current flow instead of aggressive etchants. Therefore, the electrochemical photoetching enables use of milder chemicals in order to machine difficult to etch metals.

The electrochemical photoetching takes place when the direct current flows from the anode, which becomes polarised, causing the metal ions to diffuse through the electrolyte to the cathode, removing metal atom by atom [24]. Rates of machining depend on the current passed through the electrolyte, etched area, temperature, agitation, and duration of the process [57].

¹ Etching throughout the thickness of the substrate.

² Undercut – the etchant “undercuts” the photoresist. The etchant is able to attach laterally as well as in the vertical direction when etching most metals.

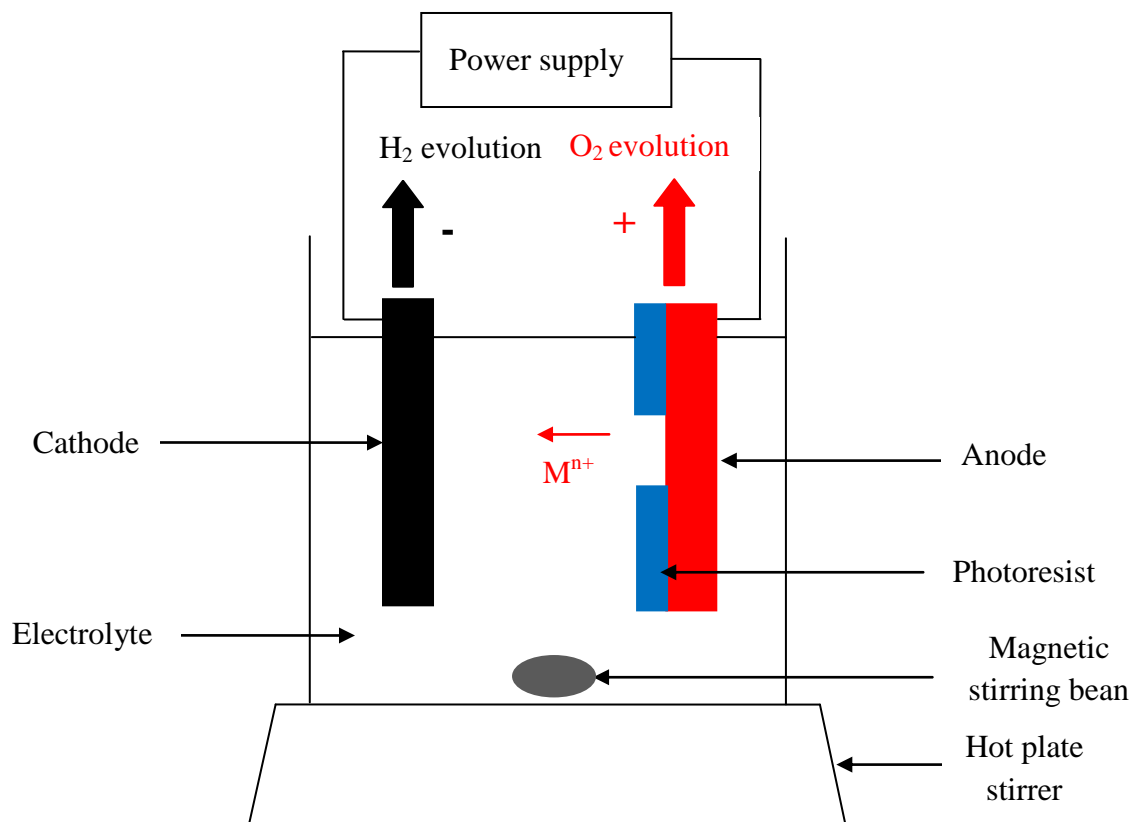


Figure 5: Layout of electrochemical photoetching reaction cell.

The type of electrolyte used in the process affects the quality of the surface finish [28], [54]. Extensive research on non-hazardous, economical and stable electrolytes was carried out at Cranfield University [28]. The outcome of this investigation highlighted best compromise chemicals³ and parameters for Ti and NiTi alloy (amongst other metals and alloys) electrolytic etching. The experiments were conducted on metal specimens (2.2 x 5 cm) masked with PVC Tape with an exposed circular area -left for etching. (The passive oxide of Ti was first removed by brief immersion in Actane 70, which is a proprietary ammonium bifluoride solution). A range of electrolytes was tested.

The results of (Continuous) Direct Current (DC) electrolytic etching performed for 15 min. at ambient temperature and with agitation (provided by a magnetic stirrer) indicated that the highest etching rates were achieved with 1M LiCl in methanol at 1.8 A/cm² and 15% NaCl at 0.7 A/cm². The surface roughness was of the order of < 0.2 µm for 1M LiCl in methanol electrolyte.

Etching conducted on **NiTi** confirmed that **1M LiCl in methanol** at 1.8 A/cm² was a best compromise for this alloy. Etch-through was achieved with the etch rate of **17.33 µm/min**. For both Ti and NiTi alloy pulsed continuous (PC)⁴ etching did not offer any advantage.

Further work on electrolytic etching of difficult-to-etch metals provided some new findings [54]. By applying **10% w/w HCl** it was possible to etch through **Ti** with an etch rate of **60.5 µm/min** during a DC cycle. PC etching resulted in decreasing the etching rate for the same current density (CD) 15.06 A/cm². For the higher applied CD = 10.13 A/cm² in 15 % NaCl, the fabricated Ti showed a significant increase of the surface roughness (10 times higher than in [28]) and the etch rate 60.5 µm/min.

One subject of extensive interest has been H₂SO₄ in methanol. Chen [44] used **5% H₂SO₄ in methanol** as the electrolyte in order to machine a NiTi stent. The combination of parameters which resulted in uniform etching within a required range of dimensional tolerances was found to be: 1:2 anode to cathode area ratio, 20 mm distance between the electrodes, CD = 1.72 A/cm² and etching at ambient temperature. The etch rate of **7.7 µm/min** was achieved.

³ “Best compromise” in terms of etch rate and surface roughness of etched area.

⁴ Where the current is periodically turned on and off. The reactions by-products are removed during the off mode.

Kantor's research [24] on developing etching technology to produce high quality components in NiTi demonstrated that a concentration of **15% H₂SO₄ in methanol** shows the **best conductivity** properties in a Hull Cell and does not generate a smut (reaction by-product).

Further adjustments of the concentrations of H₂SO₄ in methanol were applied in the work of [58], [59]. 3M and 1 mol/l respectively were used for fabrication of cp Ti and NiTi alloy at voltages 8 and 9 V. In both cases the surface finish of the etched pattern appeared regular in shape and smooth. When the experiments were repeated with the use of H₂SO₄ but in ethanol [59], the etching rate was suppressed from 16 μm/min (for H₂SO₄ in methanol) to 2.7 μm/min. Moreover, the etched finish became very rough, as also noticed by Kantor in his research [24]. Ethanol was confirmed to lower the current in electrolyte solutions in contrast to methanol. It is due to the low polarization of ethanol which results in less ionized solutes in ethanol than in methanol [59].

Ultrasonic assisted electrochemical photoetching was incorporated in order to improve the material removal rate as well as surface finish [60]. Frequencies of 40 kHz were applied to a bath filled with H₂SO₄ in methanol electrolyte at ambient temperature. It was found that the etch rate was improved by between 20 % and 50% and the surface finish was proved to be smoother.

Obtaining an uniform electric field distribution, during the process of etching through a pattern, has been the main challenge in electrochemical photoetching. A new approach to overcome this difficulty was proposed by Mineta et.al. [61]. The current distribution was enhanced with additional conductive layers of metals deposited on the backside of NiTi alloy. A thin layer of Cu/Ni was sputtered first to promote the adhesion and then a thick layer of Cu was electroplated on top of it to create a sacrificial conductive layer. The SMA sheet 35 μm thick was electrolytically etched through to the metals sacrificial layer in 5% H₂SO₄ in methanol. Then the photoresist and the Cu layer were removed by chemical etching in concentrated nitric acid.

Salt electrolytes were introduced to the fabrication of Ti and its alloys.

5M NaBr solutions were applied in the work of [58], [62] to etch cp Ti and Ti6Al4V. The pattern was successfully achieved. However, it was noted that the low potential applied (2 V) caused pitting dissolution with very rough surface, whereas a higher potential of 8 V resulted

in corrosion products entrapped in the pattern [58]. Uniform etching was obtained at potential of 5 V with no by-products present.

The results of the etched patterns with 1 mol/l electrolytes of LiCl in methanol and LiCl in ethanol, were evaluated [59]. **LiCl in methanol** was found to produce uniform etching with the etching rate higher than 10 $\mu\text{m}/\text{min}$. It was noted that this solution could **substitute** the conventional **H₂SO₄ in methanol** electrolyte.

The material removal rate was even higher when an ultrasonic agitation at a frequency of 40 kHz was added to a PC electrochemical etching in 1M LiCl in methanol solution [63]. The etch rate increased from 15 $\mu\text{m}/\text{min}$ in rotational-stirring electrolyte to 24 $\mu\text{m}/\text{min}$ for ultrasound of 50 W and 30 $\mu\text{m}/\text{min}$ for 100 W ultrasound. It was concluded that ultrasonics can be beneficial for a pattern with a large etched surface area and only high frequency ultrasound can improve microfabrication directionality.

However, LiCl in ethanol has an advantage of being non-corrosive, non-toxic and stable for a long time [59]. Moreover, when the ethanol was used as a solvent, LiCl produced a much smoother surface finish than H₂SO₄ in methanol. However, the low etch rate 3.5 $\mu\text{m}/\text{min}$ and relatively high etch factor makes this solution suitable for fine pattern etching.

Also in case of LiCl in ethanol an additional layer of metal was deposited on the NiTi specimen [64]. A 20 μm thick layer of Ni was electroplated on the backside of the metal sheet in order to maintain an even current distribution throughout etching. The achieved results suggested that the non-uniform current distribution caused the side etching which reduced the width of the line of about 100 μm . Apart from this disadvantage, the NiTi SMA spring microstructure was formed with this approach.

- **Two step patterning process**

Chauvy, et al. [65] formed a passive oxide film on a titanium substrate by applying an anodic potential in 0.5M H₂SO₄ electrolyte through a patterned photoresist. The anodised titanium was irradiated by a laser per site. The presence of the photoresist was needed during the anodization step to obtain an oxide that would withstand the aggressive environment of the etchants. The electrochemical dissolution of the Ti was performed in an electrolyte containing 3M H₂SO₄ in methanol at 0°C with an applied constant potential of 6 V. However, the use of resist limits possible applications to two dimensional only. Therefore, a new resist-free

approach was developed in order to enable three-dimensional (3D) electrochemical micromachining of structures in Ti [66]. The proposed method was based on anodization of Ti, laser lithography of the titanium oxide film, electrochemical dissolution and ultrasonic cleaning. The anodic oxidation was performed in the same solution as described in [65] but with higher voltages, 40 V for electropolished surface and 100 V for mechanically polished substrate. These corresponded to oxide films thickness of 100 nm and 250 nm, respectively. Then, the lithography pattern consisting of 10 μm x 10 μm square was achieved using a XeCl excimer laser with a pulse duration of 20 and 280 ns. Finally, the electrochemical micromachining was carried out in 3M H_2SO_4 in methanol at -10°C for 10 min with the applied potential of 20 V for 20 s, then down to 10 V for 10 s and maintaining 10 V to the end of the etching. This resulted in the microstructure of 20 μm in depth.

The same approach was applied to mechanically and electrolytically polished Ti cylinder. The anodised specimen in 0.5 M H_2SO_4 at 40 V was patterned with the two arrays of dots with the laser. Then, the anodic dissolution of the irradiated areas was carried out in H_2SO_4 in methanol electrolyte for 23 min without rotation. As the result, more than 100,000 cavities of approx. 40 μm in diameter were etched. However, it was found that the bottleneck of this method is a low patterning speed.

2.2.6 Sandwich structure microfabrication

Investigations on improving the uniformity of current distribution on the anode and reducing the environmental impact by incorporation of less hazardous etchants and the subsequent need for less durable photoresists (to avoid the use of stronger strippers) were carried out. Two approaches to these problems in electrochemical photoetching were distinguished. Both rely on the same electrochemical principals and they minimise the inter-electrode gap between the anode and the cathode in order to improve the current distribution on the workpiece.

However, the way how the electrodes are fabricated is a variable here. Two approaches were defined: by non-permanent attachment and by coating layer by layer in order to obtain a sandwich structure.

- Non-permanent structure

A new method that introduces a dielectric layer coated with a conductive layer attached to a workpiece was demonstrated [67]. A non-conductive layer acts as a patterned mask with the coated metal film that acts as a cathode in the process. This approach in electrochemical machining (Figure 6) allows reusing the mask with the cathode layer. Moreover, a thickness modification of the insulation film is responsible for current distribution on an anode.

The fabrication of the layers consists of pressing the mask patterns on the anode and clamping together with during the electrochemical machining. The mechanism of etching relies on an electrolyte flow through the imaged structure. Whereas, the exposed areas of the anode undergo a controlled dissolution when sufficient voltage is applied. Since tool wear does not occur in this process, the mask can be applied to the production of other samples.

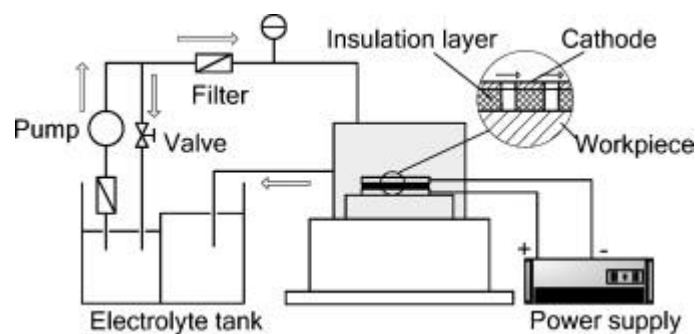


Fig. 6. Schematic diagram of ECM experimental system applied by [67].

This method was utilised in the fabrication of arrays of holes and dimples in 300 μm thick 1Cr18Ni9Ti workpiece. Two different thicknesses of the dielectric layer were verified in order to achieve an even current distribution over the anode. The applied parameters, 30 μm thick Cu cathode, insulation layer thickness of 100 μm with the addition of an electrolyte flow (16 % wt. NaNO_3) at 0.7 MPa and temperature of 26 $^{\circ}\text{C}$, produced the dimple without the convex shape in the centre. It was possible to fabricate dimples 240 μm in diameter and 4, 10, and 22 μm in depth.

It was confirmed by the Finite Element Method (FEM) as well as the experimental outputs that the lowest current distribution occurs on the centre of the trench. In order to overcome this problem, the mask aspect ratio was increased.

This method showed a potential of producing micro-holes and holes on thin metal sheet.

A modified cathode/dielectric/anode arrangement was applied to etch holes through cp Ti [60]. In this approach, a resist acting as the insulation layer between the anode and the cathode was used. Ti was dip-coated with the negative-working photoresist and imaged. In order to obtain the same pattern on the cathode, stainless steel (acting as the cathode) was imaged and etched.

Finally, the two parts: patterned Ti with 10 μm of DET 466 was clamped together with the stainless steel cathode and immersed in an electrolyte of 1M LiCl in methanol. PC electrolytic etching was performed in an ultrasonic bath at a frequency of 40 kHz. 518 μm diameter hole in 100 μm thick Ti was produced by this method.

- **Permanent structure**

Another approach to fabricate a sandwich structure, comprising of cathode, dielectric and anode was verified [68]. In this method, the layers were put together permanently.

Although, the method was utilised to **etch stainless steel AISI 304**, it showed potential in obtaining a uniform current distribution on the anode. The “sandwich structure” was built from the following materials: the anode: stainless steel AISI 304, the insulation layer: Shipley AZ1818 positive photoresist and the cathode: copper.

The results demonstrated an array of 100 μm diameter micro-holes on stainless steel AISI 304 by applying PC mode to “sandwich structure” and placed in the electrolytic cell filled with 0.1 M HCl electrolyte. The etch rate was approx. 2.4 $\mu\text{m}/\text{min}$ and the average depth of grooves was 4.85 μm .

2.2.7 Microfabrication with reduced impact on the environment

The “sandwich structure” method demonstrated the possibility of an improved current distribution over the workpiece. This resulted in the reduction of the convex shape in the centre of the machined features. It was made feasible by minimising the gap between the two electrodes to the micro-size.

As this method is an electrolytic process it eliminates the need for using aggressive etchants, due to the direct current flow which increases the power of the etching.

The development of a novel sandwich structure method in order to microfabricate Ti in a more environmentally friendly way was a subject of this research.

2.2.8 Summary of literature review

In the first chapter the following subjects were discussed:

a) Titanium biomedical devices

In the Chapter 1.1 Ti main characteristics as the metallic biomaterial have been highlighted. The amount of applications reviewed resonate its superior properties and indicate how Ti is a well-established material in the medical field.

b) Ti microfabrication techniques

The current techniques of producing micrometer features in Ti have been reviewed in Chapter 1.2. The summary of their advantages and disadvantages has been presented in Table 3. The machining techniques are in order of the appearance in the text.

Table 3: Methods of Ti microfabrication.

Machining technique	Process capabilities	Process limits
Reactive Ion Etching Lag	Complex 3 D surface profiles by using a single mask.	Low etch rate; expensive equipment; HF utilization in the process.
Laser micromachining	NiTi SMA stents manufacturing; texturing of the surface to enhance osseointegration.	Stress generated due to the metal melting affects the material's chemical and mechanical properties, i.e. formation of Ti oxide inside and outside of the HAZ.
Mechanical micro-milling	-	High tool wear and tool failure; increase of cutting speed restricted by the Ti properties.
Laser-assisted micro-milling	Elimination of top edge burrs and chips of the milled material. Possible to overcome low shear plane temperatures when small tool diameter is used.	Increase of surface roughness comparing to the conventional micro-milling.
Photochemical machining	Fabrication of complex shapes in thin metallic materials in bulk quantities on industrial scale.	Use of very aggressive and hazardous etchants. Etching reaction severe. Generation of H ₂ reduces Ti fatigue strength and the ductility. Deterioration of most of the masks during the etching process. Excessive undercut (photoresist lifting at edges

Machining technique	Process capabilities	Process limits
Electric discharge machining	Using the ultrasonic assisted EDM variation process it is possible to improve the electrolyte flow dynamics and by-products sedimentation. Fabrication of 3 mm hole in depth.	Difficulties in removing the by-products from the IEG. High voltage used.
Jet electrochemical micromachining (Jet-EMM)	High speed drilling. Can machine surfaces of any type of curvature. Generates micro-holes with high aspect ratios without implementation of photolithography stage.	High voltage up to 250 with the pressure greater than 280 kPa creates operational, economical and surface finish problems
Through mask Jet-EMM	High etch rate of machining micro-holes.	High undercut in machined micro-holes.
Electrochemical photoetching	Machining does not affect the properties of the workpiece. Enables use of milder etchants.	Non-uniform current distribution on the workpiece.
Electrochemical photoetching by sandwich structure application	Theoretically, more uniform current distribution on the workpiece. Incorporates less hazardous electrolytes.	Involves multistep processing in case of permanent sandwich structure.

Electrochemical photoetching incorporating a “sandwich structure” has shown potential in the fabrication of micro-holes in Ti. This method forms the backbone of this thesis and as such its use as a viable Ti microfabrication method will be accessed in the following chapters.

Chapter 3. Background to experimental methodology

Introduction

The construction of a sandwich structure, comprising of anode, insulator and cathode (Figure 7) is the subject of the research presented in this thesis. The experimental work was focused on developing the anode and cathode arrangement in order to improve the current distribution on the conductive workpiece (anode) during the electrochemical etching. The minimisation of the IEG between the electrodes to a few micrometers (the IEG in a conventional electrolytic photoetching is of the order 0.5 to a few centimetres) was investigated as a possibility of overcoming problems related to conventional electrolytic etching, such as: non-uniform pattern dissolution (observed as an island of a material left in a centre called “W” profile⁵), reaction product build up, resist adhesion, and heat generation in the interelectrode gap.



Figure 7: Cross section of the “sandwich structure”.

The preliminary work was aimed at the determination of:

- a) a configuration of the sandwich structure,
- b) the top two materials, and
- c) a route of building the structure on the cp Ti.

The experimental work was divided into the activities that determined the final sandwich structure layers which were subsequently patterned in order to conduct Ti selective electrochemical etching.

⁵ Arising through current concentrations on high points and edges.

The verified routes of fabrication of the sandwich structure have been summarised in this Chapter.

3.1 Determination of the configuration of the sandwich structure

3.1.1 Exploratory sandwich structure

The initial work was focused on determination of the configuration of the sandwich structure.

In the work conducted by Zhu et.al. [67] it has been shown that by simple attachment of the anode and the cathode with an insulator between them (rather than the conventional IEG occupied by the electrolyte) it is possible to etch micro holes and dimples in the substrate. They managed to fabricate a micro-dimple array in 1Cr18Ni9Ti stainless steel of hundreds of micrometers in diameter and several micrometers in depth. The experiments were aimed at eliminating a lithography step, in order to reduce the time and cost of processing by applying a prepatterned cathode and insulator and attaching this to the workpiece in the electrolytic cell.

The feasibility of an exploratory sandwich structure that could enable the production of microfeatures in Ti by putting together the workpiece and the cathode with the dielectric between them was tested. The experiments were aimed at proving the beneficial influence of etching Ti using the sandwich configuration allowing a micro-size gap between these electrodes. The following experimental set-up was applied:

Equipment

250 ml glass beaker,
Perspex jig,
2 Crocodile clips with electrical leads,
DC power supply,
PVC insulation tape.

Materials

The following materials were used in order to build the “sandwich structure”:

- Cathode and insulator: Liquid Crystalline Polymer Circuit Material (LCP) [69], used as the cathode, dielectric and a mask (LCP sheet was clad with Cu on both sides),
- Anode: Titanium, grade 2 (98.885% pure Ti), 250 μm thick.

Chemicals

35⁰Bé FeCl₃,

2% Micro® cleaning solution,

acetone (99.0%),

10% w/v HCl electrolyte.

Experimental procedure

Cu from one side of the Cu-LCP sheet was removed from the polymer surface with a Chemcut spray etching machine using 35⁰Bé FeCl₃ for approx. 10 minutes cycle, at ambient temperature. Next, Ti and Cu-LCP specimens were cut to size of 2cm x 4cm and immersed in the 2% Micro® cleaning solution and placed in an ultrasonic bath (40 kHz) for 10 minutes, then rinsed with deionised (DI) water. To remove grease, the titanium sample was immersed in acetone (99.0%) with ultrasonic agitation applied for 15 minutes, then rinsed with DI water and dried with a compressed air gun.

The Ti specimen was attached using insulation tape to the copper clad LCP. The pattern was made by drilling different size holes through the Cu-LCP with a small twist drill. The prepared sample was placed in the electrolytic cell, filled with electrolyte and connected to the DC power supply. The experimental conditions, with selected the size hole of 110 μm , have been summarised in the Table 4.

Table 4: The experimental conditions for the non-permanent “sandwich structure” etching.

Hole diameter in the cathode/insulator tool	110 μm
Cathode (copper clad) thickness	18 μm
Insulator thickness	50 μm
Substrate (Ti, grade 2) thickness	250 μm
Current Density	18.18 A/cm ²
Temperature	Ambient
Time of etching	2 min.

Results and discussion

The etching results obtained from the series of experiments showed pits in the Ti corresponding to the areas where they were drilled in the Cu-LCP. The measurements made with an Olympus Lext Confocal Laser Microscope of one of the pits showed the depth of 5.68 μm and the width of 90 μm .

The problem, which occurred during the experiments, was the anodisation of the titanium as observed by the formation of the titanium dioxide on the surface. This was concluded as the effect of too low voltage, which caused the passivation of the substrate.

It was also noted that, although, the etched pattern in Ti corresponded to the apertures in the Cu-LCP, it was irregular in shape. This phenomenon was explained as a lack of directionality of this etching technique caused by a loose clamping system to hold cathode/dielectric and anode, which resulted in the poor finish of the drilled holes (the Cu-LCP material left at the entrance of the holes). In the consequence, it reduced the etched diameter of the pattern.

The non-permanent attachment of the anode/insulation/cathode resulted in poor dimensional control of the etched pattern in Ti. Therefore, further experimental work was focused on building a more permanent sandwich structure.

3.1.2 Sandwich structure

In order to build a more permanent sandwich structure, comprising of the Ti, the insulation layer and the cathode, an investigation of possible top two materials was undertaken (top two materials: dielectric layer and cathode, see Fig. 7).

Each layer has to fulfil certain requirements to allow further processing of the “sandwich structure”.

3.2 Determination of materials of the sandwich structure

3.2.1 Insulator

The two electrodes (see Fig. 7), have to be separated with an insulating material but in order to minimise this IEG and optimise the current distribution, a very thin layer (measuring a few micrometers) of the insulator is necessary. The insulator or dielectric layer binds the two electrodes together. In order to withstand subsequent processing of the sandwich structure, it

has to be resistant to:

- physical processing: electric current, temperatures up to 300⁰C, vacuum compatible;
- chemical processing: chemical deposition, imaging, developing, etching;
- mechanical processing: stress.

In the meantime, this dielectric material should be processable enough to be deposited on the titanium surface, to achieve good coverage but with a sufficiently thin layer so as to minimise the inter-electrode gap and be capable of obtaining high image resolution. Moreover, it should allow coatings of other materials to be applied to it, so this includes good adhesion properties. Taking into consideration the environmental impact, the dielectric cannot contain hazardous compounds and should enable the use of innocuous developing and stripping chemicals.

- **Photoresist as an insulator**

Introduction

Photoresist is an organic material, consisting of a polymer, a sensitiser, and a casting solvent. It allows for thin coating of a substrate. By exposure to radiation through a suitable mask, the polymer changes in structure making it either soluble or insoluble in a developing solution. The exposed material is then a subject of a development process, aimed at removing the soluble part of the film. The remaining - non-soluble part “masks” the substrate and protects it from attack during an etching process (this is otherwise known as a stencil).

Photoresist was found to meet the process requirements of the sandwich structure fabrication.

In the work conducted by Wang, Allen, Almond [68] the photolithography process with the use of a positive photoresist was applied to produce holes in stainless steel with a diameter of 100 µm. The two step lithography was implemented to obtain a patterned sandwich structure.

Resist tone

For purposes of this work, two types of photoresists application routes were investigated.

Negative tone resist

When exposed to UV radiation, the exposed regions of the polymer become strengthened in the negative tone resist. The insolubilisation of the resist is achieved in one of two ways: the negative resist material increases in molecular weight through UV exposure, or it is photochemically transformed to create new insoluble products. The increase in molecular weight is normally accomplished through photoinitiators that produce free radicals or cross-linking facilitated by strong acids or copolymerisation of monomers [29].

Negative photoresists usually are two-component bis(aryl)azide rubber resists, whose matrix resin is cyclised poly(cis-isoprene) [29]. Bis(aryl)azide sensitisers lose nitrogen as a consequence of a photolysis and generate very reactive nitrene. The nitrene is responsible for a cross-linking. However, oxidation is the competitive reaction to cross-linking. Therefore, the exposure of the negative resist can only be conducted under a nitrogen atmosphere or in a vacuum. The negative resist also has a disadvantage of achievable resolution which is limited by film thickness. Overexposure is needed to initiate cross-linking of the deeper parts of the film. Aromatic solvent developers are employed to remove the unexposed area of the photoresist. However, newer negative resists incorporate water-based developers [29].

Positive tone resist

The polymer, in the photochemical reaction during exposure, becomes weaker by rupture or scission of the main chains [29]. As a consequence, the exposed resist is more soluble in a developer.

There are two families of positive tone resists, the single component: poly(methylmethacrylate) (PMMA) and the two-component (DQN) resists composed of a photoactive diazoquinone ester (DQ) and a phenolic novolac resin (N).

PMMA belong to deep UV (DUV) resists requiring doses $> 250 \text{ mJ/cm}^2$. However, the UV spectral absorbency of PMMA can be increased and the lithographic sensitivity of 150 mJ/cm^2 is achieved, by the addition of a photosensitiser t-butyl benzoic acid. PMMA resists are used in electron beam, ion beam, and X-ray lithography.

The DQN represents near-UV resists which transforms into a polar, base-soluble product. The novolac resin (N) is soluble in alkali, however, it becomes insoluble by adding 20 – 50 % by wt. DQ. The resist retrieves its soluble properties through the photochemical reaction of DQ.

The resist is soluble in mild alkaline solutions and can be stripped in strongly alkaline solvents [29].

The examples of the industrial developers for positive resists are: 0.05 – 0.5 N KOH aq solutions with a surfactant, tetramethylammonium hydroxide (TMAH), ketones, and acetates [29].

Theoretical experimental procedure

Three variations of photoresists were compared in order to choose the best, i.e. which would enable imaging micron features on titanium using processing chemicals with a reduced environmental impact.

The ready-to-pattern sandwich structure comprises of two layers of the photoresists: a top – coated on a cathode and a bottom photoresist – separating an anode and the cathode (see Table 5). The aim of the bottom layer of the photoresist is to act as a dielectric but it must also contain through-features to enable selective etching of the underlying Ti substrate. The aim of the upper layer of photoresist is to provide a means of patterning the cathode layer with the desired features. These features are subsequently transferred through to the Ti substrate by electrolytic etching. The upper resist is removed prior to etching features into the substrate.

The alternative processing routes have been summarised in Table 5. The structure layers correspond to the Anode/Insulator/Cathode arrangement presented in the Figure 7.

Table 5. Alternative processing stages investigated in the formation of the “sandwich structure”.

Procedure	Photoresist (top layer + bottom layer) Cross section of the sandwich structure		
	A) Negative + negative	B) Negative + positive	C) Positive + positive
1. UV exposure through the phototool (black and transparent structure)			
2. Development			
3. Metal through etching			
4. UV flood exposure			
5. Development	Incompatible Negative photoresist cannot produce pattern which would be transferred to Ti substrate.		

Where: Negative photoresist Positive photoresist

Results and conclusions

The literature review and the conducted analysis of the photoresists [29], [70] have suggested that:

Negative photoresist:

- is sandwich structure incompatible: exposed areas become insolubilised in the developing solvent [70];

- cannot produce ultra-fine features (less than 2 μm);
- has lower step coverage than positive resist;
- dictates the use of organic solvents for developing and aromatic solvents for unexposed area of the film [29], and
- can be difficult to strip i.e. SU-8 [29].

Positive resist:

- is sandwich structure compatible;
- has better than negative resist step coverage;
- features below 0.5 μm can be produced [29];
- allows the use of aqueous based developers [29] and organic strippers [70] and therefore, is more environment-friendly.

These findings revealed that positive resist only processing route meets the sandwich structure process requirements. Therefore, it was applied in the further experimental work.

3.2.2 The cathode

Introduction

The cathode (top metal layer in the sandwich structure) naturally has to be a good conductor, in order to enable uniform current distribution and thereby improve the etching process of Ti in the electrolytic cell.

The cathode layer is responsible for the uniform current distribution through the patterned dielectric through to the Ti substrate underneath. Therefore, the metal to be used as the cathode has to possess low electrical resistance.

The comparison of the resistivity of metals has been presented in the Table 6.

Table 6. Resistivity of metals potentially involved in the processing of the “sandwich structure” [71].

Metal	Resistivity ($\times 10^{-6} \Omega \cdot \text{cm}$)
Silver	1.59
Copper	1.67
Gold	2.35
Aluminium	2.65
Nickel	6.93
Titanium	55.0

The conductive layer lies on top of the insulator, which suggests, it has to be capable of coating down on to the non-conductive layer by a physical or chemical deposition technique.

The metal used to create the cathode should be compatible with several processing routes:

- i. physical: glow-discharge deposition,
- ii. chemical:
 - liquid-phase chemical deposition,
 - etching: allow the use of non-hazardous etchants,
- iii. mechanical: stress resistant.

The aim of a metallisation of the positive resist is to produce a uniform, conductive film with a rapid as possible, repeatable process, which would be environmentally friendly and economically reasonable for large scale production. The techniques found to be capable of producing metal films on the non-conductor were: sputtering, ion beam deposition, spray-on techniques, spin-on techniques and electroless plating [29], [72].

Sputtering and electroless deposition were found to be compatible with the cathode production on the positive resist.

The metals chosen for depositing by these techniques were: copper, gold, aluminium, and nickel.

The sputtering of gold, aluminium and copper as well as electroless plating of copper and nickel were chosen as potential routes of metallisation of positive resist S1818. These were found as the most suitable metals and methods according to the specified requirements mentioned above.

3.3 Permanent sandwich structure building

In this sub-chapter, the examined processing routes of building the sandwich structure on Ti have been presented.

The flow diagram detailing the verified fabrication techniques has been enclosed in the appendix B.

3.3.1 Titanium substrate preparation

Titanium (grade 2) sheets, dimensions: 0.250 mm x 197 mm x 300 mm supplied by Datum Alloys Ltd. [73] were manually sanded with grit papers: 240, 400, and 1200 in order to improve the titanium's conductivity by removing the titanium dioxide layer. Then, the Ti sheets were cut into 40 mm x 45 mm pieces on a guillotine.

Next, cleaning procedures were introduced to remove inorganic and organic contamination from the surface. The specimens were soaked in 2% Micro® solution and placed in an ultrasonic bath (40 kHz) for 10 minutes, then rinsed with DI water. To remove grease, the titanium samples were immersed in acetone (99.0%) with applied ultrasonic agitation for 15 minutes, then rinsed with DI water and dried with a compressed air gun.

3.3.2 Photoresist coating

Microposit™ S1818 Positive Photoresist [74] was applied on to the Ti substrates using a Cookson SCS G3 – 8 Spincoat vacuum spin coater. The conditions were adjusted to give a 4 µm thick coating (1000 rpm, spin time of 60 s.).

Then, the samples were soft baked at 115°C for 30 minutes on the EMS Electro Micro Systems Precision Hot Plate, model 1000-1, to drive off the solvent in the resist. This stage was aimed at improving the adhesion to the substrate [75].

3.3.3 Metallisation of the photoresist

Two deposition techniques, sputtering and electroless plating, were employed to produce the conductive layer on top of the positive resist S1818. The experimental methodologies for each of the technique have been presented in this sub-chapter.

I. Sputtering

Introduction

Sputtering is a physical process of thin film deposition by ion implantation [76]. The sputtering takes place in a chamber filled with noble gas, typically argon at 4×10^{-2} torr where the front surface of a cathode is covered with a target material to be deposited and a substrate is placed on an anode. During sputtering, the target, which is at a high negative potential, is bombarded with the positive argon ions created in plasma [29]. The ejected surface atoms from the target are deposited onto the substrate.

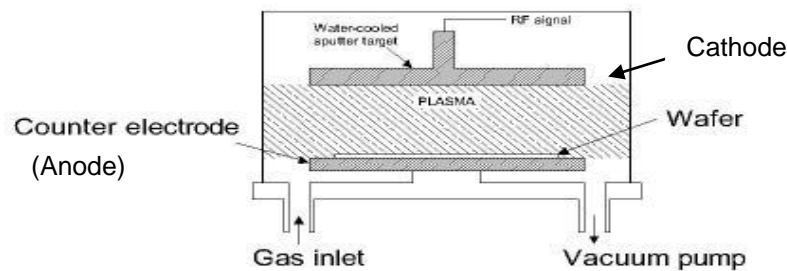


Figure 8: RF sputtering system [77].

Sputtering can be employed in a production environment [29] and it offers deposition of a wide variety of materials with better step coverage and adhesion to the substrate than evaporation techniques.

Sputtering as the method of metallisation of the positive resist S1818 has been presented in this section. Three metals were deposited in order to test their potential application as the cathode in the sandwich structure.

Equipment

The Radio Frequency (RF) Sputtering of Nordiko Sputtering System was employed to deposit metal films.

Materials

The following metal targets were used to deposit approx. 50 nm metal films on the Ti/S1818 specimens:

- a) Gold (Au),
- b) Aluminium (Al), and
- c) Copper (Cu).








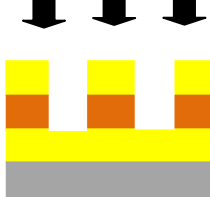

Experimental procedure

The Au, Al, and Cu films were deposited using a RF Nordiko sputtering system. The deposition was conducted with an application of high purity metal targets on the photoresist S1818 coated on the Ti substrate. No heating or cooling was carried out during sputtering.

a) Processing of the Au sputtered samples

In the schematics shown in the Table 7, the procedures followed to obtain “ready-to-etch” Ti samples are shown.

Table 7. Processing stages to obtain Ti/photoresist/Au sandwich structure.

<p>Procedure</p> <p>Equipment and parameters applied</p>	<p>Sandwich structure profile</p>
<p>1. Titanium preparation.</p> <p>Procedure described in 3.3.1</p>	
<p>2. Ti coating with the positive photoresist S1818. (4 μm thick) – bottom layer photoresist</p> <p>Procedure described in 3.3.2</p>	
<p>3. Sputtering deposition of Au on top of the S1818</p> <p>Nordiko sputtering system, Base pressure= 5×10^{-3} Torr, Power = 100W, t = 1.5 min</p>	
<p>4. Coating of second layer of the S1818 (1.8 μm thick) on top of the Au layer.</p> <p>EMS spin coater, 4000 rpm, t = 60seconds</p>	
<p>5. UV exposure of top photoresist through the phototool.</p> <p>Mask Aligner (MA) 56, UV lamps int. = 5 mW/cm², t = 38 seconds</p>	
<p>6. Developing of the positive resist (top layer).</p> <p>MF-319 Developer, T=ambient, t= 80s.</p>	
<p>7. Etching through the patterned Au.</p> <p>Etchant: aqua regia HCl (3): HNO₃(1), t=4s, T= ambient.</p>	
<p>8. UV exposure of the positive photoresist (bottom layer) through the etched pattern in Au.</p> <p>MA 56, UV lamps int. = 5 mW/cm², t = 40 seconds</p>	
<p>9. Developing the positive photoresist (bottom layer).</p> <p>MF-319 Developer, T=ambient, t= 120s.</p>	

Results and discussion

It was found during developing that it was impossible to remove the bottom layer of S1818. This in turn, prevented the next step of the sandwich processing – electrolytic etching of the Ti substrate. Moreover, the Au layer dictated the use of highly corrosive and oxidising chemicals such as aqua regia, (a combination of HCl and HNO₃) or replacing them by very expensive ones: potassium iodide with iodide. This factor was the main objection to the application of Au as the conductor material.

Furthermore, the use of the Au drastically increases the costs of the materials involved in the process which directly interferes with the objectives of the conducted research.





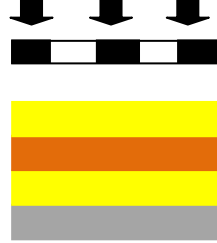


a) Processing of the Al sputtered samples

Here, the goal was to apply Al as the cathode layer in the triple sandwich structure. Al is a very good electrical conductor and can be etched with chemicals, of reduced impact on environment, such as: 20% NaOH or 12-20⁰Bé FeCl₃.

Experimental procedure

The samples were processed as shown in Table 8.

Table 8. Processing stages to obtain Ti/photoresist/Al sandwich structure.

Procedure Equipment and parameters applied	Sandwich structure profile
1. Titanium preparation. Procedure described in 3.3.1	
2. Ti coating with the positive photoresist S1818 – bottom layer. Procedure described in 3.3.2	
3. Sputtering deposition of Al on top of the photoresist. Base pressure= 4.7×10^{-5} Torr, Power= 300W, t=2 min.	
4. Coating of second layer of the positive photoresist (1.8 μm thick) on top of Al. EMS spin coater, 4000rpm, t=60s.	
5. UV exposure of top layer of the positive photoresist through the mask. MA 56, UV lamps int. = $5\text{mW}/\text{cm}^2$, 38 seconds.	
6. Developing of the photoresist – top layer. Complete removal of Al in developing media. MF-319 Developer, T=ambient, t= 80s.	
7. Microscope assessment of developed sample. Nikon Optishot Acquisition System	

Results and discussion





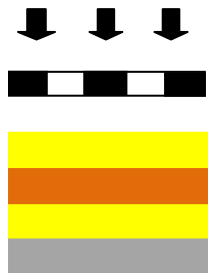


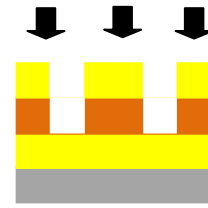
The experiments showed that the Al is incompatible with the use of a positive resist, because it did not withstand the alkaline developer used to develop out exposed regions of the top layer of resist. It is due to the alkaline etching environment of this metal. Al is amphoteric and will etch in an acid and alkaline media (MF-319 is included in the latter).



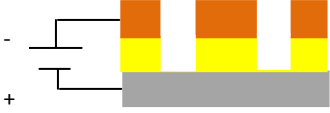


b) Processing of the Cu sputtered samples

Experimental procedure

The aim of this experiment was to apply Cu as the cathode in the sandwich structure. The processes carried out have been presented in Table 9.

Table 9. Processing stages to obtain Ti/photoresist/Cu sandwich structure.

Procedure Equipment and parameters applied	Sandwich structure profile
1. Titanium preparation. Procedure described in 3.3.1	
2. Ti coating with the positive photoresist S1818 (4µm thick) – bottom layer. Procedure described in 3.3.2	
3. Sputtering deposition of Cu on top of the photoresist. Base pressure= 4.7×10^{-5} Torr, Power= 300W, t=2 min.	
4. Coating of second layer of the positive photoresist (1.8µm) on top of Cu layer. EMS spin coater, 4000rpm, t=60s.	
5. UV exposure of top photoresist through the mask. MA 56, UV lamps int. = 5 mW/cm^2 , 38 s	
6. Developing of the positive photoresist – top layer. MF-319 Developer, T=ambient, t= 80s.	
7. Etching through the patterned Cu. Etchant: $35^{\circ}\text{Bé FeCl}_3$, T=ambient, t=15s, beaker etching	
8. UV exposure of the positive photoresist through the etched pattern in Cu. MA 56, UV lamps int. = 5 mW/cm^2 , t = 40 s	

Procedure Equipment and parameters applied	Sandwich structure profile
9. Developing of the positive photoresist (bottom layer). MF-319 Developer, T=ambient, t= 120s, beaker developing.	
10. Microscope assessment of developed sample. Nikon Optishot Acquisition System	
11. DC electrolytic etching of the sample. DC power supply, CD = 30 A/cm ² , t = 2 min., T = ambient	
12. Stripping the positive photoresist. Stripper: acetone	
13. Microscope assessment of the sample. Nikon Optishot Acquisition System	

Results and discussion

Processing of Cu sputtered samples revealed the processing problems with the photoresist S1818.

a) Step wedge test

The first conducted experiment showed that the positive resist, on the bottom layer of the sandwich structure, did not solubilise in some areas in MF-319 developer. Therefore, it was necessary to verify if the temperature and time of the soft baking stage (in the resist processing) or sputtering had affected the developing properties of this resist layer.

Soft baking temperature and time were checked with a step wedge test on the S1818 resist. The time of baking on the hot plate was increased from 30 minutes for the standard time to 40 minutes. The temperature was kept constant at 110⁰C. The 40 minutes was set as the total time of baking of whole sandwich structure before actual developing of the bottom layer of the resist. In both cases (30 min. and 40 min.) the four steps of the step wedge test were dissolved. It proved that the time and 110⁰C for baking do not affect the photoresist properties.

b) Photoresist blistering

It was also noticed that half of the deposited samples had blisters on the side where the copper was sputtered. The microscopic examination of a developed sample revealed that the bottom layer of the resist was solubilised under the blistered areas of the specimen, however, it was not dissolved on the unaffected part of the sample, see Figure 9.

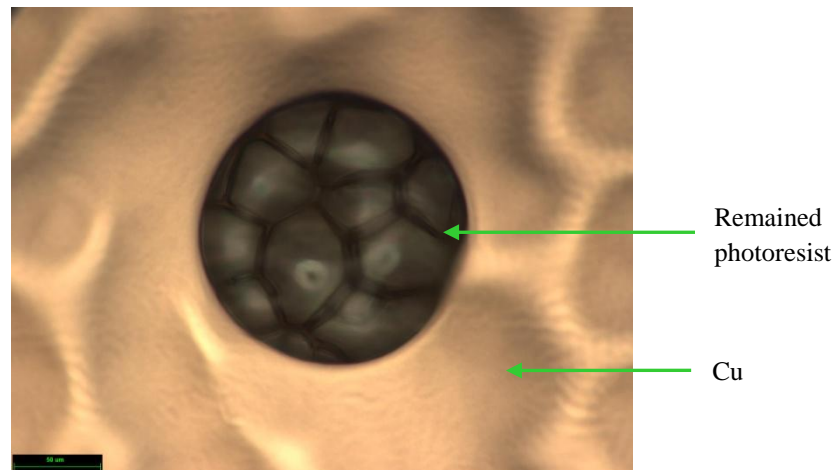


Figure 9. Undeveloped pattern in the sandwich structure. The photoresist S1818 remained in the spherical- shape pattern.

According to [78] these difficulties in photoresist developing are caused by plasma exposure during the sputtering process. It has a decompositional effect on photosensitive material. The blisters on the copper layer were due to the release of N_2 . It is released as a side product by the photo active compound diazonaphthoquinone (DNQ) in the photoresist during exposure to the plasma during sputtering. When thermally activated, it diffuses to the resist surface and remains trapped between the resist and sputtered layer of the metal thus creating blisters. Therefore, the photoresist is not compatible with the sputtering process.

It was found that for sandwich structure processing it is possible to replace the bottom resist by other non-conductive materials [79]. The literature survey showed some dielectrics that could be used in conditions of vacuum in the sputtering chamber, such as: polyimides, including PMDA-ODA Kapton[®] [80] and epoxy resin [81]. However, these materials give rise to environmental concerns due to the etchants that are required to create features in them.

- DC electrolytic etching

The sample consisting of a conductive layer with through-features (in this case a series of holes), imaged resist layer located on a Ti substrate (substrate to be etched) was taken through to the final electrolytic etching stage (stage 11 as shown in Table 9).

Equipment:

DC power supply,
2 stainless steel crocodile clips,
2 leads (red and black),
Glass beaker 250 ml,
Hot plate magnetic stirrer,
Perspex jig (to hold sample during etching)
Magnetic stirring bean,
PVC insulation tape.

Chemicals:

10% w/v HCl was applied as an electrolyte due to the results obtained during DC electrolytic etching of Ti [50].

Experimental procedure:

The specimen was connected to the DC power supply in an electrolytic cell filled with the electrolyte, see Figure 10. The current density used was approx. 30 A/cm^2 applied for 2 minutes at ambient temperature.

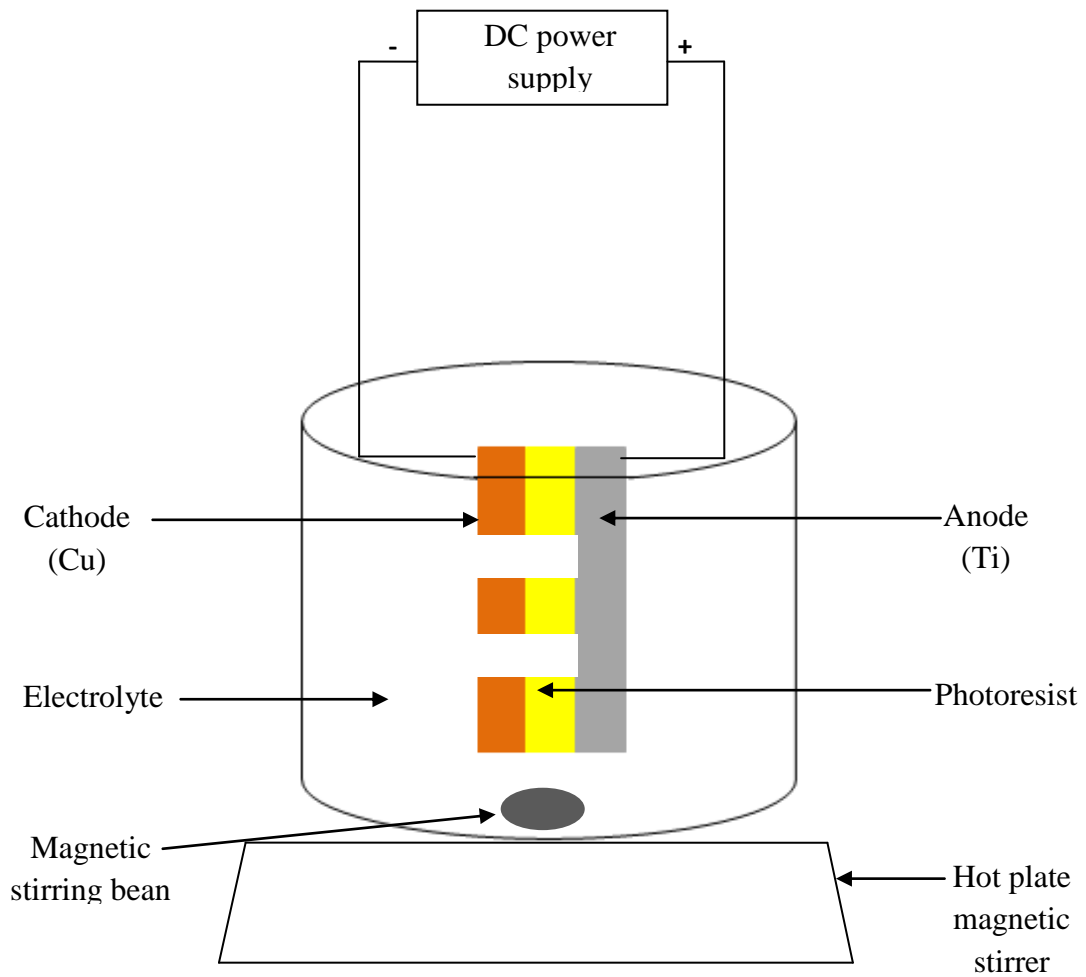


Figure 10. Cell layout for DC electrolytic etching of the sandwich structure.

Results and discussion

The microscopic assessment of the specimen showed twelve tarnished rings rather than a definite etch of 126 μm in diameter in Ti (\varnothing of test pattern 125 μm). The shape of the etched pattern corresponded to the imaged pattern. Figure 11 presents the front view of one of the rings on the Ti. The analysis was conducted with Lext Olympus Laser Microscope.

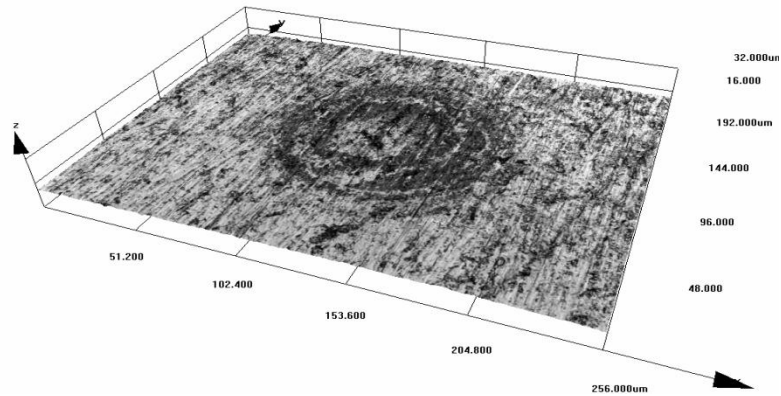


Figure 11. Tarnished ring on the Ti

Results and conclusions to the sputtering processes

The sputtering process of Au, Al, and Cu revealed many obstacles. The photoresist showed incompatibility with this way of deposition. In addition to this, sputtering as the method of coating incorporates expensive equipment. An alternative was required.

II. Electroless Plating

Introduction

Electroless plating is a method for obtaining a thin metallic film on metals, ceramics or plastics [82]. It does not require for the substrate to be conductive.

The chemical deposition of a metal from an aqueous solution of a salt of said metal has an electrochemical mechanism, involving both oxidation and reduction [82]. It is a cathalytic reaction of the anodic oxidation of a reducing agent and the cathodic reduction of metal ions.

The electroless plating bath is a complex electrolyte solution containing metallic ions, reductants, ligands and other minor components. The deposition takes place when an activated surface of the material is immersed in the plating bath [56].

The main advantage of electroless deposition is low tool cost, low processing temperature, and high quality material achieved as a result of the process [56].

The deposition of two metals was investigated: copper and nickel due to their conductive nature, compatibility with environment-friendly etching and electroless deposition properties [83].

a) Electroless plating of copper

Introduction

The electroless copper solutions incorporate one of a small number of reducing agents: formaldehyde, hypophosphite, borohydride, hydrazine or dimethylamine borane complex [84]. The majority of the plating baths use formaldehyde as the reducing agent [85], [86] and have high pH regimes (>12) which increases the deposition rate. However, aqueous alkaline solutions in which the pH-value exceeds 10 significantly attacks all AZ® cresol resins [87].

It was demonstrated by authors [86], [88] that dimethylamine borane complex (DMAB) can be run at a lower pH < 12. Moreover, it does not produce toxic fumes like formaldehyde. Therefore, the solution demonstrated by [88] was applied for Cu electroless plating on top of photoresist S1818.

Equipment

2 glass beakers 100 ml for the sensitisation and activation solutions,
250 ml glass beaker for the Cu electroless plating bath,
Hot plate stirrer,
Temperature sensor,
Metal stand,
Crocodile clip,
PVC insulation tape,
Magnetic stirring bean.

Chemicals

The sensitisation and activation solutions were prepared as follows [88]:

Sensitisation solution:

5g/l SnCl₂ + 10 ml/l HCl (conc.)

Activation solution:

0.1 g/l PdCl₂ + 0.1 ml/l HCl (conc.)

Electroless Copper Solution:

The copper electroless plating solution was prepared in the following manner [88]:

Copper (II) sulphate pentahydrate (CuSO₄ · 5H₂O) 2 g/l, Ethylenediaminetetraacetic acid (EDTA) 6 g/l, Ammonium hydroxide (NH₄OH) 50 ml/l, and Dimethylamine borane complex (DMAB) 4 g/l.

Experimental procedure for Cu electroless deposition

The Ti substrate coated with photoresist S1818 was masked with PVC insulation tape on the back side in order to allow sensitisation, activation and subsequent electroless deposition only on one side of the sample.

The specimen was then immersed in the sensitisation solution for 1 minute at ambient temperature. Then, the sample was rinsed with DI water and the procedure was repeated with the activation solution for 1 minute. Finally, the specimen was placed in the Cu electroless plating solution orientated in a vertical position. The plating bath was operated at pH = 10 at 50⁰C. The sample was plated for 70 minutes. The solution was stirred before and after immersion of the specimen.

Results and discussion

The positive photoresist S1818 did not dissolve at pH=10. During the experiments, the deposition of Cu appeared within the first 10 minutes of immersion in the solution. The fully coated samples were achieved after 70 minutes with thicknesses varying from 0.5 μm to 3.9 μm, measured with SEM.

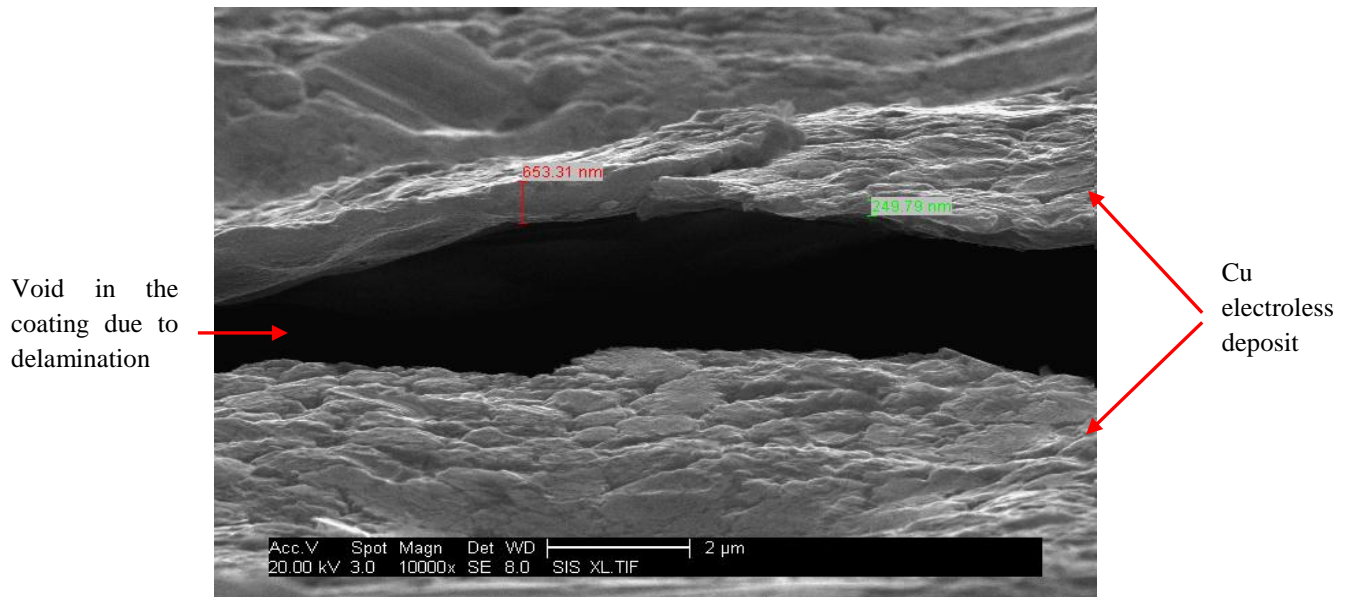


Figure 12: SEM micrograph of Cu electroless plated deposit with an indication of the thicknesses of the film.

It was proved from the processing of electroless deposited samples that photoresist S1818 withstood all conditions of the electroless Cu plating bath.

- **An alternative pre-treatment solution**

In the work of [89] the attempt was made to replace expensive activator PdCl_2 by AgNO_3 in order to reduce the cost of the plating process. Guo, et.al [89] used AgNO_3 with NH_4OH instead of the conventional solution of PdCl_2 with HCl to catalyse the reaction of Cu electroless deposition. The experiment, conducted on polyester fabrics, demonstrated a uniformly distributed and relatively dense metallic Cu layer after 20 minutes of plating at 30°C . Guo, et.al [89] proved that it was possible to successfully eliminate the use of the catalyst PdCl_2 .

Therefore, in order to improve uniformity of the Cu electroless coating as well as reduce the time of the deposition, the new pre-treatment solutions were examined.

Chemicals

The sensitisation and activation solutions were prepared in the following manner [89]:

Sensitisation solution:

10g/l SnCl₂ + 40 ml/l HCl (conc.)

Activation solution:

10 g/l AgNO₃ + 10 ml/l NH₄OH (28%)

The Cu electroless plating solution constituents remained the same [88].

Experimental procedure

A Ti specimen coated with S1818 resist and masked from the back side with insulation tape was immersed in the sensitisation solution at ambient temperature. After 10 minutes, the sample was removed and rinsed with DI water. Next, the specimen was placed in the activation solution for 20 minutes at ambient temperature. Before immersing the sample in the Cu electroless plating bath, it was rinsed with DI water and dried in an oven for approx. 30 s at 50⁰C. Finally, the activated specimen was placed in the plating bath with pH = 10 at 50⁰C for 120 s.

Results and discussion

The results of the conducted experiments showed that an application of the alternative sensitisation solutions: SnCl₂ + HCl (increased concentration of SnCl₂ and HCl) and the activation solution: AgNO₃ + NH₄OH lead to:

- Improvement of the adhesion of the Cu electroless deposit,
- Uniform Cu coating,
- Reduce time of electroless plating in comparison to route incorporating SnCl₂ + HCl and PdCl₂ + HCl pre-treatment solutions,
- Reduce costs of the chemicals used in the process (PdCl₂ is a very expensive compound which could cause a problem in commercialisation of the process).

It was verified that to obtain the uniform deposition of Cu on the S1818 resist the total time of immersion lasted 120 seconds. The thickness of the layer was 80 nm (as measured with Focused Ion Beam (FIB)).

The qualitative verification of Cu deposition taken by X-ray Diffraction (XRD) showed peaks indexed to Cu as in case of Cu where the solution with PdCl₂ + HCl was acting as the catalyst (see Fig.13 the comparison of XRD spectra).

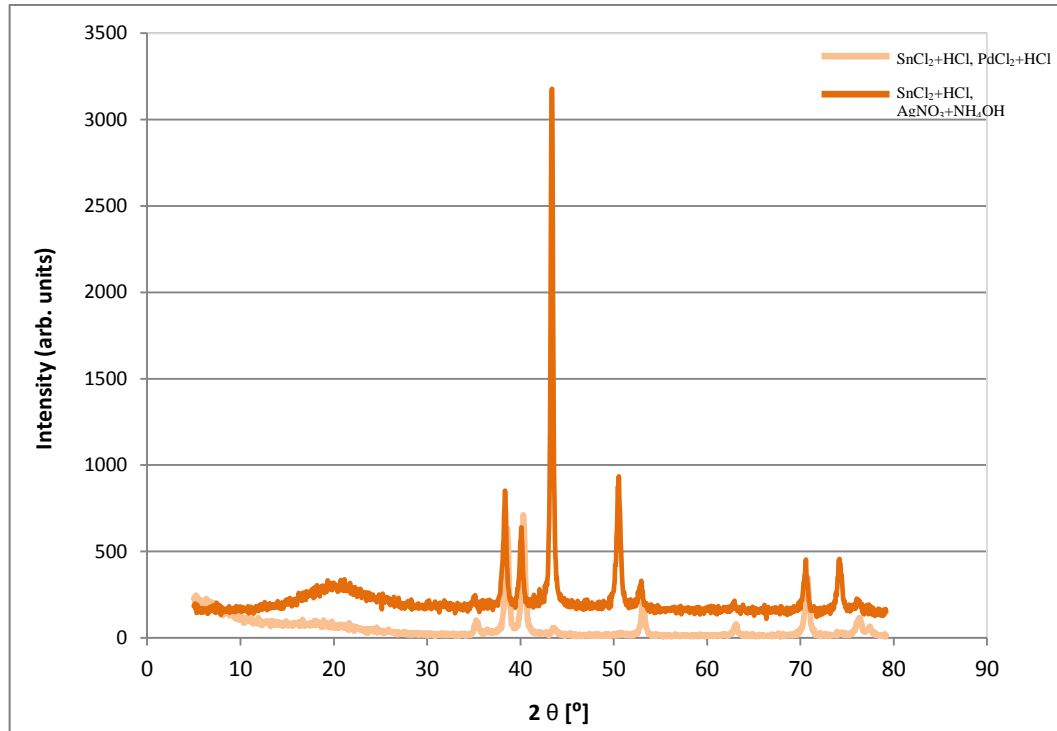










Figure 13. XRD spectra for the Cu depositions obtained from two differently activated samples. Peaks at $2\theta = 43.5^\circ$, 50.5° , and 74.0° represent Cu.

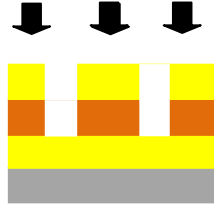


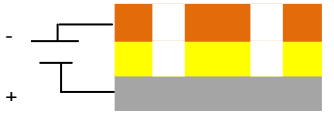


It can be seen from the XRD analysis of the two Cu electroless deposits that there are higher Cu peaks for the deposit obtained when the specimen was activated with AgNO₃+NH₄OH. This could indicate the denser Cu coating and better Cu crystallization.

- **Processing of the sandwich structure with the cathode obtained from the Cu electroless deposition**

Table 10 on the next page details the processing steps in order to achieve a “ready to etch” Ti sandwich structure with the Cu conductive layer. The Cu layer was deposited with the application of the alternative pre-treatment solutions mentioned on the page 67.

Table 10. Processing stages to obtain Ti/photoresist/Cu structure incorporating electroless copper process.

Procedure Equipment and parameters applied	Sandwich structure profile
1. Titanium preparation. Procedure described in 3.3.1	
2. Titanium coating with the positive photoresist S1818. (4 μm) – bottom layer Procedure described in 3.3.2	
3. Copper electroless plating on top of the photoresist. Prior to plating: sensitisation and activation. Plating parameters: Hot plate stirrer, Plating time = 120 seconds, T = 50°C	
4. Coating of second layer of the positive photoresist on top of copper layer. EMS spin coater, 4000rpm, t=60seconds	
5. UV exposure of the top photoresist through the mask. MA 56, UV lamps int. = 5mW/cm ² , t = 38 s	
6. Developing of the positive photoresist – top layer. MF-319 Developer, T=ambient, t= 80s	
7. Through-out etching of the patterned copper. Etchant: 35 ⁰ Bé FeCl ₃ , T=ambient, t=15s, beaker etching	
8. Microscope assessment of the sample. Nikon Optishot Acquisition System	

<p>Procedure</p> <p>Equipment and parameters applied</p>	<p>Sandwich structure profile</p>
<p>9. UV exposure of the photoresist through etched pattern in copper.</p> <p>MA 56, UV lamps int. = 5mW/cm², t = 40 s</p>	
<p>10. Developing of the bottom layer of positive photoresist. Simultaneous removal of exposed top layer of the S1818 resist.</p> <p>MF-319 Developer, T=ambient, t= 120s</p>	
<p>11. Microscope assessment of developed sample.</p> <p>Nikon Optishot Acquisition System</p>	
<p>12. DC electrolytic etching of the sample:</p> <p>DC power supply, CD = 27 A/cm², t = 2 minutes, T = ambient</p>	
<p>13. Stripping of the positive resist</p> <p>Stripper: acetone</p>	
<p>14. Microscope analysis of the etched titanium.</p> <p>Nikon Optishot Acquisition System</p>	

- **DC electrolytic etching**

The sample, consisting of the substrate, the photoresist S1818 and the cathode – built by electroless deposition, was the subject of the DC electrolytic etching.

Equipment:

DC power supply,

2 stainless steel crocodile clips,

2 copper wires with soldered copper pads in the end enabling connection with the crocodile clips,

Glass beaker 400 ml,

Hot plate stirrer,
Magnetic stirring bean,
Perspex jig,
PVC insulation tape.

Chemicals:

10% w/v HCl electrolyte

Experimental procedure:

The specimen was connected to the DC power supply in an electrolytic cell filled with the electrolyte, see Figure 10. The applied current density was 27 A/cm^2 applied for 2 minutes at ambient temperature.

Results and discussion

The DC electrolytic etching resulted in patterned Ti. The microscope examination revealed that Ti was etched and then anodised during the process, hence there were yellow circles around the etched pattern. The diameter of the transfer pattern was approx. $180 \mu\text{m}$, whereas the original diameter of the pattern was $125 \mu\text{m}$. The depth of the etched Ti could not be determined due to the Ti oxide created in the place of the transfer pattern.

Copper was successfully deposited from the electroless plating bath and utilised as the metal layer acting as the cathode in the sandwich structure. Further processing – DC electrolytic etching with the use of Cu cathode, proved the concept of an application of the sandwich structure in order to use less-hazardous etchant in order to pattern Ti but perfect etched features were not achieved.

b) Electroless plating of nickel

Introduction

Nickel is known as a good conductor (Table 6) and can be etched with chemicals such as: 42⁰Bé FeCl₃ at 49⁰C [70]. These properties were found desirable for the cathode layer in the sandwich structure.

Moreover, a pH = 5 of the nickel electroless plating solution, Nifoss 3000 [88], had met the requirements of the photoresist, as it can be operated in acidic or mild alkaline environment. Therefore, Ni electroless plating was tested in order to produce a conductive coating (the cathode) on the positive photoresist S1818.

Equipment

3 glass beakers 100 ml for the activation solutions,
250 ml glass beaker for the Ni electroless plating bath,
Hot plate stirrer,
Thermometer,
Metal stand,
Crocodile clip,
Insulation tape,
Magnetic stirring bean.

Chemicals

Activation:

- 0.5 g/l PdCl₂ + 50 ml/l HCl (conc.)
- 5g/l SnCl₂ + 10 ml/l HCl (conc.) and followed by 0.1 g/l PdCl₂ + 0.1 ml/l HCl (conc.)

Electroless plating bath:

A commercial Ni electroless plating solution Nifoss 3000 was used in the experiments [90].

Experimental procedure

Three different approaches were tested in order to receive a uniform Ni coating on the photoresist S1818.

Ti specimen was prepared by spin coating on the positive resist S1818 from one side of the sample the other side was masked with the insulation tape.

a) No surface pre-treatment of the photoresist

The first approach involved immersion of the Ti specimen in the Nifoss 3000 solution at 85 to 93⁰C without any pre-treatment of the surface.

b) Activation of the photoresist with PdCl₂ + HCl (conc.)

A second experimental approach incorporated the activation of the sample in the PdCl₂ + HCl (conc.) solution for 2 minutes. Then, the surface of the specimen was rinsed with DI water and dried in an oven. The activated specimen was placed in the electroless plating solution operated at pH = 5 and a temperature from 85 to 93⁰C.

c) Sensitisation and activation of the photoresist with SnCl₂ + HCl (conc.) and PdCl₂ + HCl (conc.)

The third procedure applied the sensitisation and the activation solutions, as they showed success in electroless Cu plating. They were used in order to reduce the Ni electroless plating time.

The experimental procedure involved sensitisation for 1 minute in SnCl₂ + HCl (conc.) solution followed by DI water rinse and 1-minute activation in PdCl₂ + HCl (conc.) solution. Prior to placing the sample in the Nifoss 3000 bath, it was rinsed once again with DI water and dried in the oven. The plating parameters remained the same as for the previous experiments.

Results and discussion

a) The first approach resulted in no Ni deposition present on the surface of the S1818.

b) In the second instance, it was possible to obtain a fully-coated sample. However, it was found that Ni plating on the photoresist is a long process. In order to plate Ni with the Nifoss 3000 over the whole area (2 x 5 cm) of the S1818, the sample had to be immersed in the solution for 8 hours.

A XRD analysis demonstrated a well-crystallized Ni deposit. Figure 14 shows the XRD of the obtained coating.

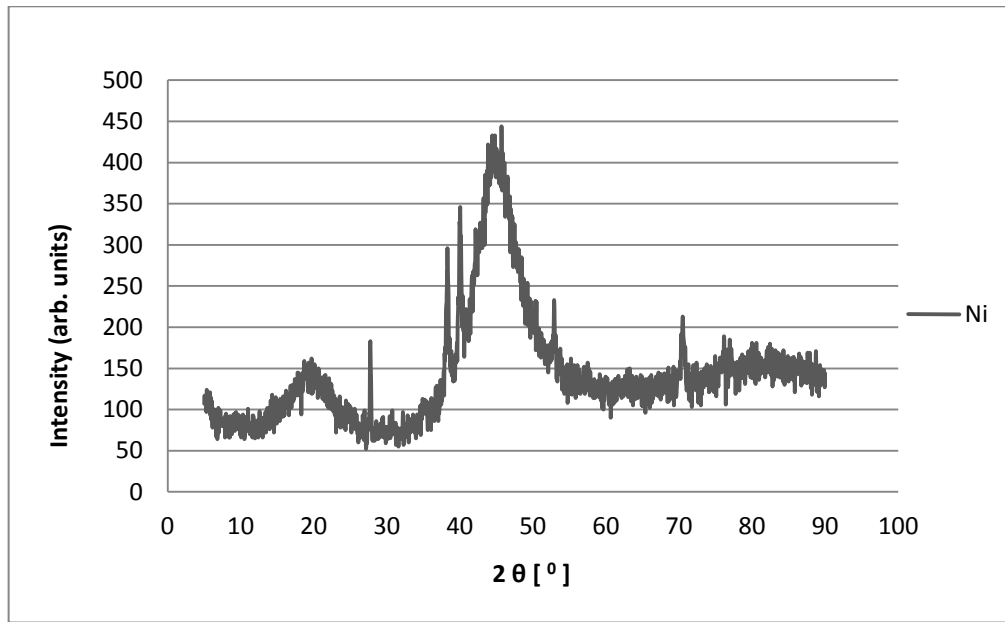


Figure 14: XRD spectrum of nickel electroless deposition.

Peaks at $2\theta = 44.5^\circ$, 51.8° , and 76.4° represent Ni.

The analysis of the deposit conducted with SEM and Focused Ion Beam (FIB) indicated different thicknesses of the Ni film varying from 3.4 μm to 7.5 μm .

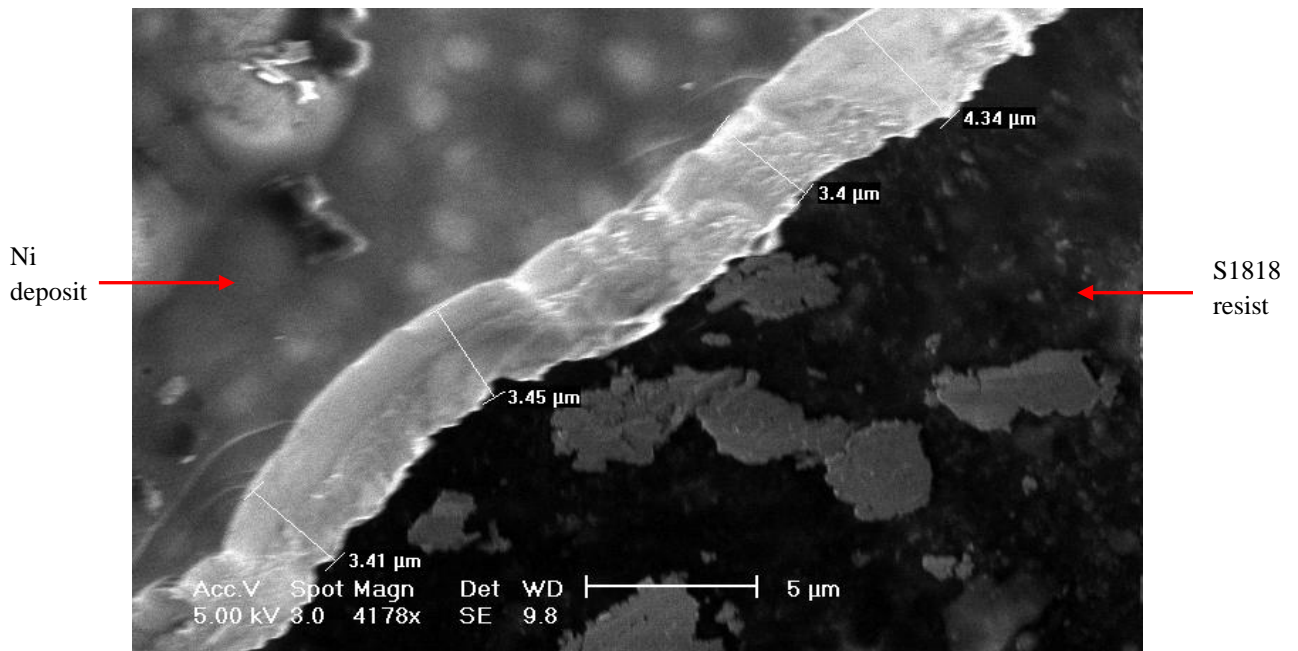


Figure 15: SEM micrograph of Ni electroless plated deposit with an indication of the thicknesses of the film.






c) In the third procedure, it was verified that $\text{SnCl}_2 + \text{HCl}$ (conc.), $\text{PdCl}_2 + \text{HCl}$ (conc.) did not have any positive impact on the plating results. What is more, there was no single sample obtained with nickel plated over the whole area of the photoresist from this variation to the experiments.




The sample obtained from the experiment incorporating activation of the photoresist S1818 with $\text{PdCl}_2 + \text{HCl}$ (conc.) (route b)) was the subject of further processing aimed at fabrication of the “sandwich structure” enabling Ti electrolytic etching.

- **Processing of the sandwich structure with the cathode obtained from the Ni electroless deposition**

Table 11 presented below details the process steps incorporating the electroless nickel plating and further fabrication steps of the sandwich structure.

Table 11. Processing stages to obtain Ti/photoresist/Ni sandwich structure incorporating nickel electroless plating process.

Procedure Equipment and parameters applied	Sandwich structure profile
1. Titanium preparation. Procedure described in 3.3.1	
2. Titanium coating with the positive photoresist S1818 – bottom layer. Procedure described in 3.3.2	
3. Nickel electroless plating on top of the photoresist. Hot plate stirrer, Plating time = 8 hrs, T = 85 - 93°C	
4. Coating of second layer of positive photoresist on top of nickel layer. EMS spin coater, 4000rpm, t=60s	
5. UV exposure of the top photoresist through the mask. MA 56, UV lamps int. = 5mW/cm ² , t = 38 s	

Procedure Equipment and parameters applied	Sandwich structure profile
6. Developing of the positive photoresist – top layer. MF-319 Developer, T=ambient, t= 80s	
7. Etching through the patterned nickel. Etchant: 42% FeCl ₃ , T=49°C, t=1.5 hrs, beaker etching.	
8. Microscope assessment of the sample. Nikon Optishot Acquisition System	

Results and conclusions

After obtaining a deposit on the resist (from the experiment using PdCl₂ + HCl (conc.) as the activation solution, it was found that it was impossible to etch an imaged pattern through the nickel layer. The microscope examination of the nickel coated sample revealed damaged photoresist underneath.

The Ni electroless plating showed many difficulties in processing such as a long plating time in comparison to Cu electroless deposition. In addition to this, the positive resist S1818 did not withstand the immersion in the nickel plating bath at temperature from 85 to 93°C. Therefore, this method of utilisation of the cathode was suspended.

Results and conclusions to the electroless processes

The electroless plating of two metals: Cu and Ni, was verified as the method of obtaining the cathode layer on the positive resist S1818. It was possible to deposit metals from both electroless solutions, however, Ni electroless deposition showed complications due to the operating conditions and repeatability of the plating.

The Cu electroless plating with the applications of two alternative pre-treatment solutions were found to be the sandwich structure compatible method of obtaining the cathode layer.

Summary

The route of obtaining the sandwich structure was determined in this Chapter. The permanent arrangement of the anode/insulator/cathode was developed. The materials for the dielectric layer and the cathode were analysed and empirically verified. Two techniques of metallisation of the non-conductor layer were investigated: RF sputtering and electroless deposition. Sputtering was eliminated, as the process revealed an incompatibility with the positive resist used as the insulator. The second route of the metal deposition, electroless plating, showed potential as the most economical and time efficient method of obtaining a conductive layer. Copper electroless plating was determined as the process to be employed in a fabrication of the cathode layer in the “sandwich structure”.

The results of the conducted experiments focused on building the sandwich structure, applying the lithographic process to pattern Ti, and finally, on DC electrolytic etching the substrate, proved the concept of the structure and enabled the use of less hazardous etchant, such as 10% w/v HCl.

The following chapters will present the established “sandwich structure” comprising of the Ti substrate (anode), a positive photoresist S1818 (insulator), and the copper coating (cathode). They have been broken down into the three chapters. The separate Chapter has been dedicated to the microfabrication process of the complete sandwich structure.

The layout of the experimental methodology was dictated by the layers order of the “sandwich structure”.

Chapter 4. Experimental procedures – stage 1 of sandwich structure building using titanium as the anode

4.1 Introduction

a) Ti classes

Titanium alloys, classified as: α , β , and $\alpha+\beta$, corresponding to hexagonal close-packed (hcp) crystal structure, body-centered cubic (bcc) crystal structure, and mixture of $\alpha+\beta$, have different properties, which are determined by the arrangement, volume fraction, and individual properties of the two phases α and β . The physical, mechanical, and technological properties of the three alloy classes have been outlined in Table 12.

Table 12. Properties of α , $\alpha+\beta$ and β Ti alloys [9].

Property/Phase	α	$\alpha+\beta$	β
Density	+	+	-
Strength	-	+	++
Ductility	-/+	+	+/-
Fracture toughness	+	-/+	+/-
Creep strength	+	+/-	-
Corrosion behaviour	++	+	+/-
Oxidation behaviour	++	+/-	-
Weldability	+	+/-	-
Cold formability	--	-	-/+

Where: ++ corresponds to very good; + corresponds to good; -/+ corresponds to average

According to the presented properties, Ti α alloys exhibit superior corrosion resistant behaviour compared with $\alpha+\beta$ or β alloys. Hexagonal α can also be characterized by the higher resistance to plastic deformation and reduced ductility. Its diffusion rate is at least two orders of magnitude lower than body-centered cubic β [9].

In contrast to α alloys, $\alpha+\beta$ and β alloys have high and very high strength achieved by hardening.

b) Chemical composition of Ti α alloys

One of the factors that determine titanium alloys' properties is the chemical composition.

The cp titanium grades of unalloyed titanium are fully alpha alloys of metal and non-metal. The various cp Ti grades differ in oxygen content, which is intentionally alloyed. Other elements like carbon and iron are considered impurities brought during the manufacturing process. The additional elements of α alloys are the α -stabilizing element aluminium and the neutral elements tin and zinc.

The detail chemical composition of the cp Ti alloys compared with the most popular Ti alloy ($\alpha+\beta$) has been presented in Table 13.

Table 13: Chemical compositions of four cp Ti alloys compared with $\alpha+\beta$ alloy [10].

Element	Grade 1	Grade 2	Grade 3	Grade 4	Ti6Al4V ^a
Nitrogen	0.03	0.03	0.05	0.05	0.05
Carbon	0.10	0.10	0.10	0.10	0.08
Hydrogen	0.015	0.015	0.015	0.015	0.0125
Iron	1.20	0.30	0.30	0.50	0.25
Oxygen	0.18	0.25	0.35	0.40	0.13
Titanium	Balance				

^a Aluminium 6.00% (5.50 – 6.50), vanadium 4.00% (3.50 – 4.50) and other elements 0.1% maximum or 0.4% total.

- Ti (cp), grade 2

Due to its excellent corrosion resistance, Ti grade 2 is commonly used for corrosion-resisting structural applications for chemical processing. It is also applied in aerospace, marine as well as medical industry [9], [91].

The most widely used unalloyed titanium grade 2, was selected, by the sponsor company of the project, as the subject of this research. Ti, commercially-pure (cp), grade 2 was used as the anode in the process of fabrication of the novel “sandwich structure”.

The chemical composition of the Ti grade 2 used in the experiments, has been outlined in Table 14.

Table 14: Chemical composition of the investigated Ti substrate [73].

C	N	Fe	O	H	Ti
0.01%	0.04%	0.08%	0.15%	0.0094%	Balance%

It should be noted that Ti, grade 2 has a minimum Ti content requirement of 98.905% [91].

4.2 Titanium substrate preparation

4.2.1 Titanium sanding

Titanium (grade 2) sheets, dimensions: 0.250 mm x 197 mm x 300 mm supplied by Datum Alloys Ltd. [73] were manually sanded with SiC papers: 220 and 400 grit size in order to remove the inherent titanium dioxide layer. Then, the titanium sheets were cut into 40 mm x 50 mm pieces with a guillotine.

4.2.2 Cleaning

The Ti sanding procedure was followed by cleaning of the cut pieces in order to remove inorganic and organic contamination from the surface.

The specimens were soaked in 2% Micro-90® solution for approx. 24 hours and then, immersed in acetone with an applied ultrasonic agitation (40 kHz) for 10 minutes. The final stage of cleaning was spraying with DI water and drying with a compressed air gun.

4.2.3 Electrical resistivity measurements of Ti substrate

Titanium possesses high electrical resistance compared to silver (see Table 6). In addition, its natural ability to develop titanium dioxide (Resistivity (ρ) = 10^{12} $\Omega\cdot\text{cm}$ [92]) decreases its conductivity.

Minimising the resistivity of the substrate, improves the electrolytic etching process. Therefore, manual sanding of titanium was applied in order to remove the oxide layer and to improve its conductivity.

Equipment

A “four- point probe” was selected as a convenient tool for the measurement of resistivities [93]. The following set-up of the equipment was used to measure the electrical resistivity of Ti specimens: Four-Point Probe, DC power supply, and Multimeter ISO tech IDM 91E.

Experimental procedure

The resistivity of the as-received and sanded Ti specimens was measured by applying the set current of 4.53 mA and reading the voltage on the Multimeter in mV. Three readings were taken per sample from three different parts of the specimen (top, centre, and bottom). Then, the mean of the measurement was calculated with a standard deviation.

The resistivity (ρ) was calculated according to the equation:

$$\rho = 4.53 \frac{V t}{I} \quad (\Omega \cdot \text{cm}) \quad (7)$$

Where:

V – measured voltage (V),

t – thickness of the specimen (cm),

I – current (A)

Results and discussion

The following results were obtained for the as-received and sanded titanium samples.

Table 15: The measured resistivity with standard deviation of the as-received and sanded titanium samples.

Ti sample	Resistivity ($\Omega \cdot \text{cm}$)	Standard deviation
As-received	$5 \cdot 10^{-5}$	$5.77 \cdot 10^{-5}$
Sanded	$4.32 \cdot 10^{-5}$	0

The registered resistivities indicate that the incorporated Ti oxide removal process using grit papers resulted in the lower resistivity of the titanium.

4.2.4 Roughness measurements

The surface roughness of the Ti has an effect on the roughness of the subsequent process layers, which are deposited on top of the substrate. What is more, the roughness of the Ti determines an adhesion of these coatings. Therefore, roughness was a subject of the analysis of the as-received and sanded Ti samples.

Equipment

Surface roughness measurements were conducted with an Olympus Lext Confocal Laser Scanning Microscope. The system consists of an optical microscope and laser scanner. The laser is a Class 2 with a wavelength of 400 nm. Both the optical microscope and the laser are controlled by a computer system which is used to produce a quantitative 3D image of surface [94].

Experimental procedure

Five measurements were taken from the scan. Then, a mean was calculated and a standard deviation.

Results and discussion

Figure 16 presents the results obtained from the roughness measurements. The images show the surface finish of as-received and sanded samples taken with SEM.

The manually sanded of the Ti specimen resulted in a shinier surface with an increase of the roughness of 60%.

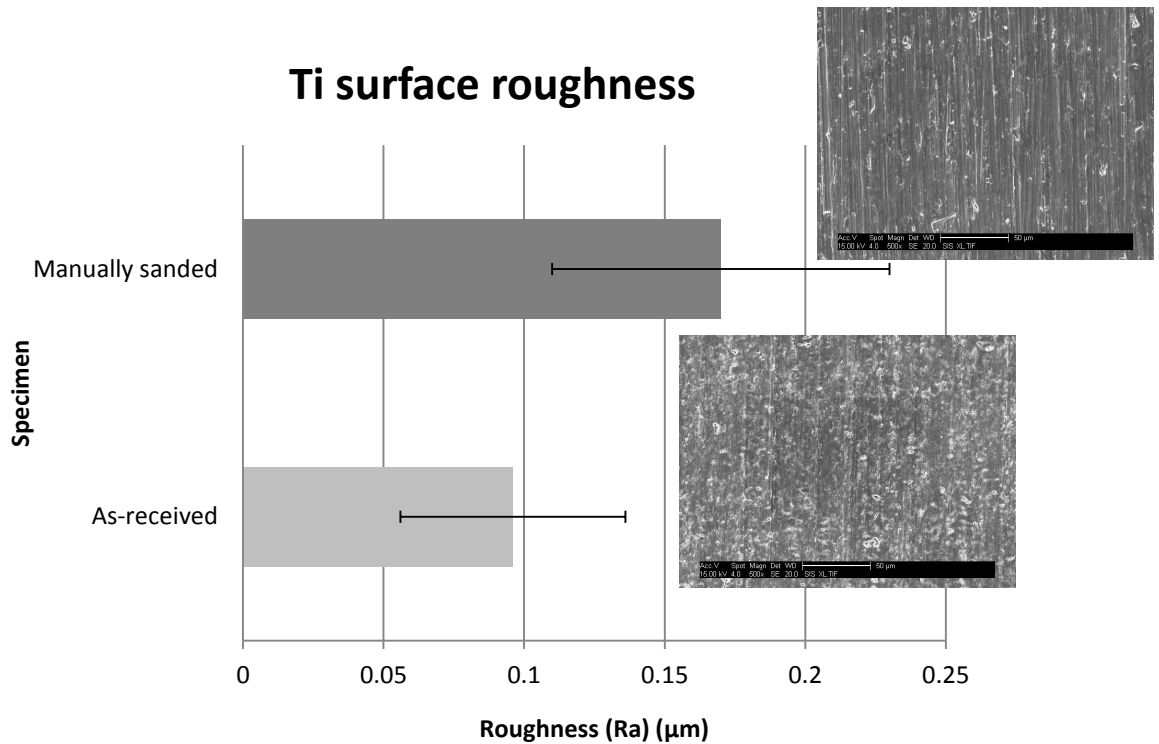


Figure 16: Surface roughness of the as-received and sanded Ti samples with the corresponding SEM micrographs of the surface textures.

In order to evaluate the grinding effect on removing the initial oxide layer of Ti, the XRD analysis was conducted.

4.2.5 XRD analysis

The difference between Ti specimens: as-received and manually sanded was studied by conducting the X-ray analyses with the use of SIEMENS D5005 X-Ray Diffractometer.

Results and discussion

The following spectra were obtained for the two investigated Ti specimens.

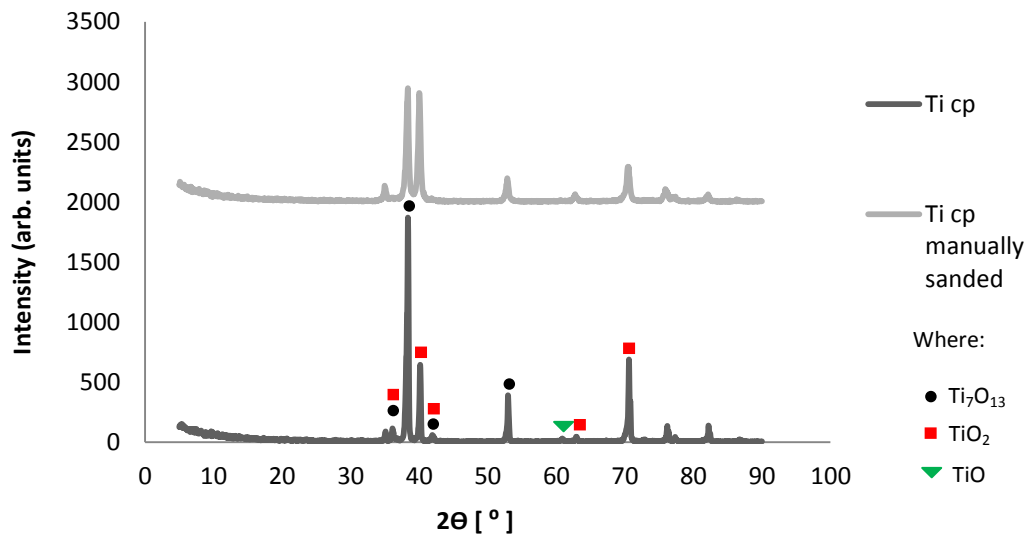


Figure 17: XRD spectra for the as-received and manually sanded Ti samples. All peaks, on the spectrum of the Ti manually sanded specimen, represent Ti.

Titanium can reach valence numbers up to 4^+ , hence there are many possible oxidation stages [95]. It undergoes a series type of oxidation sequence. The oxide states change from lower to higher as oxidation progresses and as temperatures rises [96]. The following oxides states are formed by Ti:



Moreover, the morphology and composition of oxide films on titanium alloys depend on the type of surface treatment applied [96].

It can be seen from the XRD spectrum of the as-received specimen that three titanium oxides were detected: Ti_7O_{13} , TiO_2 , and TiO . TiO_2 and the Magnèli Phases, the oxides between $\text{Ti}_{10}\text{O}_{19}$ and Ti_4O_7 , represent high oxidation stages of titanium [95]. TiO_2 was found in three phases: rutile ($2\theta = 36^\circ, 42^\circ, 63^\circ$), anatase ($2\theta = 70.5^\circ$), and brookite ($2\theta = 40^\circ$).

The XRD analysis of the manually sanded Ti specimen revealed that all three oxides types found in the as-received Ti sample with the X-ray spectroscopy were successfully removed.

4.2.6 Ti microstructure

Ti microstructure was a subject of the analysis. The aim was to investigate the possible change in microstructure during Ti manual sanding. Two samples, Ti as-received and sanded, were prepared in order to see their grains and then analyse under the optical microscope.

Experimental procedure

Two Ti samples: as-received and sanded, were sectioned with the Guillotine. The size of prepared specimens was approx: 2 x 2 cm.

a) Polishing of the Ti samples

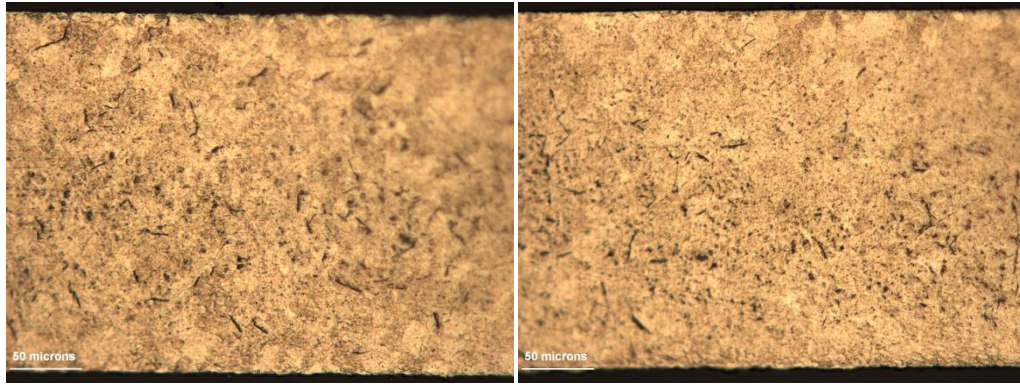
The cross-sectioned Ti specimens were mounted in the epoxy resin and left to cure. After 48 hrs, the specimens were polished with a Grinder-Polisher, Buehler Meteserv Motopol 12. The samples were polished with the following grit papers: P240, P1200, P2500, and P4000. The polishing speed was set at 150 rpm for 2 minutes. The final polishing with the use of P4000 at 100 rpm was conducted with the addition of OP-S Suspension and followed with OP-A Suspension in order to achieve a smooth and scratch-free surface on the cross-sectioned titanium specimens.

b) Etching of the samples etching

In order to distinguish grain boundaries in the investigated metal, the cross-sectioned Ti samples – surface sanded and as-received, were etched with Kroll's solution, which contained: 10 ml HF, 5 ml HNO₃, and 85 ml H₂O [97]. The reagent was applied by swabbing the Ti samples for 15 seconds and then it was rinsed off with tap water.

c) Microstructure analysis

An optical microscope Nikon Eclipse ME-600 was used for an investigation of the metallographic Ti specimens. The analysis conducted on the processed samples revealed the following microstructures.



a)

b)

Figure 18: Microstructure of the etched cross-sectioned cp-Ti samples; a) as-received specimen, b) sanded specimen.

The conducted microstructure examinations of the Ti specimens showed no change in the grain size or boundaries.

Summary to chapter

The established processing stages of the titanium, grade 2 were presented in this Chapter.

The manual sanding of the substrate was introduced with the cleaning regime.

The sanding was confirmed, by the XRD analysis, to remove the inherent titanium oxides that exist on the Ti surface. The titanium specimen with removed oxides (sanded) showed slightly lower resistivity than the as-received titanium sample. No change in the Ti microstructure appeared to be induced by the manual sanding procedure.

Chapter 5: Experimental procedures – stage 2 of sandwich structure building using photoresist as a dielectric

Introduction

According to the results of the experimental work, dedicated to the selection of the dielectric material (Chapter 3.2.1), it was found that the positive tone photoresist can be applied in the sandwich structure as an insulator. It meets process requirements by being resistant to electric current and compatible with the chemical deposition process used to make the copper cathode. In addition to this, it allows processing of the sandwich structure through selective patterning, developing, and etching. Moreover, the positive photoresist is more environment-friendly due to the use of aqueous developers [29] and organic strippers [70].

The S1818 photoresist was selected as the dielectric layer between anode (workpiece) and cathode and as the photosensitive layer applied on top of the copper layer, Figure 19.

The top layer of the S1818 photoresist allows selective patterning of the sandwich structure layers.

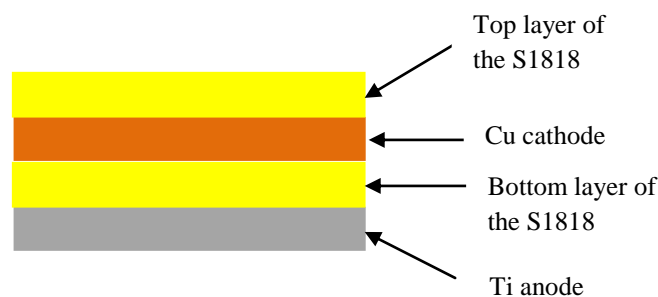


Figure 19: Cross section of the complete sandwich structure prior patterning.

5.1 S1818 constituents characterisation

The S1818 belongs to the family of two-component positive resists, consisting of a Novolac and a diazonaphthoquinone photoactive compound (PAC) [98].

The Novolac is a cresol resin synthesized from phenol and formaldehyde [87]. The properties of the resist, such as: film-forming, adhesion, chemical and thermal resistance characteristics, are influenced by the molecular chain length [87], [98]. Long chains improve the thermal

stability; reduce the “dark erosion” and the development rate. Short chains improve the adhesion, but also are responsible for lowering softening temperature [87]. The Novolac resin is soluble in organic solvents as well as in aqueous base solutions [98].

The radiation chemistry, responsible for the resist’s photochemical reaction, occurs in the PAC. The PAC of the S1818 belongs to the group of diazonaphthoquinone-sulphonates (DNQ-sulphonate) [87]. An arylsulphonate is a substituent of the diazonaphthoquinone. It is also referred to as a “ballast” group, which influences the solubility characteristics of the sensitizer molecule and has an impact on the absorption characteristics of the chromophore [98].

DNQ-sulphonate presence in photoresist reduces its alkaline solubility, compared with pure Novolac resin, and makes it soluble only in organic solvents but insoluble in aqueous base [87], [98]. However, the DNQ-sulphonate upon exposure to matched UV-light (typically < 440 nm) transforms into a carboxylic acid, accompanied by the release of nitrogen and the absorption of water [87]. The photoproduct is extremely soluble in aqueous base solutions due to the carboxylic acid functionality [98].

Positive photoresist formulations consist of the Novolac resin and the DNQ-sulphonate dissolved in an organic solvent. The solvent of the S1818 photoresist is propylene-glycol-mono-methyl-ether-acetate (PGMEA) [87]. It acts as a main ingredient of the photoresist due to the concentration of approx. 55 – 85 %. During softbake, the remaining solvent concentration decreases to approx. 5 %.

In addition to the mentioned ingredients, the positive photoresist may also contain anti-oxidizing and levelling agents, as well as adhesion promoters.

5.1.2 Chemical composition of the S1818 resist

The positive photoresist MICROPOSIT™ S1818 (referred to as S1818 resist) is a liquid of a red amber colour with characteristic ester-like odour. It has neutral pH, boiling point ca. 146 °C and flash point of 40 to 46 °C [74].

The S1818 resist physical and chemical properties are the departure of the properties of its constituents.

The chemical composition of the S1818 resist applied throughout the research has been outlined in Table 16.

Table 16. Chemical composition of the positive photoresist MICROPOSIT™ S1818 [74].

Component	Concentration
Electronic grade propylene glycol monomethyl ether acetate	65.0 - 95.0 %
Mixed cresol novolac resin	< 30.0 %
Diazo photoactive Compound	1.0 – 10.0 %
Fluoroaliphatic Polymer Esters	< 1.0 %
Cresol	< 0.9 %

a) Propylene glycol monomethyl ether acetate

$C_6H_{12}O_3$ - Propylene glycol monomethyl ether acetate (PGMEA) acts as a solvent and is the main constituent of the S1818 resist. It is a colourless, hygroscopic liquid, with characteristic odour [99]. The PGMEA belongs to flammable substances which react with strong oxidants. It can form explosive vapour/air mixture above 42 °C, therefore the PGMEA should not be exposed to open flames, sparks, or heat [99], [100].

b) Mixed cresol novolac resin

The empirical formula of cresols is C_7H_8O . They represent isomeric substituted phenols with a methyl substituent at either the ortho (2-methyl phenol, o-cresol), meta (3-methyl phenol, m-cresol) or para (4-methyl phenol, p-cresol) position relative to the hydroxyl group. They exhibit similar chemical properties to phenol and undergo electrophilic substitution reactions at the vacant ortho or para position relative to the hydroxyl group [101]. The o-cresol and p-cresol can occur either as a solid or in a liquid form, whereas the m-Cresol occurs only as a liquid. They all have phenol-like odour and are soluble in the solvents such as: ethanol, ethyl ether, acetone, benzene, and aqueous alkali hydroxides.

The novolac resin can contain two different cresols: m-cresol and p-cresol [102]. According to [103], m-cresol and p-cresol incorporated into the resin affect important properties such as resist photospeed.

More importantly, the novolac copolymer with an optimum percentage of m-cresol and p-cresol (around 60:40) is useful for positive photoresist formulations, due to the fact that it increases the alkaline solubility of the novolac resin [104].

c) Diazo photoactive compound

The DNQ derivative is commonly used as the PAC in the positive photoresists mixtures. The base-insoluble sensitizer - DNQ, is commercially available in the following formulations:

- Sodium 1,2-naphthoquinonediazide-5-sulfonate, $C_{10}H_6N_2O_4S \cdot Na$;
- 1,2-Naphthoquinonediazide-5-sulfonyl chloride, $C_{10}H_5ClN_2O_3S$;
- 2,3,4-Trihydroxybenzophenone tris(1,2-naphthoquinonediazide-5-sulfonate), $C_{43}H_{22}N_6O_{13}S_3$;
- 2,3,4-Trihydroxybenzophenone 1,2-naphthoquinonediazide-5-sulfonate, $C_{13}H_{10}O_4 \times C_{10}H_6N_2O_4S$.

The five-substituted derivatives of DNQ was found to exhibit the strongest absorption at the wavelengths of mercury emission lines of 365 nm and 405 nm and a lower absorption at 436 nm [105].

d) Fluoroaliphatic polymer esters

Fluoroaliphatic polymer esters are the compounds of a fluorinated hydrocarbon nonionic surfactant [106]. Fluorosurfactants are used in nonaqueous media, i.e. adhesive formulations [107].

5.2 Processing stages of the S1818 resist in the sandwich structure

There are two layers of the S1818 resist applied in the sandwich structure (see Fig.19). Therefore, the processing stages of the S1818 resist have been split in order to allow transfer of a pattern down to the Ti substrate (an anode) whilst maintaining the insulating properties of a photoresist.








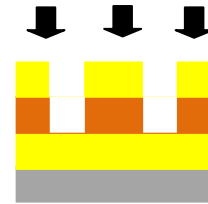

The S1818 resist:


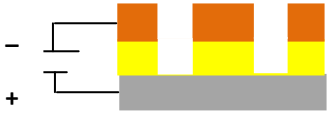
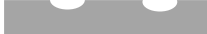

- a) Top layer of the resist: transfers pattern to the cathode.
- b) Bottom layer of the resist: separates cathode from anode and transfers pattern to the anode (Ti).

Through a combination of a) and b) the “geometry” in the shaped cathode is ultimately imparted to the Ti anode.

The detailed process steps for the Ti sandwich structure, incorporating the S1818 resist processing have been outlined in Table 17.

Table 17: Process steps for the fabrication of the sandwich structure with an indication of the photoresist processing conditions.

Procedure Equipment and parameters applied	Sandwich structure profile
1. Titanium preparation. Procedure described in 3.3.1, 3.3.2	
2. Ti coating with positive photoresist S1818 (4µm thick)– bottom layer photoresist	
3. Deposition of Cu layer	
4. Coating of second layer of positive photoresist (1.8µm) on top of Cu layer. EMS spin coater, 4000rpm, t=60s.	
5. UV exposure of top photoresist through the mask. Mask Aligner (MA) 56, UV lamps int. = 5mW/cm ² , 38 s.	
6. Developing of the positive photoresist (top layer). MF-319 Developer, T=ambient, t= 80s, beaker developing.	
7. Etching through the patterned Cu. Etchant: 35 ^o Bé FeCl ₃ , T=ambient, t=15s, beaker etching.	
8. UV exposure of positive photoresist (bottom layer) through the etched pattern in Cu. MA 56, UV lamps int. = 5mW/cm ² , 40 s.	
9. Developing of positive photoresist (bottom layer). MF-319 Developer, T=ambient, t= 120s	

Procedure Equipment and parameters applied	Sandwich structure profile
10. Microscope assessment of developed sample. Nikon Optishot Acquisition System	
11. DC electrolytic etching of the sample. DC power supply, $CD = 30 \text{ A/cm}^2$, $t = 2 \text{ min.}$, $T = \text{ambient}$	
12. Stripping the positive photoresist. Stripper: acetone	
13. Microscope assessment of the sample. Nikon Optishot Acquisition System	

5.2.1 Photoresist coating

Spin coating was selected to apply the S1818 resist onto the Ti substrate (anode) and Cu layer (cathode) in the sandwich structure. This method has long been accepted as the best approach to obtain a uniform, adherent, defect-free polymeric film over the entire substrate [98].

The Ti specimen (dimensions: 4 x 5 cm) was placed on a chuck in an EMS vacuum spinner model 4000. Next, the MicropositTM S1818 Positive Photoresist [74] was applied on to the Ti specimen with a plastic pipette by a flooding the entire sample with the resist solution prior to spinning (static dispense). Finally, the programmed spinner was adjusted to give a 4 μm thick coating for bottom layer resist and a 1.8 μm thick coating for top layer resist, respectively (see Fig. 19).

All S1818 photoresist spin coating conditions have been summarised in Table 18.

Table 18: The S1818 resist spin coating conditions using the EMS vacuum spinner.

S1818 resist layer	Start delay	No of steps	Ramp	Speed (rpm)	Dwell	Final ramp	Stop delay	Resist thickness (μm)
Bottom	0	1	50	1000	60	0	0	4
Top	0	1	50	4000	60	1	0	1.8

Ramp refers to the acceleration or deceleration rate of the rotating chuck. Ramp can have values programmed up to 250, whereas, a final ramp can have values of up to 100. The ramp = 50 is a very quick acceleration. When only a single step process is programmed, the ramp value of the step determines both the acceleration and the deceleration of the process [108].

During spin coating, the solvent concentration drops and saturates at a value of approx. 15 – 25 % which depends on the film thickness and is higher for thicker coatings. The subsequent softbake (prebake) reduces the remaining solvent concentration to the value of approx. 5 % [87].

5.2.2 Softbake

The softbake is used prior to UV exposure in order to remove residual solvent and to anneal the built-in stress caused by the shear forces encountered during the spin coating process. The evaporation of the solvent from the photoresist is crucial [87]:

- It prevents subsequent mask contamination and/or sticking to the mask,
- Prevents foaming of the resist due to N_2 created during exposure,
- Improves resist adhesion to the substrate,
- Minimises dark erosion during development,
- Prevents “bubbling” of the resist during subsequent thermal processes.

The softbake optimisation of the S1818 resist has been described in the section 4.3. Where, heating equipment, temperature and time of the soft bake were investigated.

5.2.3 Exposure

The correct exposure time for the photoresist is important for transferring a good image from the mask on to the photoresist-coated sample. Over-exposure of a photoresist will lead to difficulties in maintaining correct line widths, whereas, under-exposure will create problems in developing the image [109].

The UV exposure of the S1818 photoresist layers applied in the sandwich structure was conducted with a Karl Suss MA56 Mask Aligner.

- Phototool

During the photolithography process, UV radiation transfers the pattern from the phototool (photomask) to the photosensitive resist.

In the experimental work, a chrome-on-glass photomask was incorporated. This type of phototool is usually produced by sputtering chromium metal onto a glass sheet, coating with photoresist, UV exposure from a silver emulsion master, developing the resist image and finally etching the chromium film [70]. The advantages of using the chrome-on-glass photomask are: dimensional stability, durability and as a result suitability for long production uses [67]. However, disadvantages include brittle nature of glass.

A chrome-on-glass photomask with a pattern of circular arrays 16 x 16, with a single circle of \varnothing 125 μm was used throughout the experimental work in order to transfer image to the Ti substrate. The pattern consists of the circles at a distance of 375 μm from each other in the array and 1.73 mm from the neighbour array, according to the optical measurements conducted with a Nikon Optishot Microscope.

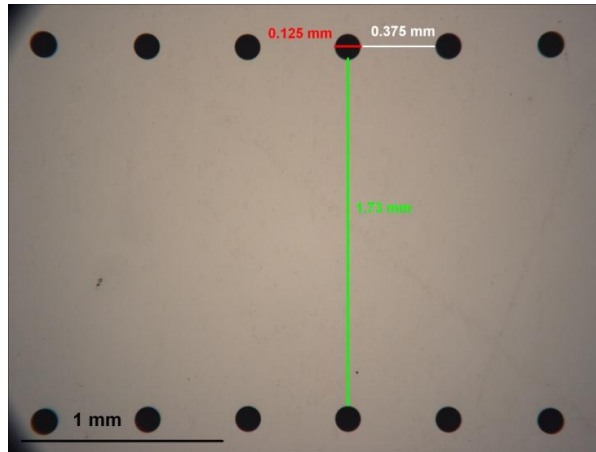


Figure 20. An optical micrograph of the chrome-on-glass pattern used for the sandwich structure patterning.

5.2.4 Development

Development of the positive photoresist coating consists of dissolving away areas of the photoresist that were exposed to the UV light. The S1818 was developed by immersion in a tank (dimensions of approx. 12 x12 x 5 cm) filled with a proprietary solution of Microposit® MF®-319 Developer [109]. This is an alkaline corrosive solution containing tetramethyl ammonium hydroxide. It is designed for high resolution semiconductor device fabrication [109].

The development process was performed at the following conditions: ambient temperature, development time: 80 s. for top layer of the S1818 and 120 s. for bottom layer of the S1818, assisted with a mild agitation. After the development, the specimens were rinsed with DI water followed by blow drying with a N₂ gun.

5.2.5 Hardbake

This process is aimed at drying off the resist completely and increasing the thermal and chemical stability of developed photoresist structures for subsequent processes [70], [87].

The hardbake optimisation of the S1818 resist has been described in the section 4.3. Where, the heating equipment, temperature and time of the bake were analysed.

5.2.6 Photoresist removal

The final step in the lithographic process is resist stripping [98]. Its' purpose is to remove the photoresist from the metal substrate without staining or corroding the metal surface [70].

The use of acetone accompanied by ultrasonic agitation (40 kHz) was used to strip the S1818 from the Ti substrate. This final step of the sandwich structure processing, simultaneously removes the deposited Cu cathode by dissolving the underlying bottom layer of S1818 (this is known as a lift-off process).

5.3 Baking stage optimisation of the S1818 resist

Introduction

An optimal temperature and time as well as suitable heating equipment are required for conducting the soft and hardbaking of the photoresist.

Too short/cool or too long/hot soft/hardbaking causes deterioration in processability of the resist.

Insufficient time and temperature during softbake can result in N₂ formation during exposure and the creation of bubbles in the resist structure. Moreover, the remaining solvent concentration increases dark erosion.

Hardbaking performed above 120 °C can cause embrittlement due to the variation between thermal expansion coefficients of both substrate and resist. Too high a temperature can also lead to thermal cross-linking of the photoresist making it more difficult to develop.

In addition to this, above the softening point, the resist structures start rounding off (flowing).

It is also crucial, to use baking hardware that ensures temperature control, cleanliness and that transfers the heat uniformly to the whole area of the specimen.

According to the literature, the following temperatures and times were applied for soft/hardbaking of the S1818 photoresist with respect to its thicknesses and type of used heating equipment:

Table 19: Review of applied temperatures and time to soft/hardbake of the S1818 photoresist.

	Hotplate	Oven
Softbake	<ul style="list-style-type: none"> - Thickness: 1.65 μm 110 \pm 5$^{\circ}\text{C}$ for 45 \pm 5 sec. [110] - Thickness approx. 1.8 μm 95 $^{\circ}\text{C}$ for 1 min. [111] - Thickness: 2 μm 120 $^{\circ}\text{C}$ for 2.5 min. [112] 	<ul style="list-style-type: none"> - Thickness: 1.65 μm 95 \pm 5$^{\circ}\text{C}$ for 30 min. [110] - Thickness: 2 μm 90 $^{\circ}\text{C}$ for 30 min. [112]
Hardbake	<ul style="list-style-type: none"> - Thickness approx. 1.8 μm 115 $^{\circ}\text{C}$ for 1 min. [111] 	<ul style="list-style-type: none"> - Thickness: 1.65 μm 115 \pm 5$^{\circ}\text{C}$ for 30 min. [110]

It can be noted from Table 19 that applied temperature and time versus the thicknesses of the S1818 resist is compliant with the rule to perform the softbake at 100 $^{\circ}\text{C}$ for 1 min. per μm resist film thickness on a hotplate in order to maintain sufficient solvent evaporation and to minimise DNQ-loss [87].

Equipment

Hot plate and oven, utilised in the experiments, represent different heat transfer mechanism.

- a) A hot plate transfers heat by conduction. When a contact hot plate (no gap between the hotplate and the substrate) is used, the thickness and heat conductivity of different substrates have minor impact on attaining the required temperature.

The EMS Electro Micro Systems Ltd. Model 1000-1 Precision Hot plate was utilised in the experimentations.

- b) Ovens which transfer heat by convection reveal more distinct temperature hysteresis [87]. However, a time interval is required to attain the expected final temperature.

The Gallenkamp convection oven was used during the experimentations.

Experimental procedure

Process steps of the Ti sandwich structure comprise two stages of S1818 softbake and two stages of the hardbake, as illustrated in Table 17. Experimental work was carried out to assess suitable equipment.

a) Hotplate

- Approach I.

In the first attempt the vacuum hotplate was incorporated for both soft and hardbake. The following parameters were applied, see Table 20.

The 30 min. softbake of the bottom layer was introduced in order to remove the N₂ from the bottom layer of the S1818. The rest of parameters of the soft/hardbake were established according to the literature review presented in Table 19.

Table 20: The S1818 resist baking parameters for the hot plate (Approach I).

S1818 layer	Bottom layer	Top layer
Softbake	115 °C for 30 min.	115 °C for 3.5 min.
Hardbake	115 °C for 3.5 min.	115 °C for 3.5 min.

- Approach II.

A shorter time for the hardbake of the bottom layer and for the soft/hardbake of top layer of the S1818 resist was applied.

Table 21: The S1818 resist baking parameters for the hot plate (Approach II).

S1818 layer	Bottom layer	Top layer
Softbake	100 °C for 30 min	100 °C for 45 s.
Hardbake	100 °C for 45 s.	100 °C for 45 s.

b) Hot plate and oven

In this approach, the soft bake of the bottom layer of the S1818 on the hot plate was shortened in order to minimise the stress. An oven hardbake for both bottom and top layer of the S1818 resist was introduced.

Table 22: The S1818 resist baking parameters for the hot plate and the oven.

S1818 layer	Bottom layer	Top layer
Softbake (hot plate)	100 °C for 3.5 min	100 °C for 45 s.
Hardbake (oven)	100 °C for 10 min.	100 °C for 10 min.

c) Oven

- Approach I.

In this attempt, all thermal processing stages of the S1818 were performed in the convection oven. The variables, such as time of baking were arbitrary, aimed at testing stress generation in layers of the sandwich structure.

Table 23: The S1818 resist baking parameters for the oven (Approach I).

S1818 layer	Bottom layer	Top layer
Softbake	100 °C for 30 min	100 °C for 15 min
Hardbake	100 °C for 10 min	100 °C for 10 min

- Approach II.

The parameters for oven curing were set-up in accordance with the literature review and the findings from the experiments summarised in Table 24.

Table 24: The S1818 resist baking parameters for the oven (Approach II).

S1818 layer	Bottom layer		Top layer
Softbake	100 °C for 60 min	50 °C for 60 min	50 °C for 60 min
Hardbake	50 °C for 60 min	50 °C for 60 min	50 °C for 60 min

Results and discussion

a) Hot plate

Approaches I and II

Processing of the sandwich structure revealed cracks in the Cu layer after spin coating of the top layer of S1818 resist. This resulted in an undesired exposure of the bottom layer of S1818 through the Cu stencil and poor image transfer, as a consequence, limited etching of the pattern in the Ti substrate.

The damage of the Cu deposit after spin coating was concluded to be the result of the stress caused by the shear forces or the stress generated at a high softbake temperature of the bottom layer of the S1818 resist.

b) Hot plate and oven

The shorter softbake time on the bottom layer of S1818 did not improve the performance of the Cu layer during the spin coating of the top layer of the S1818 resist. The cracks appeared similar to the examples described above.

c) Oven

The experiments, where the oven was employed, revealed that the sandwich structure neither had cracks in the photoresist nor in Cu deposit.

Convection oven curing was established as the appropriate method for the S1818 resist soft and hardbakes.

5.4 Mechanical properties of the S1818 photoresist cured at different temperatures

Introduction

Mechanical properties of S1818 were investigated by conducting nanoindentation tests. The experiments were aimed at evaluation of the hardness and reduced elastic modulus of resist, soft baked at two temperatures.

5.4.1 Nanoindentation

Nanoindentation has been applied for mechanical characterisation of thin-film and thin-surface layers recently [113]. The hardness and elastic modulus are the most common properties measured by this technique.

The test is based on applying an indenter, of well-defined shape, into the material under investigation where an elastic and plastic deformation occurs [114]. When the indenter is withdrawn the elastic deformation of the specimen is recorded. This enables the plotting of the loading and unloading force (F) data against the indentation depth (h).

The hardness (H) and the reduced elastic modulus (E_r) can be determined from the following equations:

$$H = \frac{P_{max}}{A} \text{ Pa} \quad (8)$$

Where: P_{max} is a peak load, N

A represents the projected area, m^2 .

The hardness is defined as the mean pressure that a material can support under loading [115].

The reduced elastic modulus – E_r stands for the elastic deformation of both the specimen and the indenter. It is presented as follows:

$$E_r = \frac{\bar{\pi}}{2\beta} \frac{S}{A} \text{ Pa} \quad (9)$$

Where: S is a contact stiffness which is a slope of the unloading curve and is equal to:

$$S = 2 \beta \frac{\bar{A}}{\pi} E_r (N/m) \quad (10)$$

Where: β is a constant and depends on the geometry of the indenter, here it applies to standard Berkovich indenter, $\beta = 1.034$.

A is a function of the contact depth. For a perfect Berkovich indenter, it can be presented as a function:

$$A = f h_c = 24.56 h_c^2 (m^2) \quad (11)$$

Where: h_c is the contact depth, m.

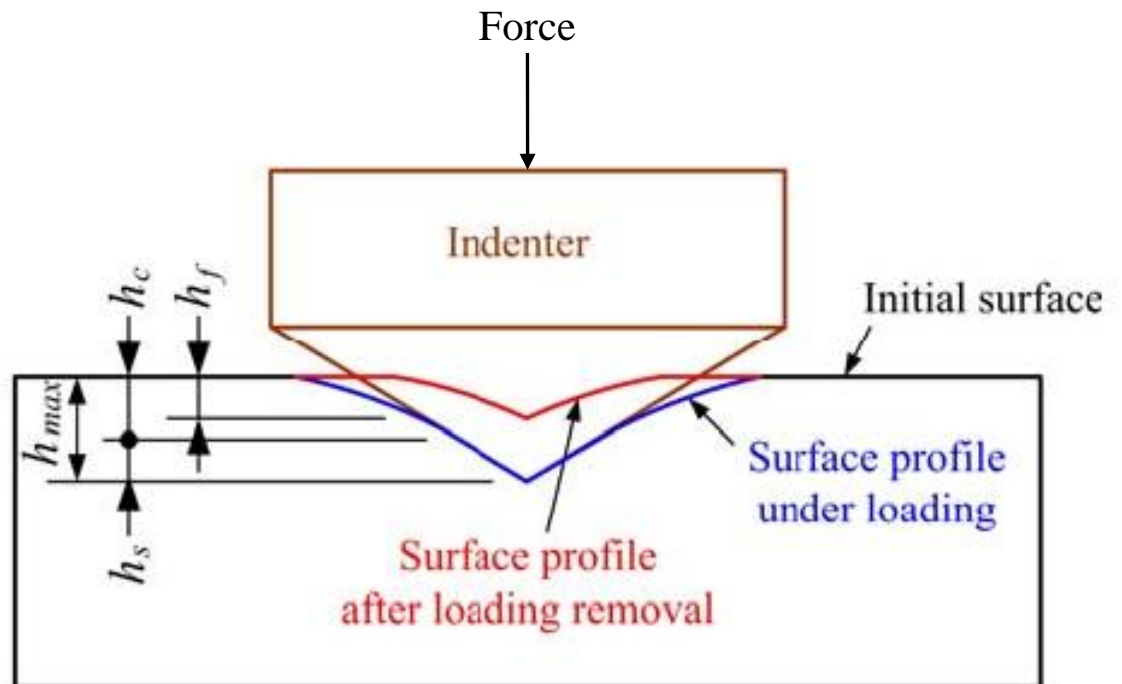


Figure 21: Sketch of nanoindentation profile, modified from [116].

5.4.2 Nanoindentation tests

Indenter

In this work the measurements were performed using a diamond Berkovich-shaped nano indenter, illustrated in Figure 21. Its geometry comprises of a sharp pointed 3-sided pyramid.

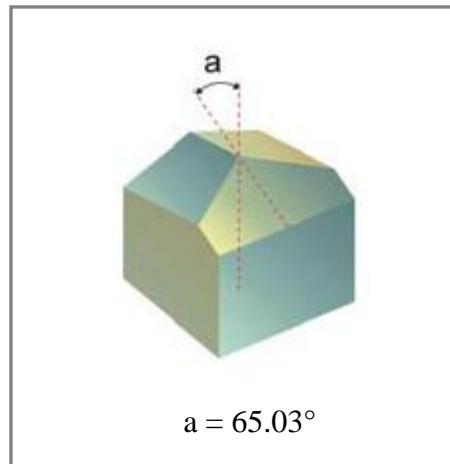


Figure 22: The Berkovich-shaped nano indenter from [117].

The defining angle a is the angle between the axis and any of the faces. The faces are symmetrically placed around the axis 120° apart [117].

Equipment

Convection oven Gallenkamp,

Thermometer

Thermo-Hygrometer Pen, model 8708 for measuring relative humidity (RH).

Experimental procedure

The manually sanded and cleaned Ti specimens, in accordance with the procedure described in Chapter 3.3.2, were spin coated with the S1818 photoresist. The parameters were set to receive the $4\ \mu\text{m}$ thick coating, see Table 18, corresponding to the bottom layer of the resist in the sandwich structure. Then, the samples were softbaked at two different temperatures: 50°C

and 100⁰C for 60 min in the convection oven. These two temperatures were chosen to evaluate their application for the softbake in the sandwich structure.

The samples were stored in the conditions of RH 42 % at 22⁰C 24 hours prior to performing the nanoindentation tests.

Results and discussion

The Berkovich-shaped nanoindenter at the surface of the S1818 resist has been shown in Figure 23.

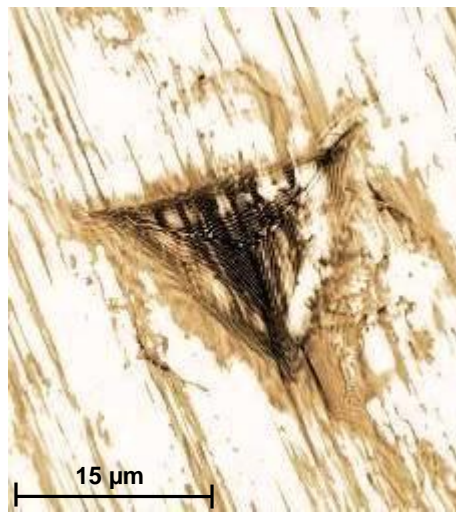


Figure 23: An optical micrograph of a trace of the Berkovich indent at the S1818 surface.

The results of the nanoindentation tests have been presented in plots of hardness and elastic modulus versus applied load. The load-displacement curves of the S1818 resist softbaked at temp. of 50⁰C and 100⁰C have been illustrated in Figure 24. The analyses of the E_r have been presented in Figure 25. Whereas, H of the S1818 resist have been illustrated in Figure 26.

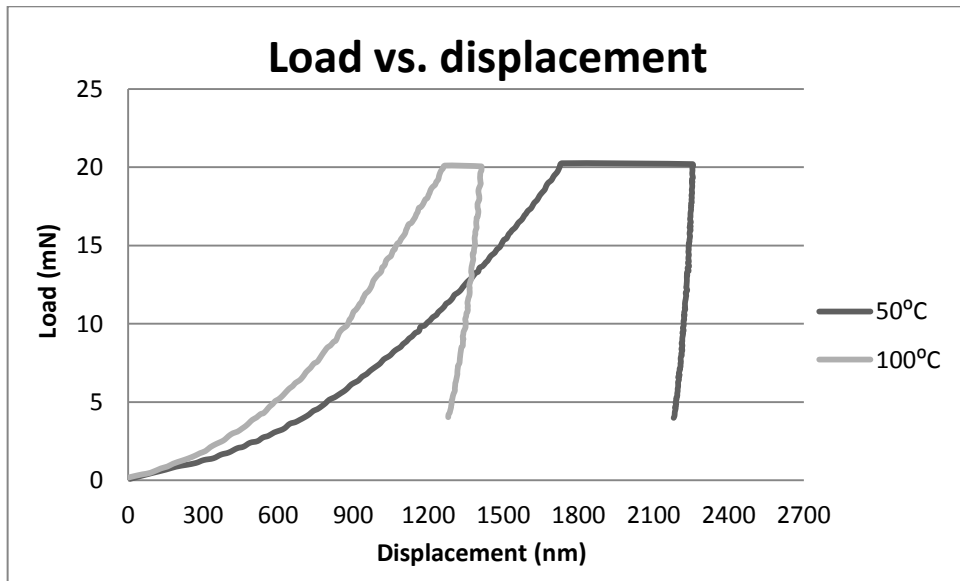


Figure 24. Load vs. displacement of the S1818 resist softbaked at 50⁰C and 100⁰C for 60 min.

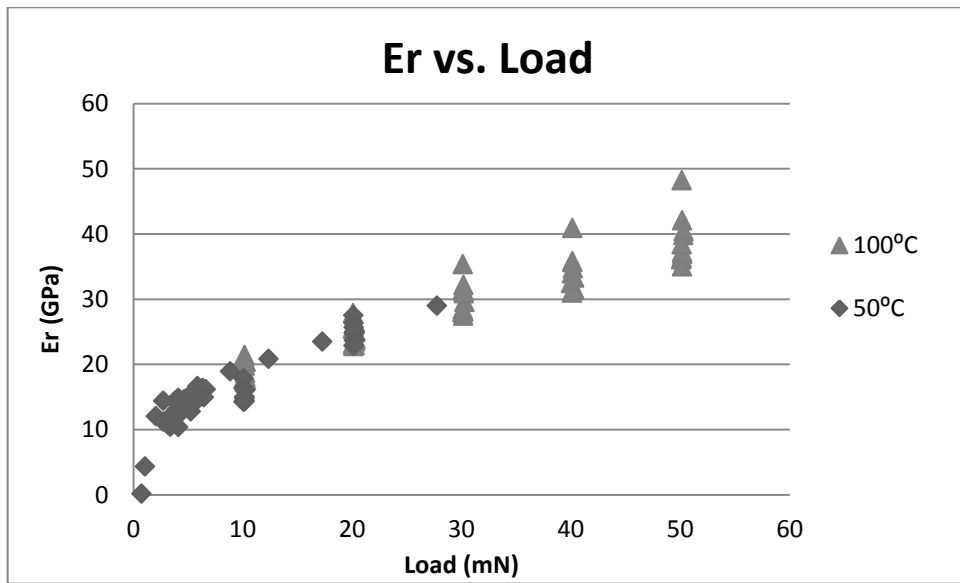


Figure 25. Reduced elastic modulus of the S1818 resist softbaked at 50⁰C and 100⁰C for 60 min.

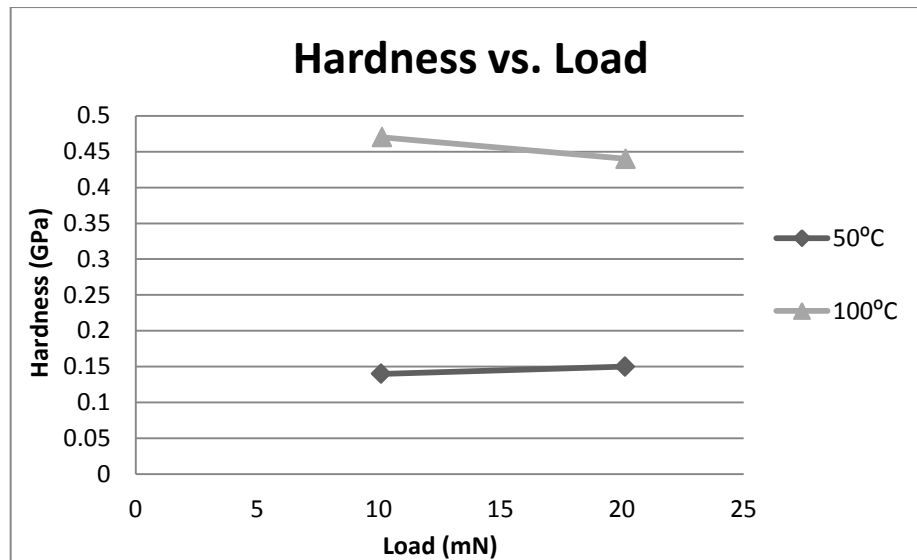


Figure 26. Hardness of the S1818 resist softbaked at 50⁰C and 100⁰C for 60 min.

The analysis of the load-displacement curves, of the S1818 resists, shows a higher displacement of the resist softbaked at the temperature of 50⁰C. The displacement measured about 2.2 μm. Whereas, the displacement of about 1.3 μm was noted in case of the resist softbaked at 100⁰C.

Reduced elastic modulus is increasing linearly in case of both resists, softbaked at 50⁰C and 100⁰C. The highest E_r value, of 48 GPa for the applied load of 50 mN, was noted for the sample baked at 100⁰C. In case of the S1818 softbaked at 50⁰C the max. E_r = GPa for 29 mN applied.

The presented analysis of hardness value of the S1818 resist indicates that the highest value was measured of the resist softbaked at 100⁰C. It achieved max. H value of 0.46 GPa This is in compliance with the rule that the higher bake temperature results in higher hardness. The resist softbaked at 50⁰C the max. H of 0.15 GPa was measured.

During patterning stages of the Ti sandwich structure it was found that the resist softbaked at 100⁰C for 60 min. required higher UV exposure dosage (120 s, lamp int. 5.2 mW/cm²) than the resist baked at 50⁰C for 60 min (80 s). In addition to this, the edges of the developed features in the resist softbaked at 100⁰C were not round. The pattern developed in the resist softbaked at 50⁰C corresponded to the image from the mask and had an even edges.

Therefore, the softbake of the bottom layer of the S1818 resist at 50⁰C for 60 min. was applied in further experimental work.

5.5 Investigation of the Ti/S1818 resist interface

Analyses of the interface of Ti and S1818 were conducted in order to assess whether the baking stages in a convection oven result in an oxide growth on the Ti substrate.

The Ti oxide may lead to a detachment of the S1818 resist from the substrate and make Ti etching uncontrollable. The Ti oxide is very inert, therefore, a higher voltage is required to electrolytically etch the Ti and what is more, the oxide causes lack in adhesion of the photoresist to the substrate.

Experimental procedure

Two Ti specimens were manually sanded and cleaned using the standard procedure, then, the photoresist S1818 was spin coated down at speed of 1000 rpm for 60 seconds. Next, each of the specimens was baked in the convection oven for a total of four hours with 10 minutes breaks after every hour, when the samples were removed from the oven to allow cooling (this was aimed at imitating the normal processing conditions). After the baking step, the specimens were cut to size of 1.2 x 3 cm and sputtered with platinum to conduct FIB analyses. Pt was applied in order to make a conductive layer on top of S1818 to prevent from charge build-up on a dielectric material (S1818) during FIB milling.

The applied parameters have been presented in Table 25.

Table 25: The parameters used to evaluate the Ti and the S1818 resist interface.

Baking step	1	2, 3, 4
Sample 1	50 ⁰ C for 60 min.	50 ⁰ C for 60 min.
Sample 2	100 ⁰ C for 60 min.	50 ⁰ C for 60 min.

Results and discussion

The results of the conducted analysis have been presented below, Figure 27.

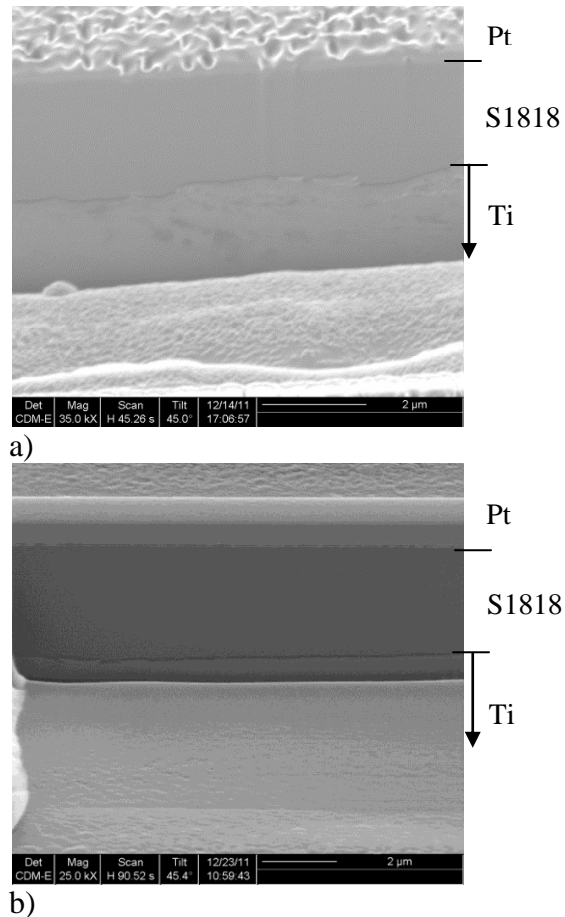


Figure 27. FIB micrographs of the milled specimens: a) sample 1; b) sample 2 in Table 26.

The irregular line of the Ti border in example a) Figure 27 is due to the fact that Ti is more difficult to mill than the S1818.

In both cases there was no Ti oxide creation observed at the Ti and the S1818 photoresist interface. The Ti oxide is very tenacious, therefore, it would strongly affect the final Ti electrolytic etching process. Higher current densities would have to be applied in order to break through the passivating oxide layer.

Summary

The following themes, related to the S1818 positive resist processing in the sandwich structure, were investigated in this Chapter:

- The S1818 positive photoresist was characterised in terms of chemical composition and its properties.
- The processing stages of the resist in the sandwich structure were described and illustrated.
- The soft and hardbake conditions of the S1818 resist were determined as well as the heating equipment. The oven baking was selected as the method which did not produce cracks in the sandwich structure layers.
- The mechanical properties of the S1818 resist soft baked at different temperatures were investigated. The lower displacement (1.3 μm), higher reduced elastic modulus and hardness (0.46 GPa) were observed in case of the S1818 treated at 100⁰C. Whereas, the resist soft baked at 50⁰C was observed to have lower reduced elastic modulus, higher displacement (2.2 μm) and lower hardness (0.15 GPa).
- The high temperature of soft bake: 100⁰C for 60 min. was found to affect its UV sensitivity and developing properties. The soft bake at 50⁰C for 60 min. did not deteriorate the UV sensitivity or developing properties of the resist.
- The FIB analyses of the Ti and the S1818 interface showed no Ti oxide creation after processing the specimens in the convection oven.

Chapter 6: Experimental procedures – stage 3 of sandwich structure building using a copper cathode

Introduction

Cu electroless plating was determined in Chapter 3 as the process employed to produce the cathode layer in the “sandwich structure”. This method of metallisation was found to be compatible with the other fabrication routes of the sandwich structure.

The Cu electroless solution was the subject of analyses and further modifications. The aim of the studies of the Cu electroless deposit was to produce a dense coating with low resistivity and roughness with the film thickness enabling further building-up by a process of electroplating.

6.1 Role of Cu layer in Ti sandwich structure

The Cu layer plays an important role in the Ti sandwich structure. It acts as the cathode which is separated from the anode (Ti) with the S1818 photoresist. The cathode has to be a very good conductor, in order to enable uniform current distribution over the anode. Therefore, the conductive deposit has to be dense (good coverage of the dielectric layer) in order to prevent electrolyte penetration, since the Ti sandwich structure is submerged while electrolytic etching is performed.

6.2 Cu electroless deposition

Electroless deposition is an autocatalytic process that must be preceded by an activation pretreatment of the dielectric surface [118].

The main advantage of electroless deposition is low tool cost, low processing temperature, and high quality material achieved as a result of the process [83].

Cu electroless deposition has a commercial potential due to the fact that it can be utilised to metallise large insulating substrates with simple processes using equipment at low cost [119].

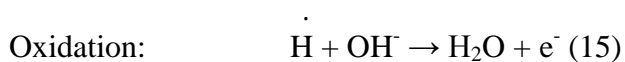
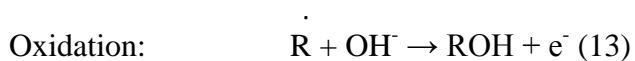
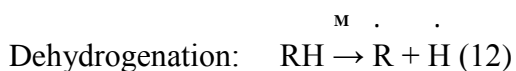
6.2.1 Mechanism of Cu electroless deposition

The electrochemical mechanism of electroless plating is characterised by two half reactions that occur simultaneously, an oxidation half reaction: anodic oxidation of a reducing agent and a reduction half reaction: cathodic reduction of metal (here Cu) ions.

The process is thermodynamically favourable. It has an activation energy that prevents deposition at room temperature and the reaction has to be activated on a catalytic surface [83].

Electroless plating solution exhibits a mechanism which can be summarised by the following anodic and the cathodic partial reactions [84]:

- **Anodic**



- **Cathodic**



Where: R – reductant radical, H - hydrogen radical, M – metal to be deposited.

The dehydrogenation step determines the catalytic nature of the electroless process [84]. It is crucial at this stage to determine a reductant for the metal to be deposited. The dehydrogenation can also be initiated by the energy to break the chemical bond between R-H. Oxidation of reductant (reaction 13) must be stimulated with a higher pH.

Oxidation or recombination of H: only one of the reactions 14 or 15 occurs on the metal surface. Which one depends on the properties of the metal, the pH of the solution and the mixed potential of the reaction. When the reaction 14 precedes the overall anodic reaction is:



When reaction 15 proceeds:



The final efficiency of electroless deposition depends on which one of these two reactions overtakes in the process.

Cathodic reactions: metal reduction and hydrogen evolution depend on the reductant used.

- Aspects of catalysts in copper electroless plating

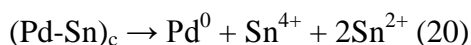
The oxidation of the reducing agent on the surface of the base material is an essential for a catalyst. Through the activation process, active colloids are absorbed on the substrate surface and work as catalysts [120].

A catalyst acts as the anodic site at which a reductant can be absorbed and oxidized. The electrons released on oxidation, migrate through the metal and allow copper reduction. Therefore, the catalytic particles are responsible for an electron transfer from the reducing agent to the metal ions.

The role of a heterogeneous catalyst is to absorb the reactant and transform it to the species that can more readily undergo the desired chemical reaction. Hence, the oxidation of the reducing agent depends on the activation step in electroless copper plating. The energy of the absorption must be high enough to attract the reactant to the surface and low enough to release the reaction product into the solution.

The most commonly utilised catalysts in the electroless copper plating process comprise Sn and Pd [50].

The process of activation of a non-catalytic surface has two steps. First, the specimen is treated by an acidic solution of SnCl_2 , followed by an immersion in an acidic solution of PdCl_2 . The reaction proceeds according to the equation:



Where: $(\text{Pd-Sn})_c$ denotes a complex.

The mechanism of electroless plating is determined by the catalytic reaction. Listed below are certain conditions which are stimulated by the presence of a catalyst and can summarise the electroless deposition process:

- Electroless deposition occurs selectively on an active surface.
- A catalysing reaction is necessary for electroless deposition to take place on a non-active surface such as plastics and ceramics.
- There is an induction period before the deposition takes place.
- A specific combination of metal and reductant is necessary for electroless plating to occur.
- Electroless plating usually accompanies hydrogen evolution, the rate of which is not directly related to that of metal deposition [82].

6.2.2 Cu electroless process for Ti sandwich structure

In order to initiate copper electroless deposition from the solution, the substrate is activated in two stage immersions. The solutions are prepared in the following manner:

a) Sensitisation solution

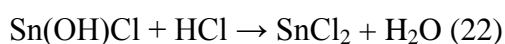
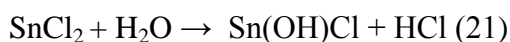


Table 26: Sensitisation solution constituents with the quantities per litre.

Constituent	Quantity per l
SnCl ₂	10 g
HCl	40 ml
DI H ₂ O	To make up volume to 1 l

b) Activation solution

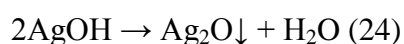
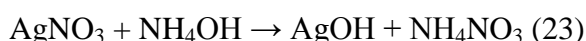
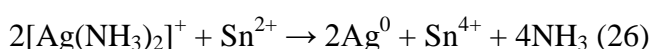


Table 27: Activation solution constituents with the quantities per litre.

Constituent	Quantity per l
AgNO ₃	10 g
NH ₄ OH	10 ml
DI H ₂ O	To make up volume to 1 l

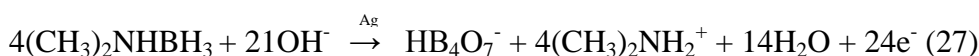
It has been noted in the literature that after putting a non-conductor in an acidic SnCl₂ bath, Sn²⁺ ions are absorbed on to the surface, forming a uniform layer [89]. The immersion in the solution 22, attracts [Ag(NH₃)₂]⁺ ions onto the already sensitised surface. The Sn²⁺ ions reduce Ag complex to Ag⁰ according to the reaction:



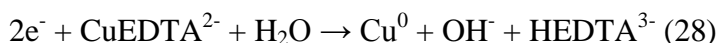
c) Cu electroless plating

The deposited metallic silver catalyses the subsequent Cu deposition in the electroless plating bath. The following reactions take place in the solution:

- On the anode, the oxidation of the reducing agent occurs:



- Cathode reaction illustrates the reduction of the copper-EDTA complex:



The following composition of the Cu electroless solution was established. Its chemistry was previously proved (Chapter 3.3.3) to be compatible with the processing demands of the Ti sandwich structure.

Table 28: Copper electroless plating solution constituents with the quantities per litre.

Constituent	Quantity per l
CuSO ₄ ·5H ₂ O	2 g
Na ₂ EDTA	6 g
28%NH ₄ OH	50 ml
DMAB	4 g
DI H ₂ O	To make up volume to 1 l

Where: $\text{CuSO}_4 \cdot 5\text{H}_2\text{O}$ is a source of copper ions, Na_2EDTA acts as a complexing agent, DMAB is a reducing agent, and $28\% \text{NH}_4\text{OH}$ delivers OH^- groups, what levels the pH of the solution.

Figure 28 shows the overall process:

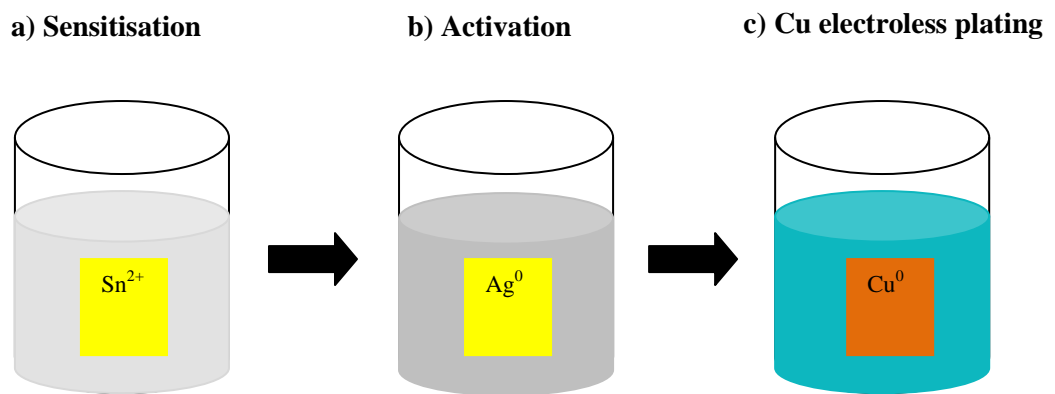


Figure 28: Cu electroless process stages. The colours of the solutions a) and b) do not present their actual appearance. The colours were selected to differentiate the solutions one from the other.

Figure 29 presents the layer structure achieved.

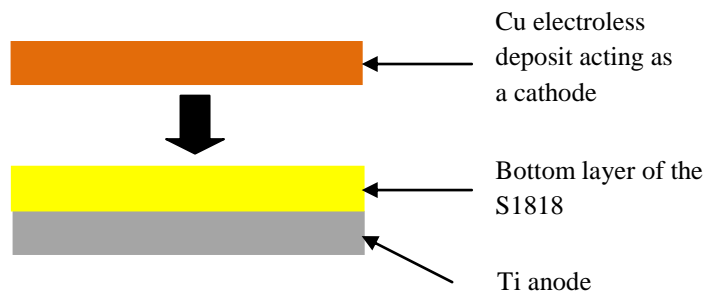


Figure 29: Cross section of the process of Cu electroless deposition in the Ti sandwich structure.

Chemicals

- a) Sensitisation: SnCl_2 (Tin (II) Chloride) dihydrate 98%, HCl (Hydrochloric acid) 32 %.
- b) Activation: AgNO_3 (Silver (I) Nitrate) 99.8+%, NH_4OH (Ammonium Hydroxide) 28-30%.
- c) Cu electroless plating: $\text{CuSO}_4 \cdot 5\text{H}_2\text{O}$ (Copper (II) Sulphate 5-hydrate) 98% extra pure, Na_2EDTA (Ethylenediaminetetraacetic acid disodium salt dehydrate) 99.0-101.0%, NH_4OH 28-30% and DMAB (Borane-dimethylamine complex) 98+%.

DI H_2O was applied to all prepared solutions.

Equipment

- a) Sensitisation and activation stages

100 ml glass beaker x 2; filled with the solutions to the level that allows submerging specimens in a vertical position⁶,

plastic tweezer x 2 (one for handling sample in the sensitisation solution and the second for the activation solution).

- b) Cu electroless plating

100 ml beaker – Cu electroless plating tank,

400 ml beaker for water jacket,

Hot plate stirrer,

Temperature sensor,

Metal stand,

Magnetic stirrer,

pH meter,

PVC insulation tape,

Stainless steel tweezers,

Crocodile clip.

Figure 30 illustrates the equipment layout.

⁶ Vertical position of the specimen was selected for all stages of the Cu electroless plating due to the fact that it caused the least damage of the coatings while handling.

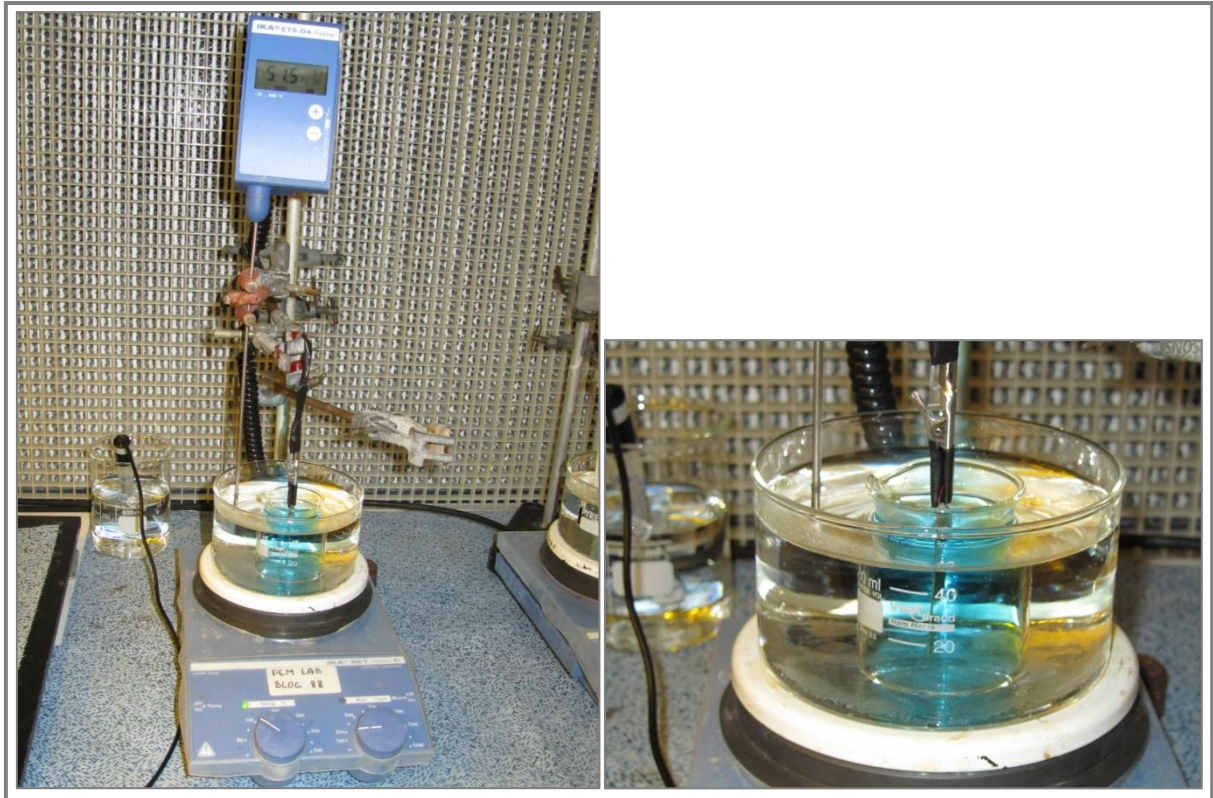


Figure 30: Experimental set-up for the Cu electroless plating. Left picture: equipment used for the Cu electroless plating. Right picture: vertical immersion of the substrate - Ti/S1818.

Experimental procedure

Firstly, the specimen, comprising of Ti substrate coated with the S1818 photoresist covered with a double layer of the PVC insulation tape on a back, was immersed in the sensitisation solution ($\text{SnCl}_2 + \text{HCl}$) for 10 minutes. The specimen was subsequently rinsed with DI water and placed in the activation solution ($\text{AgNO}_3 + \text{NH}_4\text{OH}$) for 20 minutes. The extensive DI water rinse of the sample was applied after activation in order to eliminate contamination of the plating solution with an excess of deposited species. All processes were performed at ambient temperature. Prior to the drying step, the outer layer of the PVC insulation tape was removed, to allow plating only from the S1818 resist side of the Ti sandwich structure.

Afterwards, the specimen was dried in a convection oven at 50°C . Finally, the sample was immersed in the Cu electroless plating solution for 3 minutes at 50°C . The Cu plated S1818 resist was rinsed with DI water and dried with an air gun. Lastly, the PVC tape, covering the back side of the Ti, was removed.

The summary of the operating conditions of the processes have been presented in Table 29.

Table 29: Operating conditions for the sensitisation solution, activation solution and the Cu electroless plating bath.

Solution	Operating temperature (°C)	Time of immersion (min.)	pH
SnCl ₂ + HCl	Ambient	10	0.86
AgNO ₃ + NH ₄ OH	Ambient	20	11.07
Standard Cu electroless bath	50 - 52	3	10.33– 10.43

i. Surface morphology study of a deposit obtained from the standard Cu electroless solution

The “sandwich structure” comprising of Ti/S1818/Cu layers was analysed with an Oxford Energy Dispersive X-ray (EDX) Spectrometer in order to investigate the Cu coverage of the photoresist and an element content of the electroless deposit.

The EDX Spectrometer, integrated with a Scanning Electron Microscope (SEM), include a sensitive X-ray detector, a liquid nitrogen chamber for cooling, and software to collect and analyze energy spectra. The detector, which is made of Si(Li) crystals, is mounted in the sample chamber of the SEM and cooled by the liquid nitrogen. The detector absorbs the energy of incoming X-rays by ionisation, yielding free electrons in the crystal that become conductive and produce an electrical charge bias. The X-ray absorption converts the energy of individual X-rays into electrical voltages and the electrical pulses correspond to the characteristic X-rays of the element. The EDX can determine a chemical composition of materials down to a few micrometers [121].

Results and discussion

The sample, comprising of the layers of Ti, S1818 photoresist and Cu electroless deposit, was the subject of EDX analysis. Since, the cross-sectioning of the specimen was not applicable, due to the brittleness of the Cu electroless deposit, the EDX analysis was conducted from the top of the Ti sandwich structure (Ti/S1818/Cu – top).

It was observed that the Cu was coated on the whole area of the dielectric. The SEM micrograph obtained from the conducted analysis showed a Cu deposit with some bigger clusters of Cu particles. Figure 31 indicates the coating achieved with the standard route of Cu electroless plating.

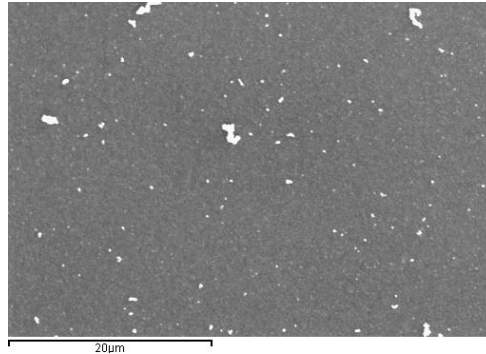


Figure 31. SEM micrograph of the Cu deposit obtained from the standard Cu electroless solution.

The element analysis of the specimen showed the presence of sulphur (S) which is the constituent of the Cu electroless solution. Sn or Ag were not detected which could indicate complete reduction. The presence of the elements: Ti, O, and C were due to the fact that the beam penetrates the material being scanned down to a few microns. The EDX analysis results for Ti/S1818/Cu with Cu obtained from the standard Cu electroless solution have been shown in Figure 32.

It should also be noted that any foreign element in the Cu coating can have an effect on the etching process during the Ti sandwich structure forming. Therefore, it is desirable to obtain as high a Cu content in the deposit as possible.

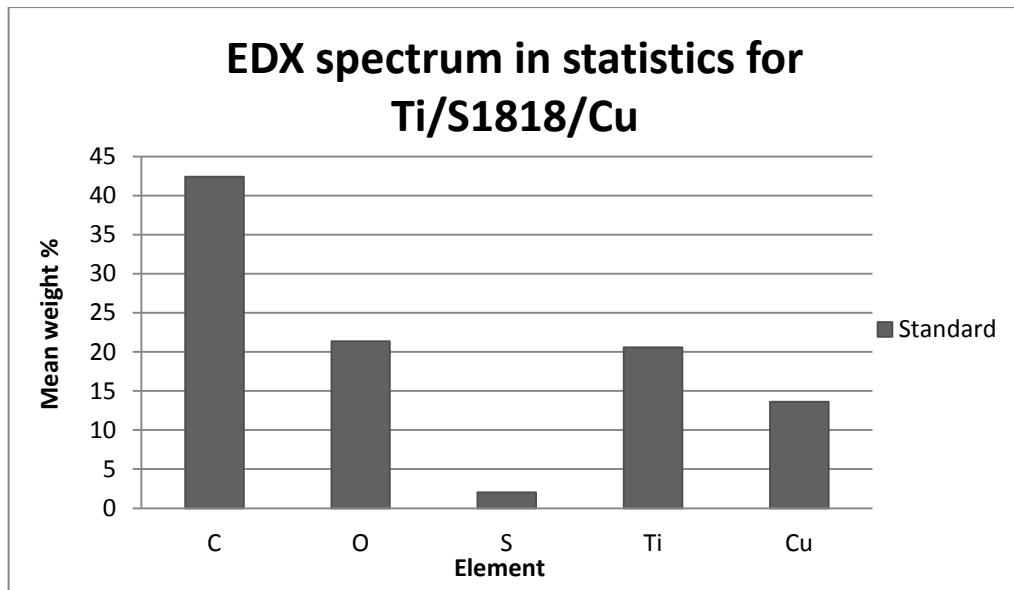


Figure: 32. EDX spectra in statistics for Ti structure: Ti/S1818/Cu - Cu obtained from standard solution.

It was found that the Cu electroless deposit produced from the standard solution to create the cathode in the Ti sandwich structure, did not withstand the applied conditions of the final stage of the electrolytic etching of Ti (an anode). The Cu coating delaminated immediately after immersion in an electrolytic cell containing 10 % (by wt.) HCl. The damage of the cathode (Cu coating) was concluded to occur due to the penetration of the electrolyte through the Cu lattice.

New experiments aimed at building a denser and therefore more robust Cu electroless film were conducted.

- **Agitation effect on Cu electroless deposit**

The agitation effect on the Cu electroless deposit was investigated in order to build a thicker and denser coating. Therefore, the influence of mechanical agitation during Cu electroless deposition was the subject of the work presented next.

It is common practice to stir a plating solution in order to enhance the movement of ions. It was reported that an application of an ultrasonic irradiation improves plating rates, physical and mechanical properties of the Cu electroless coating [122].

Therefore, ultrasonic agitation was introduced to the standard Cu electroless plating solution. The experimental procedure was conducted according to the Chapter 6.2.2.

The results showed that applied frequencies of 38 – 40 kHz did not lead to the formation of the Cu coating on the substrate.

The next step was to verify the effect of mechanical stirring on Cu electroless deposition. The mechanical agitation was found to prevent from hydrogen bubbles retention at the plating site and to improve the deposition uniformity [123].

The following agitations were applied during electroless plating, Table 30.

Table 30. Effect of a mechanical stirring on Cu electroless deposit.

Sample	Applied agitation			
	Magnetic stirring speed	Deposition time	Surface finish	XRD analysis
1	250 rpm	3 min.	Smooth	-
2	350 rpm	3 min.	Smooth	-
3	600 rpm	3 min.	Smooth	+
4	Standard – no stirring	3 min.	Smooth	+

Where: - no analysis conducted; + analysis conducted.

Results and discussion

The analysis of Ti/S1818/Cu spectra (Figure 33) implies that the same Cu crystallites were formed. No improvement in Cu coating appearance was noticed with stirring applied. Whereas, it was found that stirring of the plating solution prior to deposition enhanced the creation of the Cu nucleation sites on the substrate.

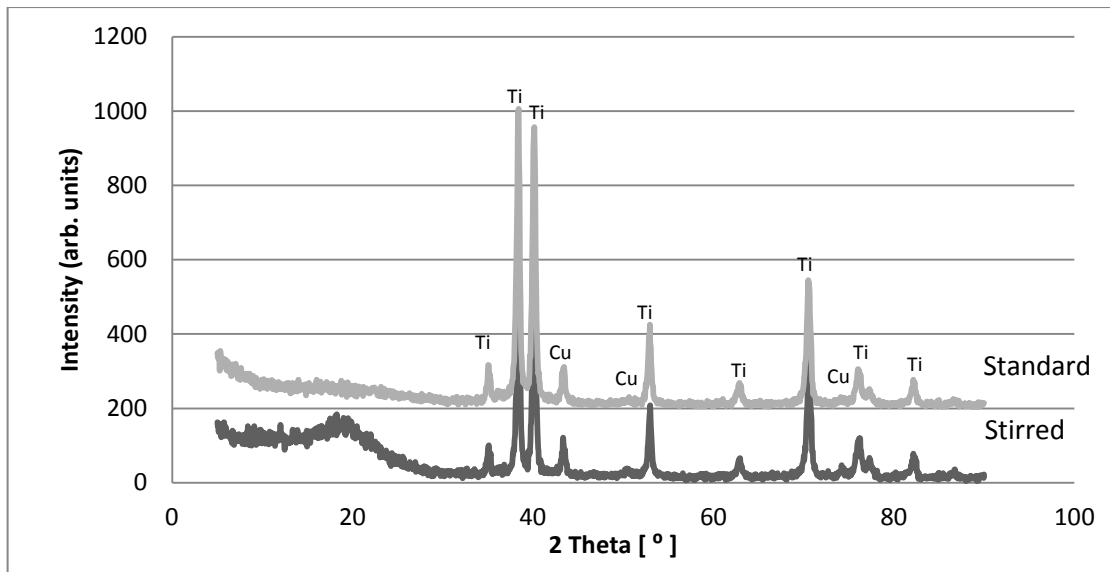


Figure 33: XRD spectra of Ti/S1818/Cu structure with the Cu coatings obtained from stirred and unstirred solutions.

Further experimental work on denser and therefore more robust Cu electroless deposit, capable of being processed through all the steps of Ti sandwich structure including the final electrolytic etching, have been presented in the following section.

6.2.3 Cu electroless deposit modification

New additives were introduced to the standard Cu electroless plating solution in order to produce a denser film by enhancing the Cu content. With more Cu laid down initially this acts as a conductive 'key' for more Cu to plate down onto.

a) Organic additives

Introduction

Several organic compounds were selected (based on an extensive literature search) to build a more compact Cu electroless coating. They were: **glycerol, sorbitol, saccharin, cytosine, and gelatin.**

Both **glycerol** and **sorbitol** belong to a polyhydric alcohol. Glycerol ($C_3H_8O_3$) is a clear, colourless, viscous liquid [124]. Whereas, sorbitol ($C_6H_{14}O_6$) appears in the form of a white hygroscopic powder, granules, crystalline powder or flakes [125]. Glycerol and sorbitol are known for their plasticizing properties. A plasticizer is defined as “a substantially nonvolatile, high boiling, nonseparating substance, which changes the physical and/or mechanical properties of other material” [126]. Glycerol and sorbitol, plasticize by reducing internal hydrogen bonds and increasing intermolecular spacing. Therefore, they decrease brittleness and increase the permeability of film materials.

It was reported [127] that in the presence of moisture, glycerol imparted a greater plasticizing effect than sorbitol. This phenomena was explained by the fact that glycerol has a greater molar content per mass unit and a smaller molecular size that facilitates its penetration into the film matrix.

Cytosine ($C_7H_5NO_3S$) is a nitrogenous base derived from pyrimidine that occurs in nucleic acids. The addition of the cytosine, to the Cu electroless solution, caused a high crystal refinement. Therefore, such a property can lead to producing a tight, dense, continuous, and void-free structure [128].

Saccharin, is an organic compound of the molecular formula $C_7H_5NO_3S$, known as a strong levelling agent for the surface and a grain refiner. It also helps reduce internal stresses in a deposit [129]. It was found that the addition of saccharin did not show an effect on the thickness value or composition of the deposit, whereas, it had an influence on a surface morphology [129], [130].

Gelatin, derived from collagen, has a gel forming properties. It was reported that the addition of gelatin has prevented the particles from growing to larger sizes. It was demonstrated in the literature that gelatin had an effect on the tendency of smaller particles to agglomerate [131].

Glycerol was also tested in conjunction with saccharin. It was previously noted that such a combination is very effective in pyrophosphate zinc plating solutions [132]. The addition of glycerol and saccharin were aimed at combining their individual properties.

Chemicals

The chemical compounds of the sensitisation and activation solutions as well as the Cu electroless plating solution remained the same.

The following chemical compounds were added to the base Cu electroless plating solution:

Glycerol 98%, D-sorbitol, cytosine 99 + %, saccharin 98 + %, gelatine from bovine skin, type B, (Table 31).

Table 31. Copper electroless plating solution organic additives with the quantities per litre.

Organic compound	Quantity g per l	Reference
Glycerol	28.85	-
Glycerol 2	47.82	[131]
Sorbitol	94.60	[131]
Cytosine	0.004	[126]
Saccharin	8.00	[128]
Gelatin	0.50	[129]
Glycerol + saccharin	28.85 + 8.00	[133] + [130]

Equipment

The equipment for the sensitisation, activation as well as for electroless plating was used as described in section 6.2.2.

Experimental procedure

a) The procedure of the sensitisation and activation remained the same, as described in the section 6.2.2.

b) Cu electroless plating was performed in order to determine a plating rate for each of the Cu electroless solution enhanced with the addition of the organic compound. The specimens were prepared prior to the Cu electroless plating in the same manner as described in section 6.2.2. Then, the plating rates were determined for all Cu electroless solutions. The plating rates were investigated by registering the weight gain during the deposition process. The specimens were weighed prior to electroless plating and 24 hours after the deposition to allow water from the coating to evaporate. An analytical balance with a precision to 1×10^{-4} g was employed to weigh the samples. The plating rates of all Cu electroless solutions containing the organic additives have been presented in Appendix C.

The time to achieve a 'uniform-looking' coating for the tested Cu electroless solutions has been given in Table 32.

Table 32. Time needed to obtain a uniform copper coating by electroless deposition with the use of solution with the organic additive/s.

Solution with the additive used	Plating time (min.)
Standard (reference)	3
Glycerol	5
Glycerol 2	5
Sorbitol	5
Cytosine	3
Saccharin	60
Gelatin	5
Glycerol + saccharin	60

The sample with the most uniform-looking Cu coating for each of the Cu solutions was selected and was the subject of the analyses presented in the following sections.

i) Surface morphology study of Cu electroless deposits obtained from the modified Cu electroless solutions

The “sandwich structure” comprising of Ti/S1818/Cu layers was analysed with an EDX Spectrometer in order to investigate the Cu coatings morphology.

The SEM micrographs were analysed with regard to finding a 'dense-looking' Cu coating.

The EDX analyses present the element spectra obtained from the scans of the Cu coatings from the Ti/S1818/Cu structures.

Results and discussion

The SEM micrographs, obtained from the conducted analysis of the Cu coatings deposited from the solutions containing new organic additives, have been presented in Figure 34. It can be seen from the SEM micrographs (Figure 34) that glycerol (in both concentrations), sorbitol, saccharin, glycerol in conjunction with saccharin as well as cytosine produced compact Cu electroless deposits. Only coating from gelatin-enhanced solution (Figure 34, a)) had no uniform Cu coverage. There were observed only single Cu particles.

The Cu coatings were found to have a shiny orange colour, whereas the deposit from the solution containing gelatin, presented dark brownish colour.

The results of the EDX analyses showed conformity with the SEM observations regarding the Cu coating containing gelatin. It indicated the lowest Cu content (mean weight %) amongst other additive-enhanced deposits. The highest Cu content (mean weight %) was detected from the saccharin-and glycerol 2-containing deposits. The lowest C content (mean weight %) in the spectra was noted from the glycerol modified electroless solution which could indicate the thickest Cu coating obtained.

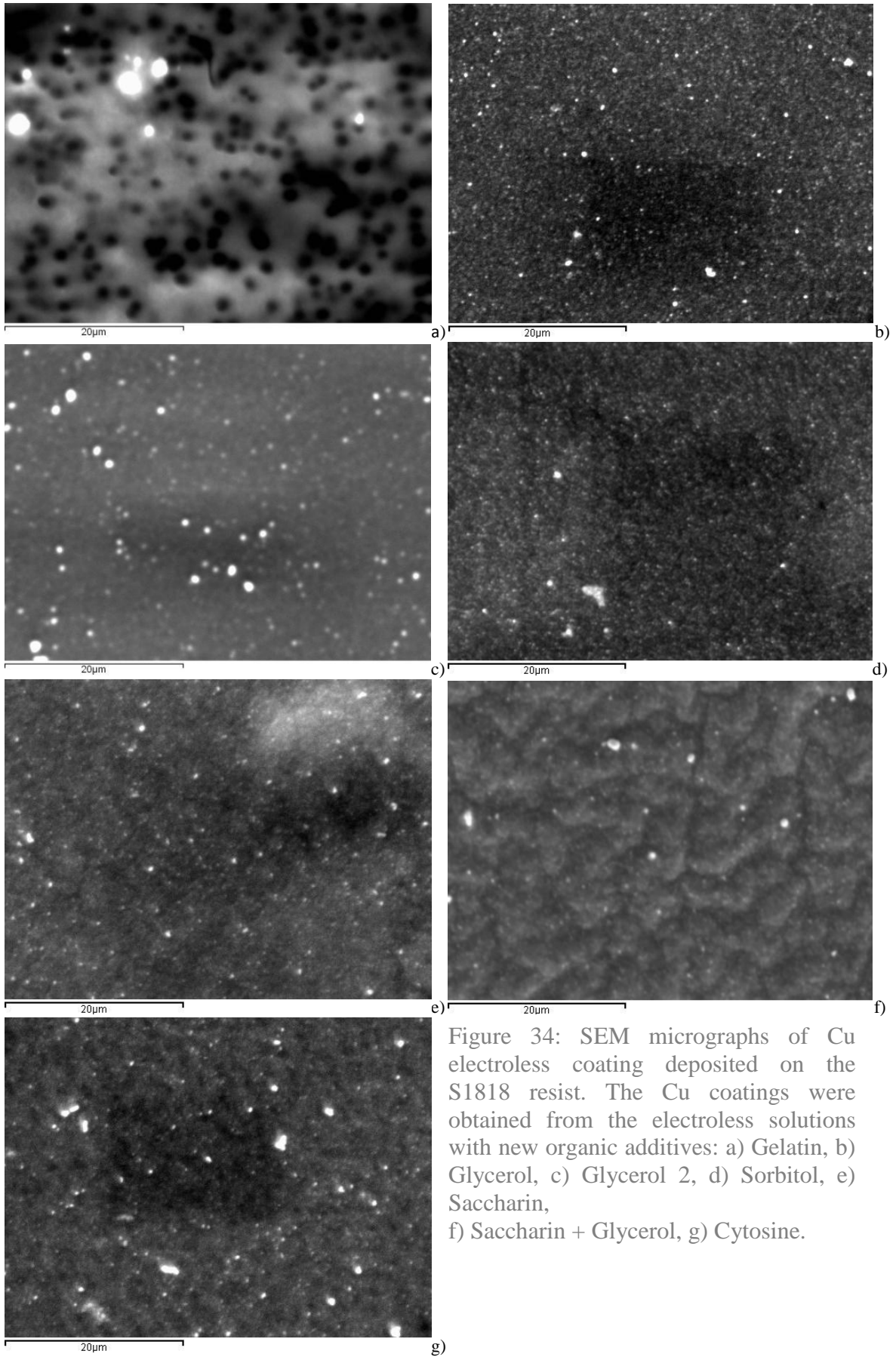


Figure 34: SEM micrographs of Cu electroless coating deposited on the S1818 resist. The Cu coatings were obtained from the electroless solutions with new organic additives: a) Gelatin, b) Glycerol, c) Glycerol 2, d) Sorbitol, e) Saccharin, f) Saccharin + Glycerol, g) Cytosine.

EDX analysis results for the structure comprising of Ti/S1818/Cu with Cu layer obtained from the modified electroless solutions containing new organic additives have been shown in Figure 35.

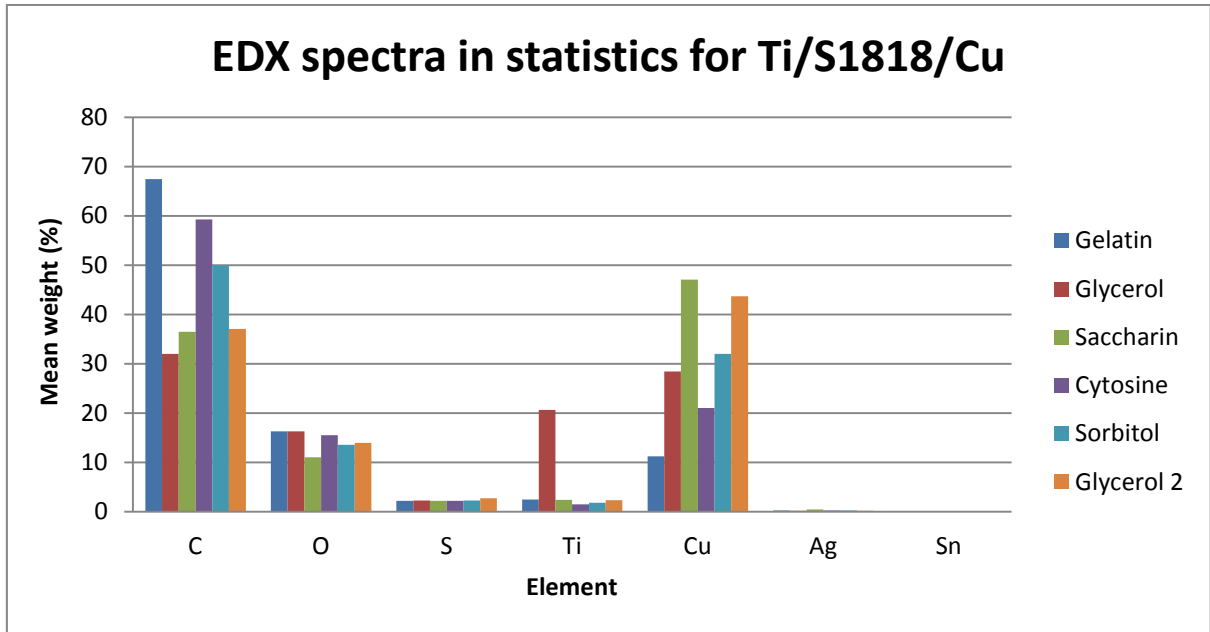


Figure 35: EDX spectra in statistics for Ti/S1818/Cu structure. The Cu coating obtained from the modified solutions.

ii) XRD characterisation of Cu electroless deposits

XRD analysis was carried out on the Ti/S1818/Cu samples. The qualitative investigation of the obtained XRD spectra was conducted in order to assess the crystallisation of the Cu deposits.

Ti and the S1818 resist were prepared in the same manner for all investigated samples. Whereas, the Cu coatings were obtained from the solutions containing the organic additives. A Siemens D5005 X-Ray Diffractometer was applied for X-ray analyses. The results are shown below (Figure 36).

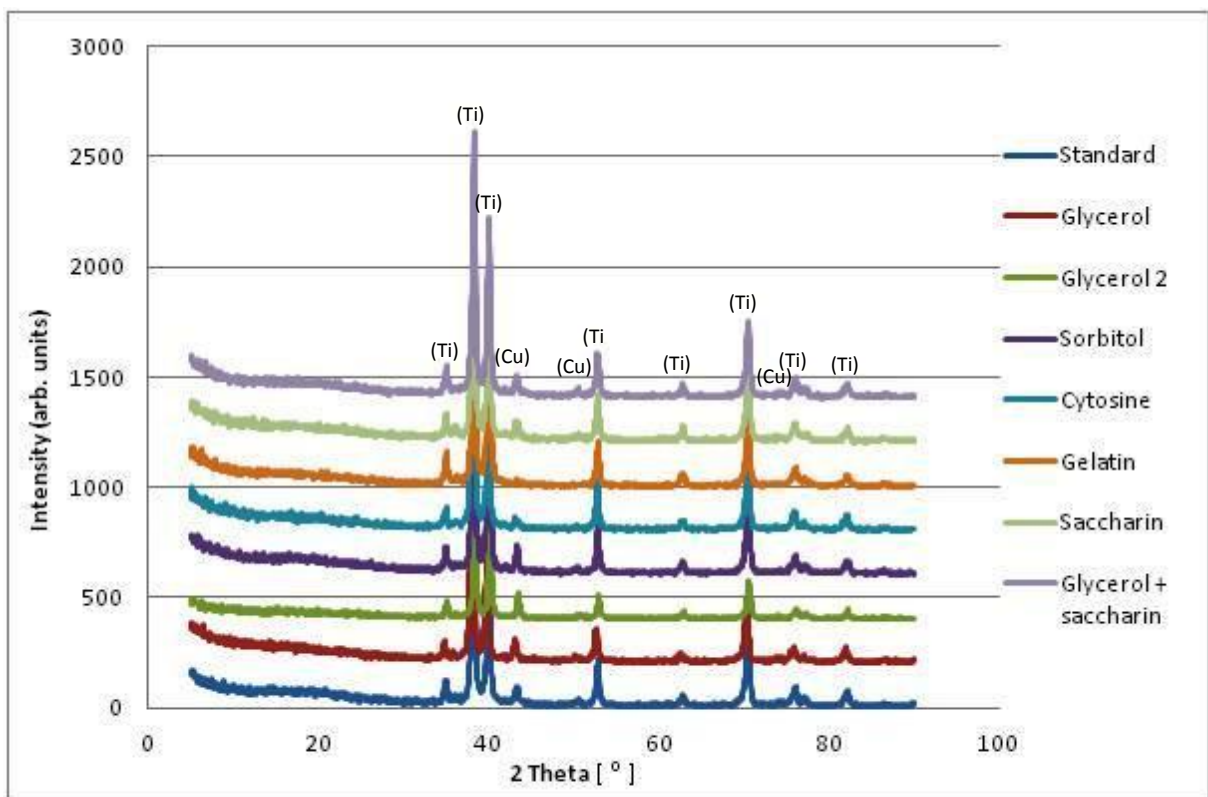


Figure 36: XRD spectra for the Cu depositions obtained from the electroless solutions containing tested organic additives.

Characteristic peaks of Cu: $2\theta = 43.5^\circ$, 50.5° , and 74.0° corresponding to the crystal faces of (111), (200), and (220).

From the qualitative analysis by XRD of the Cu deposits it was noted that all coatings showed peaks indexed to Cu. This indicated that the obtained electroless deposits were well crystallised.

It was previously observed [134] that the formation of dense Cu film is accompanied with the (111) texture.

The smallest peak indexed to (111) plane was noted for the coating obtained from the solution with the addition of gelatin. This could indicate that apart from this Cu deposit other had the compact structure.

iii) Roughness analyses of Cu electroless deposits

High uniformity of the Cu coating is very important both for the subsequent processes: electrolytic plating (applied to thicken the Cu layer) and electrolytic etching of Ti. It is due to the fact that the electric field accumulates at sharp edges (peaks) of rough films [134].

In the electroplating, the uneven surface of the seed layer could lead to rapid plating at those regions. The initially non-uniform film would become even rougher after electrolytic plating. Whereas, in the electrolytic etching scenario, the high peaks in the cathode (Cu coating) could result in current disturbance on the anode during the electrolytic etching of the Ti sandwich structure. Therefore, ideally, a continuous coating of low roughness is required for subsequent processes.

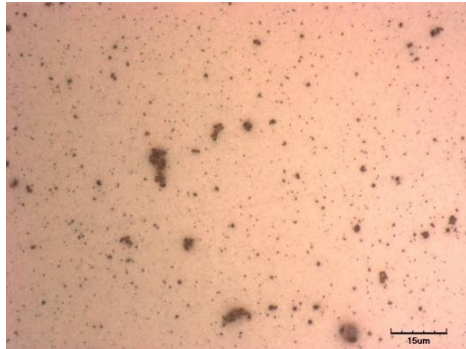
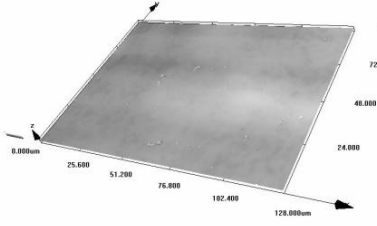
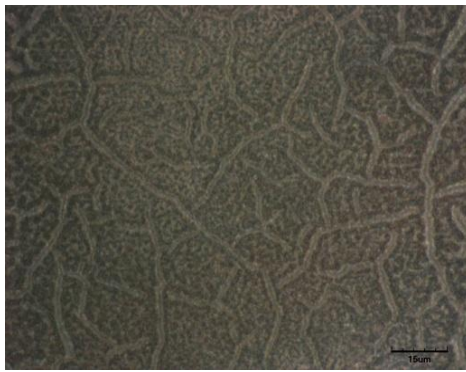
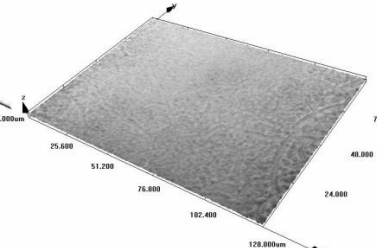
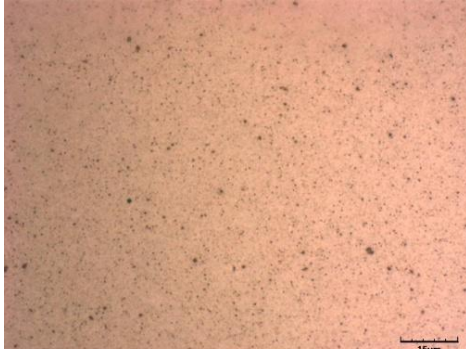
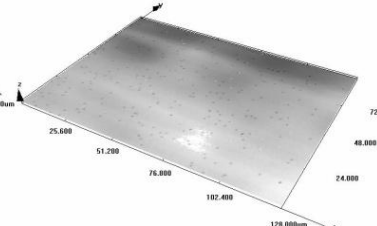

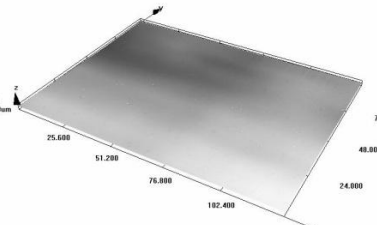
Experimental procedure

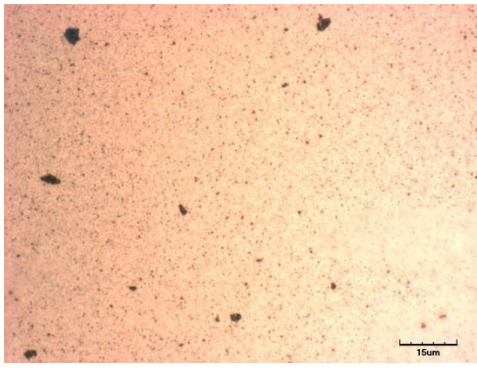
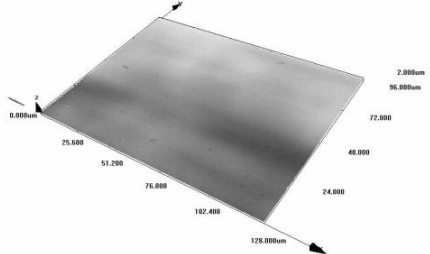
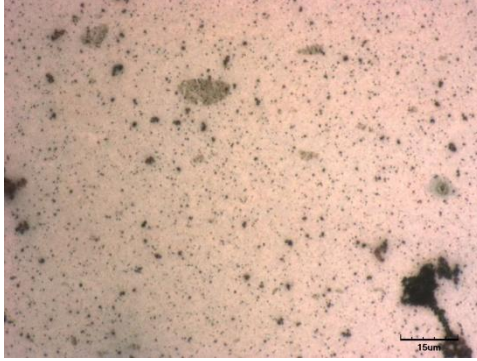
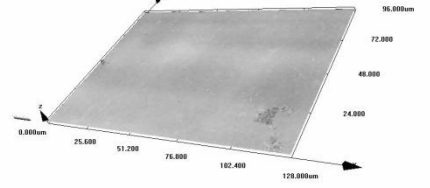
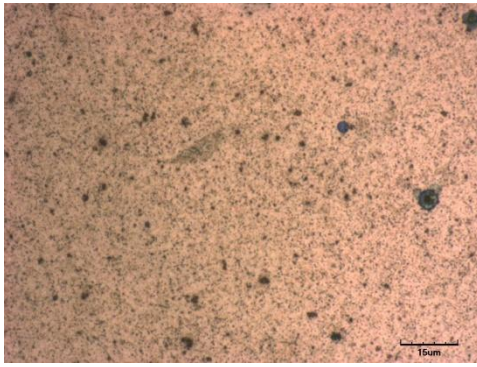
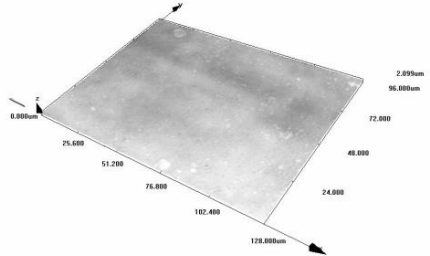
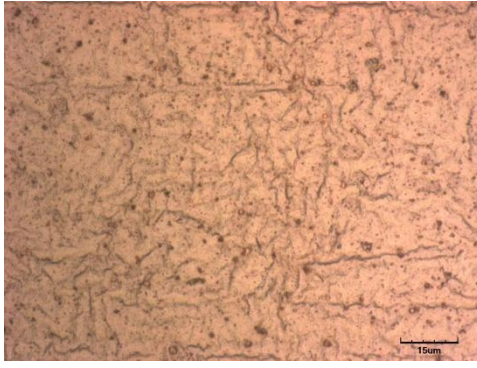
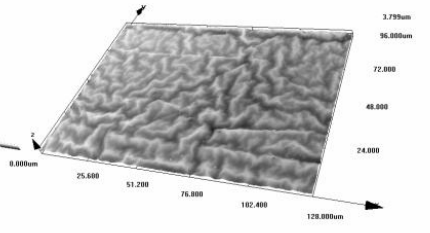
Cu coatings deposited from the modified electroless solutions were scanned with the Olympus Lext Confocal Laser Microscope in order to analyse their surface topography and their roughness. Five measurements of the surface roughness were taken for the scan per sample. Then, the mean and the standard deviation were calculated.

Results and discussion

The obtained micrographs have been presented in Table 33, where the surface of the Cu coatings on top of the Ti/S1818 structure have been shown and corresponding to it, surface topography.

Table 33. Olympus Lext Confocal Laser Microscope micrographs of the Cu deposits from Cu electroless modified solutions.

Additive used	Micrograph of the surface (top view)	Surface topography (3 D scan)
No additive - standard		
Gelatin		
Glycerol		
Glycerol 2		

Additive used	Micrograph of the surface (top view)	Surface topography (3 D scan)
Sorbitol		
Cytosine		
Saccharin		
Saccharin and Glycerol		

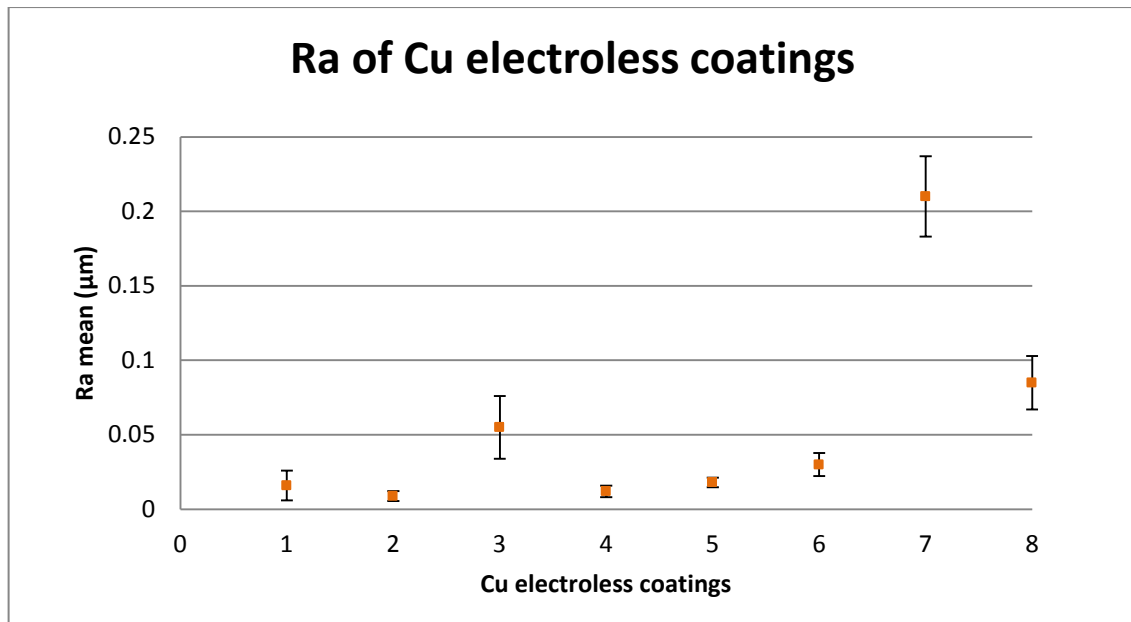


Figure 37: Roughness of Cu electroless deposits obtained from the solutions containing the following additives: 1 –standard, 2 – glycerol, 3- glycerol 2, 4 – sorbitol, 5 –cytosine, 6 – saccharin, 7 – glycerol + saccharin, 8 – gelatine.

Presented results indicate that the addition of the organic compounds: glycerol and sorbitol produced smoother Cu deposit than the coating obtained from the standard solution. The higher concentration of glycerol (here referred as glycerol 2) resulted in a higher surface roughness. The combination of glycerol and saccharin and gelatine additives had a significant influence on the higher surface roughness of the Cu coating.

It could be seen, from the Olympus Lext Confocal Laser Microscope micrographs, that the gelatine-enhanced solution produced a coating that was covered with cracks. It was concluded that this phenomena was related to the property of the gelatine behaving as a sol when warmed-up, whereas, it solidifies to form a gel as it cools. Therefore, Cu electroless coating with the addition of gelatine created a deposit with a different thermal expansion coefficient to the substrate (photoresist).

Whereas, the high surface roughness of the Cu deposit, from the solution containing glycerol and saccharin, was found to be related to the behaviour of the S1818 resist in the Cu electroless bath. The immersion of an inactivated substrate inactivated at 50⁰C for one hour caused cracks of the resist. Further analysis conducted with AFM revealed cracks of a max. depth of 3.16 µm and max. width of. 0.57 µm. Hence, the crazed surface of the Cu electroless coating from the solution containing glycerol + saccharin.

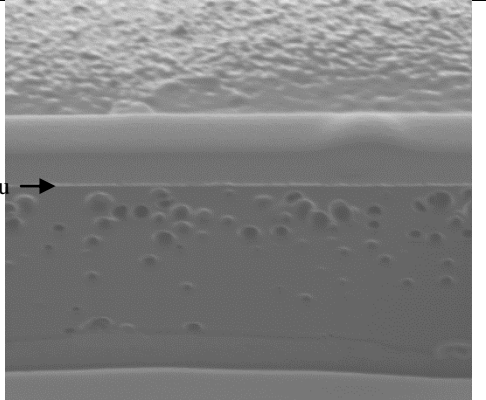
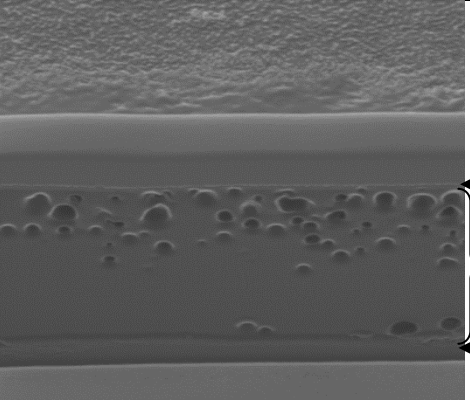
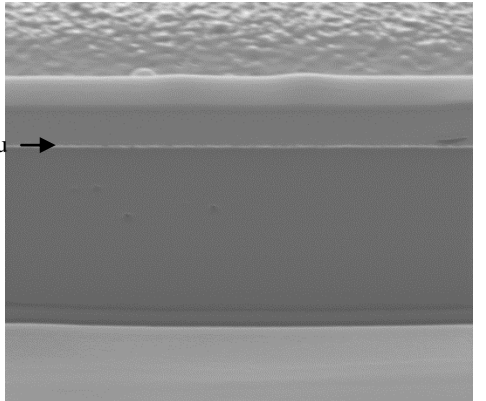
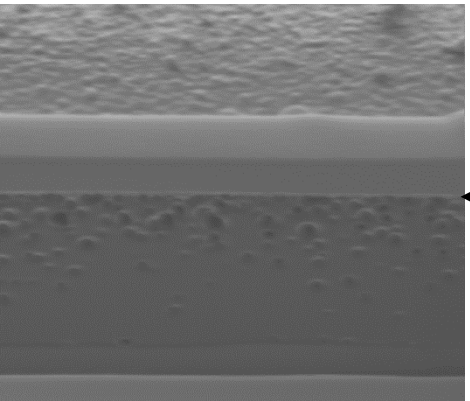
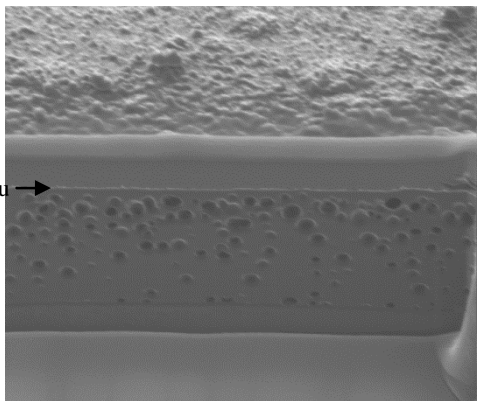
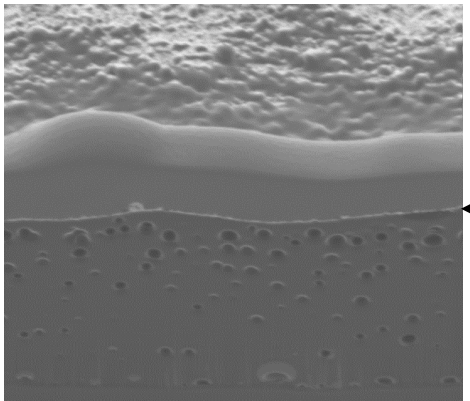
iv) Thickness measurement of Cu electroless deposits

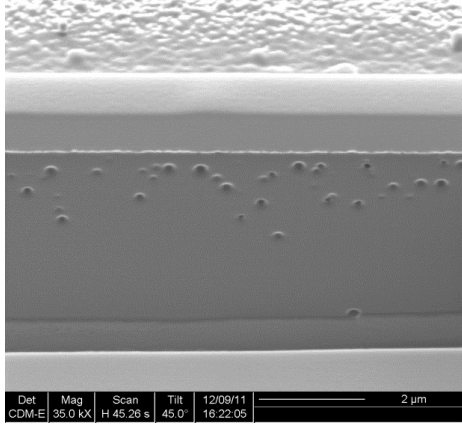
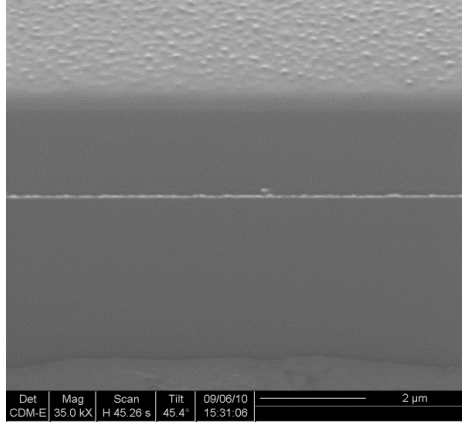
The thickness of Cu electroless deposits was investigated with the use of FIB. The Ti/S1818/Cu samples were milled in order to determine the Cu film thickness from cross-section micrographs.

Results and discussion

The FIB cross-section micrographs with the corresponding thickness values, for the Cu coatings modified with the organic compounds, have been illustrated in Table 34.

Table 34. FIB cross-section thickness measurement of Cu electroless deposits in the Ti/S1818/Cu structure.

<p style="text-align: center;">FIB cross-section micrograph of the Ti/S1818/Cu structure</p>		<p style="text-align: center;">Cu layer thickness/ additive used in the Cu solution</p>
 <p style="text-align: center;">a)</p>	 <p style="text-align: center;">b)</p>	
 <p style="text-align: center;">c)</p>	 <p style="text-align: center;">d)</p>	<p style="text-align: center;">50 nm</p> <p>a) Standard, b) Gelatin, c) Sorbitol, d) Cytosine, e) Saccharin, f) Glycerol + Saccharin</p>
 <p style="text-align: center;">e)</p>	 <p style="text-align: center;">f)</p>	

FIB cross-section micrograph of the Ti/S1818/Cu structure	Cu layer thickness/ additive used in the Cu solution
	<p>60 nm</p> <p>g) Glycerol 2</p>
	<p>70 - 100nm</p> <p>h) Glycerol</p>

The presented results showed that the addition of the organic compounds: gelatine, sorbitol, cytosine, saccharin, and a combination of glycerol + saccharin had no effect on the thickness of the Cu deposit in comparison with the thickness of the Cu coating obtained from the standard electroless solution.

However, an increase of the thickness was noted in case of the Cu films deposited from the solutions containing both concentrations of glycerol.

v) **Resistivity of Cu electroless deposits**

Low resistivity (ρ) of the Cu coating, acting as a cathode in the Ti sandwich structure, is required to improve the current flow in the electrolytic etching. Therefore, resistivity measurements of Cu electroless coatings obtained from the solutions containing organic additives were conducted.

Equipment

The measurements of the ρ were carried out with the application of the following equipment: Four-Point Probe, DC power supply, and Multimeter ISO tech IDM 91E.

Experimental procedure

The ρ of the Cu coatings was measured by applying the set current of 4.53 mA and reading the voltage on the Multimeter in mV. Three readings were taken per sample from three different parts of the Cu film (top, centre, and bottom). Then, the mean of the measurement was calculated with a standard deviation.

Results and discussion

The results of received ρ values for the Cu coatings have been presented in Figure 38.

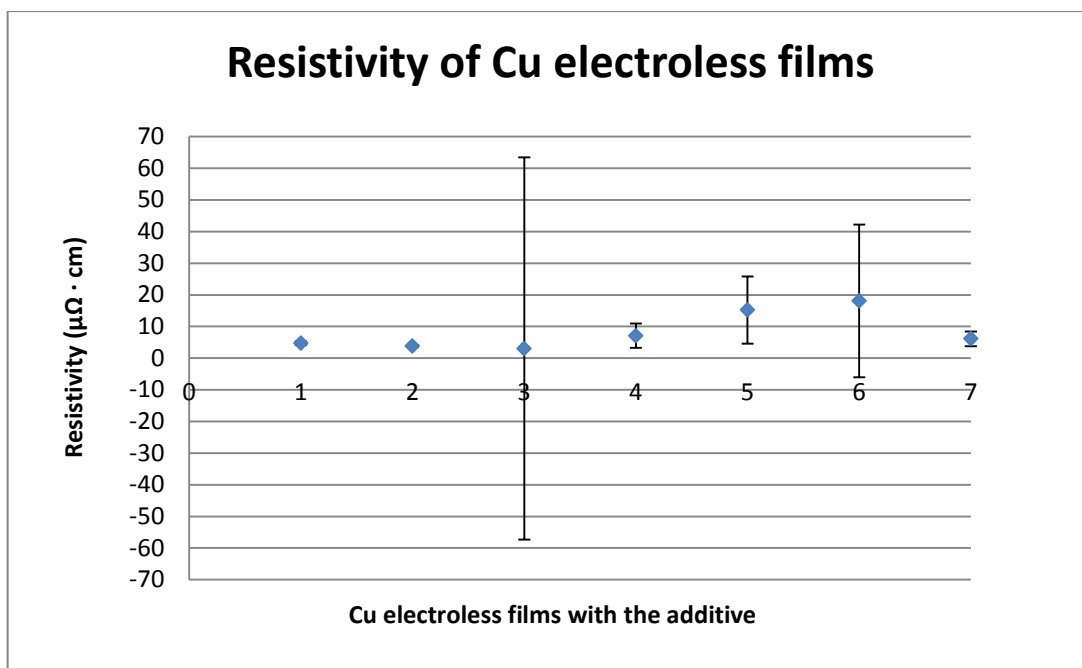


Figure 38: Resistivity of Cu electroless films; where: 1 –standard, 2 – glycerol, 3- glycerol 2, 4 – sorbitol, 5 –cytosine, 6 – saccharin, 7 – glycerol + saccharin.

Figure 38 illustrates that the lowest ρ values were achieved from the Cu coatings deposited from the solutions containing glycerol – in both concentrations. Whereas, the highest ρ was registered for coating obtained from saccharin-enhanced plating bath.

Conclusions regarding the Cu electroless deposits obtained from the modified solutions with the organic additives

A number of the organic compounds were tested as the additives to the Cu electroless solutions. The main goal of this work was to produce a dense and uniform Cu coating which acts as a cathode in the Ti sandwich structure and which could act as a seed layer for Cu electroplated film. (Electroplating is subsequently used on top of electroless plating to achieve a suitably thick Cu layer).

It was possible to produce Cu deposits from the electroless solutions containing the organic additives. The conducted analyses provided qualitative and quantitative characteristics of the obtained Cu films.

The XRD qualitative analysis showed that all Cu coatings were well crystallized except the coating produced from the solution containing gelatin.

It was found from the EDX analysis that the lowest C content occurred for the Cu coating electrolessly plated from the solution containing glycerol. This result was concluded to be in accordance with the film thickness which was confirmed with FIB measurements. It was found that the solution containing glycerol produced the thickest Cu coating (70 – 100 nm). Whereas, the standard Cu coating had the thickness of 50 nm.

The roughness analysis conducted with the Olympus Lext Confocal Laser Microscope showed that the Ra of 0.01 and 0.012 μm was achieved by the Cu coatings produced from the solutions containing glycerol and sorbitol and these were the lowest measured Ra. The Ra of 0.016 was noted for the standard Cu coating. Whereas, the lowest resistivity of 3.04 and 3.83 $\mu\Omega \cdot \text{cm}$ was obtained by the Cu coatings deposited from the solutions containing glycerol in concentrations: 47.82 g/l and 28.85 g/l respectively. ρ of 4.73 $\mu\Omega \cdot \text{cm}$ was measured for the Cu standard deposit.

It was noted from the obtained results, that the preferred parameters were obtained by a Cu coating deposited from the electroless solution containing glycerol (28.85 g/l). Therefore, the further modifications of the Cu electroless solution were conducted with the addition of the glycerol to the standard Cu solution composition presented in Table 28.

b) Surfactants

Introduction

The term 'surfactant' refers to molecules that are surface-active, usually in aqueous solutions [135]. These molecules have a property of strong adsorption at the water-air interface, hence, they reduce surface energy (Gibbs theorem). This phenomenon is due to the fact that surfactants have both hydrophilic and hydrophobic moieties. In addition to this, surfactants exhibit an ability to form self-assembled structures – micells, in aqueous solution. The structures are created to reduce the exposure of the hydrocarbon chains to water.

The metal deposition in electroless plating is accompanied by H₂ evolution on a cathode (substrate). Incorporation of the surface-active compound into the electroless plating bath plays a crucial role in the removal of hydrogen bubbles from the surface of the substrate by adsorption at the H₂-liquid interface [136]. Hence due to this, it is possible to achieve uniform and pit-free deposit from electroless plating.

Three surface-active compounds were selected as possible additives to the Cu electroless plating solution. They were the non-ionic surfactants: Tween 20, PEG M. W. 4600, and Triton X-100 (TX-100). The reason for incorporation of the non-ionic surface active agents was dictated by their property to not ionize in aqueous solution, because of the hydrophilic group which does not dissociate [137].

The purpose of this experiment was to build a dense and uniform Cu coating with the assistance of a surface active agent, which could be thickened, if applicable for Ti sandwich structure process.

Chemicals

The chemical composition of the sensitisation and activation solutions remained the same.

The following chemical compounds were added to the base Cu electroless plating solution (Table 29): glycerol 98% (28.85 g/l) + one of the following surfactants: Tween 20, PEG M. W. 4600, and TX-100.

The quantities were adjusted according to the studied literature or were modified. The used surface active agents with the quantities applied have been presented in Table 35.

Table 35. Non-ionic surfactants applied to Cu electroless plating solution.

Surfactant	Quantity g per l	Reference
Tween	0.05	Modified from [136]
PEG	0.1	[138]
TX-100	0.04	Investigated independently

Equipment

a) Sensitisation and activation stages

250 ml glass beaker x 2; filled with the solutions to the level that allows submerging specimens in a vertical position,

plastic tweezers x 2 (one for handling sample in the sensitisation solution and the second for the activation solution).

b) Cu electroless plating

250 ml beaker – Cu electroless plating tank,

500 ml beaker for water jacket,

Hot plate stirrer,

Temperature sensor,

Metal stand,

Magnetic stirrer,

pH meter,

PVC insulation tape,

Stainless steel tweezers,

Crocodile clip.

Experimental procedure

Firstly, the specimens, comprising of Ti substrate, size of 4 cm x 5 cm, coated with the S1818 photoresist covered with a double layer of the PVC insulation tape, were immersed in the sensitisation solution ($\text{SnCl}_2 + \text{HCl}$) for 10 minutes. The specimens were subsequently rinsed with DI water and placed in the activation solution ($\text{AgNO}_3 + \text{NH}_4\text{OH}$) for 20 minutes. The extensive DI water rinse of the sample was applied after activation in order to eliminate contamination of the plating solution with an excess of deposited species. All processes were performed at ambient temperature. Prior to the drying step, the outer layer of the PVC insulation tape was removed, to allow plating only from the S1818 resist side of the Ti sandwich structure.

Afterwards, the specimens were dried in a convection oven at 50°C . Finally, the samples were immersed in the Cu electroless plating solutions for 1, 2, 3, 4, 5, 10 and 15 min. to determine plating rates for each of the solution at $50 - 52^\circ\text{C}$ and pH of 10.35 – 45. Then, the Cu plated S1818 resists were rinsed with DI water and dried with the air gun. Lastly, the PVC tape, covering the back side of the Ti, was removed.

i) Plating rate of the solutions containing the additions of the surfactants

The plating rate of the solutions containing the additions of glycerol and one of the tested surfactants was investigated by registering the weight gain during the deposition process. The specimens were weighed prior to electroless plating and 24 hours after the deposition to allow water from the coating to evaporate. An analytical balance with a precision to 1×10^{-4} g was employed to weigh the samples.

Results and discussion

The results of the investigated plating rates for the solutions containing the additions of the glycerol and one of the tested non-ionic surface active agents have been presented in Figure 39.

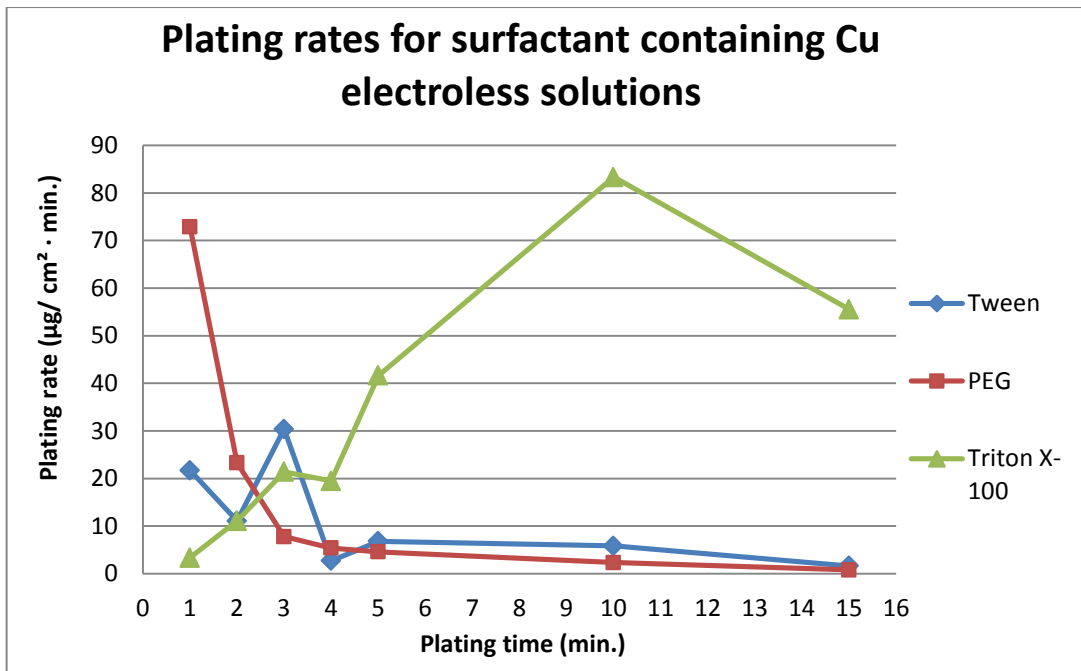


Figure 39: Plating rates for the Cu electroless solutions containing additions of glycerol and three different surfactants.

Figure 39 shows that the maximal deposition rate of $82 \mu\text{g}/\text{cm}^2$ at 10 min of plating was achieved from the solution containing the additions of glycerol (28.85 g/l) and TX-100 (40 mg/l). After approx. 13 minutes, it was found that the coating started to delaminate. Therefore, it was determined that 10 minute-deposit from the solution Cu base plating bath + glycerol and TX-100, in the quantities mentioned above, would be further investigated.

An optical micrograph of the coating which was analysed has been presented in Figure 40.

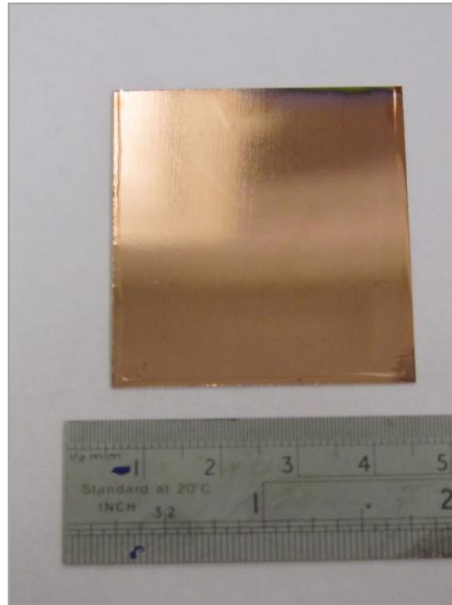


Figure 40: Optical micrograph of the Cu electroless coating obtained from the Cu electroless solution containing the additions of glycerol and Triton X-100.

ii) Surface morphology study of a deposit obtained from the Cu electroless solution containing glycerol and TX-100

The “sandwich structure” comprising of Ti/S1818/Cu layers, with the Cu coating obtained from the solution modified by the additions of glycerol and TX-100, was analysed with an EDX Spectrometer in order to investigate the Cu coverage of the photoresist and an elemental content of the electroless deposit.

Results and discussion

The SEM micrograph of the Cu coating has been presented in Figure 41.

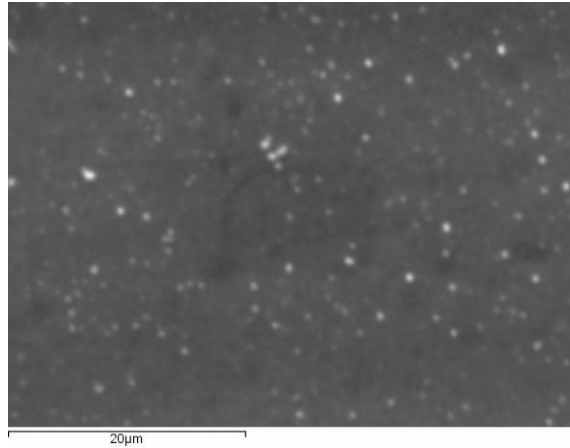


Figure 41: SEM micrograph of the Cu deposit obtained from the Cu electroless solution containing the additions of glycerol and TX-100.

It can be seen from the SEM micrograph of the Cu deposit that the coating is compact and it exhibits uniform grain size.

The results of the EDX analysis of the structure comprising of the Ti/S1818/Cu have been shown in Figure 42.

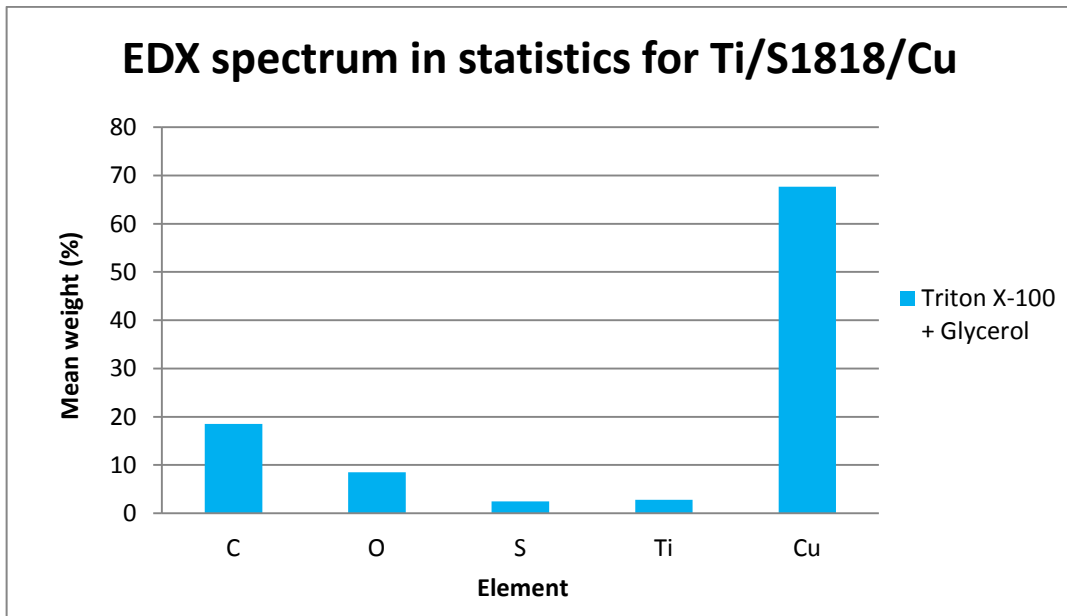


Figure 42: EDX spectra in statistics for Ti structure: Ti/S1818/Cu - Cu obtained from the Cu electroless solution containing the additions of Glycerol and Triton X-100.

The element analysis of the sample showed a high Cu content (mean weight 68 %). This could indicate a compact deposit plated from the modified solution. The detected C, O and Ti

come from the subsequent Ti/S1818 layers due to the electron beam penetration. Whereas, present S in the EDX spectrum, come from the Cu electroless plating solution, containing $\text{CuSO}_4 \cdot 5\text{H}_2\text{O}$.

iii) Characterisation of the Cu deposit obtained from the electroless solution containing glycerol and TX-100

Further analyses of the Cu coating deposited from the electroless solution containing additions of glycerol and TX-100 were carried out in order to evaluate its properties and compare with the standard Cu electroless coating.

The investigated parameters were: thickness, roughness, and resistivity. All the measurements were conducted in accordance with the procedures described in the Chapter 6.2.3, section a).

Results and discussion

The results of the conducted measurements of the Cu coating deposited from the electroless solution containing additions of glycerol and TX-100 were compared with the Cu electroless plating deposited from the standard solution (Table 36).

Table 36. The parameters obtained from the Cu coating deposited from the Cu electroless solution containing the additions of glycerol and TX-100.

Parameter (unit)	Glycerol + TX-100	Standard
Thickness (nm)	60	50
Roughness (μm)	0.031; Std. Dev. 5.95×10^{-3}	0.016; Std. Dev. 0.01
Resistivity ($\mu\Omega \cdot \text{cm}$)	2.37; Std. Dev. 4.09×10^{-6}	4.73; Std. Dev. 0.59×10^{-6}

It can be seen from the obtained results, that the Cu coating produced with the addition of glycerol and TX-100 was 10 nm thicker than that from the standard electroless solution. In addition to this it exhibited lower resistivity than that of the standard plating bath. Moreover, the registered resistivity was the lowest amongst all tested before Cu electroless coatings,

described in the Chapter 6.2.3, section a). This phenomenon was previously described by [139] that an increase in the density of electroless copper films might be the reason the lower resistivity.

The roughness parameter of the Cu electroless deposit from standard solution was noted to be lower than that of additive-enhanced one.

Conclusions to the Cu electroless deposit modified with the addition of glycerol and TX-100

The achieved Cu coating from the modified Cu base solution by the additions of glycerol (28.85 g/l) and TX-100 (40 mg/l) was the subject of an in-depth investigation.

Firstly, it was found that the as-modified Cu electroless solution exhibits the highest plating rate compared to the other tested solutions. As a result it was possible to deposit a uniform, dense Cu coating with a mirror-finish appearance. Moreover, it achieved a thickness of 60 nm (50 nm standard Cu coating) and the lowest measured resistivity of $2.37 \mu \Omega \cdot \text{cm}$ amongst the other tested Cu electroless coatings.

A feasibility of the modified Cu coating to be a base to a Cu electrolytic deposit have been presented in the Chapter 6.3.

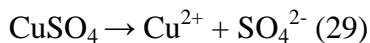
6.3 Cu electroplating

Introduction

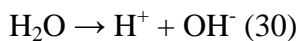
Electrodeposition is a method of applying metallic coatings to conductive surfaces by electrochemical processes. The metallic or conductive substrate to be electroplated is immersed in a solution containing a dissolved salt of the metal to be deposited and is connected as a cathode (negatively charged) to a power supply. Positively charged - one or two anodes (if plating from both sides of the substrate) are immersed in the electrolyte and complete the electrical circuit.

In the cell where the Cu electroplating is conducted, the following reactions take place [140]:

- Copper sulphate on dissolution in water dissociates into ions:



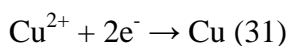
- Water itself to some extent also dissociates



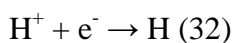
Under the influence of a potential applied between two electrodes immersed in the electrolyte the ions migrate. The positively charged ions migrate towards the cathode and the negatively charged ions move towards the anode.

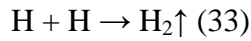
Cathode

At the cathode surface the positive charges of the Cu ions are neutralised by acceptance of electrons from the cathode and as a result Cu atoms are formed.



Most of the H is evolved from the cathode surface as a gas. Only a small proportion is built into the cathode deposit, this phenomenon is called hydrogen embrittlement.

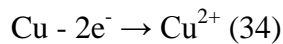




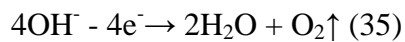
Anode

At the anode the reaction depends on the material from which the anode is made. When the anode is made of Cu, the following reactions occur:

The Cu anode dissolution which forms Cu ions in the solution replenishes those Cu ions removed from the electrolyte by Cu deposition at the cathode.



The other reaction which takes place is a discharge of hydroxyl ions which results in O₂ evolution.



Electroplating, in Ti sandwich structure, was applied in order to build-up the thickness of the Cu electroless film, according to the schematic presented in Figure 43. The Cu electroless coating deposited on the non-conductor was used as a seed layer prior to electroplating. Both layers: Cu electroless and Cu electroplated deposits form the cathode in the Ti sandwich structure.

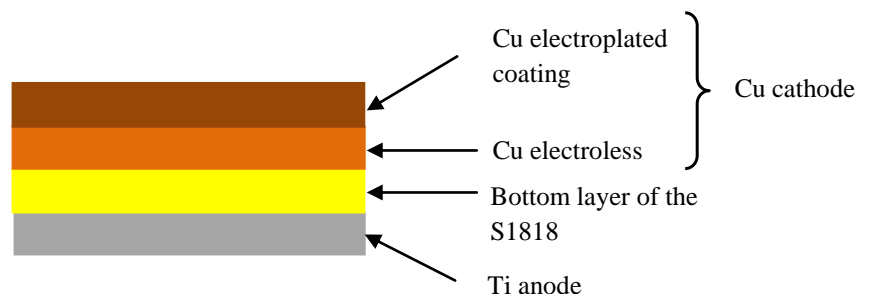


Figure 43: Cross section of the sandwich structure with the Cu double layer.

Chemicals

The Cu electrolyte for electroplating consisted of the following chemical compounds: Copper (II) sulphate 5 hydrate 98% extra pure ($\text{CuSO}_4 \cdot 5\text{H}_2\text{O}$), sulphuric acid 98% (H_2SO_4), saccharin 98 + % ($\text{C}_7\text{H}_5\text{NO}_3\text{S}$), sodium chloride (NaCl), and DI water.

Equipment

DC power supply,

Multimeter,

Metal stand,

2 stainless steel crocodile clips,

2 copper wires with soldered copper pads in the end enabling connection with the crocodile clips,

500 ml glass beaker,

Hot plate stirrer,

Magnetic stirring bean,

PVC insulation tape,

Perspex jig for positioning the anode and the cathode,

Anode: Cu sheet of the Cu content mean weight 99.01 % and O of mean weight 0.99%.

Cathode: Cu electroless deposit, obtained from the solution containing the additions of glycerol and TX-100, on top of the Ti/S1818 structure.

Experimental procedure

The Cu electroplating was carried out with the electrolyte prepared in the proportions presented in Table 37.

Table 37. Cu electroplating electrolyte constituents with quantities used per litre.

Chemical compound	Quantity (unit per l)	Reference
$\text{CuSO}_4 \cdot 5\text{H}_2\text{O}$	75 g	[141]
H_2SO_4	100 ml	[141]
$\text{C}_7\text{H}_5\text{NO}_3\text{S}$	240 mg	[142]
NaCl	50 mg	[141]
DI H_2O	To make up volume to 1 l	-

The plating conditions which were kept constant during all conducted experiments were: ambient temperature of the electrolyte, stirred at 350 rpm, cathode current density (CD) of 15 mA/cm² and IEG of 2.5 cm.

Plating rates of Cu electrolyte were determined by applying the constant parameters: CD, IEG, temp., and stirring speed, while time of plating varied from 10 to 60 minutes in 10 min. intervals.

The plating rates of Cu electroplating solution were determined by registering the weight gain of the sample after electrodeposition.

Results and discussion

The measurements of the thickness of the Cu electroplated deposits were conducted with the use of FIB. Figure 44 presents the cross section micrographs of the structure comprising of (from the bottom) Ti, S1818 resist, Cu electroless coating and Cu electroplated deposit for picture a) and the structure of S1818/Cu electroless coating and Cu electrodeposited coating in case of pictures b, c, d, e, and f.

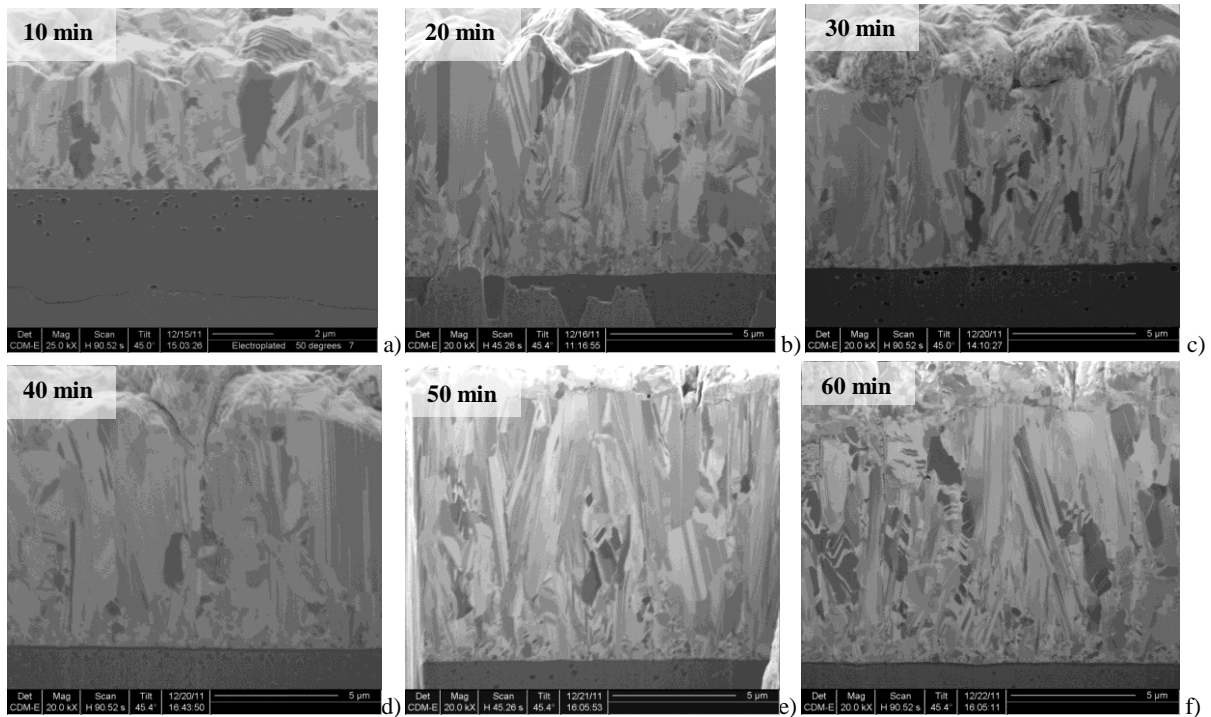


Figure 44: FIB cross section of the Ti/S1818/Cu structure with the Cu electroplated at different times on top of Cu electroless deposit.

All obtained micrographs of the Cu electrodeposits show a compact coating with no indication of any detachment or voids in the structure. It can be noted that after 20 minutes of electroplating the Cu coating doubled the thickness. Whereas, the 30-minute plating resulted in no significant gain in thickness of the Cu coating. The growth of bigger lumps is observed from 30 to 60 minute-plating. This could be explained by the growth of Cu grains while plating is continued.

Thickness measurements of the Cu electrodeposits have been illustrated in Figure 45.

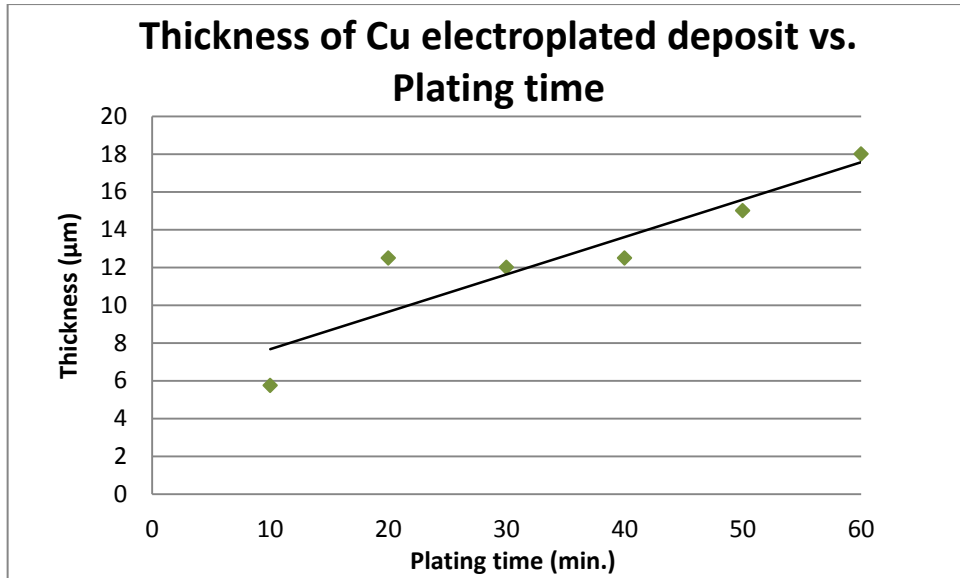


Figure 45: Thickness of Cu electroplated deposit measured with FIB vs. plating time.

It can be noted from the obtained results of the measurements that thickness increases almost linearly to plating time.

Plating rates for Cu electroplating have been presented in Figure 46.

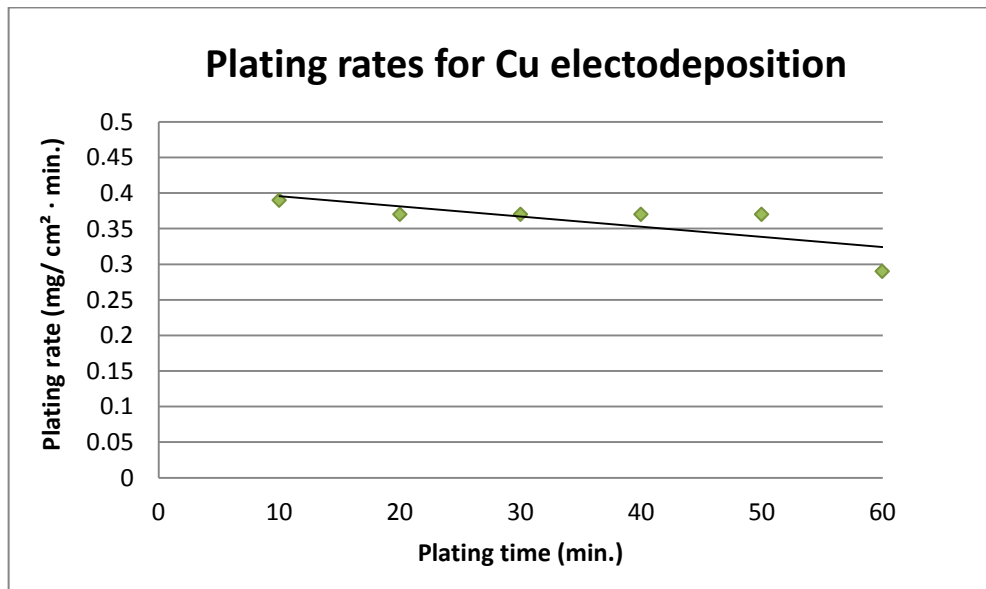


Figure 46: Plating rates for Cu electrodeposition.

The results for the plating rates indicate that the rate of deposition remains the same for 20, 30, 40, and 50 minutes plating, whereas there is slightly higher plating rate for 10 minute deposition. A drop in plating rate was noted in case of 1 hour electrodeposition.

The optical micrograph which illustrates the deposition steps with an indication of the surface finish of the Cu electroless deposit (middle) and Cu electroplated (right) coating have been presented in Figure 47.

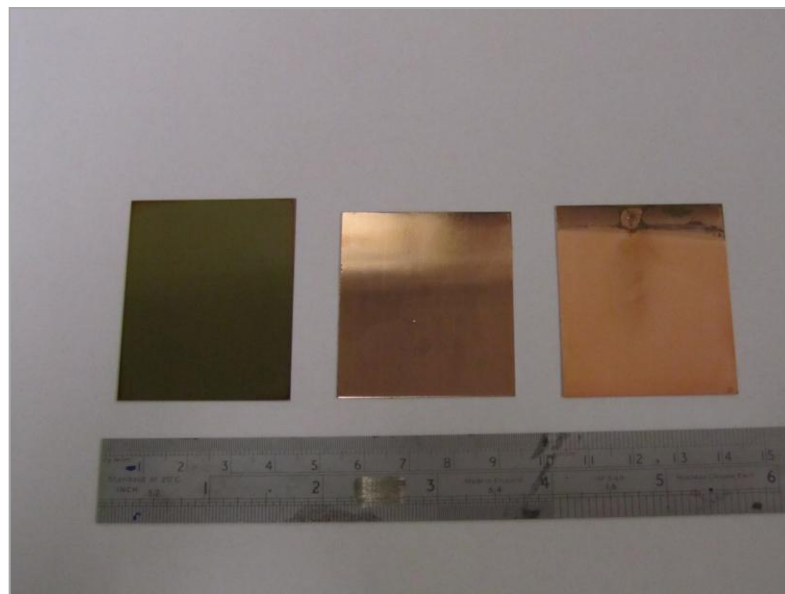


Figure 47: Optical micrographs illustrating the deposition process steps; from left: specimen coated with the S1818 resist, then coated with the Cu electroless deposit, and Cu electroplated layer on top of electroless deposit.

The finish of the Cu electroplated coating was observed to be matt which was in accordance to what was reported in the literature [140].

6.4 Summary of fabrication of the cathode in the Ti sandwich structure

The Cu cathode was successfully obtained. The electroless plating was selected as a method for deposition of the Cu film. It was found that the Cu electroless solution (Table 28) containing the additions of glycerol (28.85 g/l) and surfactant TX-100 (40 mg/l) exhibited the highest plating rate amongst the other solutions which were tested. Moreover, it produced Cu coating with the preferential parameters such as the lowest resistivity ($2.37 \mu\Omega \cdot \text{cm}$) and thickness of 60 nm (10 nm thicker than the coating obtained from the standard solution).

The selected Cu electroless coating was tested also with the success as the seed layer to Cu electrodeposition. The Cu electroplating coatings showed dense structure of the film.

Both layers of the Cu coatings: Cu electroless deposit and Cu electroplated created the cathode for the Ti sandwich structure electrolytic etching.

Chapter 7: Experimental procedure – Titanium sandwich structure microfabrication

Introduction

In this Chapter, the Ti microfabrication process steps have been presented. The emphasis was put on the experimental work carried out on electrolytic etching of Ti by application of a novel sandwich structure.

7.1 Ti sandwich structure microfabrication

The established three steps of the Ti sandwich structure building have been presented in Chapters 4, 5, and 6. Each of these process stages determines the next one and has an impact on the final Ti sandwich structure electrolytic etching.

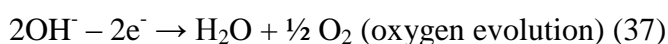
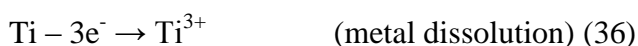
The complete Ti sandwich structure microfabrication route, in the form of a flow diagram, has been presented in Appendix D.

7.2 Mechanism of electrolytic etching of Ti sandwich structure

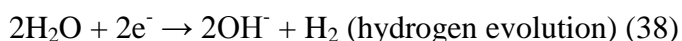
The electrolytic etching of Ti in the sandwich structure is governed by Faraday's Laws of Electrolysis which were described in Chapter 2.2.5.

The electrolytic etching of the Ti sandwich structure incorporates cathodic and anodic partial reactions following the electrochemical laws. The reactions which take place at the electrodes in the electrolytic cell are presented below.

At the anode (substrate) (+ ve):



At the cathode (- ve):



Other reactions also take place in the reaction chamber:

$2\text{Ti} + 6\text{HCl} \rightarrow 2\text{TiCl}_3 + 3\text{H}_2$ (39) where TiCl_3 is very soluble in water

$\text{Ti}^{3+} + 3(\text{OH})^- \rightarrow \text{Ti}(\text{OH})_3 + 3\text{e}^-$ (40) (reaction by-product)

$2\text{Ti}(\text{OH})_3 + 2\text{H}_2\text{O} \rightarrow 2\text{Ti}(\text{OH})_4 + \text{H}_2$ (41)

- **Current distribution in the Ti sandwich structure**

During electrolytic etching, material dissolution is ascribed to current density distribution on an anode surface. In through-mask process it also determines the shape evolution [51].

Primary and tertiary current distributions are the controlling factors in the uniformity and directionality of the etching [143]. The primary current distribution depends on the geometry of the electrochemical system [51]. In the electrolytic etching additional factors play a role as well. On the pattern scale, the current distribution is influenced by the spacing of the pattern and its geometry. High current density was found to be on features distributed further apart, leading to an increased rate of those features [51], [143]. The mask aspect ratio also has a significant influence on the current distribution [144]. The current density decreases on the anode as the mask aspect ratio increases. A higher aspect ratio improves the current distribution due to the enhancement of the current scattering effect of the mask edge step [145]. However, when the thickness of the mask is too high, the current density is not sufficient to dissolve metal.

The novel Ti sandwich structure was introduced in order to allow more uniform current distribution on the substrate (Ti), which acts as an anode, by minimising the gap between the two electrodes to the order of microns.

The cathode (Cu) is a very good conductor and it enables a uniform current distribution and thereby improves the etching process of Ti in an electrolytic cell. The two electrodes (Ti and Cu) are separated with a very thin layer (4 μm) of a dielectric material (S1818 resist) in order to minimise an inter-electrode gap (IEG) and to optimise the current distribution.

The electrolyte flow through the patterned cathode/insulator/anode is responsible for the ion exchange between the electrodes, while the current distribution defines the shape evolution of the pattern at the anode (Ti). Figure 48 shows the diagram of the Ti sandwich structure immersed in the electrolyte and ready to be electrolytically etched where h is thickness of the

dielectric – here the IEG (S1818 resist), b is the anode thickness, and c is the cathode thickness. D is the hole diameter in the resist and a is the hole spacing. B indicates the diameter of the etched hole and d its depth.

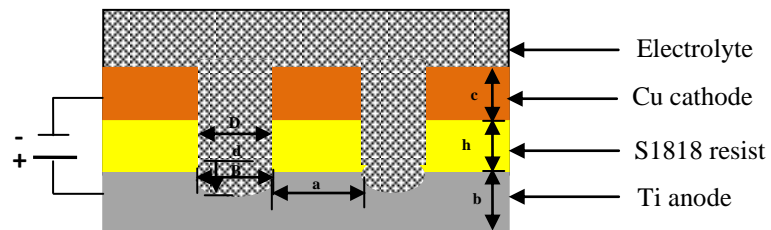


Figure 48: Schematic diagram of the Ti sandwich structure during electrolytic etching.

6.3 Chemicals

10 % w/v HCl, diluted from concentrated HCl, specific gravity of 1.16 g/cm³, 32 %, classified as a corrosive acid, was applied as the etchant for the electrolytic etching of Ti in the sandwich structure.

The selection of the etchant and its concentration was dictated by the results of the work conducted by [54]. It was reported that 10 % w/v HCl used in conjunction with a DC electrolytic etching resulted in etched-through Ti.

The acid electrolytes usually produce fewer by-products than common salt electrolytes [144], [146]. In contrast to salt electrolytes, the acid etchants dissolve the metal and the metal ions are transported away by the electrolyte [55]. This becomes especially important in the process of the Ti sandwich structure, where the IEG measures 4 µm. The accumulation of the by-product can interfere with the ion exchange during electrolytic etching and cause short-circuits.

In addition to this, HCl electrolyte is beneficial due to the fact that the chloride ions prevent anode (Ti) passivation [145].

6.4 Equipment

In the process of electrolytic etching of Ti in the sandwich structure, the following equipment was incorporated:

- Pulse Reverse Rectifier M-O-T, Micro und Oberflächen Technik GmbH
- Multimeter, Precision Gold M218
- 2 stainless steel crocodile clips
- 2 copper wires with soldered copper pads in the end enabling connection with the crocodile clips
- Glass beaker (250 ml) used in work presented in the section 6.5.1
- Glass beaker (400 ml) used for samples in work described in 6.5.2,
- Hot plate stirrer
- Magnetic stirrer
- Perspex jig

- PVC insulation tape
- Double-sided tape used to attach the Ti sandwich structure to the insulated stainless steel sample, acting as a support in the Perspex jig.

7.5 DC electrolytic etching of Ti sandwich structure

Two approaches were applied to electrolytically etch Ti in the sandwich structure.

In both cases DC was used.

The electrolytic etching was applied to the Ti sandwich structure, consisting of:

- a) Ti/S1818/Cu electroless films, and
- b) Ti/S1818/Cu electroless + electrodeposited films.

The processing routes of these two Ti sandwich structures with the results of the final electrolytic etching stage are presented in detail below.

7.5.1 DC electrolytic etching of Ti sandwich structure with an electroless Cu cathode





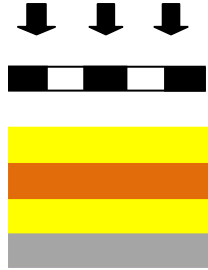


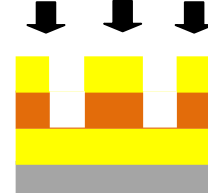
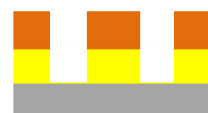
The Ti sandwich structure comprising of Ti, S1818 resist and the Cu electroless film, deposited from the solution containing addition of glycerol 28.85 g/l, was the subject of the DC electrolytic etching.


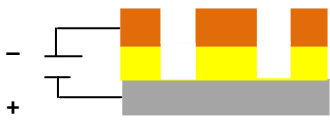


Experimental procedure

The specimen was connected to the DC power supply through the Multimeter (to measure a current flow) and placed in an electrolytic cell filled with the electrolyte (10 % w/v HCl). The applied current density (CD) was 20 A/cm² for 1 minute at ambient temperature.

Table 38 illustrates the details of the process steps of microfabrication of the Ti sandwich structure.

Table 38: Process steps for the fabrication of the Ti sandwich structure with Cu cathode electrolessly deposited.

Procedure Equipment and parameters applied	Sandwich structure profile
1. Titanium preparation. Procedure described in 4.2.1 and 4.2.2	
2. Ti coating with the positive photoresist S1818 (4µm thick)– bottom layer photoresist	
3. Deposition of Cu electroless layer t = 5 min. T = 50°C, pH = 10.35	
4. Coating of second layer of the positive photoresist (1.8µm) on top of Cu layer. EMS spin coater, 4000rpm, t=60s.	
5. UV exposure of top photoresist through the mask. MA 56, UV lamps int. = 5mW/cm², 38 s.	
6. Developing of the positive photoresist (top layer). MF-319 Developer, T=ambient, t= 80s, beaker developing.	
7. Etching through the patterned Cu. Etchant: 35%Bé FeCl₃, T=ambient, t=15s.,(beaker etching). 150 µm in diameter of etched pattern in Cu.	
8. UV exposure of the positive photoresist (bottom layer) through the etched pattern in Cu. MA 56, UV lamps int. = 5mW/cm², 40 s.	
9. Developing of the positive photoresist (bottom layer). MF-319 Developer, T=ambient, t= 120s, beaker developing.	

Procedure Equipment and parameters applied	Sandwich structure profile
10. Microscope assessment of developed sample. Nikon Optishot Acquisition System	
11. DC electrolytic etching of the sample. DC power supply, CD = 20 A/cm ² , t = 1 min., T = ambient	
12. Stripping the positive photoresist. Stripper: acetone	
13. Microscope assessment of the sample. Olympus Lext Confocal Laser Microscope	

Results and discussion

The following results of the DC electrolytic etching were observed regarding the Ti sandwich layers:

- Ti: the DC electrolytic etching resulted in half-etched Ti.
- S1818 resist withstood the DC electrolytic etching, however some damage was observed, in the form of a burn, in the place where the electrode connection was placed.
- Cu electroless cathode: the Cu film cracked and consequently delaminated from the S1818 resist from the start of the electrolytic etching.

- **SEM analysis of half-etched Ti**

The SEM analysis was conducted of the half-etched Ti. The surface finish of the half-etched micro-holes was optically evaluated.

Results and discussion

The SEM micrographs (Figure 49) of the half-etched microholes in Ti indicated that:

A spherical shape of the etched dimples corresponded to the imaged pattern and the etched surface showed a relatively smooth and shiny finish. The investigation of the edges of the etched pattern showed an even finish of the Ti micro-holes.

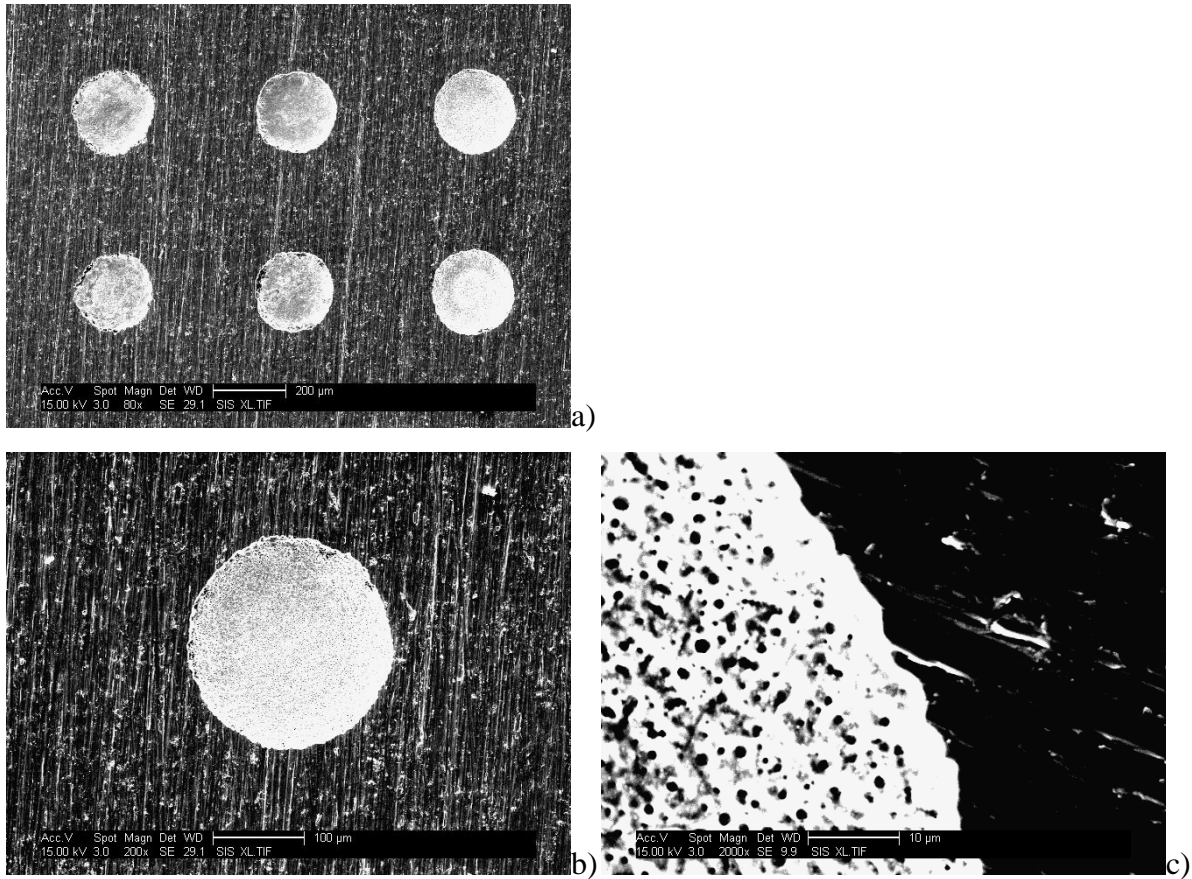


Figure 49: SEM micrographs of a) half-etched micro-holes, b) selected half-etched micro-hole, and c) the edge of the micro-hole.

- **Analysis with Olympus Lext Confocal Laser Microscope**

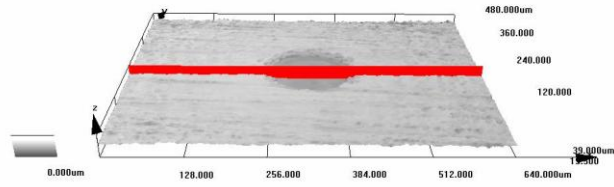
The half-etched Ti was the subject of the analysis with the Olympus Lext Confocal Laser Microscope. The microscope was used to scan the surface of the etched Ti in order to receive 3 D optical micrograph and a 2 D profile micrograph of the half-etched micro-hole. The 3 D image was used to assess the shape of etched pattern, whereas the profile image provided information about the shape of the base of the micro-hole. The base shape was an indication of current distribution on the anode (Ti) during the electrolytic etching of the sandwich

structure. A “W profile” could imply that the current distribution was not uniform over the whole area of the pattern.

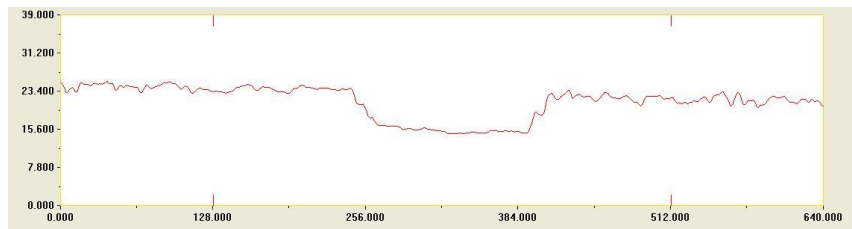
Results and discussion

The results of the conducted analysis with the Olympus Lext Confocal Laser Microscope are shown in Figure 50. The micro-holes presented on the next page do not correspond to those illustrated in Figure 49.

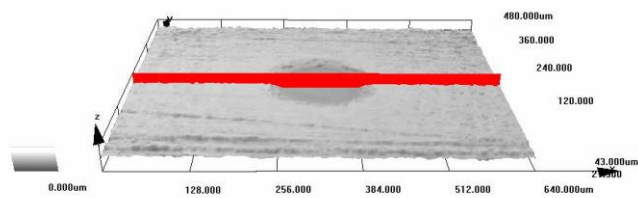
1a)



b)



2a)



b)

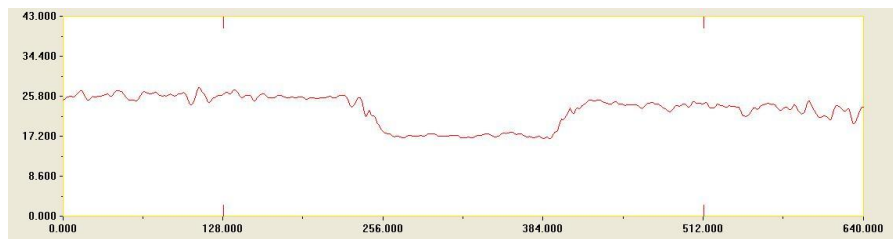


Figure 50: Olympus Lext Confocal Laser Microscope micrographs of half-etched microholes etched at $CD = 20 \text{ A/cm}^2$, for 1 min. 1a), 2a) 3D scans of the half-etched microholes with corresponding 2D images of the profiles of the etched micro-holes: 1b), 2b).

The 3D micrographs of the etched micro-holes showed a spherical finish. Both presented micrographs of the half-etched micro-holes in Ti had flat-base profiles. The micro-holes of approx. 8 μm in depth were etched by applying 20 A/cm² for 1 minute.

- **Analysis of etched Ti**

The etched Ti was the subject of further analysis conducted with the Olympus Lext Confocal Laser Microscope. The half-etched micro-holes in Ti were scanned with the microscope in order to measure the etch depth, width of the etched pattern and surface roughness. The obtained values were used to calculate etch rate and etch factor. The surface roughness presented below, was received from the plane roughness analysis of the half-etched micro-holes measured individually.

Results and discussion

The results of the conducted analysis are presented in Figures 51 and 52.

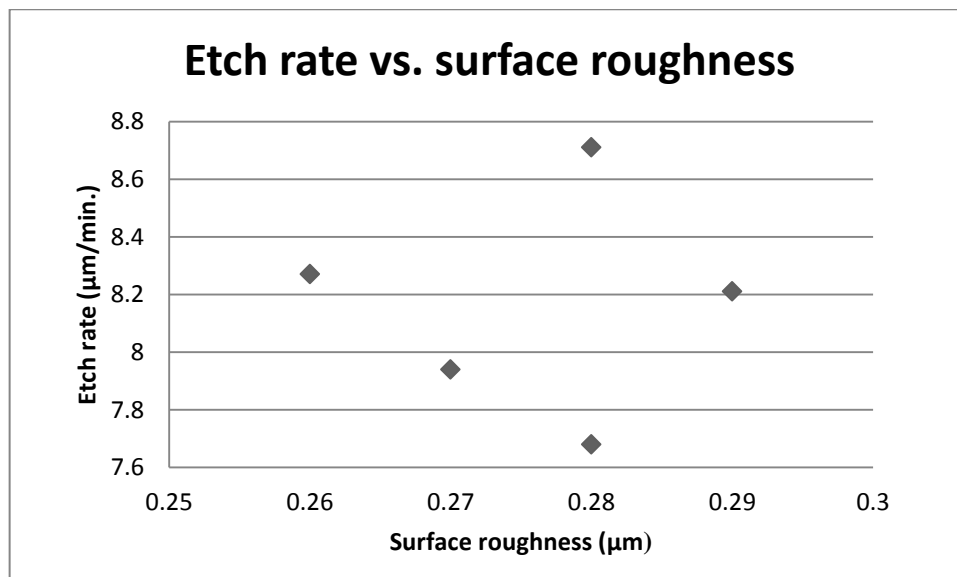


Figure 51: Etch rate vs. surface roughness of half- etched micro-holes in Ti with the use of Cu electroless cathode.

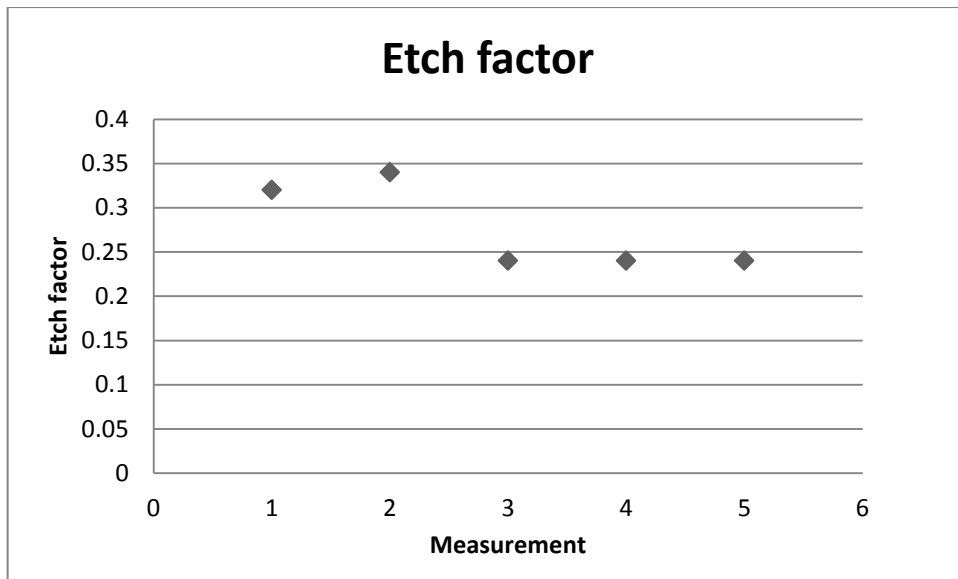


Figure 52: Etch factor of half- etched micro-holes in Ti with the use of Cu electroless cathode.

It can be noted from the Figure 51 that an increase of the etch rate does not correspond with the increase of the surface roughness. The maximum measured etch rate was of order of 8.7 $\mu\text{m}/\text{min}$.

The etch factor, illustrated in Figure 52, was of order of 0.34 to 0.24.

Conclusions to Ti sandwich structure microfabrication with the electroless Cu cathode

It was possible to conduct the electrolytic etching of the Ti sandwich structure with the Cu cathode obtained from the electroless deposition. The applied parameters were a CD of 20 A/cm^2 for 1 minute at ambient temperature. The depth of the etched micro-holes varied from 7.7 to 8.7 μm with the surface roughness from 0.26 to 0.29 μm . The process showed limitations in the form of a delamination of the Cu electroless cathode in the electrolyte during electrolytic etching. As a consequence of this, the process could not exceed 1 minute or be repeated.

7.5.2 DC electrolytic etching of Ti sandwich structure with the Cu cathode obtained from electroless and electrodeposition









The Ti sandwich structure comprising of Ti, S1818 resist and the Cu double films, was electrolytically etched during the DC cycle. The Cu cathode comprised a Cu electroless coating (60 nm) deposited from the solution containing the additions of glycerol and TX-100 to the base solution and the electrodeposited layer of Cu (12.5 μm). Different current densities were tested in order to determine the etch rate, surface roughness, and etch factor of the produced pattern in Ti.

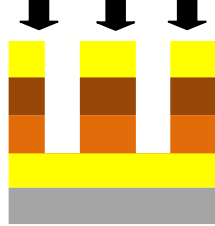
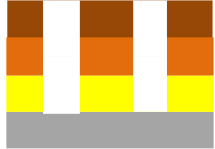

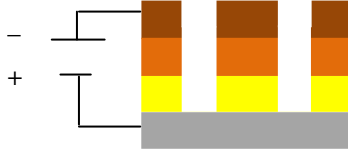


Experimental procedure

The specimen was connected to the DC power supply through the Multimeter and placed in an electrolytic cell filled with the 10 % w/v HCl. The CDs of 10, 15, 20, and 25 A/cm^2 were applied for 1 minute at ambient temperature. Stirring of the electrolyte at 250 rpm was applied throughout the experiments.

The Ti sandwich structure microfabrication process steps have been outlined in Table 39.

Table 39: Process steps for the fabrication of the Ti sandwich structure with Cu cathode obtained from electroless and electrodeposition.

Procedure Equipment and parameters applied	Sandwich structure profile
1. Titanium preparation. Procedure described in 4.2.1 and 4.2.2	
2. Ti coating with the positive photoresist S1818 (4µm thick)– bottom layer photoresist)	
3. Electroless deposition of Cu layer t = 10 min., T = 50°C, pH = 10.45	
4. Electrodeposition of Cu layer t = 20 min., T= ambient, CD = 15 mA/cm ²	
4. Coating of second layer of the positive photoresist (1.8µm) on top of Cu layer. EMS spin coater, 4000rpm, t=60s.	
5. UV exposure of top photoresist through the mask. MA 56, UV lamps int. = 5mW/cm ² , 38 s.	
6. Developing of the positive photoresist (top layer). MF-319 Developer, T=ambient, t= 80s, beaker developing.	
7. Etching through the patterned Cu layers. Etchant: 35 ⁰ Bé FeCl ₃ , T=ambient, t= 60s, (beaker etching)	

Procedure	Sandwich structure profile
<p>Equipment and parameters applied</p> <p>8. UV exposure of the positive photoresist (bottom layer) through the etched pattern in Cu.</p> <p>MA 56, UV lamps int. = 5mW/cm², 80 s</p>	
<p>9. Developing of the positive photoresist (bottom layer).</p> <p>MF-319 Developer, T=ambient, t= 240s, beaker developing.</p>	
<p>10. Microscope assessment of developed sample.</p> <p>Nikon Optishot Acquisition System</p>	
<p>11. DC electrolytic etching of the sample.</p> <p>DC power supply, CD = 10, 15, 20, 25 A/cm², t = 1 min., T = ambient, stirring 250 rpm</p>	
<p>12. Stripping the positive photoresist.</p> <p>Stripper: acetone</p>	
<p>13. Microscope assessment of the sample.</p> <p>Olympus Lext Confocal Laser Microscope</p>	

- **SEM analysis of half-etched Ti**

The SEM analysis of the half-etched Ti was carried out produced by applying 20 A/cm² for 1 minute. The surface finish of the half-etched micro-holes was investigated.

Results and discussion

Figure 53 shows the SEM micrographs of the micro-holes in Ti.

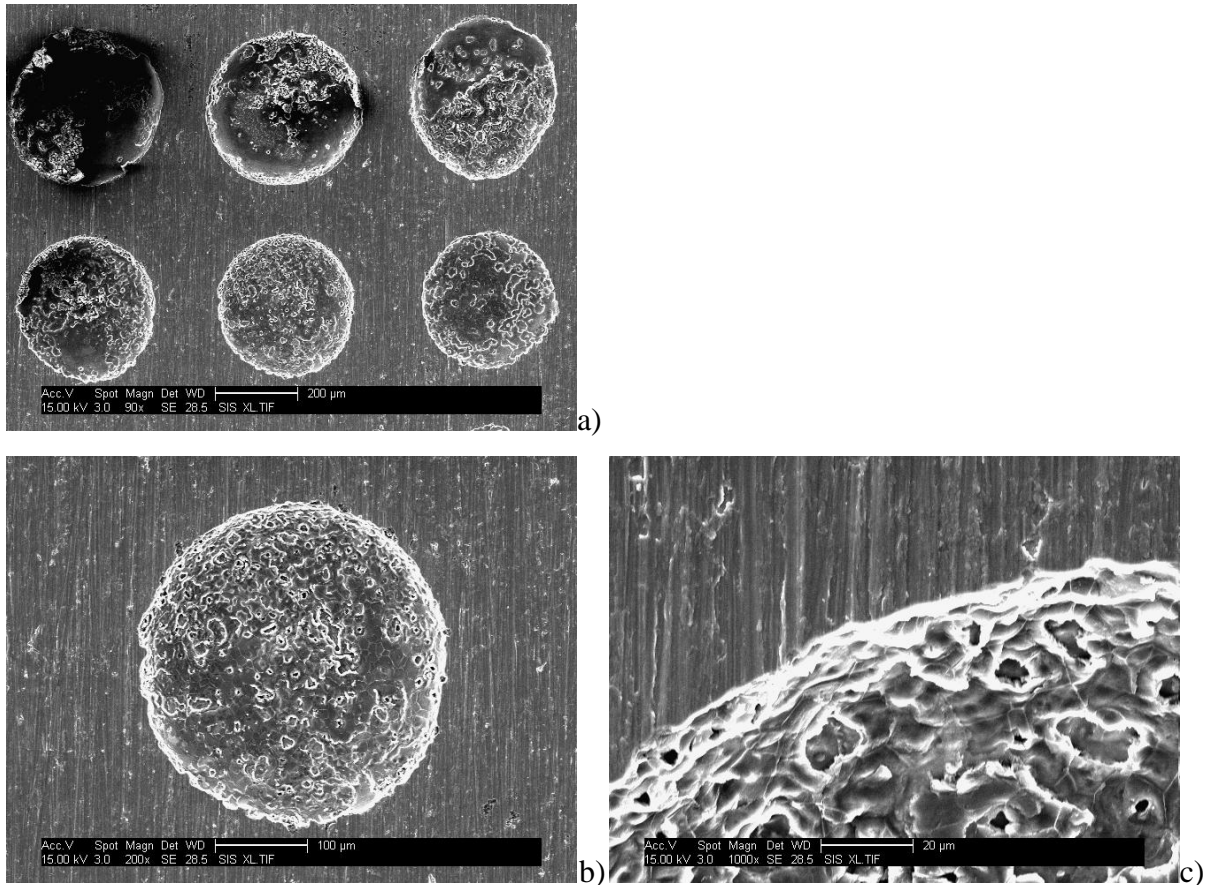


Figure 53: SEM micrographs of a) half-etched micro-holes, b) selected half-etched micro-hole, and c) the edge of the micro-hole, produced by applying 20 A/cm^2 for 1 minute at ambient temperature.

The obtained SEM micrographs presented the spherical shapes of the etched micro-holes in Ti, corresponding to the imaged pattern. The edges of the etched micro-holes were found to have a rough appearance. The uneven-looking areas of the etched micro-holes were due to different surface roughnesses.

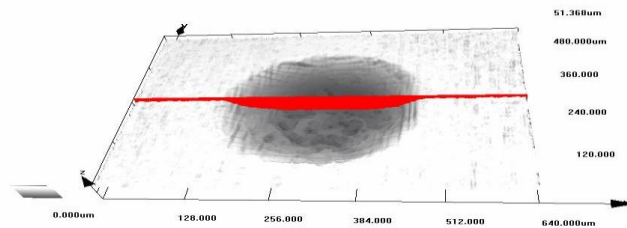
- **Analysis with Olympus Lext Confocal Laser Microscope**

The analysis of the half-etched Ti sample, obtained by applying CD of 20 A/cm^2 for 1 minute, was conducted with the Olympus Lext Confocal Laser Microscope. The shape of the pattern from 3D scan and a shape of a profile in 2D were the subjects of the investigation.

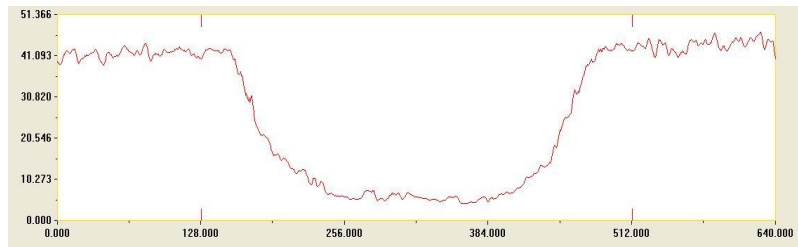
Results and discussion

The results of the Olympus Lext Confocal Laser Microscope analysis are outlined in Figure 54.

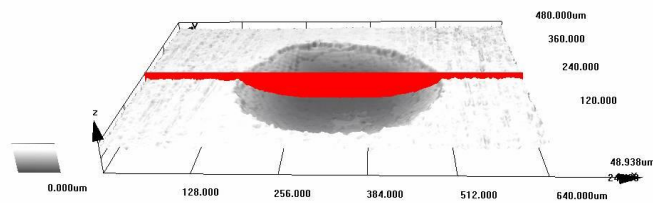
1a)



b)



2a)



b)

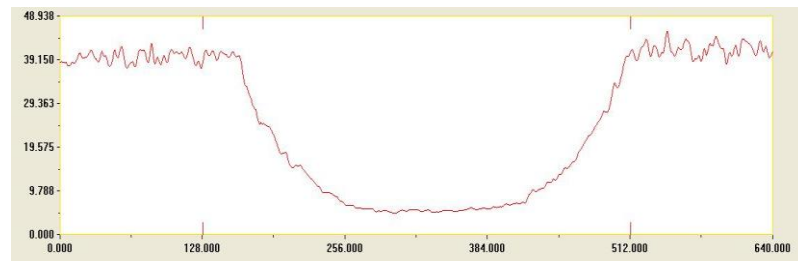


Figure 54: Olympus Lext Confocal Laser Microscope micrographs of half-etched microholes etched at $CD = 20 \text{ A/cm}^2$ for 1 min. 1a), 2a) 3D scans of the half-etched microholes with corresponding 2D images of the profiles of the etched micro-holes: 1b), 2b).

The micrograph obtained from the Olympus Lext Confocal Laser Microscope analysis indicated flat base profiles of the half-etched micro-holes and no “W” effect was observed on the 2D scans of the etched micro-holes.

The micro-holes of approx. 37 μm in depth were etched by applying 20 A/cm^2 for 1 minute.

- **Analysis of etched Ti**

Further analyses, of the samples electrolytically etched by applying CD of 10, 15, 20, and 25 A/cm^2 , were carried out with the Olympus Lext Confocal Laser Microscope. The half-etched micro-holes in Ti were measured in order to determine the etch depth, width of the etched pattern and surface roughness. The obtained values were used to calculate etch rate and etch factor. The surface roughness values were received from the plane roughness analysis of the half-etched micro-holes measured individually.

Results and discussion

The obtained data, from the conducted analyses, have been presented in the following Figures: 55, 56, 57, and 58.

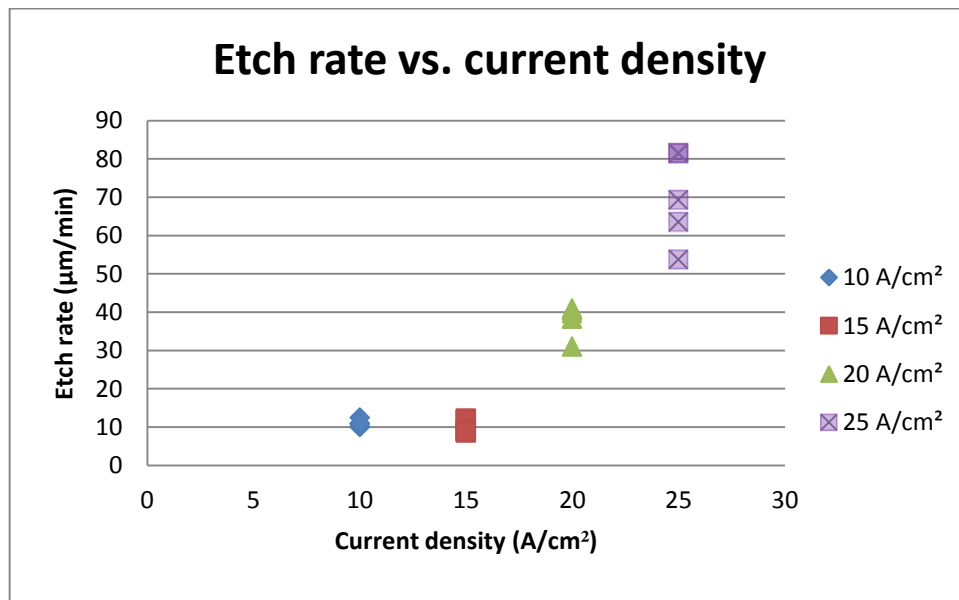


Figure 55: Etch rate vs. current density.

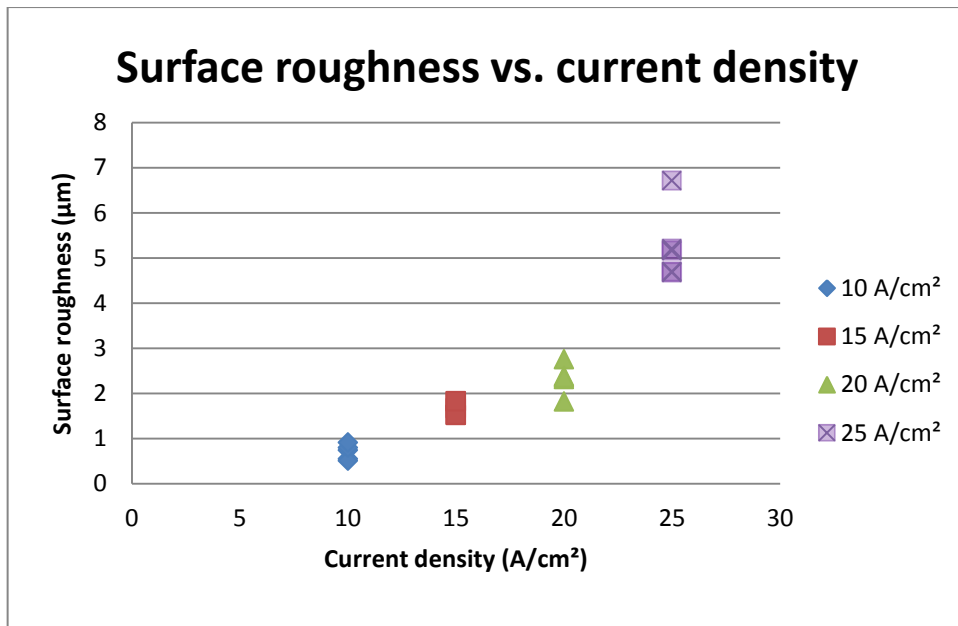


Figure 56: Surface roughness vs. current density.

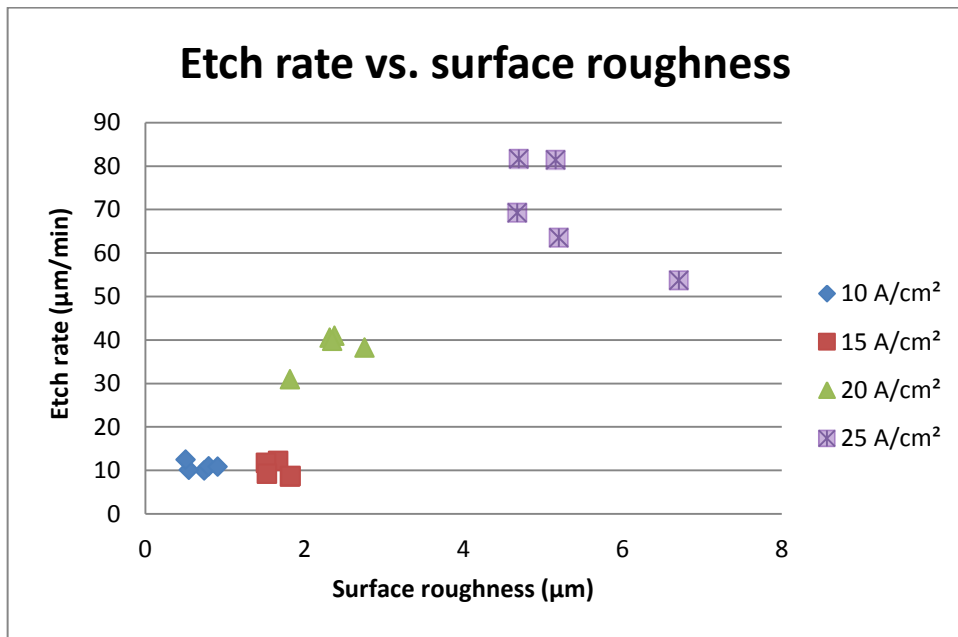


Figure 57: Etch rate vs. surface roughness.

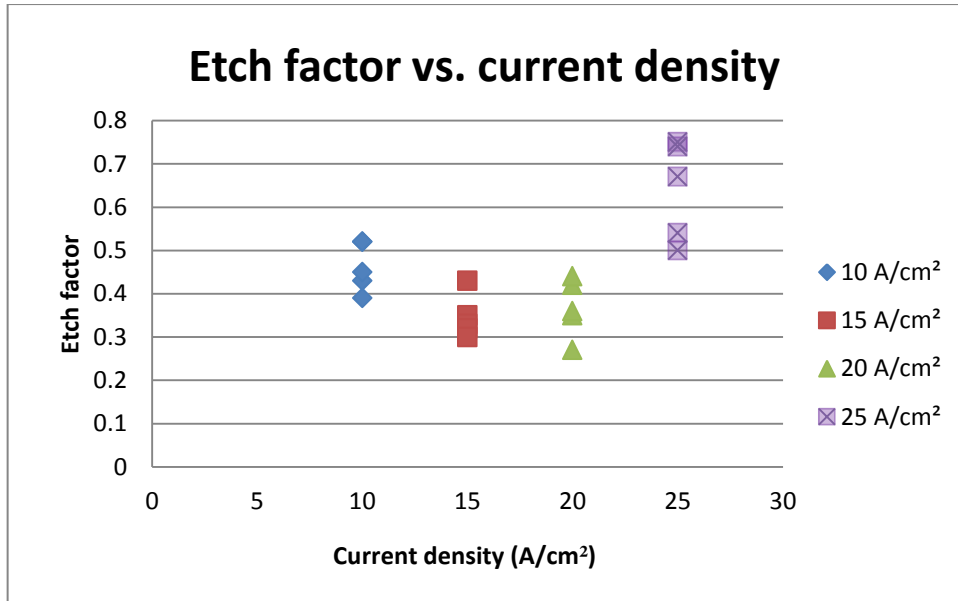


Figure 58: Etch factor vs. current density.

The results of the conducted analyses showed that the etch rate increased with an increase of the current density. The minimum etch rate of 10 $\mu\text{m}/\text{min}$. was noted for two current densities: 10 and 15 A/cm^2 . The maximum etch rate of 82 $\mu\text{m}/\text{min}$. was observed in case of CD of 25 A/cm^2 , which was found to be in accordance with Faraday's Law.

The surface roughness was found to increase linearly with increasing current density and increasing etch rate. A minimum Ra from 0.5 to 0.9 μm was noted for the CD of 10 A/cm^2 . Whereas, the maximum Ra from 4.7 to 6.7 was observed in the case of CD of 25 A/cm^2 .

There was no obvious trend observed with the etch factor. An etch factor of the order of 0.3 to 0.7 was measured, whereas, the highest etch factor of 0.75 was observed when CD of 25 A/cm^2 was applied.

i. Effect of number of electrode connections on electrolytic etching uniformity

It was observed in the results of the previous electrolytic etching of Ti in sandwich structure that the half-etched microholes were distributed non-uniformly over the area of the anode (Ti).

Any influence of an additional two electrode connections on improvement of uniformity of electrolytic etching on all area of the sample was the subject of the analysis. Two crocodile clips per electrode were introduced to improve the current distribution over the whole area of the anode in the sandwich structure.

Equipment

The equipment utilised in the electrolytic etching remained the same as described in section 6.4 apart from 4 stainless steel crocodile clips and 4 copper wires, with soldered copper pads in the end enabling connection with the crocodile clips.

Experimental procedure

In this section the experiments on DC electrolytic etching of a novel Ti sandwich structure were carried out by applying the CD of 20 A/cm^2 . This value of CD was chosen as a compromise between a high etch rate (approx. $40 \text{ }\mu\text{m/min.}$) to relatively low surface roughness (max. $2.7 \text{ }\mu\text{m}$) shown in Figure 57.

The specimens were connected, 2 crocodile clips per electrode, to the DC power supply through the Multimeter and placed in an electrolytic cell filled with the 10 % w/v HCl. The CD of 20 A/cm^2 was applied for 1 minute at ambient temperature. Magnetic stirring of the electrolyte (250 rpm) was applied during the experiments.

Results and discussion

The results of the conducted experiments, presented in Figure 59 and 60, were compared with the measurements taken of the half-etched Ti achieved by DC electrolytic etching at the same conditions but with the application of 1 crocodile clip per electrode.

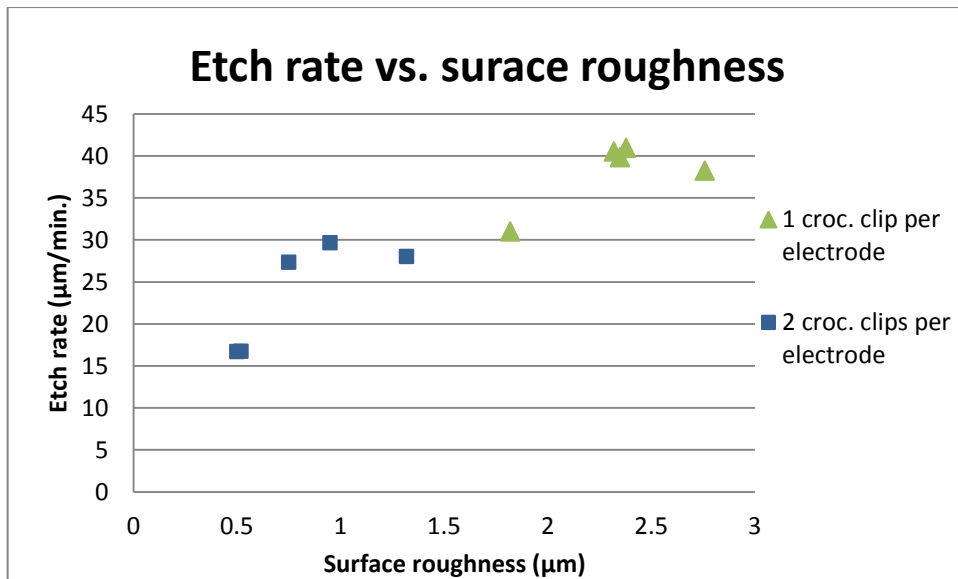


Figure 59: Etch rate vs. surface roughness etched Ti in sandwich structure electrolytic etching process utilising different number of electrode connectors.

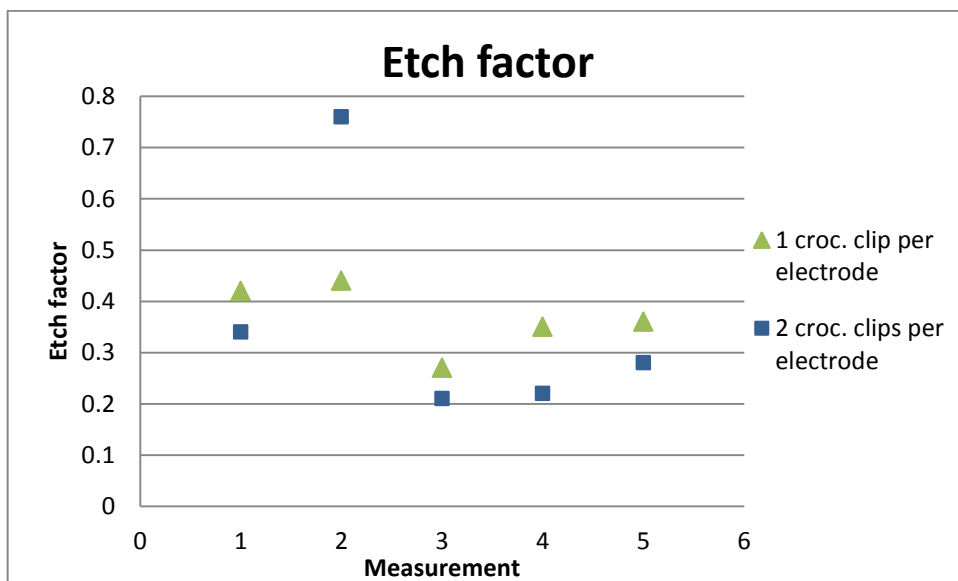


Figure 60: Etch factor of etched Ti in sandwich structure electrolytic etching process utilising different number of electrode connectors.

It can be seen from Figure 59, where the etch rate vs. surface roughness have been plotted that the additional 2 electrode connectors resulted in a decrease of surface roughness of the micro-

holes by approx. 50 %. It also caused a drop of the etch rate by approx. 10 $\mu\text{m}/\text{min}$ and the etch factor.

However, the observation of the sample etched with 2 crocodile clips per electrode revealed that the half-etched micro-holes were distributed on a larger area of the patterned sandwich structure. Therefore, further work on electrolytic etching of Ti sandwich structure was carried out with the applications of 4 crocodile clips and 4 copper wires with soldered copper pads.

ii. Effect of stirring speed on electrolytic etching uniformity

Strong stirring was previously reported to improve the etching rate and the dimensional distribution in the anode [44]. This phenomenon was explained by dissipation of the by-products. However, the stirring resulted also in rough surface finish of the edges of etched pattern.

In this work two different mechanical stirring speeds were tested in order to improve the etch rate and a uniformity of Ti etching in the sandwich structure over a bigger area of the substrate. The mechanical stirrer incorporating a magnetic follower was utilised to increase the electrolyte flow rate.

Equipment

The following equipment was applied during the electrolytic etching of the Ti sandwich structure:

- Pulse Reverse Rectifier M-O-T, Micro und Oberflächen Technik GmbH,
- Multimeter, Precision Gold M218,
- 4 stainless steel crocodile clips,
- 4 copper wires with soldered copper pads in the end enabling connection with the crocodile clips,
- Glass beaker 400 ml,
- Hot plate stirrer,
- Magnetic stirring bean,
- Perspex jig,

- PVC insulation tape,

Double sided tape to attach the sandwich structure to the insulated stainless steel sample – acting as a support in the Perspex jig.

Experimental procedure

The DC electrolytic etching of the Ti sandwich structure was conducted by applying a CD of 20 A/cm² for 1 minute. Two mechanical stirring speeds were tested; 250 and 800 rpm.

The specimens were connected to the DC power supply through the Multimeter by 2 crocodile clips per electrode and placed in the electrolytic etching chamber filled with 10 % w/v HCl.

Results and discussion

The summary of the conditions applied and the observations of the electrodes have been presented in Table 40.

The results of the conducted work have been illustrated in Figures: 61 and 62.

Table 40. Conditions applied for electrolytic etching of Ti sandwich structure with 2 stirring speeds with the observations of the electrodes.

Sample no.	Current density (A/cm²)	Etching time (min.)	Stirring speed (rpm)	Number of crocodile clips applied	Anode observation	Cathode observation
1	20	1	250	4	Half-etched; anode attacked around the edges, pattern transferred and anodized	Black “smut” present around the edges and on the top of the cathode
2	20	1	800	4	Half-etched; pattern etched over a larger area of the anode	Black “smut” on the cathode corresponding to the area of the etched pattern on the anode

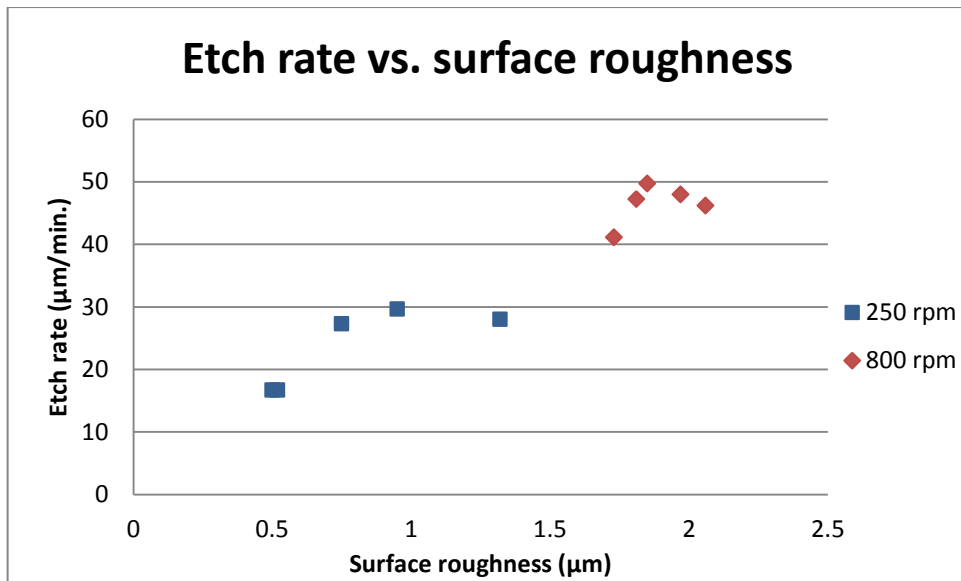


Figure 61: Etch rate vs. surface roughness of the etched Ti at two mechanical stirring speeds.

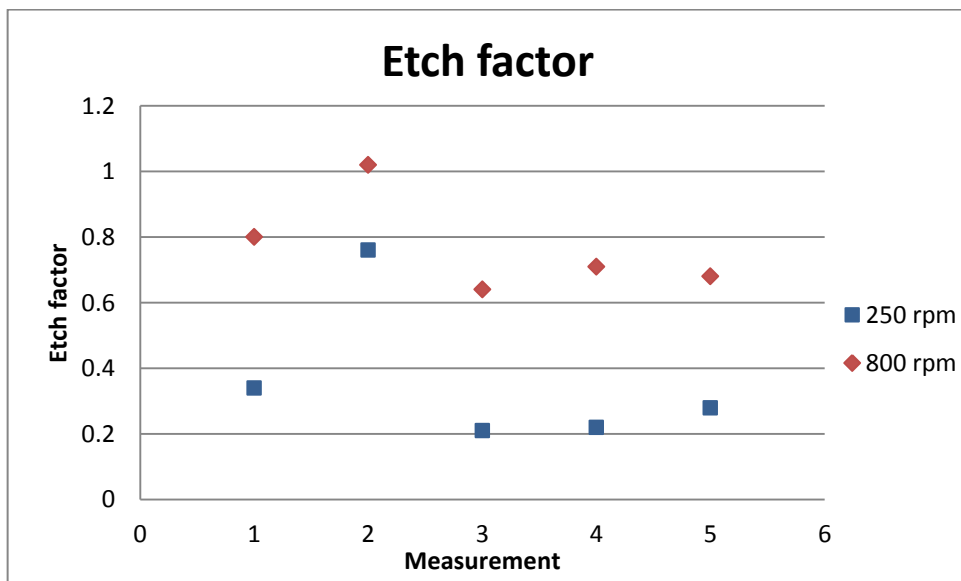


Figure 62: Etch factor of the etched Ti at two mechanical stirring speeds.

It can be noted from Figure 61, illustrating the etch rate of etched micro-holes in Ti substrate vs. surface roughness, that the etch rate was increased by the factor of 2 when the mechanical stirring speed of 800 rpm assisted the electrolytic etching. The increase was also observed in case of the surface roughness of the etched micro-holes, when the same etching conditions

were applied. The values of the surface roughness of the etched pattern, when 800 rpm mechanical stirring was used, were found to be within the range of 1.8 to 2.0 μm , whereas the surface roughness of the etched micro-holes, when the stirring speed of 250 rpm was applied, was observed to be from 0.5 to 1.3 μm . The etch factor, Figure 62, was found to be higher of the pattern etched with the stirring speed of 800 rpm the factor of 2 and 3, respectively.

- **Electrolytic etching with a high mechanical stirring speed**

The electrolytic etching of the Ti sandwich structure was performed for 1, 2 and 3 minutes with the mechanical stirring of the electrolyte. The aim of this work was to achieve a higher etch rate and observe the uniformity of the etched pattern over the area of the anode.

Experimental procedure

The DC electrolytic etching of the Ti sandwich structure was conducted by applying a CD of 20 A/cm^2 for 1, 2, and 3 minutes. The specimens were connected to the DC power supply through the Multimeter by 2 crocodile clips per electrode and placed in the electrolytic etching chamber. The mechanical stirring of the electrolyte, 10 % w/v HCl, was incorporated at the speed of 800 rpm.

Results and discussion

The results of the experimental work are presented in the form of a table with an indication of the observation taken of the anode and the cathode, see Table 41, and in Figures: 63, 64, and 65. The measurements were taken from the same area of each of the sample (top array of the etched micro-holes).

Table 41. Conditions applied for electrolytic etching of Ti sandwich structure with a high mechanical stirring speed.

Sample no.	Current density (A/cm²)	Etching time (min.)	Stirring speed (rpm)	Number of crocodile clips applied	Anode observation	Cathode observation
	20	1	800	4	Half-etched; pattern etched over a larger area of the anode	Black “smut” on the cathode corresponds to the area of the etched pattern on the anode
2	20	2	800	4	Half-etched; pattern etched over a larger area of the anode	Black “ smut” on the whole area of the cathode
3	20	3	800	4	Half-etched; pattern etched over a larger area of the anode	Black “ smut” on the whole area of the cathode

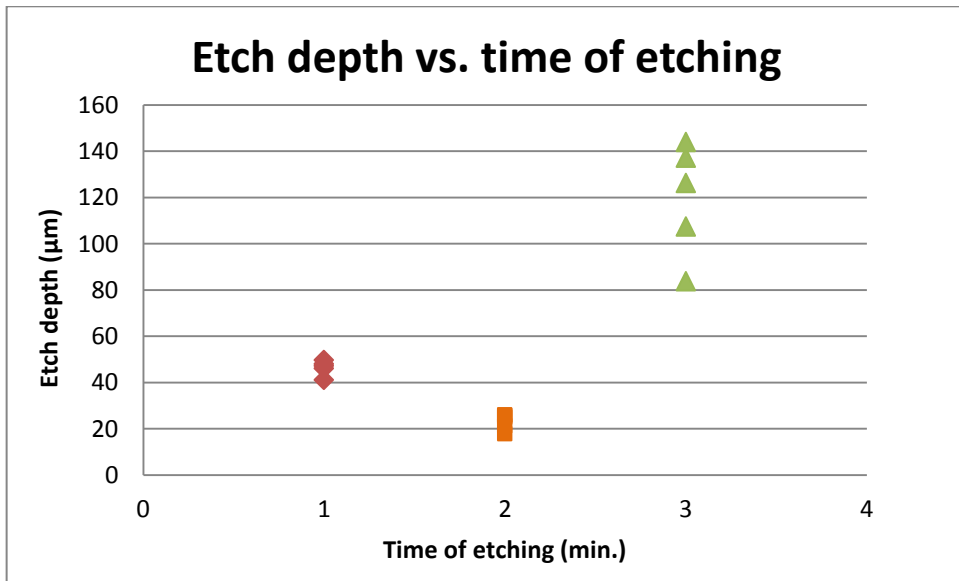


Figure 63: Etch depth vs. time of etching of Ti at high mechanical stirring speed.

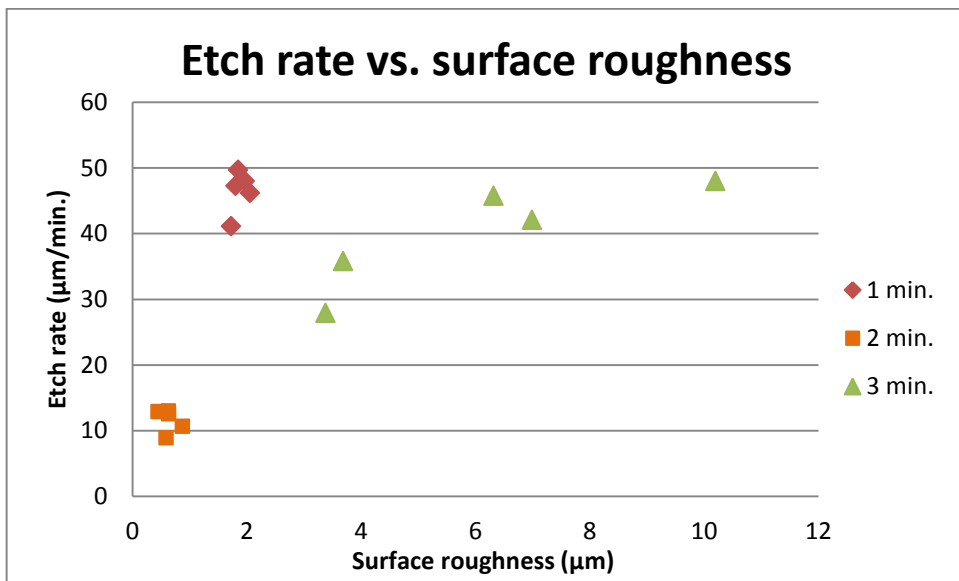


Figure 64: Etch rate vs. surface roughness of the etched Ti at a high mechanical stirring speed.

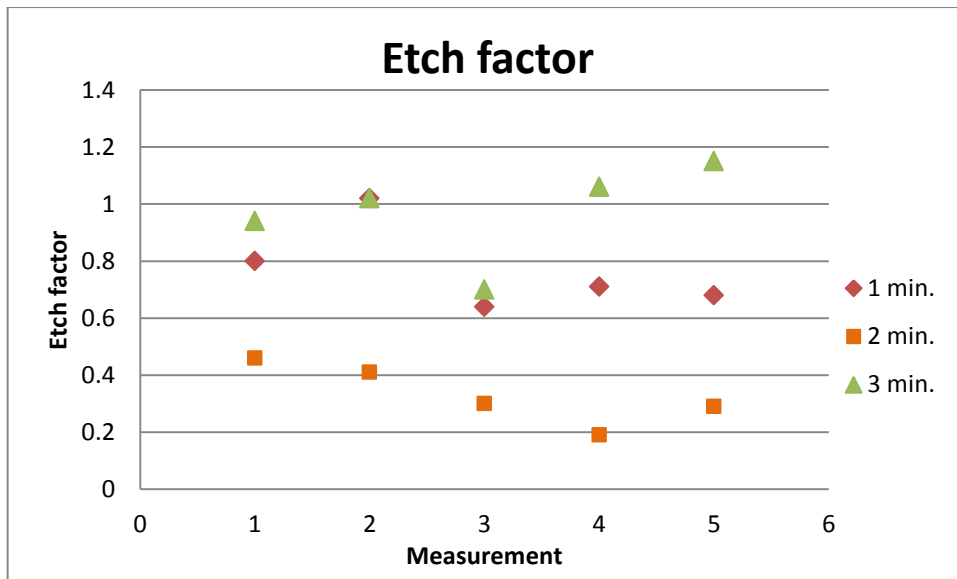


Figure 65: Etch factor of the etched Ti at a high mechanical stirring speed.

Figure 63 illustrates the etch depth of the micro-holes, electrolytically etched for 1, 2, and 3 minutes. It indicates that the significant linear increase of the etch depth was measured for the micro-holes etched for 3 minutes. Whereas, the sample which was etched for 2 minutes noted a decrease of the etch depth compared to 1 minute-etching. These results could indicate that the process was not reproduced. This could be explained by the rapid mechanical stirring (800 rpm) applied during electrolytic etching which could cause the electrolyte turbulence and non-uniform etching as well as the by-products build-up.

The maximum etch depth of 143.9 μm was measured for the micro-hole etched for 3 minutes.

Figure 64 illustrates the correlation between the etch rate and the surface roughness of the etched micro-holes in Ti. It can be noted that 1 minute of electrolytic etching effected in the highest etch rate of 49 $\mu\text{m}/\text{min}$. and the surface roughness of average 1.8 μm . The micro-holes etched for 3 minutes were also produced at a high etch rate (maximum) of 48 $\mu\text{m}/\text{min}$., but with high surface roughness of average 6.1 μm whereas, the measurements taken of the etched pattern for 2 minutes showed the lowest etch rate to surface roughness ratio. The lowest surface roughness could indicate that the parameters applied during electrolytic etching did not cause the by-products to build-up.

The etch factors, presented in Figure 65, of the etched Ti, shows that the highest etch factor was calculated for the micro-holes etched for 3 minutes, and the lowest for a 2 minute etched pattern.

The other observation made was the appearance of the anode and the cathode stressed in Tables 40 and 41. It was observed that the electrolytic etching of Ti sandwich structure, when 4 crocodile clips were applied (2 per electrode), were accompanied by the black film generation on the cathode. Further work was carried out in order to explain the reason why this phenomenon took place and a chemical composition of the black film.

- **Analysis of the black film generated on the cathode**

The cathode from the Ti sandwich structure, consisting of the Cu electroless film and electrodeposited Cu on top of it, was the subject of the analyses conducted. The cathode from the sandwich structure was detached, after electrolytic etching for 3 minutes with an application of 4 connectors to the electrodes, to be analysed with SEM and XRD techniques in order to verify the chemical composition.

Results and discussion

The results of the carried out analysis have been presented in Figures 66 and 67.

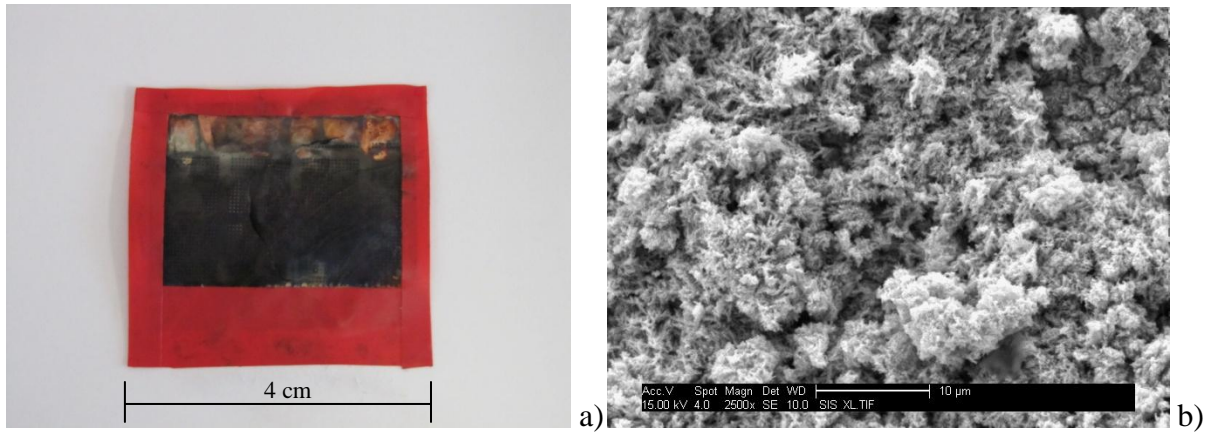


Figure 66: a) An optical micrograph of the cathode after electrolytic etching; b) SEM micrograph of the black film on top of the Cu cathode.

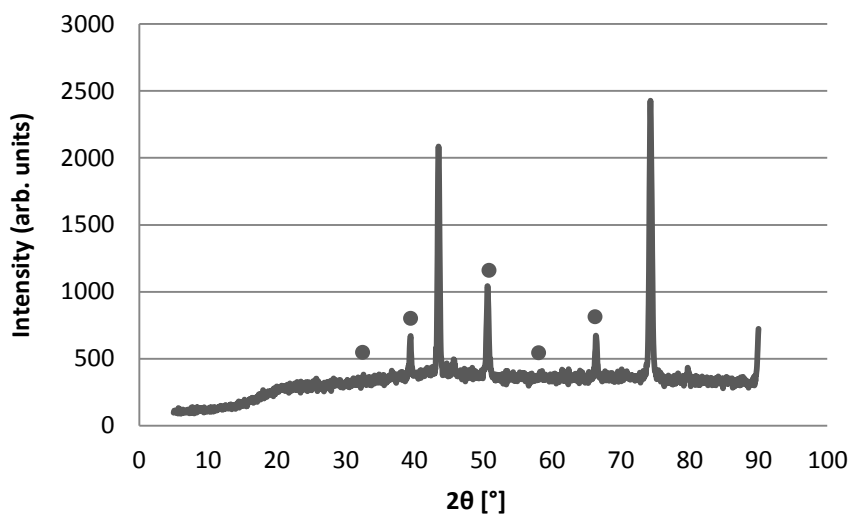
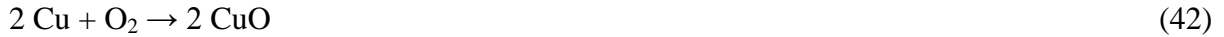


Figure 67: XRD spectrum of the Cu cathode from the Ti sandwich structure after electrolytic etching where the dot above the peak indicates detection of CuO.

SEM observation conducted on the cathode from the Ti sandwich structure after 3 minutes of electrolytic etching showed the deposit had the appearance of a sponge. It could be noted from Figure 66 b) that this deposit had also conducting properties. Further elemental analysis conducted with EDX revealed that the major constituent of the cathode was Cu 83.5%, O 10.1%, C 4.1%, the other detected elements were Cl and Ti. The detected O and C could indicate that they were formed during electrolytic etching as an effect of Joule heating.

XRD analysis carried out on the same cathode showed the peaks of CuO. This chemical compound is formed by oxidising Cu in air. In this case the Cu cathode reacted with O₂ released from the anode (Ti) during the electrochemical dissolution, reaction (42).



It is reduced to Cu metal in a reaction with H₂, presented in (43). In electrolytic etching, H₂ evolution takes place on the cathode.



iii. Effect of cooling of electrolyte on Ti sandwich structure etching

It was previously demonstrated that the electrolytic etching for 3 minutes when 4 electrodes connectors were applied for the electrodes resulted in CuO creation on the Cu cathode due to Joule heating. In order to eliminate this, an ice-cooled water jacket was applied.

Equipment

The equipment utilised in the electrolytic etching remained the same as described in section 6.5.2 ii) apart from:

- Plastic container, capacity approx. 1000 ml for cooled water with ice,
- Temperature controller.

Experimental procedure

The DC electrolytic etching of the Ti sandwich structure was conducted by applying a CD of 20 A/cm² for 3 minutes. The electrolytic etching was assisted with a mechanical stirring at a speed of 800 rpm.

The specimens were connected to the DC power supply through the Multimeter by 2 crocodile clips per electrode and placed in the electrolytic etching chamber filled with 10 % w/v HCl in an ice water jacket. The temperature of the electrolyte was kept at 13⁰C.

Results and discussion

It was observed that the application of the cooling of the electrolyte successfully prevented Joule heating and eliminated the formation of CuO on the cathode.

The results of the conducted work on cooling the electrolyte during electrolytic etching of the Ti sandwich structure are shown in Figures 68 and 69.

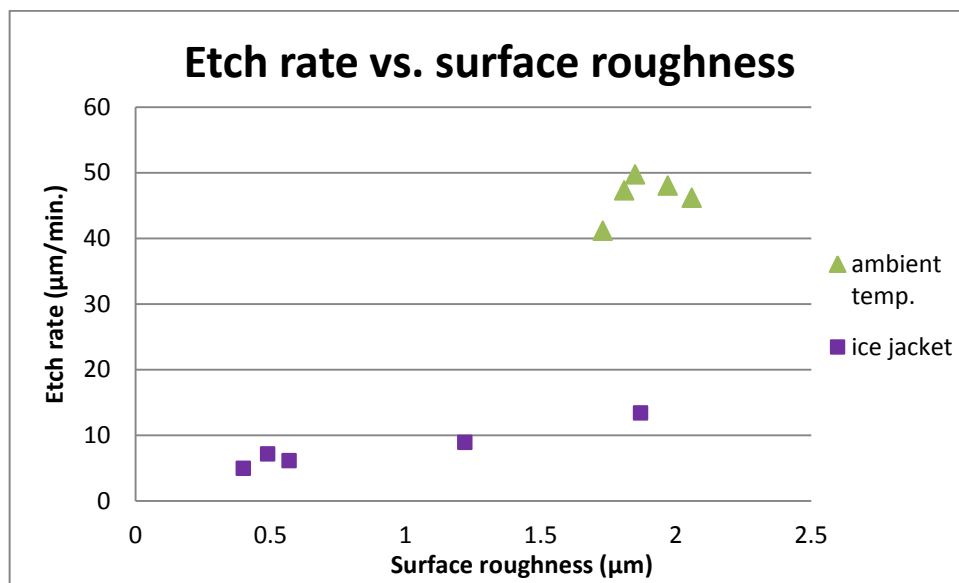


Figure 68: Etch rate vs. surface roughness of the etched Ti micro-holes at ambient temperature and with an ice jacket applied.

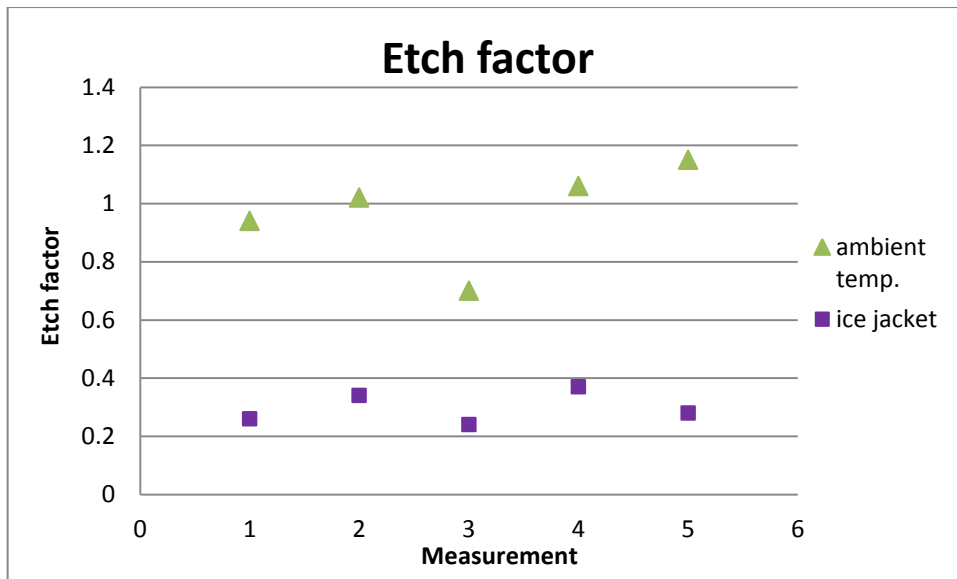


Figure 69: Etch factor of the etched Ti micro-holes at ambient temperature and with an ice jacket applied.

It was observed from Figure 68 that the etch rate decreased when the temperature of the HCl decreased. This was explained by the fact that conductivity of the electrolyte decreased with a drop in temperature. The etch rate was noted to decrease from average 46 $\mu\text{m}/\text{min}$ at ambient temperature to average 8 $\mu\text{m}/\text{min}$ when the electrolyte was cooled. Also the surface roughness was observed to decrease, however, some single micro-holes in Ti were found to have surface roughness of the order of 2 μm similar to the ones etched at ambient temperature.

The electrolyte cooling effected also a decrease of the etch factor in the range of 1 to 0.2 to 0.4, Figure 69.

iv. Effect of an ultrasonic agitation on etching performance of Ti sandwich structure

An application of ultrasonic vibration in an electrolytic etching or EDM was previously proved to have a beneficial effect [53], [60], [63]. Ultrasonic-assisted photoetching was reported to improve the material removal rate and the surface finish [63]. It was also found that with the ultrasonically-assisted electrolytic etching it was possible to achieve straight sidewalls on the edges of the holes and on the sidewalls and to obtain a polished surface on

the etched Ti [60]. Introducing ultrasonic vibration can improve the liquid flow and prevent erosion-products sedimentation [53] in the IEG.

Ultrasonic agitation was applied to the electrolytic etching of Ti in the sandwich structure in order to decrease the surface roughness of the half-etched micro-holes and to investigate the dissolution rate of the substrate.

Two temperature conditions of the electrolyte were tested in the ultrasonic-enhanced electrolytic etching: ambient temperature and 13⁰C achieved by cooling the water in the ultrasonic bath.

Equipment

The equipment remained the same as presented in section 6.5.2 ii) except:

- Ultrasonic bath 40 kHz,
- Metal stand.

Experimental procedure

The ultrasonically-assisted DC electrolytic etching of the Ti sandwich structure was performed by applying the CD of 20 A/cm² for 3 minute. The specimens were connected to the DC power supply through the Multimeter by 2 crocodile clips per electrode and placed in the electrolytic etching cell filled with 10 % w/v HCl and placed in the ultrasonic bath filled with water. Two temperatures of 10 % w/v HCl were tested: ambient temp. and 13⁰C achieved by cooling the water in the ultrasonic bath with ice.

Results and discussion

The quantified results of the conducted experiments are presented in Figures 70 and 71.

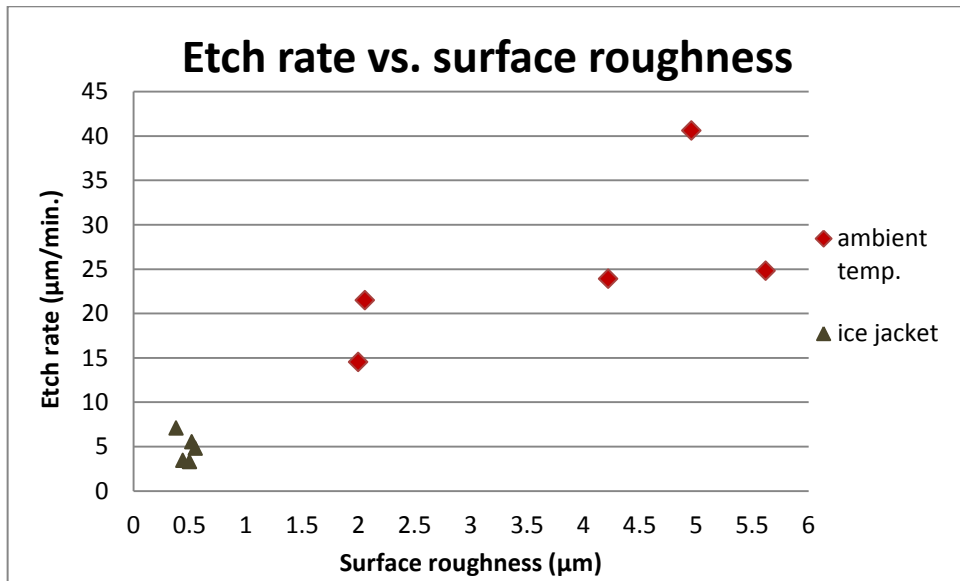


Figure 70: Etch rate vs. surface roughness of the etched Ti micro-holes at ambient temperature and cooled electrolyte in the ultrasonic bath.

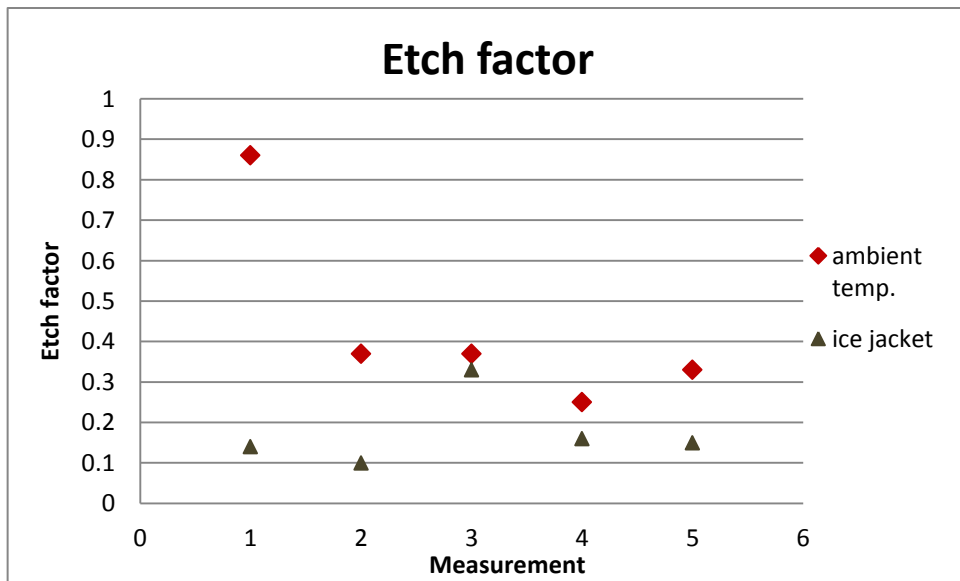


Figure 71: Etch factor of the etched Ti micro-holes at ambient temperature and cooled electrolyte in the ultrasonic bath.

The results obtained from the electrolytic etching of Ti in the sandwich structure in the ultrasonic conditions showed a decrease in the etch rate and surface finish in comparison with the electrolytic etching when a high mechanical stirring (800 rpm) was applied. The values of the surface roughness of the etched pattern in Ti were observed to decrease and to be more scattered than those when the etching was conducted without the ultrasonics at ambient temperature.

The ultrasonic agitation in conjunction with the cooling of the electrolyte caused a significant drop of the etch rate and the surface roughness of the etched half-etched micro-holes. The etch factor decreased also at the temperature of 13°C.

The ultrasound effect resulted in improved surface roughness of the half - etched micro-holes in Ti in comparison with the usual rotational-stirring method. However, the dissolution rate did not increase. This can be further investigated by changing the ultrasound power density [60].

Conclusions to Ti sandwich structure microfabrication with the Cu cathode obtained from electroless- and electro-deposition

The Ti sandwich structure with the Cu cathode obtained from electroless- and electro-deposition was the subject of a series of electrolytic etching experiments. The parameters such as: different current densities, number of electrical connectors per electrode, different time of etching at a high mechanical stirring speed and an effect of cooling the electrolyte as well as an ultrasonic agitation were tested in order to achieve a uniform etched pattern and to increase the etch depth in Ti.

The summary of the experimental work dedicated to electrolytic etching of the Ti sandwich structure has been presented in Table 42.

Table 42. Summary of the Ti sandwich structure electrolytic etching results.

Factor	Etching results	Surface roughness	Comment
Cu cathode obtained from electroless deposition			
CD = 20 A/cm ² t = 1 min., T = ambient, Stirring 250 rpm	Etch rate max. = 8.7 µm/min. Etch factor = 0.24 to 0.34	Ra max. = 0.29 µm	- Flat-base profiles of etched micro-holes, - Process suspended due to a delamination of Cu electroless cathode during electrolytic etching.
Cu cathode obtained from electroless and electrodeposition			
CD = 10, 15, 20, 25 A/cm ² , t = 1 min., T = ambient, Stirring 250 rpm	Etch rate max. = 82 µm/min. for 25 A/cm ² Etch factor from 0.3 to 0.7 Etch rate = 40 µm/min. for 20 A/cm ²	4.7 – 6.7 µm for 25 A/cm ² 2.8 µm for 20 A/cm ²	Flat-base profiles of etched micro-holes in Ti.
CD = 20 A/cm ² , t = 1 min., T = ambient, Stirring 250 rpm <u>4 croc. connectors (2 per electrode)</u>	Etch rate max. = 30 µm/min. Slight decrease of etch factor comparing to etch factor of 20 A/cm ² with 1 connector per electrode used.	Max. 1.5 µm	- Decrease of Ra, - Decrease of etch rate, - Improved distribution of half- etched micro-holes on the substrate.
CD = 20 A/cm ² , t = 1 min., T = ambient, 4 croc. connectors (2 per electrode) <u>Stirring 800 rpm</u>	Etch rate max. = 50 µm/min. Etch factor max. = 1	Max. 2.0 µm	Half-etched micro- holes etched over a larger area of the anode.
CD = 20 A/cm ² , <u>t = 3 min.</u> , T = ambient, 4 croc. connectors (2 per electrode) Stirring 800 rpm	Etch depth max. = 143.9 µm Etch rate = 46 µm/min. Etch factor approx. 1	Max. 10 µm	Observations as above
CD = 20 A/cm ² , t = 3 min., <u>T = 13°C</u> , 4 croc. connectors (2 per electrode) Stirring 800 rpm	Etch rate average = 8 µm/min. Etch factor from 0.2 to 0.4	Average 0.9 µm	- Significant decrease of etch rate and Ra.

Factor	Etching results	Surface roughness	Comment
Cu cathode obtained from electroless and electrodeposition			
CD = 20 A/cm ² , t = 3 min., T = 13 ⁰ C, 4 croc. connectors (2 per electrode) <u>Ultrasonic agitation</u> (40 kHz)	Etch rate max.= 7 μm/min. Etch factor from 0.1 to 0.32	0.5 μm	- Uniform depth of etch and Ra of half-etched micro-holes.
CD = 20 A/cm ² , t = 3 min., <u>T = ambient</u> , 4 croc. connectors (2 per electrode) Ultrasonic agitation (40 kHz)	Etch rate from 15 to 40 μm/min. Etch factor from 0.25 to 0.35	From 2 to 5.5 μm	- The values of etch rate and Ra very scattered in comparison to the results when the mechanical agitation was applied (800 rpm).

According to the obtained results, presented in Table 42, the following recommendations can be made for:

- One-sided etching:
 - High etch rate: CD = 20 A/cm², 4 crocodile connectors (2 per electrode), mechanical stirring at 800 rpm.
 - Fine feature patterning: requires low etch rate and low Ra: ultrasonic-assisted (40 kHz) etching for 3 minutes at CD = 20 A/cm², 4 crocodile connectors (2 per electrode), T = 13⁰ C of electrolyte.
- Etching through: CD = 20 A/cm², 4 crocodile connectors (2 per electrode), mechanical stirring at 800 rpm, 3 minute-etching.

It should be stressed that in a conventional photochemical etching of titanium, incorporating HF as an etchant, has a detrimental effect on the surface roughness of etched features. It also results in a non-uniform etching [44] [147]. Although no reference was found in the literature available as to a typical surface roughness achieved with the use of HF, it is believed to be of the order of several micrometers – certainly visibly “rough” to the naked eye.

The etch factor for HF based etchants of NiTi SMA was found to be 0.16 [147], [148]. In both cases the surface finish was reported to be poor (no quantitative value mentioned).

The results of the Ti electrolytic etching with the use of the sandwich structure indicated that it was possible to obtain an etch factor of 1 with an etch rate of 50 $\mu\text{m}/\text{min}$. The surface roughness, in this case, was found to be 2.0 μm . It was also empirically determined that the half-etched micro-holes in Ti had a spherical shape corresponding to the imaged pattern and a “preferred” flat-base profiles as opposed to the W-profile typically achieved with conventional electrolytic etching where preferential etching occurs at the edges of the features.

Chapter 8: Experimental procedure – scale-up of titanium sandwich structure process

8.1 Introduction

The preliminary work dedicated to scaling-up the process of microfabrication of the Ti sandwich structure is presented in this Chapter. The scale of the anode on which the sandwich structure was planned to be built was increased by a factor of 4. Figure 72 shows a manually sanded Ti substrate.



Figure 72: 4 inch diameter manually sanded Ti substrate.

The sanded 4 inch Ti specimen is processed according to the established sandwich structure process route presented in the Flow Diagram, see Appendix D. The flow diagram was prepared considering the laboratory-scale process which was then assessed under its feasibility to be scaled-up.

8.2 Test pattern

A new phototool (Figure 73), designed and delivered by Datum Alloys Ltd., was introduced to be applied for patterning the Ti sandwich structure. The phototool presents a characteristic pattern of a microfluidic device and series of test features with given dimensions where the smallest feature measures 1 μm .

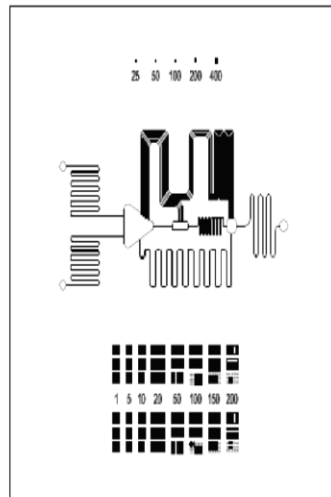


Figure 73: A design of the phototool for patterning the scaled-up Ti sandwich structure.

8.3 Equipment

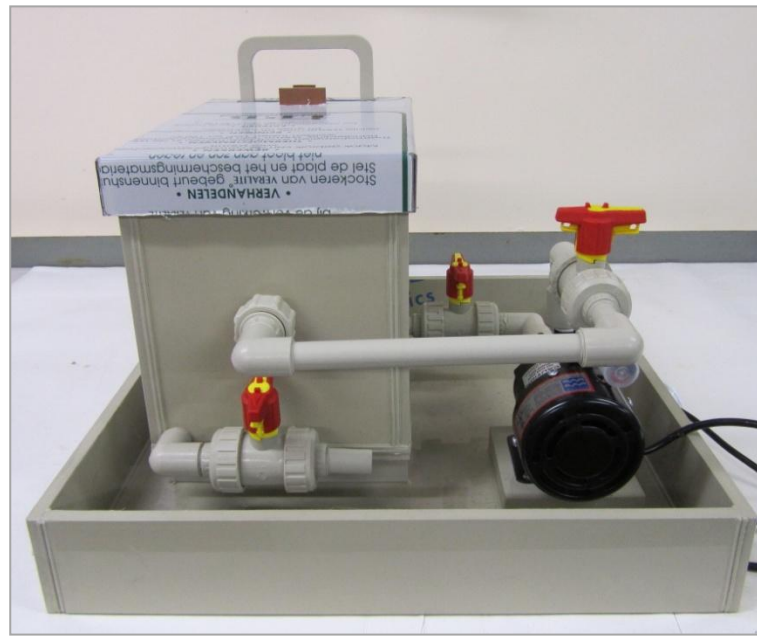
The scale-up of the Ti sandwich structure process involve introduction of new equipment and changing the size of the equipment which had been used previously in the laboratory-scale process.

8.3.1 Electrolytic etching machine

The electrolytic etching machine (Figure 74), designed by Datum Alloys Ltd., was constructed to allow processing of the 4 inch Ti sandwich structure.

The machine consists of a rectangular reaction chamber covered with a lid. The chamber of length 34.5cm (measured from inner wall), width: 22.3 cm, height: 26 cm had a wall thickness of 1.2 mm. The etching machine is placed in a shallow square container, of length 52.5 cm and height of 8.5 cm, to hold the liquid in case of any spillage.

The Ti sandwich structure is located in a vertical position in the reaction chamber, filled with 10 l of 10 % w/v HCl. The electrolyte penetrates the exposed areas of the sandwich structure through an aperture in the sandwich structure holder illustrated in Figure 74 b). The electrolytic etching machine is equipped with a pump which maintains a constant circulation of the electrolyte in front of the Ti sandwich structure.



a)



b)



Electrical connections

c)

Figure 74: New electrolytic etching machine for the scaled-up process of the Ti sandwich structure, a) side view of the machine; b) front view of the loaded Ti workpiece to the Ti sandwich structure holder; c) top view of the machine with the indicated electrical connections to the sandwich structure and the electrolyte pump.

Table 43. Process steps and required equipment for the scaled-up Ti sandwich structure microfabrication process.

Process	Main equipment utilized	Equipment specification
1. Ti preparation: a) Cutting, b) Cleaning	a) Guillotine, b) – Glass beaker, and ultrasonic bath	a) Able to cut A4 sheet of metal of the thickness max. 1.2 mm, b) Ultrasonic bath 40 kHz
2. Photoresist coating	Spin coater	Loading 1 sample per spin coating
3. Soft bake	Convection oven	Enables processing several samples per loading
4. Cu electroless plating process a) Sensitization, b) Activation, c) Cu electroless plating	a) Glass beaker b) Hot plate stirrer, c) Temperature controller	a) 2000 ml
4. Cu electroplating	a) Glass beaker b) Hot plate stirrer c) DC power supply	a) 3000 ml
5. Photoresist coating	Spin coater	As mentioned in 2.
6. Soft bake	Convection oven	As mentioned in 3.

Process	Main equipment utilized	Equipment specification
7. UV exposure	a) Mask aligner or b) Riston PC-Printer 130	a) Allows exposure of 1 sample b) Allows several samples to be exposed simultaneously
8. Developing	Glass container	Approx. 1000 ml
9. Hard bake	Convection oven	As mentioned in 3.
10. Cu etching	Glass beaker	2000 ml
11. UV exposure	a) Mask aligner or b) Riston PC-Printer 130	As mentioned in 7.
12. Developing	Glass container	Approx. 1000 ml
13. Hard bake	Convection oven	As mentioned in 3.
14. Electrolytic etching	a) Electrolytic etching machine, b) Rectifier, max. input 50 A and 80 V.	a) described in section 7.3.1

Process	Equipment	Equipment specification
15. Stripping	Glass tray	Approx. 1000 ml

It can be noted from Table 43 that the majority of the machinery is being reused in the scaled-up process which was used previously in the laboratory-scale process. They are: spin coater, mask aligner, hot plate stirrer, and DC power supply.

8.3.2 Chemicals

The chemicals incorporated in the laboratory-scale process were applied for the scaled-up Ti sandwich structure process. A list of the utilised chemicals has been summarised in Appendix E.

8.4 Future work on the scale-up of Ti sandwich structure

The work presented here is the analysis of the initial stages of scaling up of the laboratory-scale process. It highlighted the main concepts on how the scale-up of the Ti sandwich structure will be approached.

The main challenge is to produce high-quality components with controlled parameters, such as: side walls profile, desirable dimensions and surface roughness. In addition to this, the future work will be focused on the test pattern analysis on the features distribution and a size in order to obtain a uniform etch over the whole area of the substrate.

Chapter 9: Discussion and summary of the feasibility of producing titanium microparts using a novel sandwich structure

The research presented in this thesis was dedicated to the development of a novel Ti sandwich structure entailing electrolytic etching of Ti (cp) with the use of 10 % w/v HCl as the electrolyte/etchant.

Two approaches were distinguished to fabricate the sandwich structure in the literature. First, a “non-permanent” structure, incorporated the clamping of a dielectric layer coated with a conductive layer attached to a workpiece [67] and coating of a substrate with a photoresist in order to image it and attach a conductive cathode with the corresponding pattern [60].

Second, a “permanent” sandwich structure fabrication process involved coating of the substrate AISI 304 with the photoresist AZ1818 and deposition of a copper film [68]. The results of microfabrication of the sandwich structures, both non-permanent and permanent, demonstrated the feasibility of this process to produce micro-features in the substrates: 1Cr18Ni9Ti [67], Ti [60], and AISI 304 [68] with an application of electrochemical machining [64] and electrochemical photoetching [60], [68].

The results obtained from the microfabrication of the non-permanent sandwich structures showed relatively shallow micro-holes of 4, 10, and 22 μm in depth when 16% NaNO_3 electrolyte was employed [67]. Whereas, the substrate was etched through (100 μm thick Ti) when 1M LiCl in methanol as the electrolyte was incorporated. However, the use of methanol as the solvent raises serious environmental implications.

Electrolytic etching of the permanent structure in 0.1 M HCl resulted in etched dimples of 4.85 μm in diameter and an etch rate of 2.4 $\mu\text{m}/\text{min}$.

The Ti sandwich structure, described in this thesis, relied on building a permanent structure, comprising of the anode (Ti), the dielectric (photoresist) and the cathode.

The technique utilised the same photolithography process as used in a conventional PCM process, in order to achieve selective etching on a metal substrate. However, for the electrolytic etching stage, the IEG between the anode and the cathode was substantially reduced to 4 μm . The purpose of the dielectric layer being reduced to a minimum is to improve the distribution of the current on the conductive workpiece (Ti) by minimising the electric field and ensure even etching during subsequent electrolytic dissolution.

A process to build a novel sandwich structure was developed which would be integral in the subsequent microfabrication of features in the Ti base layer.

The work on the three sandwich structure layers resulted in the findings presented below.

i. Sandwich structure building

a) Ti anode (bottom layer of sandwich structure)

The manual sanding of the Ti substrate removed the inherent Ti oxides that increased the resistivity of the substrate.

b) Dielectric S1818 photoresist (middle layer of sandwich structure and also used as temporary top layer to image features onto copper cathode layer)

The positive resist S1818 was selected as the insulator between the anode and the cathode. It allowed selective patterning, developing and etching of the sandwich structure. It enabled a reduced impact on the environment by incorporation of aqueous developers and organic strippers. In the work carried out on the S1818 resist layers within the sandwich structure, the soft- and hard-bake temperatures, its duration and a heating equipment were determined.

The nanoindentation tests of the S1818 resist softbaked at temperatures of 50⁰C and 100⁰C for 60 min. revealed that an increase of the temperature of curing increases the hardness of the resist.

It was confirmed by FIB milling of the Ti/S1818 structure that there was no Ti oxide creation observed at the interface when the specimens were soft-baked in a convection oven.

c) Cu cathode

Cu electroless deposition was incorporated in obtaining the Cu cathode for the Ti sandwich structure. The solution prepared for this process: CuSO₄·5H₂O (source of copper ions), Na₂EDTA (complexing agent), DMAB (reducing agent), and 28%NH₄OH (supplier of OH⁻ groups to adjust the pH of the solution). Several organic additives were tested in order to obtain a denser Cu deposit. As a result, 28.85 g/l of glycerol was found to produce Cu coating with a preferential parameters, such as: thickness of 70 – 100 μm, ρ of 3.83 μΩ · cm, and Ra of 0.01 μm. The addition of a surfactant TX-100 decreased the resistivity of Cu deposit which decreased by over 60 %. The obtained Cu coating thus enabled a further building-up of the thickness by Cu electroplating. This produced a compact coating, where the selected 20-

minute deposit of the thickness = 12 μm was applied as the Cu cathode in the Ti sandwich structure.

ii. Ti sandwich structure microfabrication

The Ti sandwich structures with a Cu cathode obtained from only electroless plating and from combined electroless and electrodeposition were the subjects of electrolytic etching experiments. Both structures produced half-etched micro-holes in Ti of a spherical shape corresponding to the imaged pattern with preferred flat-base profiles. This is a departure to what would usually be achieved with conventional electrolytic etching where the bulk of etching would occur at the edge of the profile, leaving a substantial “land” in the middle.

A series of parameters was investigated in order to achieve a uniform etched pattern and to increase the etch depth in Ti. The results showed that, the application of CD of 20 A/cm^2 for 3 minutes at ambient temperature and using 4 crocodile connectors to the electrodes (2 per anode and 2 per cathode) with 10% w/v HCl mechanically stirred at the speed of 800 rpm, it is possible to achieve a maximum etch depth of 143.9 μm . The etch rate decreased by a factor of 6 when cooling (13°C) of the electrolyte was applied during electrolytic etching. In an ultrasonic-assisted electrolytic etching, the etch rate was also noted to decrease (min. 15 – max. 40 $\mu\text{m}/\text{min}$.) compared to the highest etch rate of 50 $\mu\text{m}/\text{min}$. The decrease of the surface roughness (from max. $R_a = 2.0 \mu\text{m}$ for the etch rate = 50 $\mu\text{m}/\text{min}$.) was achieved when cooling of the ultrasonic bath was introduced. This resulted in an etch rate of 5 $\mu\text{m}/\text{min}$ and R_a of 0.5 μm .

The developed sandwich structure processing route showed potential to fabricate micro-features in Ti. The obtained results of the etched Ti also indicated its advantage in a higher etch depth and etch rate as well as a significantly reduced impact on the environment over the methods described in the literature [60], [67], [68].

Chapter 10: Conclusions and recommendations for future work

10.1 Conclusions

This thesis covered the work on a novel sandwich structure utilised to produce micro-features in Ti via an electrolytic etching route. The presented research was divided into selection of compatible materials and techniques to build the Ti sandwich structure and to transfer an image through the layers to enable subsequent electrolytic etching of Ti with the use of a less hazardous etchant (10 % w/v HCl) than would be used in conventional chemical etching of Ti.

The conducted work on the Ti sandwich structure demonstrated the developed process steps aimed at building the Ti sandwich structure and its microfabrication.

- Ti anode preparation by manual sanding resulted in a decrease of the resistivity and removal of the inherent Ti oxides.
- The processing parameters of a positive resist S1818, employed as a dielectric layer between the anode and the cathode, were determined and optimised. The soft and hardbake at 50⁰C for 1 hour in a convection oven generate neither stress in the sandwich structure nor create a Ti oxide layer at the substrate and the resist interface.
- Cu electroless deposition was used to obtain the Cu cathode for Ti sandwich structure. The solution that was developed for the purpose contained: CuSO₄·5H₂O, Na₂EDTA, DMAB, 28%NH₄OH, glycerol, and the addition of surfactant TX-100. The obtained Cu coating was sufficient to enable further building-up of the thickness by Cu electroplating. This produced a compact coating of the thickness of 12.06 μm which was applied as the Cu cathode in the Ti sandwich structure.

The results of electrolytic etching of Ti proved the concept that by applying the structure comprising Ti/ S1818 resist/Cu to etch microholes, it is possible to overcome the problem of preferential attack at the circumference leaving a raised “land” of material in the middle which arises when conventional electrolytic etching is applied. The optical micrographs revealed the flat-base profiles of the half-etched micro-holes in Ti. Obviously, this effect would translate to other etched profiles other than microholes

The extensive work focused on achieving a uniformly etched pattern over a whole area of the anode (Ti) indicated that parameters, such as: a) agitation of the electrolyte, b) applied

electrical connectors, c) temperature of the electrolyte, and finally d) size and spacing of features on the phototool, control the distribution of the etched pattern, etch depth, and surface finish in Ti substrate.

The Ti sandwich structure electrolytic etching was completed with the following conclusions:

- One-sided etching:
 - High etch rate: CD = 20 A/cm², 4 crocodile connectors (2 per electrode), mechanical stirring at 800 rpm. Results for 1 minute-etching: etch rate of 50 μm/min., etch factor max = 1, surface roughness = max. 2 μm.
 - Fine feature patterning requires low etch rate and low Ra: ultrasonic-assisted (40 kHz) etching for 3 minutes at CD = 20 A/cm², 4 crocodile connectors (2 per electrode), T = 13 °C of electrolyte. Results for 3 minute-etching: etch rate max. of 7 μm/min., etch factor max. of 0.32, and surface roughness of 0.5 μm.
- Etching through: CD = 20 A/cm², 4 crocodile connectors (2 per electrode), mechanical stirring at 800 rpm, 3 minute-etching: etch depth of 143.9 μm, etch factor max = approx. 1.

10.2 Recommendations for future work and its relevance to industry

The results obtained from electrolytic etching of Ti sandwich structure on a laboratory-scale showed a potential of this method to produce micro-features with a preferred parameters such as shape of the micro-holes corresponding to the imaged pattern and flat-base profiles. Utilising 10 % w/v HCl as an electrolyte makes it a more environment-friendly method to produce micro-size pattern in Ti.

10.2.1 Current distribution control

The current distribution was reported in the literature [51] to be controllable on a workpiece, pattern and a feature scale. The Ti sandwich structure proved to be responsible for a uniform current distribution on the feature scale by producing the flat-base profiles of the micro-holes in Ti. The Ti sandwich structure electrolytic etching showed differences in the etched pattern distribution over the area of the specimen. The improvement was obtained by introducing a high mechanical stirring (800 rpm) and 4 electrode connectors. However, further work should be focused on dimensional control of the etched pattern on the whole area of the substrate by

phototool and mask aspect ratio modifications. Both factors play a role in the uniformity of current distribution on a pattern scale and an increase of the etch rate.

i. Finite element method (FEM)

FEM is a numerical technique for solution of the shape evolution problem. This tool can be applied to optimise the current distribution on the pattern scale by investigating the effect of the spacing and open ratio of the pattern on the anode.

ii. Pulsed reverse current (PRC) etching

PRC consists of an anodic and cathodic pulse as well as off or relaxation periods. It includes anodic (positive or “forward”) and cathodic (negative or “reverse”) duty cycles. PRC offers an improvement of dimensional accuracy by focussing the current. Current density is controlled by the processes related to charge transport at the electrode surface and mass transport from the electrolyte to the electrode surface [54]. The other advantages of PRC include improvements of hydrodynamic uniformity of electrolyte and of surface finish by minimising or eliminating oxide film formation. During the off-time, both heat and by-products are removed. Therefore, smoother surface, more uniform etching and improved dimensional accuracy is produced. Replacing DC etching by PRC cycle in the Ti sandwich structure could therefore improve the parameters mentioned above. As the project was aimed at developing a method of DC electrolytic etching due to the less expensive power supply it seems justified in applying PRC etching in the Ti sandwich structure process.

10.2.2 Double-sided sandwich structure

In this thesis, the cavity etching in Ti was presented. The next step is performing a through etching. This can be carried out by one-sided or two-sided attack. The initial analysis of the double-sided Ti sandwich structure was conducted in order to enable etching through the substrate. The materials incorporated in the one-sided Ti sandwich structure remained the same, whereas, the deposition of the S1818 resist was performed by a dip coating technique in order to enable the double-sided coating. The Cu electroless- and the Cu electro-plating were also conducted on both sides without the need for masking. The stage of the sandwich structure building was finished successfully. The Ti double-sided sandwich structure could not have been finished due to the time limit of the project. Therefore, the further work could

be focused on taking this structure through the patterning stages to perform the final Ti sandwich structure electrolytic etching from both sides.

10.2.3 Scale-up process

In Chapter 7 the initial stages of the Ti sandwich structure process scale-up was presented. The presented etching results of the Ti sandwich structure showed great potential. However, in order to develop the industrial process, the process optimisation on a laboratory-scale is required. Overall, the processes involved in the Ti sandwich structure have to be characterised in terms of the inputs, outputs and wastes generation. Then, the statistical process control can be applied.

References

- [1] Ekelman, K. B., *New Medical Devices. Invention, Development and Use*, National Academy Press, Washington D.C., 1988.
- [2] European Commission, available at: <http://ec.europa.eu>, access date August 2011.
- [3] OJ L 169, 12.7, *Council Directive 93/42/EEC of 14 June 1993 concerning medical devices*, 1993, p. 1.
- [4] Jacobson, B. and Murray, A., *Medical Devices. Use and Safety*, Churchill Livingstone, 2007.
- [5] OJ L 189, 20.7, *Council Directive 90/385/EEC of 20 June 1990 on the approximation of the laws of the Member States relating to active implantable medical devices*, 1990, p. 17.
- [6] OJ L 331, 7.12, *Directive 98/79/EC of the European Parliament and of the Council of 27 October 1998 on in vitro diagnostic medical devices*, 1998, p. 1.
- [7] Paul, J. P., et.al., *Biomaterials in artificial organs*. Strathclyde Bioengineering Seminars. Proceedings of a seminar on biomaterials held at the University of Strathclyde, Glasgow, September, 1983.
- [8] Bruck, S. D., *Properties of Biomaterials in the Physiological Environment*. Boca Raton, FL: CRC Press, 1980.
- [9] Leyens, C. and Peters, M., *Titanium and Titanium Alloys, Fundamentals and Applications*, WILEY-VCH Verlag GmbH & Co. KGaA, Weinheim, 2003
- [10] Wong, J.Y. and Bronzino, J. D., *Biomaterials*, CRC Press, Taylor & Francis Group, Boca Raton, 2007

- [11] Zheng, Q. X., et.al., Artificial bone of porous tricalcium phosphate ceramics and its preliminary clinical application, *Journal of Tongji Medical University*, Vol. 12, Issue 3, 1992, pp. 173 – 178.
- [12] Pruitt, L. and Furmanski J., Polymeric Biomaterials for Load-bearing Medical Devices, *JOM*, Vol. 61, No. 9, 2009, pp. 14 – 20.
- [13] Davis, H. E. and Leach, J. K., *Hybrid and Composite Biomaterials in Tissue Engineering. Topics in Multifunctional Biomaterials and Devices*, Ed. N. Ashammakhi, 2008.
- [14] Lakes, R., *Composite Biomaterials. The Biomedical Engineering Handbook: Second Edition*, Ed. J. D. Bronzino, Boca Raton, CRC Press, LLC, 2000.
- [15] Bannon, B. P. and Mild, E. E., *Titanium Alloys for Biomedical Applications: An Overview*, Luckey, E. H. A. and Kubli, F., A symposium sponsored by ASTM Committee F-4 on Medical and Surgical Materials and Devices and ASTM Committee B-10 on Reactive and Refractory Metals and Alloys Phoenix, Ariz., 11-12 may 1981, ASTM Special Technical Publication 796, 1983.
- [16] Heisterkamp, F. and Carneiro, T., *Niobium: Future Possibilities – Technology and the Market Place*, available at:
<http://www.cbmm.com.br/portug/sources/techlib/science techno/table content/sub 5/images/pdfs/057.pdf>, access date August 2011.
- [17] *Niobium and Alloys of Niobium*, available at: <http://www.elitematerial.co.uk>, access date August 2011.
- [18] International Titanium Association – *Medical Data Sheet*, available at: www.titanium.org, access date August 2011.
- [19] Kasemo, B. and Lausmaa, J., Surface properties and processes of the biomaterial-tissue interface, *Materials Science and Engineering*, CI, 1994, pp. 115 – 119.
- [20] Kasemo, B., Biological surface science, in: *Surface Science*, 500, 2002, pp. 656 – 677.

- [21] *Titanium Alloys in Medical Applications*, The Titanium Information Group, available at: <http://www.azom.com/article.aspx?ArticleID=1794>, access date August 2011.
- [22] Wang, K., The use of titanium for medical applications in the USA, in: *Materials Science and Engineering A213*, 1996, pp. 134 – 137.
- [23] Schuh, A., et.al., Second generation (low modulus) titanium alloys in total hip arthroplasty, in: *Mat.-wiss. U. Werkstofftech.* Vol. 38, No. 12, 2007, pp. 1003 – 1007.
- [24] Kantor, N., *Component Fabrication by Etching Nickel Titanium Alloys*, MSc by Research Thesis, School of Industrial and Manufacturing Science, Cranfield University, May 2001.
- [25] Federspil. P. A., Implant-retained craniofacial prostheses for facial defects, Review article, in: *GMS Current Topics in Otorhinolaryngology – Head and Neck Surgery*, Vol. 8, 2009, pp. 9 – 16.
- [26] International Titanium Association – *Medical Data Sheet*, available at: www.titanium.org, access date 2011.
- [27] *Titanium Implants in a Human Body*, available at: <http://www.profimedia.si/picture/titanium-implants-in-a-human-body/0015021831/>, access date August 2011.
- [28] Dr Almond, H. and Prof. Allen D., “*Difficult-to-etch*” *Metals and Alloys*, Photochemical Machining Research Consortium No.3., School of Industrial and Manufacturing Science, Cranfield University, Bedford MK43 0AL, UK, 2003.
- [29] Madou, M. J., *Fundamentals of Microfabrication. The Science of Miniaturization*, Second Edition, CRC Press LLC, Florida, United States of America, 2002.
- [30] Lu, X. and Leng, Y., Electrochemical micromachining of titanium surfaces for biomedical applications, in: *Journal of Materials Processing Technology*, Vol. 169, 2005, pp. 173-178.

- [31] Gantz, K., et.al., Development of a comprehensive model for RIE-lag-based three-dimensional microchannel fabrication, in: *Journal of Micromechanics and Microengineering*, 18, 2008, pp. 9.
- [32] Rao, M.P., et.al., *Single-Mask, High Aspect Ratio, 3-D Micromachining of Bulk Titanium*, in: 18th IEEE International conference on Micro Electro Mechanical Systems, 2005, pp. 64 -67.
- [33] Allen, D., et.al., *A technical comparison of micro-electrodischarge machining, microdrilling and copper vapour laser machining for the fabrication of ink jet nozzles*, Proceedings of Design Test, Integration and Packaging of MEMS/MOEMS, 9-11 May, Paris, France, 2000, pp. 531 – 540.
- [34] Ramsden, J. J., et.al., *The Design and Manufacture of Biomedical Surfaces*, in: *Annals of the CIRP*, Vol. 56/2/2007, pp.687 -711.
- [35] Reimers, H., et.al., Topographical and surface chemical characterization of nanosecond pulsed-laser micromachining of titanium at 532-nm wavelength, in: *Applied Physics A: Materials Science and Processing*, Vol. 77, 2003, pp. 491-498.
- [36] Liang, C., et.al., Surface modification of cp-Ti using femtosecond laser micromachining and the deposition of CA/P layer, in: *Materials Letters*, Vol. 62, 2008, pp. 3783-3786.
- [37] Jaffery, S.I., et.al., Proceedings of the 36th International Matador Conference, Editors: S. Hinduja, L.Li, 2010.
- [38] Zelinski, P., *The Right Tool for Milling Titanium: Modern Machine Schop*, available at: <http://www.mmsonline.com/articles/the-right-tool-for-milling-titanium>, access date October 2011.
- [39] Shelton, J.A., and Shin, Y.C., Comparative evaluation of laser-assisted micro-milling for AISI 316, AISI 422, Ti-6Al-4V and Inconel 718 in a side-cutting configuration, in: *Journal of Micromechanics and Microengineering*, Vol. 20, 2010, pp. 12.

- [40] Ding, H., et.al., Thermal and mechanical modeling analysis of laser-assisted micro-milling of difficult-to-machine alloys, in: *Journal of Materials Processing Technology*, article in press, 2011, pp. 13.
- [41] Almond, H. and Allen, D.M., *Electrolytic Machining of Difficult-to-etch Metals and Alloys*, in: Proceedings of the 20th International Conference on Computer-Aided Production Engineering, CAPE, Scotland, UK, 6-8 June 2007, pp. 53-62.
- [42] Pornsin-sirirak, T. N., et.al., Titanium-alloy MEMS wing technology for micro aerial vehicle application, in: *Sensors and Actuators A*, Vol. 89, 2001, pp. 95 – 103.
- [43] Zhao, G., et.al., *Fabrication of Bulk Titanium Out-of-plane Microneedles*, in: Proceedings of the 2009 4th IEEE International Conference on Nano/Micro Engineered and Molecular Systems, January 5-6, 2009, Shenzhen, China, pp. 428 – 431.
- [44] Chen, T.T., *Electrochemical micromachining of microdevices from NiTi shape memory alloys*, PhD Thesis, School of Industrial and Manufacturing Science, Cranfield University, May 1999.
- [45] Fisher Scientific Safety Data Sheet, *Hydrofluoric acid, 48% solution in water*, creation date 06 Jul 2010, revision date 13 Jan 2011, revision number 2, pp.8
- [46] Minnesota Poison Control System, 24 hours a day, 7 days a week, *Hydrofluoric Acid (HF)*, *Newsletters and Reviews*, Revised December 2009, available at: <http://www.mnpoison.org/index.asp?pageID=151>, access date October 2011.
- [47] Prentice, G., *Electrochemical Engineering Principles*, Prentice-Hall International Editions, 1991.
- [48] Groves, P. D., *Modern Chemistry Background Readers, Electrochemistry*, John Murray, Albemarle Street, London, 1984.
- [49] Edwards, J., Committee for Promotion of Electroplating, *Electroplating. A guide for designers and engineers*, Institute of Metal Finishing, Birmingham, 1983.

- [50] Mallory, G.O. and Hajdu, J.B., *Electroless Plating. Fundamentals and Applications*, American Electroplaters and Surface Finishers Society, Inc., Orlando, Reprint Edition.
- [51] Datta, M. and Landolt, D., Fundamental Aspects and Applications of Electrochemical Microfabrication, in: *Electrochimica Acta*, Vol. 45, 2000, pp. 2535-2558.
- [52] Lu, X. and Leng, Y., Electrochemical micromachining of titanium surfaces for biomedical applications, in: *Journal of Materials Processing Technology*, Vol. 169, 2005, pp. 173 – 178.
- [53] Wansheng, Z., et.al., Ultrasonic and electric discharge machining to deep and small hole on titanium alloy, in: *Journal of Materials Processing Technology*, Vol. 120, 2000, pp. 101 – 106.
- [54] Dr Almond, H. and Prof. Allen, D., *The Pulse Reverse Etching of “Difficult- to- etch” Metals and Alloys*, Photochemical Machining Research Consortium No.7 School of Applied Sciences, Cranfield University, Bedford MK43 0AL, UK, 2007.
- [55] Sen, M. and Shan, H.S., A review of electrochemical macro- to micro-hole drilling processes, in: *International Journal of Machine Tools & Manufacture*, Vol. 45, 2005, pp. 137 – 152.
- [56] Sen, M. and Shan, H.S., Analysis of hole quality characteristics in the electro jet grilling process, in: *Journal of Machine Tools & Manufacture*, Vol. 45, 2005, pp. 1706 – 1716.
- [57] McGeough, J., Electrochemical Machining, July 2005, available at: <http://electrochem.cwru.edu/encycl/art-m03-machining.htm>, access date October 2011.
- [58] Madore, C. and Landolt, D. Electrochemical micromachining of controlled topographies on titanium for biological applications, in: *Journal of Micromechanics and Microengineering*, Vol. 7, 1997, pp. 270 – 275.
- [59] Mineta, T., Electrochemical etching of a shape memory alloy using new electrolyte solutions, in: *Journal of Micromechanics and Microengineering*, Vol. 14, 2004, pp. 76 - 80.

- [60] Allen, D. M., et.al., *Extending the Process Capability of Electrolytic Photoetching with Ultrasonics and Ultra-Short Voltage Pulses*, in: unpublished results, 2008, pp.4.
- [61] Mineta, T., et.al., An active guide wire with shape memory alloy bending actuator fabricated by room temperature process, in: *Sensors and Actuators A*, Vol. 97 - 98, 2002, pp. 632 – 637.
- [62] Lu, X., et. al., Comparative study of osteoconduction on micromachined and alkali-treated titanium alloy surfaces in vitro and in vivo, in: *Biomaterials*, Vol. 26, 2005, pp. 1793 – 1801.
- [63] Wang, W., et.al., *Improved Electrolytic Photoetching of Titanium with Ultrasonics*, unpublished results, 2008, pp. 6
- [64] Namazu, T., et. al., Titanium-Nickel Shape Memory Alloy Spring Actuator for Forward-Looking Active Catheter, in: *Journal of Metallurgy*, Vol. 2011, Article ID 685429, pp. 9.
- [65] Chauvy, P.-F., et.al., Electrochemical Micromachining of Titanium Through a Patterned Oxide Film, in: *Electrochemical and Solid-State Letters*, Vol. 2 (3), 1999, pp. 123 - 125.
- [66] Chauvy, P.-F., et.al., Applications of laser lithography on oxide film to titanium micromachining, in: *Applied Surface Science*, Vol. 208 – 209, 2003, pp. 165 – 170.
- [67] Zhu, D., et.al., Electrochemical micromachining of microstructures of micro hole and dimple array, in: *CIRP Annals – Manufacturing Technology*, Vol. 58, 2009, pp. 177 – 180.
- [68] Wang, W., et.al., *Improved electrolytic photoetching utilising ultra-short voltage pulses*, unpublished results, Cranfield University, 2008.
- [69] Data Sheet RF 1.3000, Ultralam® 3000, *Liquid Crystalline Polymer Circuit Material, Double-Clad Laminates*, Rogers Corporation, Advanced Circuit Materials Division 100 S. Roosevelt Avenue, Chandler, AZ 85226.

- [70] Allen, D.M., *The principles and Practice of Photochemical Machining and Photoetching*, Cranfield Institute of Technology, Adam Hilger, IOP Publishing Limited, Bristol, 1986.
- [71] Brodie, I. and Muray, J. J., *Physics of Microfabrication*, Plenum Press, New York, 1982.
- [72] Kern, W. and Schuegraf, K.K., *Deposition Technologies and Applications: Introduction and Overview*, William Andrew Publishing/Noyes, 2002, available at: www.knovel.com, access on June 2009.
- [73] Datum Alloys Packing Slip No. 15572, *Titanium, grade 2*, Datum Alloys Ltd., Unit B, Bridge Works, Station Yard Industrial Estate, Kingsbridge, TQ71ES, UK, 04 February 2009.
- [74] Microposit™ S1818™ *Positive Photoresist Material Safety Data Sheet*, Rohm and Haas Electronic Materials LLC, 455 Forest Street, Marlborough, MA 01752 United States of America.
- [75] Kirby, P., *Basic Silicon MST Fabrication Techniques, Overview of MEMS Device Fabrication (including fabrication techniques taken from the IC industry)*, MSc in Microsystems and Nanotechnology, Lecture notes, Microsystems Technology I, pp. 17 - 21 November 2008.
- [76] Wasa, K., et.al., *Thin Film Materials Technology. Sputtering of Compound Materials*, William Andrew Publishing, Springer, 2004.
- [77] Deposition Processes, MEMS Thin Film Deposition Processes, available at: <http://www.mems-exchange.org/MEMS/processes/deposition.html>, access date January 2012.
- [78] *Lithography, Theory and Applications of Photoresists, Developers, Solvents and Etchants*, MicroChemicals, 2007.
- [79] *Discussion conducted with Dr Glenn, L.*, Research Fellow in Microsystems and Nanotechnology, SAS, Cranfield University, 14 September 2009.

[80] Cho, S.H., et.al., Micro-scale metallization on flexible polyimide substrate by Cu electroplating using SU-8 photoresist mask, in: *Thin Solid Films*, Vol. 475, 2005, pp. 68 - 71.

[81] Epoxy Resin, available at:

<http://www.techsil.co.uk/Products/EpoxyResin/tabid/92/Default.aspx>, access date January 2012.

[82] Ohno, I., Electrochemistry of Electroless Plating , in: *Materials Science and Engineering*, A146, 1991, pp. 33 - 49.

[83] Shacham- Diamand, Y. and. Dubin, V.M., Copper electroless deposition technology for ultra-large-scale-integration (ULSI) metallization, in: *Microelectronic Engineering*, Vol. 33, 1997, pp. 47 -58.

[84] Van Den Meerakker, J. E. A. M., On the Mechanism of Electroless Plating. II. One Mechanism for Different Reductants, in: *Journal of Applied Elechtrochemistry*, 11, 1981, pp. 395 - 400.

[85] Hsu, D. T., et.al., Electroless Copper Deposition Solution Induced Chemical Changes in Low-K Fluorinated Dielectrics, in: *Materials Science in Semiconductor Processing*, Vol. 2, 1999, pp. 19 - 22.

[86] O'Connel, M. P., et.al., *Selective Electroless Copper Deposition at a High Rate Using Dimethylamine Borane as a Reducing Agent*, National Microelectronics Research Centre, Lee Maltings, Prospect Row, Cork, Ireland, available at: www.electrochem.org/docs/2006/9034/letter.html, access date July 2009

[87] MicroChemicals, *Lithography. Theory and Application of Photoresists, Developers, Solvents and Etchants*, 2008/2009.

[88] Pearlstein, F. And Weightman, R.F., Electroless Copper Plating Using Dimethylamine Borane, in: *Plating*, Vol. 60, 1973, pp. 474 - 476.

[89] Guo, R. H., et.al, An alternative process for electroless copper plating on polyester fabric, in: *Journal of Materials Science: Materials in Electronics*, Vol. 20, 1, January, 2009, pp. 33 - 38.

[90] W. Canning Materials Ltd., *User Instructions*, Great Hampton St., Birmingham B18 6AS.

[91] *Titanium alloy Ti6Al4V*, Technical Datasheet, January 2000, available at: <http://cartech.ides.com/datasheet.aspx?i=101&E=269>, access date: March 2012.

[92] *Titanium Dioxide (TiO₂)*, January 2002, available at: <http://www.azom.com/Details.asp?ArticleID=1179>, access date: January 2012.

[93] Smits, F. M., *Measurement of Sheet Resistivities with the Four-Point Probe*, Manuscript received October 15, 1957, pp. 711 – 718.

[94] Dyer, A. G., Senior Technical Officer, *Standard Operating Procedure, Olympus Lext Confocal Laser Microscope*, SOP ML 22 version 1, 1 April 2009.

[95] Bolivar, V. and Friendrich, B., *Synthesis of Titanium via Magnesiothermic Reduction of TiO₂ (Pigment)*, in: *Proceedings of EMC 2009*, pp. 1 – 17.

[96] Fraker, A.C., et.al., *Surface Preparation and Corrosion Behavior of Titanium Alloys for Surgical Implants in Titanium Alloys in Surgical Implants*, Luckey, E. H. A. and Kubli, F., A symposium sponsored by ASTM Committee F-4 on Medical and Surgical Materials and Devices and ASTM Committee B-10 on Reactive and Refractory Metals and Alloys Phoenix, Ariz., 11-12 may 1981, ASTM Special Technical Publication 796, 1983.

[97] Medlin, D.J., et.al., *Metallographic Preparation of Orthopaedic Medical Devices*, available at: http://www.georgevandervoort.com/mic_met_pdf/MetallographicPrepMedicalDevices.pdf, access date: March 2012.

[98] Thompson, L.F., et.al., *Introduction to Microlithography*, second edition, ACS Professional Reference Books, American Chemical Society, Washington, DC, 1994. ISBN 0-8412-2848-5

[99] Propylene Glycol Monomethyl Ether Acetate, September 1997, available at: www.inchem.org/documents/icsc/icsc/eics0800.htm, access date April 2012.

[100] Sigma-Aldrich, Material Safety Data Sheet, *Propylene glycol monomethyl ether acetate*, available at www.sigmaaldrich.com/catalog/DisplayMSDSContent.co, access date April 2012.

[101] International Programme on Chemical Safety, Environmental Health Criteria 168, *Cresols*, available at: <http://www.inchem.org/documents/ehc/ehc/ehc168.htm#SectionNumber:1.1>, access date April 2012.

[102] Roy, D., et.al, Photoresists for Microlithography. 2. The Role of Polymer Microstructure, in: *Resonance*, August 2002, pp. 59 – 66.

[103] Fitzgerald, E., Determination of Composition of Mixed meta- and para-Cresol/Formaldehyde Novolaks by ¹³C-NMR Spectroscopy, in: *Journal of Applied Polymer Science*, Vol. 41, 1990, pp. 1809 – 1814.

[104] Roy, D., et.al, Optimization of monomer content and degree of linearity in lithographically interesting novolac copolymers using NMR spectroscopy, in: *Microelectronic Engineering*, Vol. 70, 2003, pp. 58 – 72.

[105] Integrated Laboratory Systems, Inc. Research Triangle Park, NC Under Contract No. N01-ES-35515, *Chemical Information Review Document for Diazonaphthoquinone Derivatives Used in Photoresists*, Supporting Nomination for Toxicological Evaluation by the National Toxicology Program, January 2006.

- [106] *Novolac polymer planarization films for microelectronic structures*, United States Patent 5858547, Publication Date: 01/12/1999, available at <http://www.freepatentonline/5858547.html>, access date April 2012.
- [107] Barthélémy, P., et.al, Fluorocarbon-Hydrocarbon Nonionic Surfactants Mixtures: A Study of Their Miscibility, in: *Langmuir*, Vol 18, 2002, pp. 2557 – 2563.
- [108] SOP, Microsystems and Nanotechnology Centre, Cranfield University, 2011.
- [109] Shipley, *Microposit® MF®-319 Developer*, MD MF-319 B 0391, pp.4.
- [110] Marvell Nanofabrication Laboratory, University of California, Berkeley, Lab Manual, *General Resist Parameters*, Table 1, available at: <http://www.microlab.berkeley.edu>, access date 02.2010.
- [111] Technology Institute, University of Toronto, *Shipley S1818 Positive resist*, Bahen Cleanroom, Document Number: ECTI-REC-001, Revision date 07.2008, pp.2
- [112] Mathies: *Photolithography*. available at: <http://openwetware.org/wiki/Mathies:Photolithography>, access date: October 2011.
- [113] Chien-Jung, et.al., A nano-indentation study of the reduced elastic modulus of Alq₃ and NPB thin-film used in OLED devices, in: *Organic Electronics*, Vol. 11, 2010, pp. 450 – 455.
- [114] Al-Halhouli, A.T., et.al., Nanoindentation testing of SU-8 photoresist mechanical properties, in: *Microelectronic Engineering*, Vol. 85, 2008, pp. 942 – 944.
- [115] Chang, R.-C., Dynamic mechanical properties of photo resist thin films, in: *Journal of Mechanical Science and Technology*, Vol. 21, 2007, pp. 1739 – 1744.
- [116] Chang, R.-C., et.al, Mechanical Properties of Photoresist Thin Films at Various Temperature, in: *Journal of the Chinese Society of Mechanical Engineers*, Vol. 27, No. 2, 2006, pp. 237 – 242.

- [117] Micro Star Technologies, *Nano indenters*, Revision 2.3, p.9
Available at: www.microstartech.com, access date: July 2011.
- [118] García-Gabaldón, M., et.al., Electrochemical study of the activating solution for electroless plating of polymers, in: *Journal of Applied Electrochemistry*, Vol. 37, 2007, pp. 1145 – 1152.
- [119] Yanagimoto, H., et.al., Selective electroless copper deposition on an aluminium nitride substrate with patterned copper seed layer, in: *Thin Solid Films*, Vol. 491, 2005, pp. 18 – 22.
- [120] Steinhäuser, E., Potential low-cost palladium-alternatives for activating electroless copper deposition, in: *Circuit World*, Vol. 36/3, 2010, pp. 4-8.
- [121] *Energy-Dispersive X-Ray Spectroscopy (EDS)*, available at:
www.serc.carleton.edu, access date: July 2012.
- [122] Touyeras, F., et.al., Electroless copper coating of epoxide plates in an ultrasonic field, in: *Ultrasonics Sonochemistry*, Vol. 8, 2001, pp. 285-290.
- [123] Rohan, J. F., et.al., Selective electroless nickel deposition on copper as a final barrier/bonding layer material for microelectronics applications, in: *Applied Surface Science*, Vol. 185, 2002, pp. 289 – 297.
- [124] Glycerol, available at: www.britannica.com, access date July 2012.
- [125] Sorbitol, available at: www.pubchem.ncbi.nlm.nih.gov, access date July 2012.
- [126] Kim, K.W., et.al., Mechanical Properties, Water Vapor Permeabilities and Solubilities of Highly Carboxymethylated Starch-Based Edible Films, in: *JFS: Food Engineering and Physical Properties*, Vol. 67, No. 1, 2002, pp. 218 – 222.
- [127] Cheng, L.H., et.al, *Interactive effects of water-glycerol and water-sorbitol on physical properties of konjac glucomannan films*, paper submitted to Food Research International, p. 26.

- [128] Hanna, F., et.al., Controlling factors affecting the stability and rate of electroless copper plating, in: *Materials Letters*, Vol. 58, 2003, pp. 104-109.
- [129] Kim, S.-H., et.al., Effect of saccharin addition on the microstructure of electrodeposited Fe-36 wt% Ni alloy, in: *Surface Coatings and Technology*, Vol. 199, 2005, pp. 43-48.
- [130] Hsu, J.-C., and Lin, K.-L., Effect of internal stress on elemental diffusion and crystallization of electroless Ni-Cu-P deposit on Al, in: *Journal of Materials Research*, Vol. 18, No. 9, 2003, pp. 2221 -2227.
- [131] Guilherme, J., et.al., Production of metallic copper powder by autocatalytic reaction in suspension, in: *Materials Research*, Vol. 9, No. 2, 2006, pp. 131 – 135.
- [132] Boto, K., Organic additives in zinc electroplating, in: *Electrodeposition and Surface Treatment*, Vol.3 1975, pp. 77 – 95.
- [133] De Oliveira, E. M., et.al., ZnNi alloy electrodeposition from acid baths containing sorbitol or glycerol and characterization of ZnNi deposits, in: *Journal of Applied Electrochemistry*, Vol. 39, 2009, pp. 1313 – 1321.
- [134] Ee, Y. C., et.al., Effect of processing parameters on electroless Cu seed layer properties, in: *Thin Solid Films*, Vol. 462 – 463, 2004, pp. 197 – 201.
- [135] Pashley, R. M. and Karaman, M. E., *Applied Colloid and Surface Chemistry*, John Wiley & Sons, Ltd. England, 2004.
- [136] Chen, B – H., et.al. Effects of Surfactants in an Electroless Nickel-Plating Bath on the Properties of Ni-P Alloy Deposits, in: *Ind. Eng. Chem. Res.*, Vol 41, 2002, pp. 2668 – 2678.
- [137] Salager, J. – L., *Surfactants Types and Uses*, Firp Booklet # E300-A, Mérida-Venezuela, Version # 2, 2002, p. 49,
Available at: nanoparticles.org/pdf/Salager-E300A.pdf, access date July 2012.

- [138] Sone, M., et.al., Electroless copper plating using Fe^{II} as a reducing agent, in: *Electrochimica Acta*, Vol. 49, 2004, pp. 233 – 238.
- [139] Lantsov, Y., et.al., New plating bath for electroless copper deposition on sputtered barrier layers, in: *Microelectronic Engineering*, Vol. 50, 2000, pp. 441 – 447.
- [140] *The Canning Handbook on Electroplating*, W. Canning Limited, Birmingham.
- [141] Luke, D. A., Electroplating Copper for Printed Circuit Manufacture, *Circuit World*, Vol. 13, No. 1, 1986, pp. 18 – 23.
- [142] Gnanasekaran, K. S. A., et.al., Stress Measurements in Electrodeposited Lead Dioxide, in: *Electrochimica Acta*, Vol. 15, 1970, pp. 1615 – 1622.
- [143] M. Datta, M. and Harris, D., Electrochemical micromachining: An environmentally friendly, high speed processing technology, in: *Electrochimica Acta*, Vol. 42, 1997, pp. 3007 – 3013.
- [144] Li, D., et.al., Microstructure of electrochemical micromachining using inert metal mask, in: *Int. J. Adv. Manuf. Technology*, published online 25 November 2010, p. 6.
- [145] Li, W., et.al., Finite element simulation and experimental study on the through-mask electrochemical micromachining (EMM) process, in: *Int. J. Adv. Manuf. Technol.*, Vol. 51, 2010, pp. 155 – 162.
- [146] Surface Finishing Tutorial, #035 *Electrolytic etching – Electrolytic machining*, available at: <http://www.misumi-techcentral.com/tt/en/surface/2010/03/034---1.html>, access date: October 2011.
- [147] Simoutre, C., *Manufacture of micro-actuators from shape memory alloys*, MSc Thesis, Cranfield Institute of Technology, School of Industrial and Manufacturing Science, 1992.

[148] Kamra, V. P., Photochemical machining of TiNi shape memory alloy, MSc Thesis, Cranfield Institute of Technology, School of Industrial and Manufacturing Science, 1993.

[149] *Olympus Confocal Scanning Laser Microscope Lext OLS3100/OLS3000*, User's Manual, Ver. 6.0.

Appendices

Appendix A

Step wedge

A neutral density step wedge is an essential tool for the determination of correct exposure for photoresist.

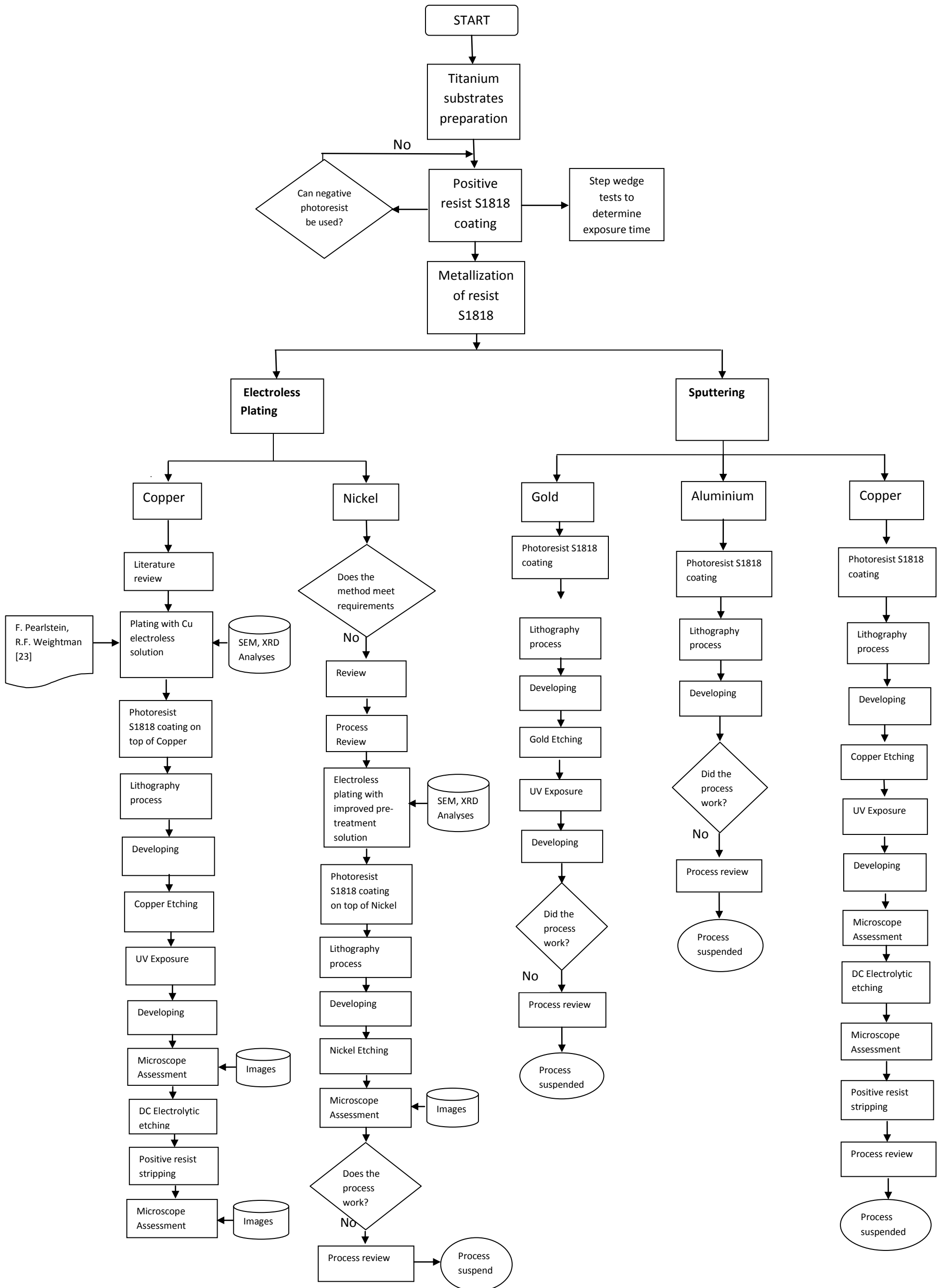
It is a strip of photographic film which is divided into areas of different optical density (usually in increments of 0.15) [70].

The determination of correct exposure time for positive-working resist is done by exposing through the step wedge and calculating the smallest exposure which will effect in completely solubilised photoresist when developed. It can be achieved by developing the over-exposed photoresist coating. The number of steps completely developed off the substrate corresponds for the percentage transmission. This is then divided by 100 and multiplied by the original exposure time to give the correct exposure time for the positive resist.

Table: calculation of step wedge transmission [70].

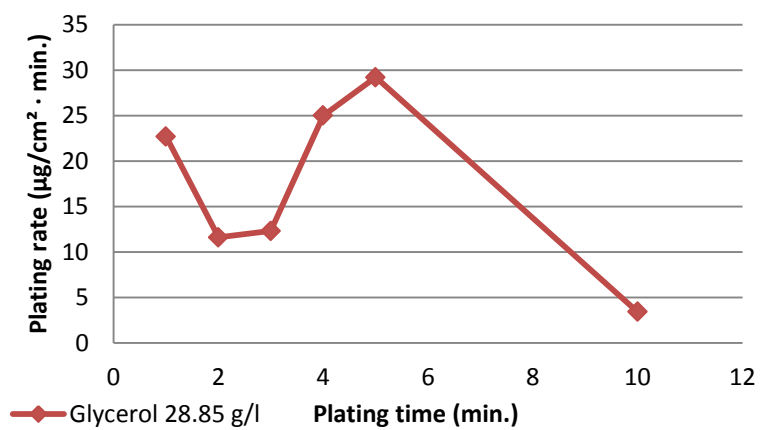
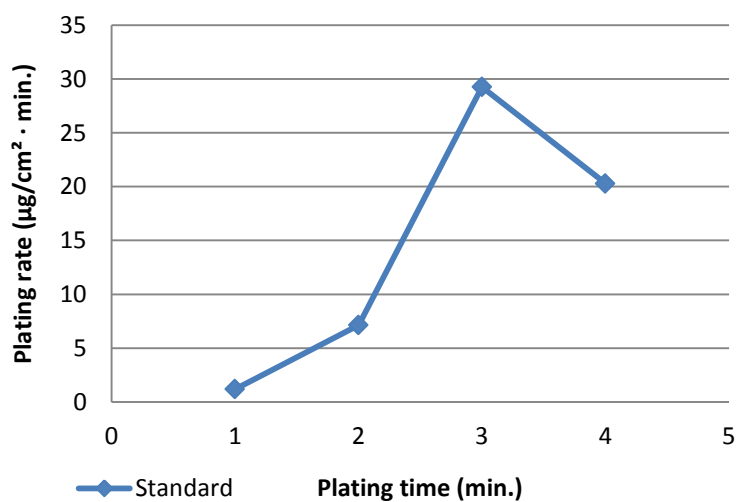
Step	Transmission optical density = \log_{10} (100% transmission)	% transmission
1	0.05	89.0
2	0.20	63.2
3	0.35	44.8
4	0.50	31.6
5	0.65	22.4
6	0.80	15.9
7	0.95	11.2
8	1.10	7.8
9	1.25	7.5
10	1.40	7.24

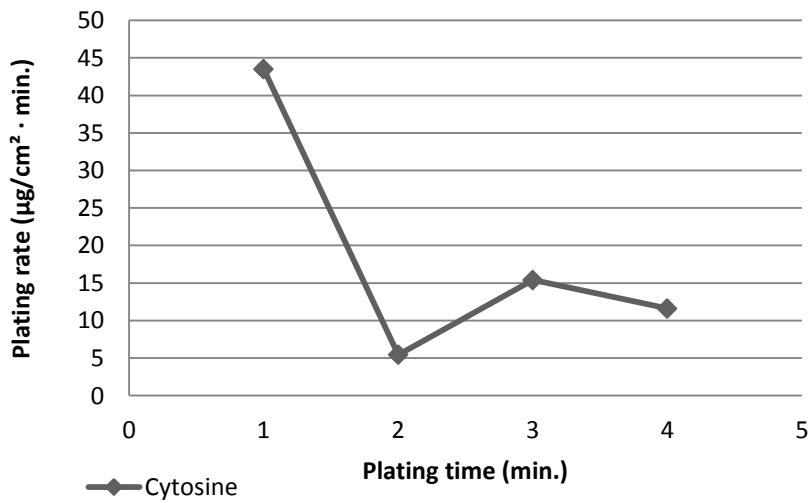
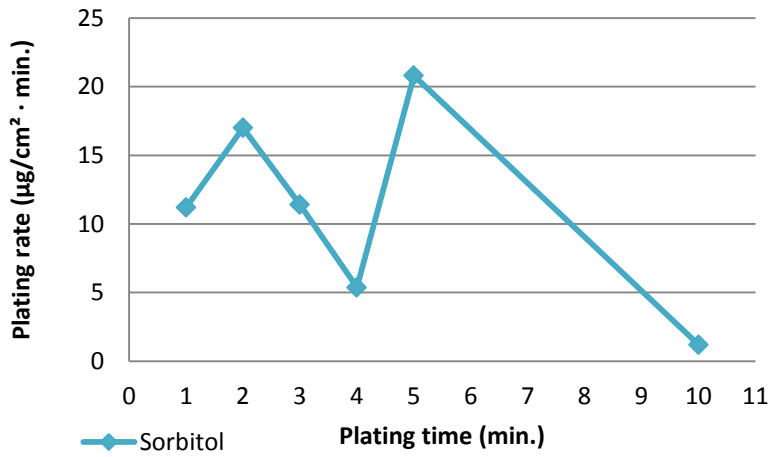
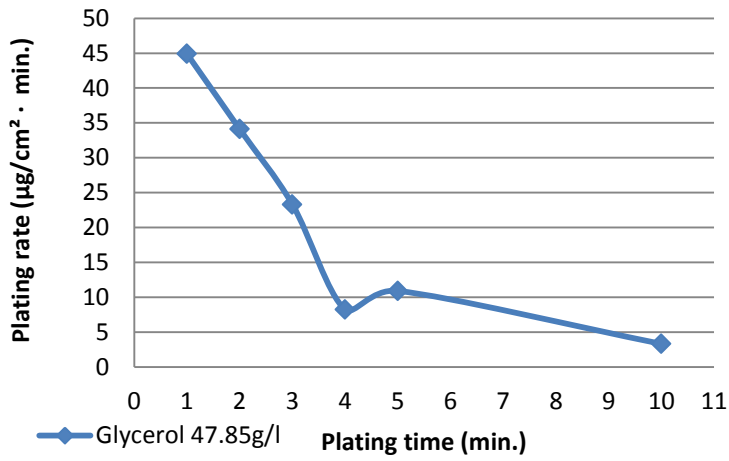
Appendix B: FLOW DIAGRAM DETAILING EXPERIMENTAL WORK INVOLVED IN FABRICATION OF THE “TRIPLE SANDWICH STRUCTURE”

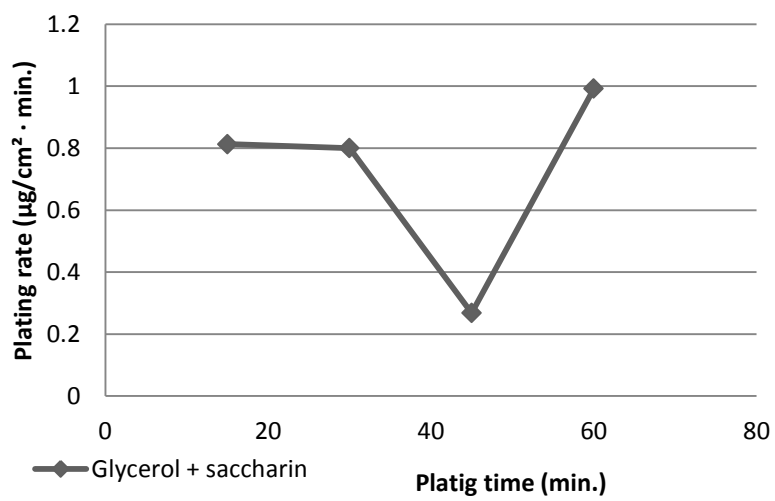
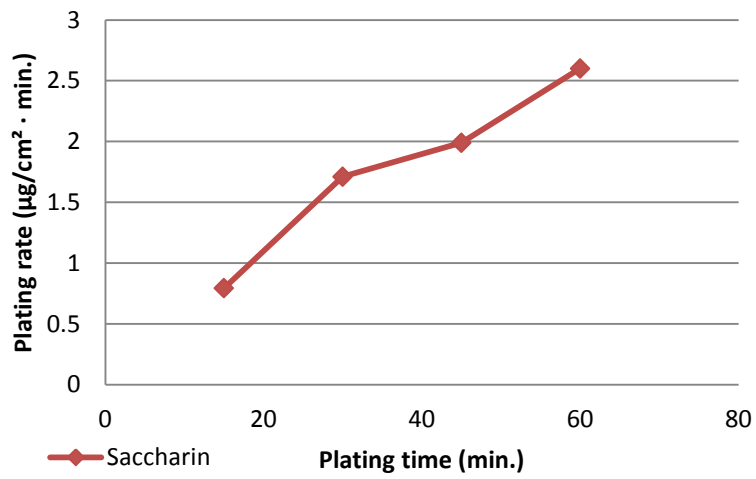
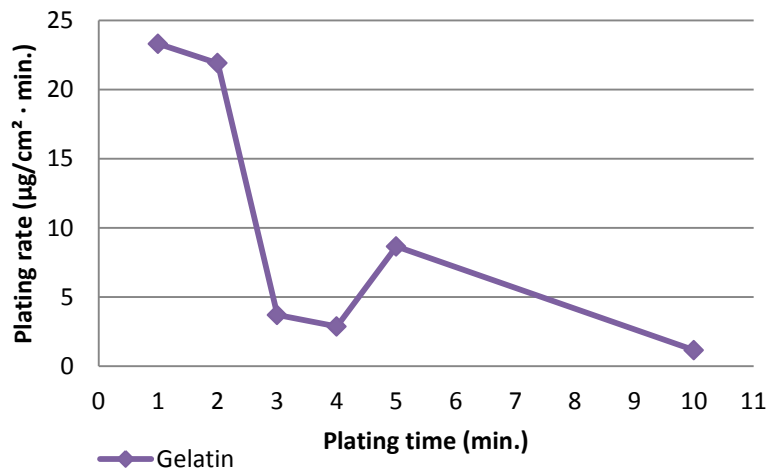


Appendix C

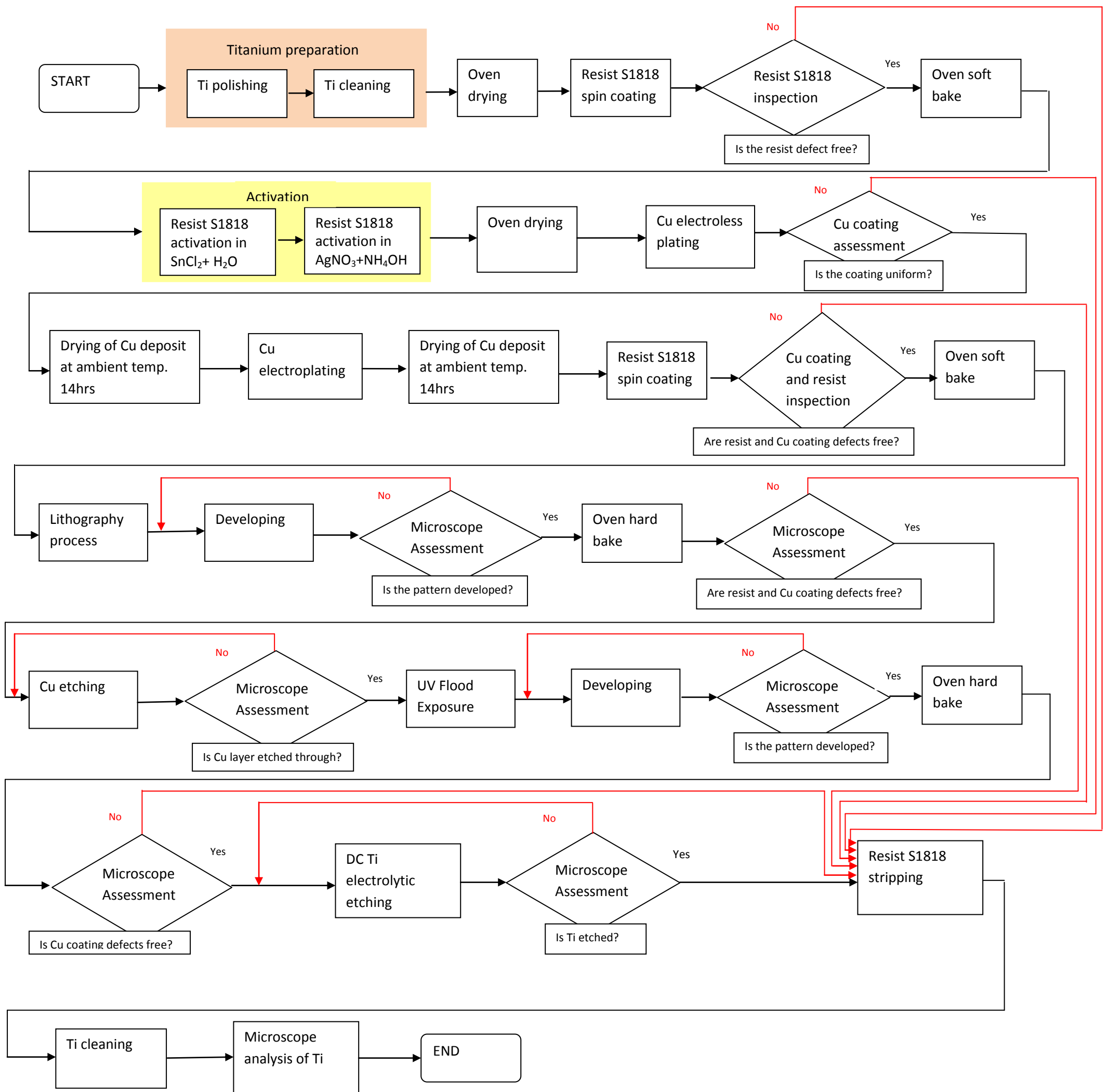
Plating rates for Cu electroless solutions containing the organic additives.







Appendix D: FLOW DIAGRAM OF ESTABLISHED SANDWICH STRUCTURE PROCESS



Appendix E

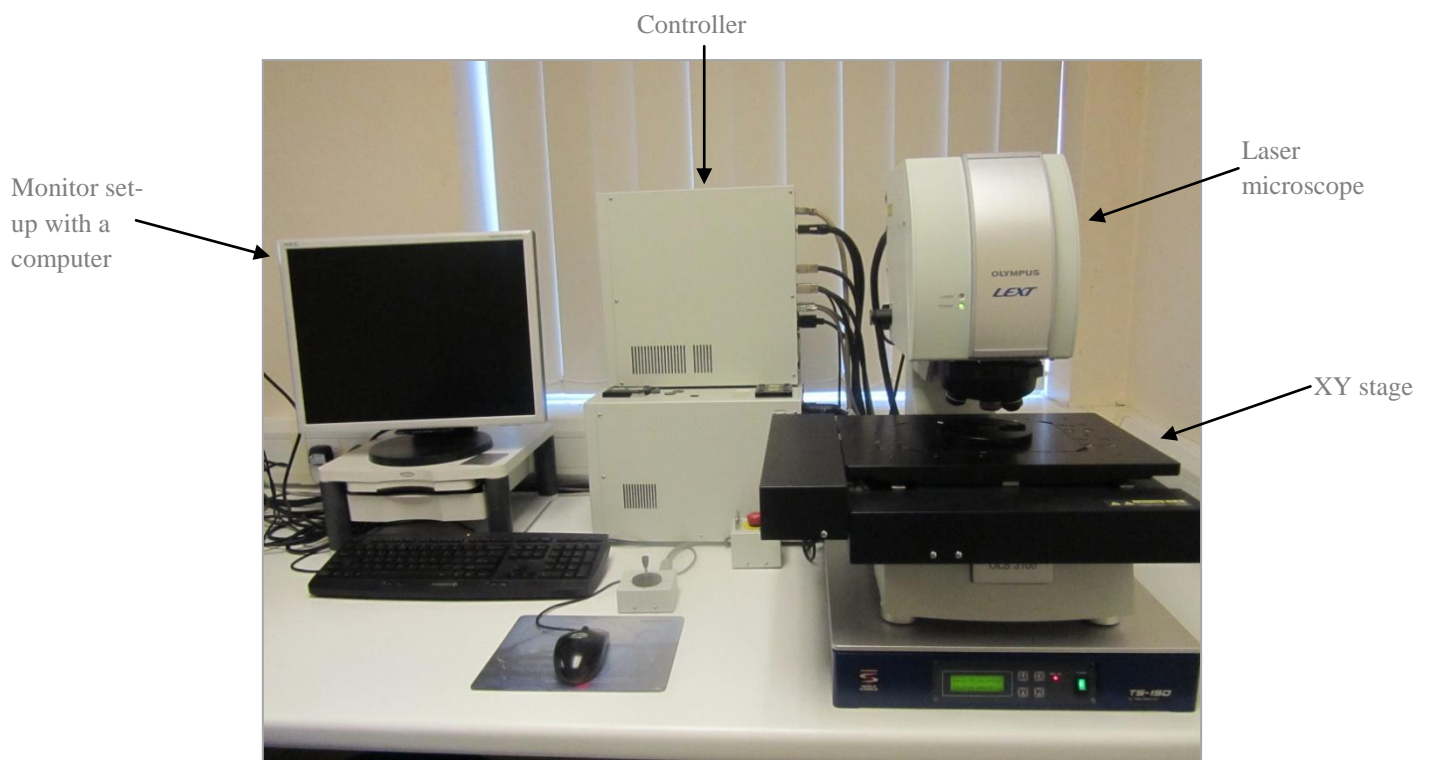
List of chemicals incorporated in Ti sandwich structure microfabrication

Process	Chemical
Cleaning	Micro-90
	Acetone
Lithography	S1818 G2
	MF- 319 Developer
Cu electroless plating	Tin (II) Chloride dihydrate, reagent grade, 98%
	Silver Nitrate, analytical reagent grade
	Borane-dimethylamine complex 98+%
	Ethylenediaminetetraacetic acid disodium salt dihydrate, ACS reagent, 99.0-101.0%
	Copper (II) Sulphate 5-hydrate
	Ammonium Hydroxide 28-30%
	Hydrochloric acid
	Buffer tablets: pH 7 and pH 9.2
	Triton X-100
	Glycerol 98%, Laboratory reagent grade
Cu electroplating	Sulphuric acid
	Sodium Chloride
Cu etching	Iron (III) Chloride 6-hydrate
Electrolytic etching	Hydrochloric acid

Appendix F

Lext Olympus Confocal Scanning Laser Microscope, type OLS3100/3000, was used throughout the research for analyses of Cu electroless coatings and etched Ti.

The surface roughness analyses, as well as analyses of etched features: etch depth, diameter, and surface roughness were carried out with the use of the equipment presented below.



Confocal Scanning Laser Microscope set-up.

The laser microscope scans the specimen in X-Y direction by aiming the laser beam at a very small spot with objective lens [149]. Then, it captures a light from a specimen with detector and outputs the image of the sample on monitor.

In confocal optics, pinhole is placed at a position that is optically conjugate with focusing position (confocal plane) to repel light that comes from place other than focusing position. As the result, the part where light was repelled is truly darkened in the image and; it is possible to slice optically the specimen of shouldered shape [149].

Specifications of the units of the Confocal Microscope.

Unit of the microscope	Specification
Laser main unit	Semiconductor laser $\lambda = 408 \pm 5 \text{ nm}$
Light source for TV	White LED
Z-drive	Moving resolution $0.01 \mu\text{m}$ Scale built-in 5 nm Stroke 10 mm
Revolving nosepiece	100x, WD= 0.35 mm 50x, WD= 0.30 mm 20x, WD= 3.1 mm 10x, WD= 11.0 mm 5x, WD= 20.0 mm